MATHEMATICAL MODELLING OF SOLUTE TRANSPORT AND ITS EFFECTS ON CROP YIELDS

A
Thesis

Submitted to the
UNIVERSITY OF KOTA

in the Partial Fulfillment of the Requirements for the
Award of the Degree of
DOCTOR OF PHILOSOPHY

in
Mathematics
under the
Faculty of Science

Submitted by
Dinesh Kumar Varma
Registration No.: RS/1836/22

Under the Supervision of
Prof. Arun Kumar
Professor
Department of Mathematics
Government College, Kota

UNIVERSITY OF KOTA
KOTA (RAJASTHAN)-324 005
INDIA

October, 2025

शोध निदेशालय
कोटा विश्वविद्यालय
एम.बी.एस. मार्ग, कोटा
(राजस्थान)–३२४००५
फोन नम्बर: ०७४४–२४७१०३७

Directorate of Research
University of Kota
MBS Marg, KOTA
(Rajasthan)-324005
Phone No.: 0744-2471037

CERTIFICATE

I feel great pleasure in certifying that the Ph.D. thesis entitled **"MATHEMATICAL MODELLING OF SOLUTE TRANSPORT AND ITS EFFECTS ON CROP YIELDS"** submitted by Mr. **Dinesh Kumar Varma** to the University of Kota in the partial fulfillment of the requirements for the award of the degree of Doctor of Philosophy is based on the research work carried out under my guidance.

He has completed the following requirements as per UGC Regulations and research ordinance of the University:

(a) Satisfactory Completion of the Ph.D. Course Work.
(b) Submission of Half Yearly Progress Reports.
(c) Fulfilment of residential requirement of the Research Centre (*Minimum 200 Days*).
(d) Presentation of research work before the Departmental Committee.
(e) Publication of at least one research paper in the referred research journal of national and international repute.
(f) Two paper presentations in the Conferences/ Seminars.

I recommend the submission of the Ph.D. thesis and certify that it is fit to be evaluated by the examiners.

Date:
Place:

Prof. Arun Kumar
Research Supervisor

शोध निदेशालय
कोटा विश्वविद्यालय
एम.बी.एस. मार्ग, कोटा
(राजस्थान)–३२४००५
फोन नम्बर: ०७४४–२४७१०३७

Directorate of Research
University of Kota
MBS Marg, KOTA
(Rajasthan)-324005
Phone No.: 0744-2471037

DECLARATION

I, **Dinesh Kumar Varma**, hereby certify that the research work presented in my Ph.D. thesis entitled **"MATHEMATICAL MODELLING OF SOLUTE TRANSPORT AND ITS EFFECTS ON CROP YIELDS"** which is carried out by me under the supervision of **Prof. Arun Kumar** and submitted in the partial fulfillment of the requirement for the award of the degree of Doctor of Philosophy of the University of Kota, represents my ideas in my own words and where others' ideas or words have been included in this thesis, I have adequately cited and referenced the original sources.

The work presented in this thesis has not been submitted elsewhere for the award of any degree or diploma from any other institution or university in India or abroad. I declare that I have adhered to all the principles of academic honesty and integrity and have not misrepresented or fabricated or falsified any idea / data / fact / source in my submission.

I understand that any violation of the above will cause for disciplinary action by the University and can also evoke penal action from the sources which have thus not been properly cited or from whom proper permission has not been taken when needed.

Date:
Place:

Dinesh Kumar Varma
Research Scholar

This is to certify that the above statement made by Mr. Dinesh Kumar Varma (Registration Number: RS/1836/22 Dated 29.01.2022) is correct to the best of my knowledge.

Date:
Place:

Prof. Arun Kumar
Research Supervisor

शोध निदेशालय
कोटा विश्वविद्यालय
एम.बी.एस. मार्ग, कोटा
(राजस्थान)–३२४००५
फोन नम्बर: ०७४४–२४७१०३७

Directorate of Research
University of Kota
MBS Marg, KOTA
(Rajasthan)-324005
Phone No.: 0744-2471037

Anti-Plagiarism Certificate

It is certified that the Ph.D. thesis entitled **"MATHEMATICAL MODELLING OF SOLUTE TRANSPORT AND ITS EFFECTS ON CROP YIELDS"** submitted by Mr. Dinesh Kumar Varma has been examined with the anti-plagiarism tool.

We undertake that:

a. The thesis has significant new work/knowledge as compared already published or are under consideration to be published elsewhere. No sentence, equation, diagram, table, paragraph or section has been copied verbatim from previous work unless it is placed under quotation mark and duly referenced.

b. The work presented is original and own work of the author *i.e.* there is no plagiarism. No ideas, processes, results or words of others have beenpresented as the author's own work

c. There is no fabrication of data or results which have been compiled and analyzed.

d. There is no falsification by manipulating research materials, equipment or processes, or changing or omitting data or results such that the research is not accurately represented in the research record.

e. The thesis has been checked by using **DrillBit** tool/software and found within the limits as per UGC plagiarism policy and instructions issued from time to time.

Report is also enclosed along with this Ph.D. thesis.

Date:
Place:

Dinesh Kumar Varma
Research Scholar

Prof. Arun Kumar
Research Supervisor

The Report is Generated by DrillBit Plagiarism Detection Software

Submission Information

Author Name	Dinesh Kumar Varma
Title	MATHEMATICAL MODELLING OF SOLUTE TRANSPORT AND ITS EFFECTS ON CROP YIELDS
Paper/Submission ID	4563780
Submitted by	arunkr71@gmail.com
Submission Date	2025-10-22 00:28:05
Total Pages, Total Words	184, 47786
Document type	Thesis

Result Information

Similarity **4 %**

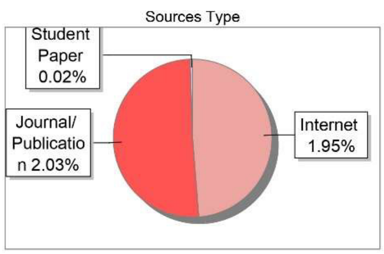

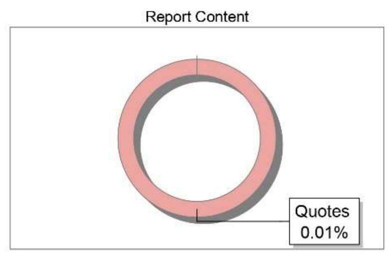

Exclude Information

Quotes	Excluded
References/Bibliography	Excluded
Source: Excluded < 2 Words	Excluded
Excluded Source	**0 %**
Excluded Phrases	Not Excluded

Database Selection

Language	English
Student Papers	Yes
Journals & publishers	Yes
Internet or Web	Yes
Institution Repository	Yes

A Unique QR Code use to View/Download/Share Pdf File

Dedication

To my beloved Parents,

Your love, support, and sacrifices have been the driving force behind my every endeavor. This thesis is dedicated to you, with gratitude and love.

Thank you for being my pillars of strength and inspiration.

ACKNOWLEDGEMENT

"No one who achieves success does so without the help of others. The wise and confident acknowledge this help with gratitude."

— Alfred North Whitehead

This thesis is not just the result of my hard work alone. It is the outcome of the support, guidance, patience, and kindness of many people around me. At this moment of completion, I want to express my heartfelt gratitude to each of them.

First and foremost, I thank the Almighty for giving me the strength, health, and determination to carry on, even when things were tough. Without His blessings, I would not have reached this stage.

I sincerely thank my research supervisor, Prof. Arun Kumar (Professor, Department of Mathematics, Govt. College, Kota, Rajasthan). From the beginning, he has been a constant source of motivation and support. His deep knowledge, honest feedback, and calm guidance helped me improve my work and stay focused. He always encouraged me to think independently and never hesitated to give his time whenever I had doubts. I feel truly lucky to have been guided by him.

I also want to thank the Principal, the Head of the Department, and all the faculty members of the Department of Mathematics, Government College, Kota, for providing a friendly, respectful, and academically supportive environment. Their encouragement, cooperation, and positive attitude made a big difference in helping me stay focused and complete my research smoothly.

I am genuinely thankful to my friends, colleagues, and fellow researchers who stood by me throughout this journey. Whether it was through a helpful suggestion, a word of encouragement, or simply being there to listen, each of them contributed in their own way. Their support — big or small — meant a lot to me and made this long research journey more manageable and meaningful.

From the deepest part of my heart, I thank my parents, Shanti Devi and Sitaram Varma, whose blessings and unconditional love have been my strength. They have always believed in me, even when I doubted myself. Their sacrifices, prayers, and support are behind every achievement of mine. My younger brother, Mahesh, also deserves special thanks. Whether it was emotional support or practical help, he was always there when I needed him. I genuinely appreciate his caring nature and encouragement during this journey.

I express my sincere appreciation to my wife, Lata, for her understanding and cooperation during the period of my research. Her constant support created a calm environment that allowed me to concentrate on my academic responsibilities.

I am also thankful to my lovely children, my daughter Yudipta and my son Dronvik. Their innocent smiles and silent support gave me emotional strength during stressful times. Their presence brought peace, purpose, and joy throughout this journey.

Lastly, I would like to thank all the friends, relatives, and well-wishers whose names may not be mentioned here, but whose support—no matter how big or small, direct or indirect—played a meaningful role in my journey. Your kind words, thoughtful gestures, and encouragement gave me strength during challenging times, and I will always be grateful for your presence and positivity.

Date: Dinesh Kumar Varma

Place: Research Scholar

ABSTRACT

Agriculture faces the dual challenge of meeting rising global food demands while managing limited resources and protecting the environment. This thesis addresses this challenge through the development and application of mathematical models to study solute transport, water flow, and nutrient uptake in soils, with a particular focus on wheat cultivation in the semi-arid region of Jaipur, Rajasthan. The work integrates theoretical modeling, computational simulations, and field-relevant insights to explore how soil–water–plant interactions shape crop yields and sustainability.

Chapter 1 set the stage by highlighting the global and regional importance of efficient water and nutrient management in agriculture. It introduced the central research objectives: to model water and solute dynamics in soil–plant systems and assess their impact on crop productivity under Jaipur's diverse soil conditions.

Chapter 2 reviewed existing literature on soil water flow, solute transport, and nutrient uptake models. Foundational contributions such as Richards' equation, the advection–dispersion equation, van Genuchten–Mualem hydraulic functions, and Michaelis–Menten uptake kinetics were discussed. The review revealed key gaps—particularly in representing root branching structures, soil heterogeneity, and local semi-arid conditions—that guided the focus of this thesis.

Chapter 3 developed models for transient soil water flow and root water uptake. Using Richards' equation coupled with Feddes root uptake functions, the study captured how water availability fluctuates with irrigation, rainfall, and evapotranspiration. Simulations showed that the upper 20–30 cm of soil supplied most plant water, while uptake sharply declined below 60 cm, underscoring the importance of topsoil management in semi-arid regions.

Chapter 4 extended the analysis to nutrient transport and uptake, incorporating root branching into the modeling framework. By combining the advection–dispersion equation with Michaelis–Menten kinetics, the study revealed that nutrient uptake followed a bell-shaped pattern—low in early growth, peaking at mid-season, and declining at maturity. The branching structure of fine lateral roots significantly

enhanced uptake efficiency in the topsoil, while soil texture strongly influenced nutrient mobility and retention.

Chapter 5 linked solute transport with crop yield responses. The findings showed that when nutrients were available at balanced levels, wheat plants made efficient use of them, leading to healthy yields. However, applying fertilizer beyond the optimal range did not improve yields significantly and instead increased the risk of nutrient losses through leaching, especially in sandy soils where water moves quickly. In contrast, finer soils were able to hold nutrients longer, supporting more stable crop performance. These results highlighted the trade-off between maximizing productivity and maintaining sustainability, underlining the importance of site-specific nutrient management.

Chapter 6 introduced a stochastic modeling framework to account for variability in soil properties, climate, and management. By using probability distributions instead of fixed values, the models estimated not just average yields but also the range and reliability of outcomes. This approach offered a more realistic perspective on agricultural systems, showing how uncertainty shapes both risks (e.g., leaching) and opportunities (e.g., efficient resource use).

Chapter 7 consolidated the findings, underscoring the importance of integrating physical models with uncertainty analysis for sustainable agriculture. It emphasized that moderate nutrient inputs maximize yield efficiency while reducing pollution risks, and that local soil conditions must guide fertilizer and irrigation strategies. Looking forward, the chapter identified future directions: extending models to multi-nutrient interactions, incorporating microbial processes, integrating climate change scenarios, and leveraging technologies such as remote sensing, GIS, and machine learning to refine predictions.

In conclusion, this thesis demonstrates that mathematical modeling provides a powerful framework for linking soil processes, root physiology, and crop yield outcomes. By focusing on Jaipur’s semi-arid soils, it offers both scientific contributions and practical guidance for improving water and nutrient management. More broadly, it highlights how integrative approaches can help achieve the global goal of sustainable and climate-resilient agriculture.

TABLE OF CONTENTS

LIST OF ABBREVIATIONS

Abbreviation	Full Form
ADE	Advection–Dispersion Equation
$C(z,t)$	Solute Concentration as a function of depth and time
C_0	Initial Solute Concentration
CDF	Cumulative Distribution Function
CDE	Convection–Dispersion Equation
C_v	Coefficient of Variation
D	Dispersion Coefficient
E[Y]	Expected Yield
ET	Evapotranspiration
ET_a	Actual Evapotranspiration
ET_c	Crop Evapotranspiration
ET_o	Reference Evapotranspiration
FAO	Food and Agriculture Organization
FDM	Finite Difference Method
FEM	Finite Element Method
HYDRUS-1D	Software for water and solute transport modeling
K_m	Michaelis Constant
K_s	Saturated Hydraulic Conductivity
LAI	Leaf Area Index
MM	Michaelis–Menten (kinetics)
PDF	Probability Density Function
P_e	Peclet Number
PDE	Partial Differential Equation
Ψ_a	Air Potential
Ψ_g	Gravitational Potential
Ψ_m	Matric Potential
Ψ_o	Osmotic Potential
$q(z,t)$	Water Flux as a function of depth and time
R	Retardation Factor
RLD	Root Length Density

SD	Standard Deviation
SVA	Stochastic Variability Analysis
SWAP	Soil–Water–Atmosphere–Plant Model
SWC	Soil Water Content
SWP	Soil Water Potential
T_r	Transpiration
t_i	Infiltration time
t_p	Ponding time
λ	Dispersivity
μ	ln λ
θ	Volumetric Water Content
θ_r	Residual Water Content
θ_s	Saturated Water Content
VG	van Genuchten (model/parameters)
v	Pore Water Velocity
V_{max}	Maximum Uptake Rate
WU	Water Uptake
$\vec{x}$	Space coordinate's vector
x	Horizontal space coordinate
y	Horizontal space coordinate
z	Vertical space coordinate
$\vec{\alpha}$	Vector of spatial random functions
$\alpha^{(j)}$	Spatial spatial random function (soil property)
Y	Crop Yield
Y_{max}	Maximum Potential Yield
$\sigma^2 Y$	Variance of Yield

LIST OF TABLES

LIST OF FIGURES

Chapter 1

Introduction

Chapter 1

Introduction

1.1 Background and Motivation

Agriculture remains the foundation of global food security, providing essential resources to sustain a rapidly growing population. By 2050, the global population is expected to reach over 9.7 billion people, which means farmers will need to produce about 70% more food to keep up with demand (FAO, 2009). The challenge is most urgent in developing countries, where agriculture contributes to GDP and employment (World Bank, 2019). To feed the growing population while coping with climate change and limited resources, farmers need to adopt new and sustainable ways to improve crop production.

Of these approaches, adequate water and nutrient management stands supreme, constituting the basis for realizing high crop production levels and sustainability of farming systems. Malnutrition or imbalance in the soils, usually exacerbated by inefficient irrigation, can result in less-than-ideal plant growth and lower production levels (White & Brown, 2010). Studies show that managing water and nutrients together can boost crop yields by making nutrients available to plants and reducing resource wastage (Fageria et al., 2003). Also, effective resource utilization stands at the center of the mitigation of environmental degradation, such as the leaching of nutrients and the salination of soils, for the sustainability of farming in the long run (Zhang et al., 2021).

Transport of solutes in soils is a highly complicated process due to the influence of the heterogeneity in soils, transitory water flows, root-soil contacts, and climatic conditions. Structural, textural, and chemical variations in the soils lead to heterogeneous availability of the nutrients (Jury & Horton, 2004), and fluctuating water moistures produce fluctuating environments that make it hard to predict the movement of the solutes through modeling (Philip, 2006). The spatially and functionally complicated root-soil relations make it hard to precisely replicate the nutrients' uptake (Willigen et al., 2002).

Additionally, the transport and accumulation of pollutants impact crop productivity and pose significant risks to ecosystems and human health (Peddinti et al., 2020). These challenges show why we need better, more integrated methods to study and manage how nutrients and chemicals move in soil and plants.

Mathematical modeling is a potent weapon to achieve this, mimicking and making sense of the interaction involving water, soils, and nutrients in different environmental conditions (Agah et al., 2017). Such models help predict the consequences of various agricultural procedures, i.e., fertilization and irrigation, on the distribution of nutrients and plants' yield (Šimůnek et al., 2006). The models also help in the production of strategies for precision agriculture, involving the saving of resources and reducing unnecessary harm to the environment (Zhang et al., 2017). Also, the addition of stochastic variability in the models aids in depicting parameter uncertainties for soils and climates to make the predictions more valid (Jury et al., 1986). Mathematical models play a significant role in promoting agricultural sustainability and formulating evidence-based strategies to address food security and environmental management challenges by bridging theoretical frameworks with field-level applications.

The research undertakes a detailed analysis of the solute transport processes in soil-plant systems to maximize the availability of nutrients and enhance crop production. Solute transport encompasses complicated processes like water-bridged movement of nutrients, diffusion, and adsorption, depending on the soil's texture, structure, and chemical nature (Jury et al., 1986). Analysis of the processes in different agronomical and environmental conditions enables the research to investigate the effects of the properties of soils, water movement, and uptake by plants to ensure a complete understanding of the dynamics of nutrients in the systems of soils and plants (Šimůnek et al., 2006).

The second primary area of focus for the work is the development of mathematical models that bring together nutrient dynamics and crop yield, and the accounting for deterministic and stochastic models in describing the physical and biological detail of the transport and root uptake of nutrients (van Genuchten & Wagenet, 1989). The models simulate the transport at the macroscopic (at the field) and microscopic (at the root) scales and establish predictive structures that can serve to guide efficient resource allocation and improved agricultural production activities (White & Brown, 2010).

Particular consideration is given to three important determinants of nutrient uptake: root architecture, soil properties, and water availability. Soil texture, pore space, and amount of organic matter control mobility and availability of nutrients (Jury & Horton, 2004), while root spatial distribution patterns and branching are significantly important in controlling absorption efficiency (de Willigen & van Noordwijk, 1994). Water availability, the primary carrier for nutrients, also assumes prominence, as the transient conditions in the water flow control the passage and uptake of nutrients (Philip, 1957). By examining these parameters in detail, the research makes important contributions to analyzing the improvement of the nutrient management results by maximizing the yield while reducing the environmental impact.

The desired impacts of this research are threefold: first, it will encourage the use of sustainable agriculture by providing models that enable the efficient use of water and fertilizers while minimizing environmental hazards like leaching and pollution (Zhang et al., 2021; Tilman et al., 2011); second, it will increase the insight into the interaction between water availability, the dynamics of nutrients, and the growth of crops by modeling the interaction at realistic field-scale conditions (White & Brown, 2010; Šimůnek et al., 2006); and third, it will supply proper instruments for irrigation and fertilization decisions by providing model-based decision-making tools that offer deterministic as well as probabilistic perspectives to enable the effective management of variability and uncertainty in agricultural systems (Jury et al., 1986; van Genuchten & Wagenet, 1989). With this comprehensive framework, the research will provide significant value in addition to the art and science of sustainable agriculture.

1.2 Objectives of the Research

This study aims to improve how we understand and manage water and nutrients in soil–plant systems through four key objectives:

1. To develop mathematical models that show how water and nutrients move in the soil under changing moisture and weather conditions.
2. To model nutrient uptake by incorporating detailed root branching structures, thereby improving predictions of nutrient use efficiency.
3. To establish sustainable thresholds for nutrient management and investigate how varying levels of nutrients and pollutants affect crop yields.

4. To introduce stochastic (probability-based) models to capture natural variability in soils and the environment, making predictions about nutrient movement and crop growth more reliable.

1.3 Soil and Its Constituents

Soil is defined as a dynamic natural body composed of mineral particles, organic matter, water, air, and living organisms, which together form the uppermost layer of the Earth's crust and serve as the primary medium for plant growth. Soils are structured into three distinct phases—solid, liquid, and gas—and comprise four primary components: inorganic solids, organic matter, water, and air. Soil's solid part is made up of minerals from weathered rocks and organic matter from plants and animals, while its liquid part is soil water, which carries dissolved nutrients like a natural solvent. In contrast, the gaseous part of soil is soil air, which is a mixture of essential gases such as nitrogen and oxygen, together with trace gases including carbon dioxide (CO_2), methane (CH_4), and nitrous oxide (N_2O) (Brady & Weil, 2017).

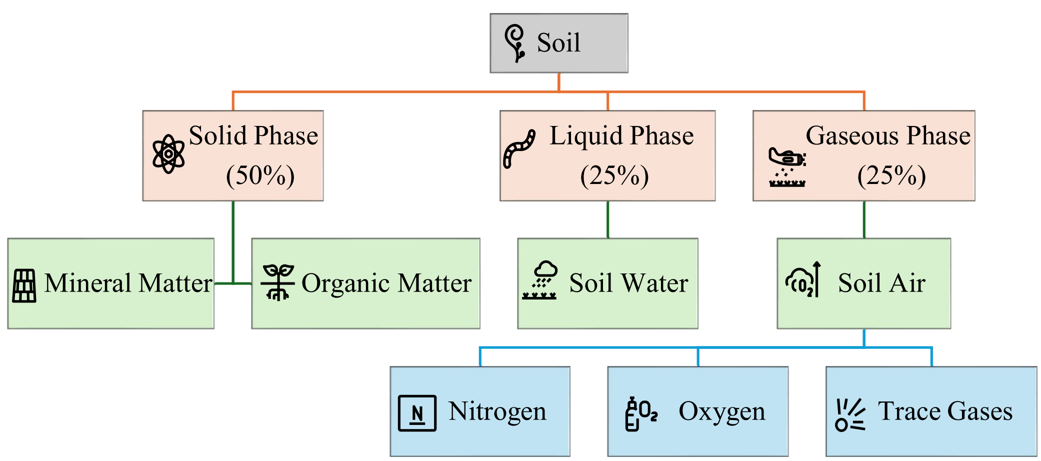

Figure 1.1 Soil Composition and Structure

Under optimal conditions for upland crops, the typical volumetric composition of soil includes about 50% solids (mainly mineral, with up to 5% organic content) and 50% pore space, which is ideally divided equally between water and air. This balance composition of soil helps plants take up nutrients, allows roots to breathe, and supports healthy soil microbes. However, this balance is dynamic and varies with environmental conditions: pore spaces may become water-saturated following rainfall or irrigation, or air-filled under dry conditions.

Soil particles are classified into different size fractions based on their diameters, and several international systems have been developed for this purpose. The two most widely used classification systems are the United States Department of Agriculture (USDA) and the International Soil Science Society (ISSS). Both systems recognize three primary soil separates—sand, silt, and clay. Sand (0.05–2.00 mm) is gritty with large pores, silt (0.002–0.05 mm) feels smooth and retains moderate moisture, and clay (<0.002 mm) is sticky with fine pores that hold water and nutrients effectively. The main difference lies in how they divide the sand fraction: the USDA defines five subcategories (from very coarse to very fine), while the ISSS uses only two (coarse and fine sand). The relative percentage of sand, silt, and clay defines the soil's textural class, which may range from loam and sandy loam to clay loam or silty clay. These types are shown on a soil texture triangle, a common chart used by soil scientists. The comparative classification ranges for both systems are summarized in Table 1.1.

Table 1.1 Soil Particle-Size Classification According to USDA and ISSS

Particle Size Range (mm)	USDA Classification	ISSS Classification
2.0 – 1.0	Very Coarse Sand	Coarse Sand
1.0 – 0.5	Coarse Sand	Coarse Sand
0.5 – 0.25	Medium Sand	Coarse Sand
0.25 – 0.10	Fine Sand	Fine Sand
0.10 – 0.05	Very Fine Sand	Fine Sand
0.05 – 0.002	Silt	Silt
< 0.002	Clay	Clay

Source: Adapted from Jury, W.A., and Horton, R., *Soil Physics*, John Wiley & Sons, Hoboken, NJ, 2004.

1.4 Soil Phases and Physical Properties

Bulk soil consists of three distinct phases: solid, water, and air. Together, these parts decide how the soil behaves. The total volume of soil $(v)[L^3]$ is the sum of the volumes of gas (v_g) $[L^3]$, liquid or water (v_l) $[L^3]$, and solids (v_s) $[L^3]$:

$$v = v_g + v_l + v_s \tag{1.1}$$

Normalizing this with respect to total volume yields the volumetric air content (a), volumetric water content (θ), and solid fraction, where:

$$a = \frac{v_g}{v}, \quad \theta = \frac{v_l}{v}, \quad \varphi = a + \theta \tag{1.2}$$

Porosity (φ) represents the total volume of pores ($v_g + v_l$) and generally accounts for about 50% of total soil volume under optimal conditions.

Bulk soil can also be described in terms of the mass of each phase.

$$m = m_g + m_l + m_s \tag{1.3}$$

where m is the total mass [M] of a soil and m_g, m_l, and m_s are the respective masses of gas, liquid, and solid [M]. The mass of gas is negligible compared to the other two phases; two important mass-based physical properties are defined.

Particle density (ρ_s), representing the density of the solid mineral component, is calculated as the mass of solids per unit volume of solids:

$$\rho_s = \frac{m_s}{v_s} \tag{1.4}$$

Most mineral soils have a particle density of about 2.65 g cm^{-3}, the same as quartz (Blake & Hartge, 2013). Soils with a lot of iron tend to be a bit heavier, while those with more organic matter are usually lighter.

Bulk density (ρ_b) of soil is more variable and is defined as the dry mass of solids per total volume:

$$\rho_b = \frac{m_s}{v} \tag{1.5}$$

Bulk density varies with soil structure, compaction, and moisture, typically ranging from 1.2 to 1.8 g cm^{-3} (Blake & Hartge, 2013). It is lowest in forest and organic soils and highest in compacted sandy soils. The relationship between porosity, particle density, and bulk density is expressed as:

Bulk density varies with soil structure, compaction, and moisture, typically ranging from 1.2 to 1.8 $\mathrm{g\,cm^{-3}}$ (Blake & Hartge, 2013). It tends to be lowest in forest and organic soils and highest in compacted sandy soils. The relationship among porosity (φ), particle density (ρ_s), and bulk density (ρ_b) is expressed as:

$$\varphi = 1 - \frac{\rho_b}{\rho_s} \tag{1.6}$$

Assuming a constant particle density, this equation highlights that changes in porosity are primarily governed by variations in bulk density.

1.5 Soil Water Content and Potential

Soil water content is a fundamental parameter in soil physics, representing the amount of water present in the soil. It can be defined in four distinct ways, each serving specific analytical and practical purposes.

Volumetric Water Content ($\boldsymbol{\theta}$) is the ratio of the volume of water (v_l) to the total volume of soil (v):

$$\theta = \frac{v_l}{v} \tag{1.7}$$

This dimensionless value is typically expressed in units of cm^3 water per cm^3 oil and is commonly used in hydrological and agricultural models.

Gravimetric water content ($\boldsymbol{\theta_g}$) is the ratio of the mass of water (m_l) to the mass of dry soil (m_s):

$$\theta_g = \frac{m_l}{m_s} \tag{1.8}$$

It is expressed in g/g or kg/kg and is useful for laboratory measurements where soil samples are oven-dried at 105°C for 24–48 hours to determine m_s (Topp and Ferre, 2002a).

The relationship between volumetric and gravimetric water contents is given by:

$$\theta = \theta_g \frac{\rho_b}{\rho_w} \tag{1.9}$$

Here, ρ_b is the bulk density of soil, and ρ_w is the density of water (approximately 1 g cm^{-3} in cgs units or 1000 kg m^{-3} in SI units).

Effective Saturation or Relative Water Content (S_e) represents the proportion of water present between the residual (θ_r) and saturated (θ_s) water contents:

$$S_e = \frac{\theta - \theta_r}{\theta_s - \theta_r} \tag{1.10}$$

This dimensionless parameter varies between 0 and 1 and is commonly used in unsaturated flow modeling (van Genuchten, 1980a).

Equivalent depth of water (D_e) provides a measure of how much water is stored in a given soil depth (D). For uniform profiles:

$$D_e = \theta D \tag{1.11}$$

For stratified profiles with n layers of varying water content and thickness, the total depth is:

$$D_e = \sum_{i=1}^{n} \theta_i D_i \tag{1.12}$$

where θ_i and D_i are the water content and thickness of the i-th layer, respectively. This definition is particularly useful in field applications and irrigation management (Hillel, 1980).

Soil Water Potential

Soil water potential (ψ) describes the energy status of water in the soil and serves as a fundamental parameter for analyzing water movement and its availability to plants. Unlike soil water content (θ), which may be misleading across different soil types, soil water potential offers a standardized way to compare water availability and flow dynamics across soils with varying textures and structures.

Formally, soil water potential is defined as the difference in energy of soil water relative to pure water at standard pressure, temperature, and elevation, expressed per unit volume, mass, or weight. It is typically represented either in Pascals (Pa), denoting energy per unit volume, or in meters (m) as potential head or hydraulic head (H), where the relationship is given by

$$\psi_t = \rho_w g H \tag{1.13}$$

where ρ_w is the density of water [ML^{-3}], g is gravitational acceleration [LT^{-2}], and H is the hydraulic head [L]. For practical purposes, these units are interchangeable, with 1 m of water head ≈ 9.8 kPa.

Components of Soil Water Potential

Total soil water potential is comprised of the potential energies due to various force fields acting on soil water. These forces include gravity, hydrostatic pressure, capillarity, solute concentration, and soil air pressure. An additional component, related to swelling soils, is rarely significant and is therefore not addressed in detail (Jury and Horton, 2004).

1. Gravitational potential (ψ_z)

Gravitational potential ($\boldsymbol{\psi_z}$) represents the influence of gravity on the energy status of soil water. It is essential for understanding vertical water movement within the soil profile. This potential is defined as the difference in energy per unit volume or weight between soil water and a reference (standard) water level, due to elevation. Mathematically, it is given by:

$$\psi_z = \rho_w g (z_{\text{soil}} - z_0) \tag{1.14}$$

where ψ_z is the gravitational potential [Pa], ρ_w is the density of water [ML^{-3}], g is the acceleration due to gravity [LT^{-2}], z_{soil} is the elevation of the soil water [L] and z_0 is the reference elevation [L].

The corresponding gravitational potential head is:

$$z = z_{\text{soil}} - z_0 \tag{1.15}$$

This head is expressed in meters (m). Usually, the soil surface is taken as the reference elevation ($z_0 = 0$). If soil water lies below this reference, the potential becomes negative, indicating lower energy due to gravity. Gravitational potential plays a key role in determining water flow direction, as water naturally moves from zones of higher to lower total potential energy.

2. Hydrostatic Potential (ψ_p)

Hydrostatic potential (ψ_p) quantifies the pressure exerted by overlying water in saturated soil zones, such as below the water table. It reflects the added energy in soil water due to the weight of water above it. In unconfined aquifers, hydrostatic potential is zero at the water table. Above it lies the capillary fringe and vadose zone (unsaturated). Temporary saturation above the water table may occur as perched water, while confined aquifers may exhibit pressure-driven flow (e.g., artesian wells).

The hydrostatic potential is calculated as:

$$\psi_p = \rho_w g(z_{watertable} - z_{soil}) \tag{1.16}$$

and the corresponding hydrostatic head (h) is:

$$h = z_{watertable} - z_{soil} \tag{1.17}$$

where z is elevation, ρ_w is water density, and g is gravitational acceleration.

This potential is always zero or positive and is measured using devices like piezometers. It is crucial in evaluating water movement in saturated soil systems.

3. Matric Potential (ψ_m)

Matric potential (ψ_m) reflects the energy reduction in soil water due to capillarity and adsorption forces in unsaturated soils. It originates from the soil matrix, where water is held in fine pores and on particle surfaces, especially clay and organic matter. Water is drawn into small pores by capillary action and adheres to solid surfaces via adsorption, both creating negative pressure (tension), thereby lowering water's energy compared to free water. This energy status is expressed as matric potential (ψ_m), and its corresponding pressure head (h) is negative in unsaturated conditions.

Matric potential does not exist in saturated soils, where water is under positive pressure and menisci (curved water surfaces) vanish. It is a critical component of total soil water potential in unsaturated zones and varies inversely with water content — becoming more negative as soil dries.

Though no direct equation exists for ψ_m, it can be measured using tensiometers or estimated through empirical relationships involving volumetric water content (θ). In modeling, both hydrostatic and matric pressures may be referred to by the same symbol h, though they apply under different saturation conditions.

4. Solute Potential (ψ_s)

Solute potential (ψ_s) represents the reduction in soil water's energy caused by dissolved solutes. When solutes are present, they attract water molecules through hydrogen bonding, thereby lowering the free energy of water compared to pure water. This energy decrease is always zero or negative.

It is defined as the difference in energy per unit volume or weight between solute-free water and soil water containing dissolved substances. The potential can be calculated using the equation:

$$\psi_s = -RTC_s \tag{1.18}$$

where C_s is the total dissolved ion concentration $[ML^{-3}]$, in moles per cubic meter, R is the universal gas constant = 8.314 $Pa \cdot m^3 \cdot mol^{-1} \cdot K^{-1}$ and T is the absolute temperature in Kelvin.

This can be converted into solute potential head (in meters) using:

$$s = \frac{-RTC_s}{\rho_w g} \tag{1.19}$$

where ρ_w is water density and g is gravitational acceleration. The solute potential is crucial in saline or fertilized soils, affecting plant water uptake by altering the osmotic balance.

5. Air Potential (ψ_a)

Air potential (ψ_a) accounts for the influence of soil air pressure on the energy status of soil water and is relevant only in unsaturated soils, where air coexists with water in pore spaces. It is defined as the difference in pressure between soil air and standard atmospheric pressure (P_0):

$$\psi_a = P_{\text{soil air}} - P_0 \tag{1.20}$$

When expressed as potential head:

$$a = \frac{P_{soil\ air} - P_0}{\rho_w g} \tag{1.21}$$

If soil air pressure is below atmospheric, it reduces soil water potential; if above, it raises it. Though difficult to measure directly and often neglected in practice, air potential can still influence readings from field instruments like tensiometers and piezometers. Variability in atmospheric pressure, compact soils, or confined spaces (e.g., caves) may cause this component to deviate significantly from standard atmospheric conditions.

Total Soil Water Potential

The total soil water potential represents the cumulative energy status of soil water resulting from all acting forces. It is the summation of the individual components of soil water potential that are active under specific conditions. These components vary primarily between saturated and unsaturated soil environments and are expressed in both potential and potential head forms.

In the absence of measurable solute and air components, total soil water potential head (hydraulic head) can be reduced to:

$$H = h + z \tag{1.22}$$

Table 1.2 Hydraulic head in saturated and unsaturated zones

Condition	Water Potential	Hydraulic Head
Saturated	$\psi_t = \psi_z + \psi_p + \psi_s$	$H = z + h + s$
Unsaturated	$\psi_t = \psi_z + \psi_m + \psi_s + \psi_a$	$H = z + h + s + a$

In saturated soils (like groundwater zones), gravitational and hydrostatic potentials dominate, whereas in unsaturated soils (such as the vadose zone), gravitational and matric potentials are more significant. Gravitational head (z) can be positive or negative based on the chosen reference level, and pressure head (h) is positive in saturated and negative in unsaturated conditions.

In most practical cases, the hydraulic head (H) describes total soil water potential, which combines all the different potential components. It is usually measured in centimeters or meters, since it can be considered the height of a water column and directly shows the direction and strength of water movement in the soil.

1.6 Water Movement in Soils

Water movement through soil is an inherent process that controls both water quantity and quality on land. Since solute transport is inherently tied to water flux, an examination of solute behavior quantitatively should commence with an in-depth explanation of water movement through the soils. This process occurs under both saturated and unsaturated conditions, each governed by distinct driving forces and flow mechanisms.

Saturated Water Flow

Saturated conditions occur below the water table, where all soil pores are filled with water. Under such conditions, the movement is predominantly horizontal due to the hydraulic gradients with a relatively small vertical component. Saturated water content (θ_s) equals the porosity (φ) of the soil when there is no air entrapment. While it is common to assume full saturation below the water table, some residual air may remain above the table, especially near the soil surface.

Unsaturated Water Flow

Unsaturated conditions predominate above the water table, in what is termed the vadose zone, where air and water coexist within the soil pores. Water movement here is vertical due to the operation of capillary forces and gravity. Horizontal movement does occur too, particularly after the occurrence of an event like rainfall or irrigation, or above an impermeable layer where local saturation forms. Generally, water movement in unsaturated soil is more complex due to its dependence on matric and gravitational potentials.

Steady and Transient Water Flow

Water movement may be classified as either steady or transient:

1. Steady flow occurs when water content and fluxes remain constant over time but may vary with depth or position.

2. Transient flow involves at least one parameter (e.g., water content, pressure head, or flux) that changes with time, reflecting dynamic redistribution.

Sources and Fate of Infiltrated Water

Water enters the soil primarily through precipitation, irrigation, or even human-made spills. When the application rate exceeds the soil's infiltration capacity, surface runoff occurs. Once inside the soil, water can do several things: it may (i) evaporate back into the air, (ii) be taken up by plant roots and released during transpiration, or (iii) move deeper down to refill groundwater. The combined processes of evaporation and transpiration are collectively called evapotranspiration (ET). If the water table lies near the surface, capillary rise may occur, drawing water upward to the root zone from the saturated layer.

Modeling Water Flow

To calculate the movement of water, the right governing equations should be used. Although analytical solutions may be possible when the conditions are steady state, the transient flow normally demands a numerical solution since it is complex. The processes listed below are normally simulated: Infiltration, Redistribution, Evaporation, Transpiration, Preferential flow and Groundwater recharge/discharge.

Numerical HYDRUS codes are widely employed to simulate these processes. They further include inverse modeling to approximate the hydraulic characteristics of the soils through matching the simulation with the observed data.

Water movement in unsaturated soil under transient conditions is commonly described by Richards' equation, which combines Darcy's law for water flow in porous media with the continuity equation. In one-dimensional vertical flow, the equation simplifies to:

$$\frac{\partial \theta}{\partial t} = \frac{\partial}{\partial z}\left[K(h)\left(\frac{\partial h}{\partial z} + 1\right)\right] - S(z,t) \tag{1.23}$$

where θ is the volumetric water content [L^3], t is the time [T], z is the vertical coordinate [L] (positive upward), h is the soil water pressure head [L], $K(h)$ is the unsaturated hydraulic conductivity [L/T], $S(z,t)$ is the root water uptake rate (sink term) [1/T].

Root Water Uptake Modeling

Root water uptake represents the removal of soil water by plant roots and is modeled through the sink term $S(z,t)$ in Richards' equation. Several modeling approaches are used to simulate root water uptake:

- **Feddes' Model (1978):** Incorporates water stress response functions to reduce uptake under dry or saturated conditions. It defines an optimal pressure head range and decreasing uptake outside of this range.
- **Van Genuchten–Feddes Model:** Couples soil hydraulic properties with plant stress response to simulate more realistic uptake patterns.
- **Macroscopic Models:** Distribute water extraction based on root length density and local soil water availability without resolving individual roots.
- **Microscopic or 3D Root Architecture Models:** Capture detailed root geometry and simulate uptake at the root-soil interface, but are computationally intensive.

1.7 Solute Transport Mechanisms in Soil

Solute transport in the soil-plant system involves the movement and transformation of solutes such as nutrients and pollutants. The main processes responsible for this movement are advection, diffusion, dispersion, sorption, root uptake, and chemical or biological degradation. These processes are typically described using the Advection–Dispersion Equation (ADE) modified with source/sink terms.

Advection

Advection refers to the transport of solutes by the bulk movement of water through the soil. The process is primarily driven by pressure gradients and is governed by Darcy's law. In three dimensions, Darcy's law is expressed as:

$$\vec{q} = -K(h)\nabla(h+z) \tag{1.24}$$

where $\vec{q}$ is the Darcy water flux vector $[LT^{-1}]$, $K(h)$ is unsaturated hydraulic conductivity as a function of pressure head $[LT^{-1}]$, h is the soil water pressure head [L] and z is the elevation head [L].

In one-dimensional vertical flow, this simplifies to:

$$q = -K(h)\left(\frac{dh}{dz} + 1\right) \tag{1.25}$$

Here, q represents the vertical water flux. The advective solute transport term in the solute transport equation is then given by:

$$\left(\frac{\partial(\theta C)}{\partial t}\right)_{\text{adv}} = -q\frac{\partial C}{\partial z} \tag{1.26}$$

where C is the solute concentration in the soil solution [ML^{-3}] and θ is the volumetric water content [$-$]. Advection dominates in coarse-textured soils or during rapid water flow, such as after irrigation or rainfall.

Diffusion

Diffusion is the process by which solutes move from regions of higher concentration to regions of lower concentration due to molecular activity. Fick's first law governs diffusive transport and, in 1-D, is expressed as:

$$J_d = -D_m\frac{\partial C}{\partial z} \tag{1.27}$$

where J_d is the diffusive solute flux [$ML^{-2}T^{-1}$], D_m is the effective molecular diffusion coefficient in soil [L^2T^{-1}] and $\frac{\partial C}{\partial z}$ is the solute concentration gradient.

Diffusion is significant in saturated or nearly saturated soils where water movement is limited, and solute gradients dominate.

Hydrodynamic Dispersion

Dispersion in porous media combines mechanical dispersion and molecular diffusion. The dispersion coefficient D accounts for the spreading of solute due to variations in pore-scale velocities and is given by:

$$D = \alpha_L|q| + \frac{D_m}{\theta} \tag{1.28}$$

where α_L is the longitudinal dispersivity [L], $|q|$ is the magnitude of Darcy water flux [LT^{-1}], D_m is the molecular diffusion coefficient [L^2T^{-1}] and θ is the volumetric water content [$-$].

In 1-D, the total solute flux from advection and dispersion is:

$$J = -D\frac{\partial C}{\partial z} + qC \tag{1.29}$$

Sorption

Sorption describes the attachment of solutes to soil particles and is a critical process that delays solute movement. The total concentration of solute in the soil, C_t, is composed of the concentration in the liquid phase and the adsorbed (solid) phase:

$$C_t = \theta C + \rho_b S \tag{1.30}$$

Where C is the solute concentration in the soil water [ML^{-3}], S is the adsorbed concentration on soil particles [MM^{-1}] and ρ_b is the bulk density of soil [ML^{-3}].

Assuming linear equilibrium sorption:

$$S = K_d C \tag{1.31}$$

where K_d is the distribution coefficient [L^{3}M^{-1}]. Substituting, the total concentration becomes:

$$C_t = \theta C + \rho_b K_d C = (\theta + \rho_b K_d)C \tag{1.32}$$

This introduces the retardation factor R:

$$R = 1 + \frac{\rho_b K_d}{\theta} \tag{1.33}$$

The advection–dispersion equation accounting for retardation in 1-D becomes:

$$R\frac{\partial C}{\partial t} = \frac{\partial}{\partial z}\left(D\frac{\partial C}{\partial z}\right) - q\frac{\partial C}{\partial z} \tag{1.34}$$

Root Uptake (Sink Term)

Root uptake represents the removal of solutes from the soil solution due to plant absorption. It is modeled as a sink term S_r in the advection–dispersion equation. In 1-D, the governing equation incorporating root uptake becomes:

$$\frac{\partial(\theta C)}{\partial t} = \frac{\partial}{\partial z}\left(D\frac{\partial C}{\partial z}\right) - q\frac{\partial C}{\partial z} - S_r \tag{1.35}$$

The root uptake sink term is typically modeled using a concentration-dependent function:

$$S_r = \alpha_r C \tag{1.36}$$

where α_r is the root uptake rate coefficient [T^{-1}] and C is the solute concentration in the soil water [ML^{-3}]. This formulation assumes linear uptake proportional to solute availability.

Chemical Reactions

Chemical reactions such as precipitation/dissolution or complexation may transform solutes into different chemical species. These reactions are modeled as source or sink terms, S_{chem}, which can be added to the transport equation:

$$\frac{\partial(\theta C)}{\partial t} = \frac{\partial}{\partial z}\left(D\frac{\partial C}{\partial z}\right) - q\frac{\partial C}{\partial z} + S_{chem} \tag{1.37}$$

An example of a first-order reaction (e.g., transformation or precipitation) is:

$$S_{chem} = -k_{chem}C \tag{1.38}$$

where k_{chem} is the first-order reaction rate constant [T^{-1}].

Degradation

Degradation, often due to microbial activity or natural decay, leads to the reduction of solute concentration over time. It is commonly modeled using first-order kinetics:

$$\frac{\partial(\theta C)}{\partial t} = \frac{\partial}{\partial z}\left(D\frac{\partial C}{\partial z}\right) - q\frac{\partial C}{\partial z} - k_d\theta C \tag{1.39}$$

where k_d is the degradation rate constant [T^{-1}]. This term reduces the solute concentration exponentially over time, depending on k_d and moisture content θ.

Combined Advection–Dispersion–Reaction Equation (1D Form)

When all mechanisms—advection, dispersion, sorption (via retardation), root uptake, chemical reactions, and degradation—are considered, the 1-D governing equation becomes:

$$R\frac{\partial C}{\partial t} = \frac{\partial}{\partial z}\left(D\frac{\partial C}{\partial z}\right) - q\frac{\partial C}{\partial z} - \alpha_r C - k_{chem}C - k_d C \tag{1.40}$$

This comprehensive form enables simulation of realistic solute behavior in soil–plant systems under transient conditions.

Numerical Simulation of Transient Soil-Plant Water Dynamics

Modeling tools such as HYDRUS-1D and HYDRUS-2D/3D are widely used to study how water moves through soil and how plant roots take it up over time and space. These simulations usually rely on inputs like soil hydraulic properties (e.g., van Genuchten–Mualem parameters), root structure and uptake behavior, weather conditions such as rainfall, irrigation, and evaporation, and the variation of soil moisture across depth and time. To make the models realistic, they are often calibrated and validated with field data collected from soil moisture probes or lysimeters.

Transient flow models have become essential in agriculture and environmental science. They assist farmers and researchers in managing irrigation more efficiently, forecasting drought stress in crops, understanding soil water movement for conservation, and assessing risks such as nitrate leaching and salinity. Yet, despite these benefits, the models continue to face important challenges. They often struggle to fully capture the variability of real soils in the field, accurately represent plant-specific responses and root dynamics, or simulate hydraulic redistribution. In addition, they require high computational power when applied to large areas.

To overcome these challenges, future research is moving toward data-driven methods. Machine learning can be used to optimize model parameters, while coupling water flow models with nutrient uptake and yield predictions can improve agricultural decision-making. Advances in modeling root–soil interactions under real-time environmental conditions will further enhance the reliability and applicability of these tools.

1.8 Nutrient Uptake Modeling in Branched Root Systems

Building upon the transient water flow framework established in Chapter 3, this section introduces a nutrient uptake model that incorporates the complexities of branched root systems. The model is grounded in the Michaelis–Menten kinetics, widely applied to describe the enzymatic uptake behavior of plant roots. The nutrient uptake rate U per unit volume of soil is given by:

$$U = \frac{V_{max} \cdot C}{K_m + C} \cdot L \tag{1.41}$$

where V_{max} is the maximum nutrient uptake rate per unit root length $ML^{-1}T^{-1}$], C is the nutrient concentration in the soil solution [ML^{-3}], K_m is the Michaelis constant, representing the concentration at which uptake is half of V_{max} [ML^{-3}], L is the root length density, representing the total root length per unit volume of soil [L^{-2}] (Barber, 1984).

This model effectively links plant physiology with soil nutrient dynamics, enabling the simulation of nutrient uptake efficiency as influenced by root branching architecture and spatial nutrient heterogeneity. By explicitly incorporating root length density, the formulation allows for dynamic analyses of how different root geometries impact overall nutrient absorption, particularly under varying soil fertility conditions.

1.9 Solute Transport Modelling and Its Impact on Crop Yield

This chapter utilizes the HYDRUS-1D model to simulate the movement of nutrients and pollutants in the soil and to assess their impact on crop productivity. The transport of solutes, whether essential nutrients like nitrates or harmful pollutants, is governed by the one-dimensional advection-dispersion equation:

$$\frac{\partial (C_T \theta)}{\partial t} = \frac{\partial}{\partial z}\left(D\frac{\partial C}{\partial z} - qC\right) + S \tag{1.42}$$

where C_T is the total solute concentration in the soil solution [ML^{-3}], θ is the volumetric water content [L^3L^{-3}], D is the dispersion coefficient [L^2T^{-1}], q is the Darcy water flux [LT^{-1}], S is the source or sink term, accounting for processes such as root nutrient uptake, decay, or chemical transformations [$ML^{-3}T^{-1}$], t is time [T], z is the vertical spatial coordinate [L].

This formulation enables the modeling of both diffusive spreading and advective transport of solutes under transient flow conditions. The HYDRUS-1D model solves this equation numerically, accommodating spatial and temporal variations in soil properties, water content, and fluxes.

Through simulation of different fertilizer application strategies and pollutant loading scenarios, the model helps quantify their effects on the solute concentration profile within the root zone. This, in turn, provides insights into how nutrient availability or contaminant accumulation influences crop yield. The model thus serves as a valuable tool for designing sustainable nutrient management plans and mitigating risks associated with soil and water pollution.

1.10 Stochastic Modeling of Nutrient Transport and Crop Yield

This study uses stochastic modeling to represent the natural variability of soils, weather, and plant processes in nutrient transport and crop yield prediction. Unlike Deterministic models, which assume these conditions are fixed, making them less able to capture the real variability found in the field, the stochastic approach introduces randomness through a stochastic differential equation,

At a single point, changes in nutrient concentration C(t) can be described using a stochastic differential equation (SDE):

$$dC = f(C,t)\,dt + g(C,t)\,dW_t \tag{1.43}$$

where $f(C,t)$ is the average change in nutrient concentration, $g(C,t)$ shows the strength of random fluctuations (diffusion), and dW_t represents small random environmental changes, such as irregular rainfall or temperature shifts (Hening et al., 2023). For nutrient movement in the soil profile, the advection–dispersion equation (ADE) can be extended with stochastic terms to include variability:

$$\frac{\partial(\theta C)}{\partial t} = \frac{\partial}{\partial z}\left(\theta D\,\frac{\partial C}{\partial z}\right) - \frac{\partial(qC)}{\partial z} - S(z,t) - k\,\theta C + \xi(z,t), \tag{1.44}$$

where $\xi(z,t)$ is a random source term representing unpredictable soil or environmental changes. Here, soil and plant parameters are not treated as fixed numbers, but as random variables that can vary from place to place.

Crop yield Y can then be linked to soil water and nutrient availability using a response function:

$$Y = \mathcal{F}(\{C(z,t)\}, \{\psi(z,t)\}, \boldsymbol{x}) + \varepsilon, \tag{1.45}$$

where $\mathcal{F}(\cdot)$ is the crop response, x represents management choices (e.g., irrigation and fertilizer timing), and ε accounts for unexplained variation. Instead of one fixed yield estimate, the model produces averages, variances, and probabilities of yield loss or environmental risk (such as nitrate leaching). This framework allows yield outcomes to be assessed not just by single predictions, but by probability distributions and risk measures, supporting more robust water–nutrient management in variable environments such as the semi-arid soils of Jaipur.

1.11 Numerical Techniques in Solute Transport

Numerical methods are essential tools in the study of solute transport in soils, particularly when analytical solutions to governing partial differential equations are not feasible due to the complexity of soil properties, boundary conditions, or transport mechanisms. Among the widely used numerical techniques, the Finite Difference Method (FDM) and the Finite Element Method (FEM) are prominent for their adaptability and effectiveness in modeling advection-dispersion-reaction processes.

Finite Difference Method (FDM)

The Finite Difference Method is a classical numerical approach that approximates derivatives in the governing equations by differences over a discretized grid in space and time. It is computationally efficient and well-suited for regular domains, making it widely used in simulating solute transport through the advection-dispersion equation. However, it requires careful attention to stability and convergence conditions.

Finite Element Method (FEM)

The Finite Element Method offers greater flexibility in handling complex geometries, heterogeneous soil properties, and boundary conditions. It is based on transforming the governing equations into their weak forms and solving them over finite elements using basis functions. FEM enables local mesh refinement and is particularly effective in capturing detailed spatial variations, making it a robust tool for coupled water flow and solute transport modeling in soils.

The chapter also highlights the use of widely adopted computational tools, including HYDRUS and MATLAB, to facilitate model development and simulation.

1.12 Introduction to HYDRUS and MATLAB

In this study, HYDRUS and MATLAB are employed as key numerical tools for simulating water and solute transport in soil systems. HYDRUS is a specialized software package designed for modeling variably saturated water flow and solute movement based on the Richards and advection–dispersion equations. Its built-in modules allow simulation of root water uptake, nutrient transport, and chemical reactions under diverse soil conditions. In parallel, MATLAB provides a flexible programming environment for implementing custom numerical algorithms, performing sensitivity analyses, and visualizing results. Together, these platforms enable robust modeling, validation, and analysis of transient flow and transport processes essential for evaluating the impact of nutrient and pollutant dynamics on crop yields.

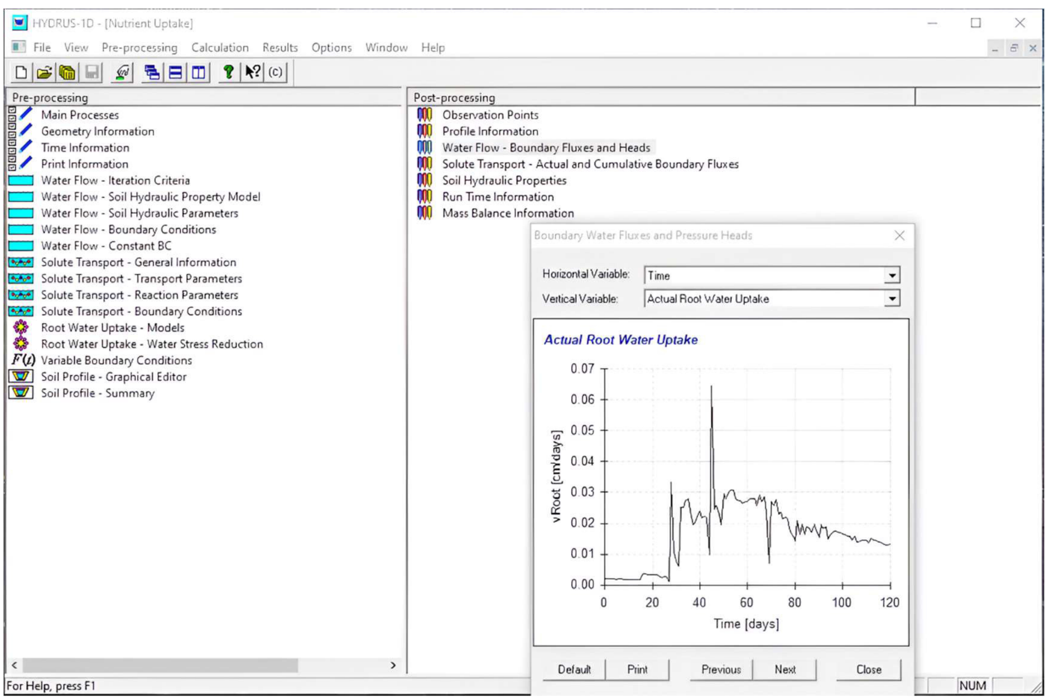

Figure 1.2 Interface of HYDRUS-1D showing main workspace for soil water and solute transport simulation.

1.13 Scope of the Study

Agricultural and Environmental Overview of Jaipur District

Jaipur, also known as the Pink City, is a prominent district in the state of Rajasthan, India. It spans a total geographical area of 11,06,148 hectares and features diverse agro-climatic and soil conditions. The district is situated in the semi-arid Eastern Plain Zone (Zone III-A), characterized by mild winters and hot summers, with temperatures ranging from 1°C in winter to 47°C during peak summer months. The average annual temperature is 24.3°C (Krishi Vigyan Kendra Jaipur-I).

The district experiences scanty and scattered rainfall, with an average precipitation of 564 mm per annum, which has decreased over the past five years. Jaipur is home to 3,088 villages and sustains a population of approximately 3.88 million people, with agriculture as a significant contributor to its economy.

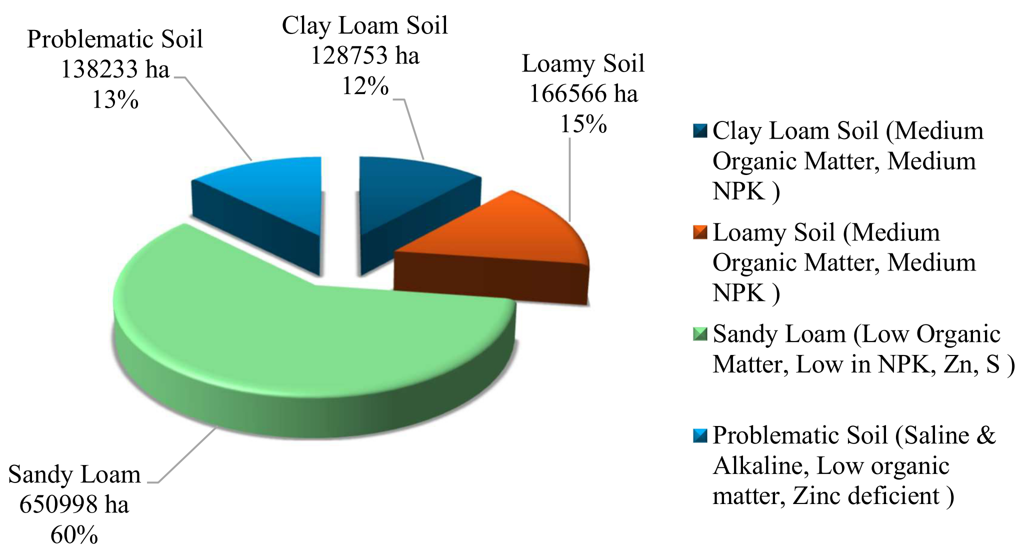

Figure 1.3 Area of Soil Types in Jaipur Region (in hectares). *(Source: Krishi Vigyan Kendra Jaipur-I. District profile. https://jaipur1.kvk2.in/district-profile.php)*

Jaipur's soils are diverse, including sandy loam, loamy, clay loam, and problematic saline-alkaline soils, which influence the district's agricultural practices and cropping patterns. The district supports a variety of crops such as pearl millet, sorghum, wheat, mustard, barley, and vegetables like tomatoes, peas, and brinjals. Horticulture, focusing on fruits like ber, amla, and guava, also holds significant potential in the region.

Table 1.3 Soil Types in Jaipur Region

Soil Type	Regions	Characteristics	Area (ha)
Sandy Loam Soil	Amer, Govindgarh, Kotputli, Jhotwara	Low Organic Matter, Low in NPK, Zn, S; Supports bajra, groundnut, mustard	650998
Loamy Soil	Kalwad, Shahpura, Virat Nagar	Medium Organic Matter, Medium NPK; Good water retention; Suitable for vegetables, barley, wheat	166566
Clay Loam Soil	Phagi, Chaksu, Dudu	Medium Organic Matter, Medium NPK, Higher water retention; Suitable for gram, mustard, barley	128753
Problematic Soils	Sambhar Lake, Dudu, Phagi, Bassi	Saline & Alkaline, Low organic matter, Zinc deficient; Low fertility; Requires reclamation or special irrigation methods	138233

Source: Krishi Vigyan Kendra Jaipur-I. District profile. https://jaipur1.kvk2.in/district-profile.php

The district is divided into four Agro-Ecological Situations (AES) based on topography, soil type, and water availability. These zones influence agricultural productivity and sustainability, highlighting Jaipur's challenges in addressing water scarcity, salinity, and soil health.

Table 1.4 Agro-Ecological Situations in Jaipur

AES Zone	Regions Covered	Characteristics
AES-I	Amer, Jhotwara, Govindgarh	Irrigated light sandy soils; plain topography; erratic rainfall
AES-II	Sanganer, Bassi, Jamwa Ramgarh	Plain to partially hilly; medium to deep soils; saline to alkaline water
AES-III	Shahpura, Kotputli, Virat Nagar	Plain topography; medium to deep soils; irregular and erratic rainfall
AES-IV	Dudu, Chaksu, Sambhar Lake, Phagi	Low rainfall; saline-alkaline soils; drought-prone; poor groundwater

Source: Krishi Vigyan Kendra Jaipur-I. District profile. https://jaipur1.kvk2.in/district-profile.php

Geographical Focus on Jaipur, Rajasthan

The study focuses on the geographical area of Jaipur, located in the state of Rajasthan, India. Jaipur is characterized by a semi-arid climate with seasonal variations in temperature and precipitation, making it an ideal location for studying solute transport dynamics in agricultural soils under different environmental conditions (Singh & Kumar, 2020). The region's diverse soil types, ranging from sandy loam to clay, provide a suitable basis for examining the variability in solute behavior across different soil textures and compositions (Gupta et al., 2015). Moreover, the focus on Jaipur is significant as agriculture is a major livelihood activity in this area, and understanding solute transport is crucial for improving local crop management practices and enhancing agricultural sustainability.

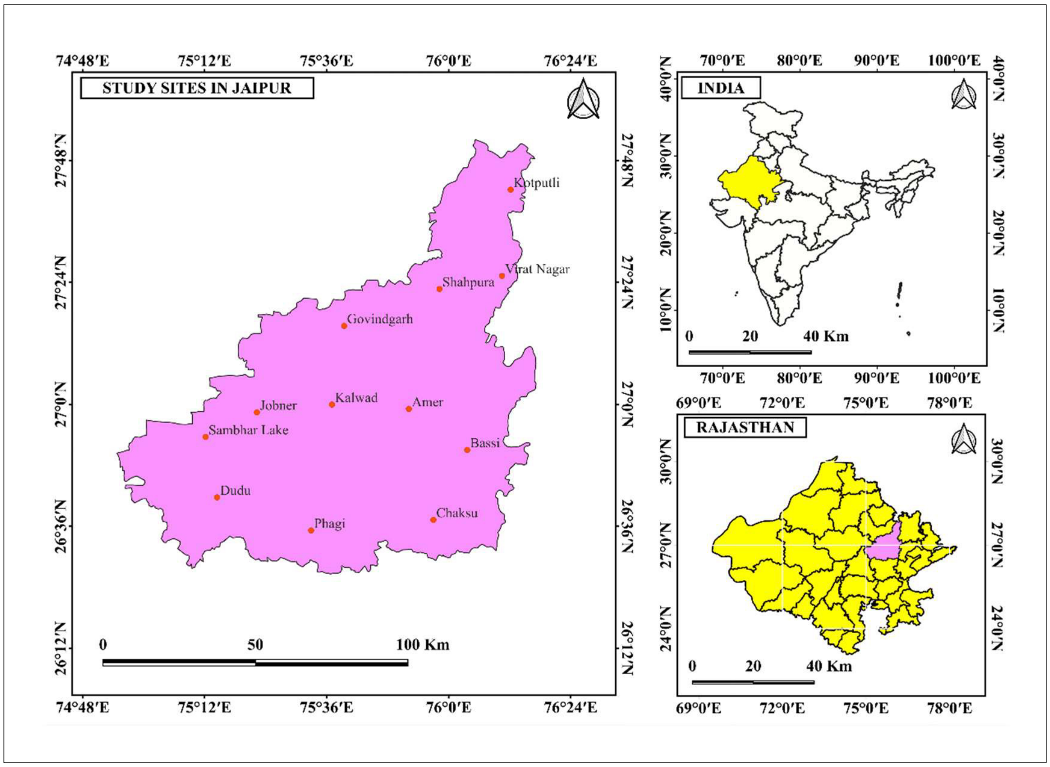

Figure 1.4 Study Area Map

Target Crops and Soil Types

The study targets major crops grown in Jaipur, including wheat, mustard, and pearl millet, which are staple crops for the region and significantly contribute to the local economy (Kumar & Sharma, 2018). These crops were selected based on their varying nutrient requirements and growth conditions, allowing for an assessment of how solute transport affects different agricultural systems. The study also considers various soil types prevalent in the region, such as sandy loam, alluvial, and black soils, to evaluate how soil texture and structure influence solute movement and nutrient availability (Sammauria et al., 2019).

Limitations and Constraints of the Study

This study has a few apparent limitations and constraints. The changing climate, especially unpredictable rainfall and temperature swings, can influence how well the models predict solute movement. Field data were not always easy to collect—some sites were difficult to access, and detailed soil and crop information was sometimes limited (Kaushik & Baghel, 2023). This study also focuses on only major nutrients like nitrogen and phosphorus. Even so, the study offers valuable insights into solute transport dynamics and their effects on crop yields and contributes to the development of sustainable agricultural practices.

1.14 Structure of the Thesis

This thesis is organized into seven interconnected chapters, each contributing to a comprehensive understanding of solute transport processes and their effects on crop yields. The progression of chapters reflects a logical flow from foundational concepts to advanced modeling approaches and practical implications.

Chapter 1: Introduction

This chapter outlines the motivation and significance of the study, emphasizing the role of solute transport in agricultural productivity. It presents the research objectives, key questions, scope of the study, and a brief overview of the methodology, thereby setting the stage for the chapters that follow.

Chapter 2: Literature Review

A detailed review of existing research is presented in this chapter, covering solute and nutrient transport in soils, root uptake processes, crop growth modeling, and hydrological modeling approaches. This review identifies critical knowledge gaps and justifies the need for the mathematical models developed in the subsequent chapters.

Chapter 3: Models for Water Flow in Soil and Its Uptake in Plants under Transient Flow Conditions

This chapter develops the mathematical framework for modeling water flow in unsaturated soil under transient conditions using Richards' equation. It also incorporates root water uptake models to simulate plant-water interactions. These foundational models serve as a basis for understanding nutrient transport and uptake.

Chapter 4: Mathematical Model for Nutrient Uptake in Plants with Multiple Root Branching Structures

Building on the water flow models, this chapter introduces a nutrient uptake model based on Michaelis–Menten kinetics, adapted for complex root architectures. It investigates how variations in root length density and soil nutrient concentration influence nutrient absorption, with implications for optimizing plant growth.

Chapter 5: Model for Nutrient/Pollutant Load and Its Impact on Crop Yield

This chapter applies the advection–dispersion equation to simulate the transport of nutrients and pollutants in the soil. The model evaluates the effects of different nutrient application rates and pollutant loads on soil solute profiles and crop yield outcomes, offering insights into sustainable land and fertilizer management.

Chapter 6: Stochastic Modeling of Solute Transport and Crop Yield Variability

To account for environmental variability and uncertainty, this chapter introduces a stochastic modeling approach using stochastic differential equations and Monte Carlo simulations. It integrates soil heterogeneity, climatic fluctuations, and random nutrient dynamics to assess their influence on yield variability.

Chapter 7: Conclusion and Future Directions

The concluding chapter synthesizes the key findings, highlighting the contributions of the developed models to understanding soil–plant interactions and solute transport. It discusses the practical implications for agricultural management and offers recommendations for future research in precision agriculture and environmental modeling.

Explanation of the Interrelationships Between Chapters

The chapters in this thesis are structured in a logical sequence, where each chapter is built upon the models and concepts developed in the preceding ones. Chapter 1 sets the foundation by establishing the research focus, objectives, and scope, while Chapter 2 grounds the study in existing literature. Chapters 3 and 4 provide the theoretical and mathematical basis for understanding water and nutrient dynamics, which are essential for developing the models presented in later chapters. Chapter 5 builds directly on the models and theories developed in Chapters 3 and 4, applying them to analyze the impact of nutrient and pollutant loads on crop yields. Chapter 6 then integrates these models with stochastic elements to account for variability, offering a more realistic and comprehensive understanding of solute transport and its effects. The insights gained from these chapters are synthesized in Chapter 7, which ties the thesis together by highlighting the overall contributions of the research and proposing practical applications and future directions. This interconnected structure ensures a cohesive flow of ideas and methodologies, progressively developing a comprehensive understanding of solute transport and its implications for crop yields.

1.15 Conclusion

This chapter introduced the fundamental concepts and importance of solute transport in agriculture, setting the context for the study. It outlined the objectives of the thesis, which include developing comprehensive mathematical models for solute transport, analyzing the impact of nutrient and pollutant loads on crop yields, and assessing the implications for agricultural sustainability. Additionally, the chapter presented the research questions guiding the investigation, defined the geographical scope, and identified the target crops and soil types, alongside the limitations and constraints of the study.

The structure of the thesis was also detailed, illustrating how each chapter builds upon the preceding ones to develop a cohesive understanding of solute dynamics and crop yield variability. This foundation is essential for understanding the complexities involved in solute transport and its effects on agricultural productivity.

As we transition to Chapter 2, the focus will shift to reviewing the existing body of literature on solute transport, soil dynamics, and crop modeling. This review will provide the theoretical and empirical background necessary to identify knowledge gaps and further refine the models developed in subsequent chapters. The literature review will also contextualize the current research within broader agricultural and environmental studies, highlighting the relevance and significance of this thesis.

Chapter 2

Literature Review

Chapter 2

Literature Review

2.1 Introduction

Transport of solutes in soil, such as water movement, movement of nutrients, root uptake, and migration of pollutants, lies at the heart of crop productivity and environmental integrity (Skaggs et al., n.d.). As modern agriculture faces the dual challenge of increasing food production and conserving natural resources, the need for robust mathematical models that accurately simulate these processes has grown substantially. These models are now necessary for modeling the intricate, dynamic processes that control solute behavior of the soil–plant–atmosphere continuum (Groenveld et al., 2021; Agah et al., 2017).

This chapter provides a comprehensive review of scientific literature related to the mathematical modeling of solute transport and its effects on crop yields. This chapter reviews foundational and cutting-edge literature in five interrelated domains that are central to the thesis: unsaturated water flow in soil, root water uptake, nutrient transport, pollutant and nutrient load impacts on crop yield, and stochastic modeling techniques to represent environmental variability and uncertainty. The review integrates findings from global studies as well as region-specific research in Jaipur and the semi-arid zones of Rajasthan, thereby providing both a broad and locally contextualized perspective.

The purpose of this chapter is to establish the theoretical and empirical foundation for the mathematical models developed in the subsequent chapters. It critically examines existing research to identify key limitations and gaps in the current understanding of solute transport processes and their impact on crop yields. The discussion in this chapter therefore serves as a bridge between past research and the modeling efforts presented in Chapters 3 to 6, where water flow, nutrient uptake, and crop response are analyzed in an interconnected manner. The findings from these models ultimately contribute to a deeper understanding of solute transport and its effects on crop productivity, providing a scientific basis for improved soil and water management strategies in semi-arid regions of Rajasthan and similar environments worldwide.

2.2 Water Flow in Unsaturated Soils

The movement of water through unsaturated soils is a critical process governing the transport and availability of nutrients, salts, and other solutes within the root zone. This movement influences plant growth, solute leaching, and pollutant dispersion, making it a central component of any agro-environmental modeling effort (Reyna et al., 2019). The mathematical description of unsaturated water flow is most commonly based on Richards' equation, which combines Darcy's law for flow through porous media with the continuity equation for mass conservation (Richards, 1941). This equation has become the foundational model for simulating water dynamics in variably saturated soils.

Richards' equation is a highly nonlinear partial differential equation due to the dependence of water content (θ) and hydraulic conductivity (K) on pressure head (h). The soil-specific functions $\theta(h)$ and $K(h)$ are typically described using the van Genuchten–Mualem model (van Genuchten, 1980; Mualem, 1976), which provides parametric relationships for unsaturated hydraulic properties. The accuracy of simulations, however, relies heavily on the correct estimation of these parameters, which are influenced by soil texture, structure, and organic matter content.

To solve Richard's equation under different boundary conditions—such as infiltration, evaporation, irrigation, and transpiration — various numerical methods have been employed. These include the finite difference method (FDM), finite element method (FEM). Such methods facilitate the numerical approximation of spatial and temporal water flow across heterogeneous soil profiles (Dam & Feddes, 2000; Timsina et al., 2021).

A few modeling tools and software packages have been developed to implement these methods. Notable among them are HYDRUS-1D/2D/3D (Šimůnek et al., 2024), SWAP (Dam et al., 2008), and MACRO (Jarvis et al., 1991). Of these, HYDRUS is particularly popular due to its flexibility in handling complex boundary conditions, soil layering, root uptake, and coupled solute transport. It has been widely used for simulating scenarios ranging from drip irrigation management to contaminant leaching in agricultural systems.

Despite advances in numerical modeling and software development, challenges remain. The scale transition problem—translating soil hydraulic parameters from laboratory-scale measurements to field-scale applications—introduces uncertainty. Additionally, soil heterogeneity in texture and structure makes parameter estimation difficult and often site-specific. Moreover, limited field validation of numerical models under dynamic natural conditions continues to hinder their generalizability and predictive reliability (Schaap & Leij, 2024; Vogel, 2019)

In the context of semi-arid regions like Jaipur, where soil water availability fluctuates sharply with rainfall and irrigation events, accurate modeling of unsaturated flow is essential. Studies in Rajasthan report significant spatiotemporal variability in soil moisture and infiltration, reinforcing the need for robust, locally calibrated unsaturated flow models (Yadav et al., 2023).

2.3 Root Water Uptake Processes

Root water uptake is a vital physiological process that governs not only plant hydration and transpiration but also influences solute redistribution, nutrient availability, and water movement in the soil profile. This process is regulated by a variety of factors, including root system architecture, soil moisture gradients, plant developmental stage, and environmental stresses such as drought and salinity. A detailed understanding and accurate modeling of root water uptake are essential for understanding crop performance and optimizing water use, particularly in water-scarce regions like semi-arid Rajasthan.

The most widely used empirical framework for modeling root water uptake is the Feddes model, which describes uptake as a function of soil matric potential and introduces stress reduction functions to represent physiological limitations in water absorption (Feddes et al., 1976). The Feddes model has been integrated into widely used numerical models like HYDRUS and SWAP, which solve Richards' equation for variably saturated flow and incorporate root uptake as a sink term (Dam et al., 2008; Šimůnek & Hopmans, 2008).

To improve upon empirical models, mechanistic root water uptake models simulate flow at the scale of individual root segments. These models incorporate radial and axial conductance, xylem water potentials, and root branching structures. For instance, Roose and Fowler (2004) proposed a mathematical model that couples root architecture with water transport based on Darcy's law, allowing 3D simulation of root-soil interactions

(Roose & Fowler, 2004). Doussan et al. (2006) extended this by modeling internal water fluxes within branched root networks under heterogeneous soil moisture conditions. These models provide a more realistic representation of water uptake dynamics and spatial variability in soil water distribution (Doussan et al., 2006).

Although there have been many advancements, most models still simplify root architecture by assuming a uniform root distribution and ignoring how roots change in response to the environment. These simplifications reduce the accuracy of simulations, especially for crops with complex and changing root systems. Collecting detailed root data in the field is also difficult, and running high-resolution models can be computationally demanding. Including realistic, branching root structures in mechanistic models remains an important research goal. Some recent models, like CRootBox and OpenSimRoot, try to address this issue, but they are not yet widely integrated with large-scale soil water flow models (Postma et al., 2017). This kind of modeling is especially important in semi-arid areas like Jaipur, where root behavior under uneven moisture conditions greatly affects water and nutrient uptake.

In the Indian context, particularly in semi-arid regions like Jaipur, understanding root uptake processes is critical due to the limited and highly variable availability of soil moisture. Studies in Rajasthan have documented that under deficit irrigation and rain-fed agriculture, root depth and architecture significantly affect crop yield responses (Choudhary et al., 2017; Soni et al., 2022). Research on wheat and mustard in Jaipur district has shown that deeper and more branched root systems are associated with greater water use efficiency and resilience under moisture stress, supporting the integration of detailed root parameters in local agro-hydrological modeling (Meena et al., 2020). Field-scale studies also highlight how local soil texture variability interacts with root distribution to influence uptake zones, reinforcing the need for location-specific calibration of root uptake models.

2.4 Nutrient Transport in Soil

The movement of nutrients through the soil profile is a fundamental process that directly affects their availability for plant uptake and their potential to contaminate groundwater. Nutrient transport occurs primarily through advection, dispersion, and diffusion. These mechanisms are mathematically described by the advection–dispersion equation (ADE), which forms the theoretical basis for simulating the fate and movement of dissolved solutes such as nitrate (NO_3^-), ammonium (NH_4^+), phosphate (PO_4^{3-}), and a wide range of agrochemicals in both saturated and unsaturated soils (Bear, 2005; Genuchten & Wagenet, 1989).

The advection term in the ADE accounts for solute movement with flowing water, while the dispersion term represents the spreading of solutes due to molecular diffusion and soil heterogeneity. This duality makes the ADE particularly effective for capturing solute dynamics under transient flow conditions, such as during irrigation or rainfall events.

Sorption–desorption processes further influence nutrient transport. These processes determine how strongly nutrients bind to soil particles, affecting their mobility and bioavailability. They are typically modeled using the Freundlich or Langmuir isotherms, which describe the equilibrium relationships between solute concentrations in soil solution and on solid phases (Sparks, 2003). Soils with higher clay content and organic matter tend to exhibit stronger sorption capacity, thereby reducing nutrient leaching but also potentially limiting nutrient availability to plants.

Leaching of nutrients, especially nitrates, is a critical concern in agricultural areas with intensive irrigation or high seasonal rainfall. Nitrate, being highly mobile, is particularly prone to leaching beyond the root zone into groundwater. This not only reduces fertilizer use efficiency but also contributes to environmental problems such as groundwater contamination and eutrophication (Addiscott & Wagenet, 1985). Modeling tools like HYDRUS-1D and HYDRUS-2D have been widely used to simulate such scenarios, enabling researchers to assess the impact of different fertilizer application strategies and irrigation regimes on nitrate leaching and solute distribution in the soil (Šimůnek et al., 2008).

In the context of semi-arid regions like Jaipur, recent studies highlight increasing nitrate concentrations in groundwater due to fertilizer overuse and inefficient irrigation practices. For instance, research conducted in Jaipur and surrounding areas shows that nitrate inventories below irrigated fields can be up to 75 times higher than those under rainfed conditions, posing a significant groundwater pollution risk (Scanlon et al., 2005). Additionally, studies in Sanganer and industrial belts of Jaipur report elevated levels of dissolved solutes, including nitrates, sulfates, and heavy metals, which further complicate the dynamics of nutrient transport in polluted soils (Shahnawaz et al., 2020).

Despite the usefulness of current models, linking solute transport to crop yield remains a major challenge. Most models focus primarily on the physical and chemical processes involved in solute movement, but do not adequately incorporate plant response functions or account for root zone uptake variability. Moreover, model accuracy is often limited by uncertainties in key parameters (e.g., hydraulic conductivity, dispersion coefficients), spatial heterogeneity, and lack of long-term field validation (Šimůnek & Hopmans, 2008). This underscores the need for integrated models that connect solute dynamics with plant growth, nutrient uptake efficiency, and yield outcomes under diverse environmental conditions.

2.5 Nutrient Uptake by Plant Roots

Nutrient uptake by plant roots is a complex and nonlinear process governed by multiple interacting factors, including root system morphology, nutrient concentration gradients in the soil, water availability, and physiological characteristics of the plant. The efficiency of this process determines nutrient use efficiency and ultimately influences crop yield and environmental sustainability.

One of the most widely applied mathematical frameworks for modeling nutrient uptake is the Michaelis–Menten model, originally adapted from enzyme kinetics. This model describes uptake as a function of external nutrient concentration and is characterized by two key parameters: the maximum uptake rate ($V_{\max}$) and the Michaelis constant (K_{m}), which defines the nutrient concentration at which uptake is half of $V_{\max}$ (Barber, 1984; Nye and Tinker, 1977). While this model effectively captures the saturation behavior of nutrient uptake, it assumes a uniform root distribution and neglects the spatial and dynamic interactions between root architecture and heterogeneous nutrient availability in the soil matrix.

To overcome these limitations, multi-compartment and spatially explicit models have been developed. These models incorporate detailed representations of root branching patterns, diffusion zones, and soil nutrient gradients. For example, Darrah (1993) introduced a diffusion–convection model that linked radial nutrient transport with root geometry. Leitner et al. (2010) further advanced this approach by coupling root growth dynamics with soil nutrient transport in a 3D domain, showing that nutrient uptake efficiency is highly sensitive to the spatial configuration of root segments and local nutrient concentration.

These mechanistic models are particularly useful for evaluating the effects of different fertilizer regimes, crop species, and soil types on nutrient use. However, their widespread adoption is limited by several factors. First, detailed root system data—such as root length density, branching angles, and radial growth rates—are rarely available, especially at field scales. Second, computational complexity increases rapidly with model resolution and spatial domain size, which poses challenges for large-scale or long-term simulations.

In the Indian context, particularly in semi-arid regions like Jaipur, accurate modeling of nutrient uptake is critical for improving fertilizer efficiency and reducing environmental losses. Studies on mustard and wheat crops in Rajasthan have demonstrated that root depth, branching density, and lateral spread significantly influence nutrient uptake under moisture-limited conditions (Meena et al., 2020; Choudhary et al., 2017). Local research highlights the importance of synchronized irrigation and nutrient application (fertigation) to enhance uptake efficiency in calcareous and sandy loam soils prevalent in the region. Furthermore, field experiments in Jaipur district have shown that nitrogen use efficiency declines sharply when root access to mobile nutrients is constrained by soil texture or uneven moisture distribution (Yadav et al., 2021).

2.6 Nutrient/Pollutant Load and Crop Yield

The productivity of crops is closely linked to the availability of essential nutrients in the soil and the presence or absence of harmful pollutants. Nutrients such as nitrogen (N), phosphorus (P), and potassium (K) are vital for plant physiological processes, and their balanced supply is necessary for achieving optimal biomass and yield. Conversely, nutrient deficiencies impair metabolic activity and limit crop performance, while excessive nutrient application can result in nutrient leaching, soil degradation, and environmental pollution (Fageria et al., 2006).

Crop yield response models aim to quantify the relationship between nutrient inputs and plant output (e.g., grain, biomass, or fruit yield). Classical models such as the Mitscherlich equation, quadratic response functions, and linear-plateau models offer empirical representations of diminishing returns with increasing fertilizer inputs. While useful for experimental interpretation and agronomic recommendations, these models do not account for the underlying biological and physical processes (Chien et al., 2009).

In contrast, mechanistic crop models such as DSSAT (Decision Support System for Agrotechnology Transfer) and AquaCrop (developed by FAO) incorporate plant physiology, water–nutrient interactions, and environmental variability to simulate crop growth and yield under varying soil and climate conditions (Jones et al., 2002; Raes et al., 2009).

Field experiments and simulation studies worldwide have demonstrated the importance of optimizing fertilizer regimes to balance yield improvement and environmental sustainability. For instance, DSSAT-based studies in sub-tropical regions have shown that site-specific nutrient management (SSNM) can increase nitrogen use efficiency by 15–30% while maintaining comparable yields (Timsina et al., 2010). However, overuse of fertilizers can lead to nitrate leaching, phosphorus runoff, and the accumulation of residual salts in the soil profile, especially in intensively irrigated or semi-arid areas.

Pollutants, including heavy metals (e.g., Cd, Pb, As), pesticides, and industrial effluents, enter the soil–plant system through anthropogenic activities such as industrial discharge, sewage irrigation, and over-application of agrochemicals. These contaminants can inhibit plant growth by interfering with nutrient uptake, enzyme activity, and photosynthesis. The extent of their effect depends on their concentration, chemical form, and bioavailability (Alloway, 2013). Long-term accumulation of these pollutants not only reduces soil fertility but also poses risks to human health through bioaccumulation in food chains.

In the Jaipur region, several studies have documented the impact of industrial pollutants on soil health and crop productivity. The Sanganer industrial zone has been identified as a hotspot for soil contamination due to untreated textile dye effluents and urban waste discharge. Elevated concentrations of nitrates, sulfates, and heavy metals have been reported in surface and sub-surface soils, negatively affecting crop yields and groundwater quality (Shahnawaz et al., 2020). Research in nearby agricultural zones shows that vegetables grown in these soils exhibit lower biomass and nutrient uptake efficiency, correlating with heavy metal accumulation in plant tissues (Sharma et al., 2006).

Despite the availability of advanced models for solute transport and crop simulation, there remains a notable disconnect between nutrient/pollutant dynamics and yield modeling. Most models simulate nutrient fate or pollutant transport in isolation, without integrating their combined effects on crop productivity. As a result, current decision-support systems for sustainable agriculture lack the capability to holistically evaluate trade-offs between input management, yield goals, and environmental risks. Developing integrated models that couple solute transport, plant uptake kinetics, and yield response under diverse pollutant and nutrient regimes remains an urgent research need.

2.7 Stochastic Modeling Approaches

Agricultural systems operate under conditions of high variability and uncertainty due to fluctuations in climate, soil properties, management practices, and plant physiological responses. These uncertainties significantly impact water availability, solute transport, nutrient uptake, and ultimately crop productivity. To capture this variability more realistically, researchers have increasingly adopted stochastic modeling approaches, which incorporate randomness and uncertainty into model parameters, forcing functions, and system responses (Henri & Harter, 2019; Vrugt et al., 2008).

A widely used tool in this context is the stochastic differential equation (SDE), which allows modeling of continuous-time systems affected by random perturbations. In agricultural hydrology, SDEs have been used to simulate soil moisture dynamics, rainfall variability, evapotranspiration, and nutrient transport under stochastic environmental conditions (Rodriguez-Iturbe et al., 1999). These models can account for the random nature of precipitation events, enabling more accurate estimation of water availability and leaching risks.

Monte Carlo simulation is another key technique that is often used to quantify uncertainty and assess risk in model predictions. This method involves generating thousands of realizations of input parameters (e.g., soil properties, crop coefficients, weather data) based on probability distributions and evaluating the distribution of output responses. It is particularly useful for probabilistic sensitivity analysis and decision-support systems in precision agriculture (Saltelli et al., 2005).

Random field modeling is also employed to represent the spatial heterogeneity of soil hydraulic properties, nutrient distributions, or contaminant concentrations. In this framework, variables such as hydraulic conductivity (K) or soil nitrate levels are treated as spatially correlated stochastic fields, typically characterized by variograms or covariance functions (Russo & Bresler, 1981). This approach is especially relevant when dealing with small-scale variability that influences large-scale solute transport, root zone processes, or irrigation performance.

Despite the progress in individual applications, the integration of stochastic processes into full-scale soil–plant–atmosphere models remain limited. Most crop models still rely on deterministic inputs and average conditions, which can underestimate risk and misrepresent field-level variability. There is a growing need for hybrid modeling frameworks that couple deterministic mechanistic models (e.g., Richards' equation for water flow, Michaelis–Menten for nutrient uptake) with stochastic modules that simulate uncertainty in inputs and boundary conditions.

In the Indian context, and particularly in semi-arid regions like Jaipur, the application of stochastic models has gained importance due to highly variable monsoonal rainfall, uneven irrigation, and heterogeneous soil profiles. Recent studies in Rajasthan have utilized stochastic models to predict groundwater recharge, rainfall–runoff relationships, and soil moisture dynamics under changing climatic regimes (Sharma et al., 2018; Singh & Jain, 2021). These efforts highlight the relevance of stochastic frameworks for improving agricultural planning and resilience in regions exposed to both climatic and anthropogenic uncertainties.

2.8 Integrating Small- and Large-Scale Models for Solute Transport and Crop Yield

Modeling how solutes (like nutrients and pollutants) move through the soil and affect crops involves many different scales—from the tiny root–soil contact zone to large farm fields. On a small scale, things like nutrient diffusion, root structure, and uptake rates control how well plants absorb nutrients. At larger scales, these local processes are affected by bigger factors like weather, irrigation, and land management (Vereecken et al., 2016; Roose & Fowler, 2004).

One major challenge is connecting models that work at different scales. Small-scale models give detailed, accurate results but are slow and need a lot of data. Large-scale models are faster and easier to use but often miss important details about how roots and soil really behave (Blöschl & Sivapalan, 1995; Tenreiro et al., 2020).

New approaches include multi-scale models that link detailed processes with larger, simpler models. For example, hybrid models combine Richards' equation (for water flow in soil) with realistic root architecture models like CRootBox or OpenSimRoot to better simulate nutrient uptake at the field level (Leitner et al., 2010; Schnepf et al., 2017).

Also, using both deterministic models (which follow fixed rules) and stochastic models (which include random variations) helps make predictions more reliable. Deterministic models explain known physical processes, while stochastic parts help handle things like uncertain rainfall or variable soil properties (Saltelli et al., 2019; Zhang et al., 2014).

This combined approach is especially useful in semi-arid areas like Jaipur, where rainfall, soil type, and irrigation availability can vary a lot. Studies from Rajasthan show that using local data on soil, climate, and farming practices makes nutrient transport models more accurate and useful (Meena et al., 2020; Singh & Jain, 2021). Still, a gap remains between small-scale measurements and large-scale farm planning. Bridging this gap is key to building better tools for sustainable agriculture.

2.9 Research Gaps and Purpose of This Thesis

Based on the earlier review, there are some important gaps in the current research that this thesis aims to address:

- **Separate treatment of key processes**: Many models handle water flow, solute movement, root uptake, and crop yield as different processes. They do not show how these are connected. This makes the models less realistic.
  (*This is handled in Chapters 3 to 6 through an integrated approach.*)
- **Simple root system models**: Many studies use basic root shapes that do not show the real structure of roots. This leads to poor predictions of how plants take in water and nutrients.
  (*Chapter 4 solves this by using detailed root branching structures.*)
- **Ignoring environmental changes**: Most models do not include random changes in weather, soil type, or farming practices. This makes them less reliable, especially in areas with changing conditions.
  (*Chapter 6 includes stochastic modeling to deal with uncertainty.*)

- **Few local models for areas like Jaipur**: There are not many models made for semi-arid places like Jaipur, where both water shortage and nutrient loss are problems.

  (*Chapters 5 and 6 use local data and conditions from Jaipur.*)

To solve these problems, this thesis presents a group of linked mathematical models that:

- Simulate water and nutrient movement in soil (Chapter 3),
- Include detailed root branching to improve uptake accuracy (Chapter 4),
- Study how nutrients and pollutants affect crop yields (Chapter 5),
- Use random simulations to show real-world uncertainty (Chapter 6).

Together, these models offer a simple and practical way to study solute movement and crop yields, especially in semi-arid farming systems like those in Jaipur.

2.10 Conclusion

This chapter reviewed important research on how water, nutrients, and pollutants move through the soil and how plants take them up. It looked at different models used around the world and in local studies from Rajasthan and Jaipur. While many useful models exist, most of them focus on only one part of the system and often ignore changes in the environment or real root structures. These gaps show the need for better models that connect all these parts.

The next chapter (Chapter 3) begins by developing a model for water flow in soil and how plants take up water under changing conditions. This model uses well-known equations like Richards' equation and helps set the base for later chapters that deal with nutrient transport and crop yield. The goal is to first understand water movement in soil before adding nutrients and pollutants in the following chapters.

Chapter 3

Model for Water Flow in Soil and Its Uptake in Plants under Transient Flow Conditions

Chapter 3

Model for Water Flow in Soil and Its Uptake in Plants under Transient Flow Conditions

3.1 Introduction

Water transport in soil plays a fundamental role in plant growth and development. Water is not only a vital component for photosynthesis and nutrient transport but also essential for maintaining cell turgor, which supports plant structure. The availability of water in the soil directly affects a plant's ability to absorb essential nutrients and sustain vital physiological processes. Efficient water uptake from the soil ensures healthy plant growth, optimal crop yield, and effective nutrient cycling in agricultural systems (Li et al., 2022).

Root water uptake is the primary mechanism by which plants absorb water from the soil. Water moves into plant roots through a gradient in water potential—water flows from areas of high-water potential in the soil to areas of lower potential inside the roots. Root systems, consisting of a network of fine root hairs and branching structures, maximize the surface area for water absorption. This process of water acquisition by plants depends on the architecture of roots, the content of soil moisture, and the capability of the plant to respond to changing water regimes (Gregory & Kirkegaard, 2016).

Perhaps the most essential feature of water flow within soil is its transient nature. Soil moisture content is not static; it varies due to outside influences such as rain, irrigation, evaporation, and water uptake from plants. These transient dynamics establish intricate processes that affect water supplies for the roots of plants with the passage of time. For example, with rain or irrigation, soil infiltrates with water and slowly redistributes across the root zone. As water gets absorbed by plants and evaporates from the soil surface, the soil dries out with less water supplied for roots. As soil dries out with time, water transfers at slower rates, and roots get under water stress, which impacts the uptake of nutrients and growth.

Changes in soil moisture over time can stress plants, especially when water is limited or unevenly distributed. To deal with this, it is important to understand and model how water moves through the soil. This helps predict plant responses to shifting moisture levels and supports smarter water management in farming. By studying the dynamic relationship between soil water flow and root uptake, farmers and researchers can develop more efficient irrigation practices and improve crop resilience under changing environmental conditions.

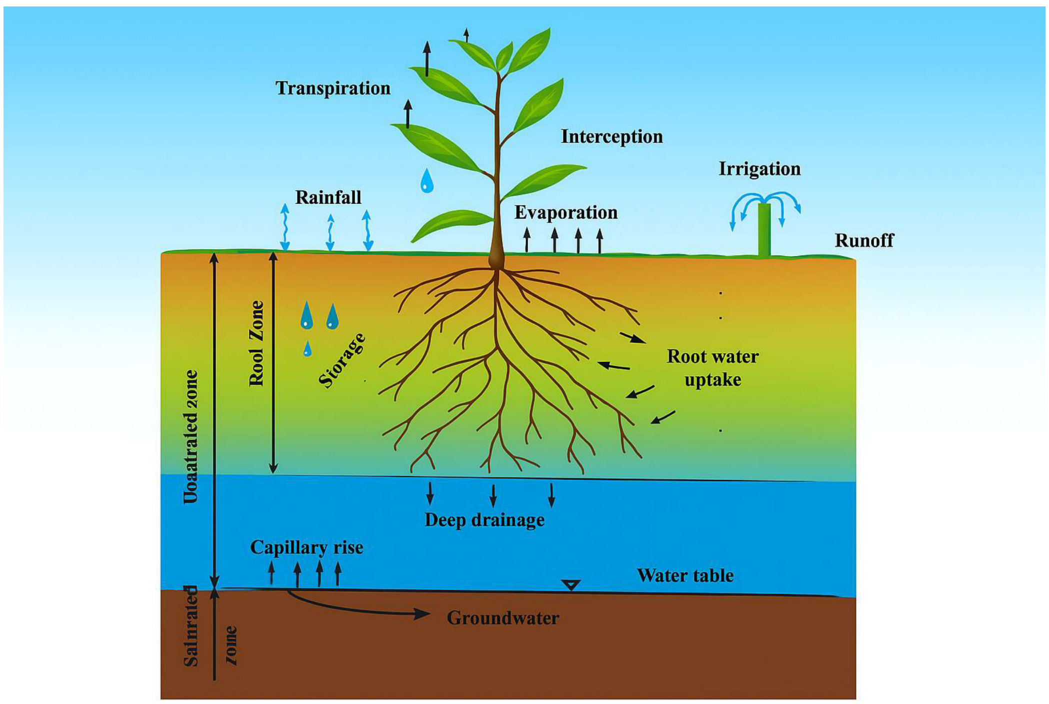

Figure 3.1 Transient Water Flow Processes in Soils (From Simunek et al., 2008)

3.2 Governing Equations for Water Flow in Soil

To understand how water moves through the soil, we need to delve into the physics of flow in porous media. The equations that govern this movement depend on whether the soil is saturated (all pores filled with water) or unsaturated (pores filled with both water and air).

3.2.1 Darcy's Equation

Darcy's Law is the foundational equation used to describe water flow in porous media, such as soil, under saturated conditions. It relates the volumetric flow rate of water through the soil to the hydraulic gradient driving the flow and the properties of the soil itself (Darcy, 1856; Hillel, 1998). For saturated flow, Darcy's law is expressed as:

$$\mathrm{q} = -K_s \cdot \frac{\partial H}{\partial z} = -K(h)\left(\frac{dh}{dz} + 1\right) \tag{3.1}$$

where q is the specific discharge or Darcy flux or water flux (m/s) - the volumetric flow rate per unit cross-sectional area of soil, K_s is the saturated hydraulic conductivity (m/s), a property that reflects the ease with which water moves through the soil when all pores are filled with water, $H = h + z$ is the total soil water potential head (hydraulic head) (m) - the sum of pressure head (h) and gravitational head (z), z is the vertical coordinate (m) (positive downward) and $\frac{\partial H}{\partial z}$ is the hydraulic gradient - the rate of change of hydraulic head with respect to distance. Darcy's Law assumes laminar flow, steady-state conditions, and fully saturated soil, enabling continuous water movement. It is widely used in groundwater flow, irrigation, and drainage system design.

3.2.2 Buckingham-Darcy Equation

The Buckingham–Darcy equation extends Darcy's Law to unsaturated soils, where pores contain both air and water, and pressure heads are negative. Unlike saturated conditions, water flow in the unsaturated zone is governed by capillary forces, soil suction, and moisture variability. Hydraulic conductivity in this zone, denoted as $K(h)$, is no longer constant but depends on pressure head or water content. Buckingham (1907) modified Darcy's equation for unsaturated flow is:

$$\mathrm{q} = -K(h)\frac{\partial H}{\partial z} = -K(h)\frac{\partial (h+z)}{\partial z} = -K(h)\left(\frac{\partial h}{\partial z} + \frac{\partial z}{\partial z}\right)$$

$$= -K(h)\left(\frac{\partial h}{\partial z} + 1\right) \tag{3.2}$$

Here, water flows under combined pressure and gravitational gradients. The capillary fringe near the water table plays a crucial role, and parameters like $K(h)$, the water retention curve $\theta(h)$, and hydraulic capacity $C_w(h)$ are strongly influenced by pore size distribution and soil texture. Flow behavior becomes especially complex at low moisture levels, where continuous water pathways may break, and vapor flow can occur.

3.2.3 Continuity equation for conservation of mass

The continuity equation represents the principle of mass conservation, stating that any change in water content within a soil volume over time must result from the balance between water inflow, outflow, and any internal sources or sinks. For vertical water movement in unsaturated soils, the equation is given by:

$$\frac{\partial \theta}{\partial t} = -\frac{\partial q}{\partial z} - S(h) \tag{3.3}$$

This equation is fundamental for modeling transient water flow and is often used in conjunction with Darcy's or Buckingham–Darcy's equations to simulate soil moisture dynamics.

3.2.4 Richards' Equation

Richards' equation, introduced by Richards (1931), is a fundamental nonlinear partial differential equation that describes water movement in unsaturated soils. It combines the Buckingham–Darcy equation for unsaturated flow with the continuity equation for mass conservation:

$$\begin{aligned} \frac{\partial \theta(h)}{\partial t} &= -\frac{\partial}{\partial z}\left[-K(h)\left(\frac{\partial h}{\partial z} + 1\right)\right] - S(h) \\ &= \frac{\partial}{\partial z}\left(K(h)\frac{\partial h}{\partial z}\right) + \frac{\partial K(h)}{\partial z} - S(h) \end{aligned} \tag{3.4}$$

This formulation shows how capillary forces (first term) and gravity (second term) drive water movement, while $S(h)$ accounts for root water uptake or other sinks. By applying the chain rule to express the water content $\theta(h)$ in terms of pressure head h, we get the pressure head formulation:

$$C_w(h)\frac{\partial h}{\partial t} = \frac{\partial}{\partial z}\left(K(h)\frac{\partial h}{\partial z}\right) + \frac{\partial K(h)}{\partial z} - S(h) \qquad (3.5)$$

Here, $C_w(h) = \frac{d\theta(h)}{dh}$ is the soil water capacity, which represents how quickly water content changes with pressure head. Richards' equation captures both capillary-driven flow and gravitational flow in the vadose zone and serves as the foundation for simulating unsaturated water transport in soils under variable boundary and initial conditions.

Richards' equation is hard to solve because it is nonlinear and depends on soil properties that change from place to place and over time. Water moves much more slowly in dry soils, and the link between water content and pressure is curved rather than straight, so special models like van Genuchten's are needed. Measuring soil properties accurately is also hard, and changing conditions such as rainfall, irrigation, and plant use make the problem even more complex. For these reasons, the equation is usually solved with computer methods like finite difference or finite element techniques, which can be slow and demanding, especially for large or layered soils.

3.2.5 Initial and Boundary Conditions

Initial Conditions

To solve Richards' equation, initial conditions must be defined using either in terms of water content

$$\theta(z,t) = \theta_i(z,0), \qquad (3.6)$$

or in terms of pressure head $h(z,t) = h_i(z,0)$ (3.7)

where θ_i and h_i are the initial values of water content and pressure head, respectively. However, it is better to use pressure head in numerical models, since it directly controls water movement. Using water content may lead to unrealistic pressure gradients and water flow, especially across different soil types, due to the non-linear nature of soil water retention curves.

Assumptions and Boundary Conditions

In modeling water flow and plant uptake in soil, certain assumptions and boundary conditions are used to simplify the system and reflect realistic field conditions. Common assumptions include treating the soil as uniform (homogeneous and isotropic), ignoring changes in soil structure (like swelling or shrinking), and neglecting air movement, focusing only on water. The system is modeled as continuous media, allowing the use of differential equations. Flow can be assumed steady or transient, depending on the situation. Boundary conditions define how water enters or leaves the soil system. They are divided into:

System-Independent Boundary Conditions

System-independent boundary conditions refer to conditions where the boundary values (such as pressure head, water content, water flux, or gradient) don't depend on soil behavior.

1. *Dirichlet Boundary Condition (Type-1)*: Specifies the pressure head at the boundary and used at water tables, lakes, or where water levels are fixed.

$$h(z,t) = h_0(z,t) \tag{3.8}$$

2. *Neumann Boundary Condition (Type-2):* Specifies the water flux across the boundary and used when a constant flux (e.g., irrigation or drainage) is applied. This is not suitable for dynamic scenarios like rainfall that exceeds infiltration, leading to ponding.

$$-K(h)\left(\frac{\partial h}{\partial z} + 1\right) = q_o(z,t) \tag{3.9}$$

3. *Gradient Boundary Condition:* Specifies the total hydraulic gradient, often used for free drainage at the bottom of a soil profile.

$$\frac{\partial h}{\partial z} + 1 = g_o(z,t) \tag{3.10}$$

System-Dependent Boundary Conditions

System-dependent boundary conditions are those where boundary values such as pressure head, water content, or flux are not fixed but are determined by the soil's current moisture condition during simulation. These are common at natural boundaries like the soil–atmosphere interface, where actual water flux depends both on external climatic inputs (e.g., precipitation, evaporation) and internal soil properties (e.g., moisture availability).

For example, when precipitation exceeds the soil's infiltration capacity, ponding occurs, and the infiltration rate is controlled by the soil, not the rainfall rate. Similarly, if evaporation demand is greater than what the soil can supply, the actual evaporation rate drops. To handle these dynamic conditions, Neuman et al. (1974) proposed the following limits:

$$K(h)\left(\frac{\partial h}{\partial z}+1\right) \leq E \quad and \quad h_A \leq h \leq h_S \tag{3.11}$$

where E is the potential infiltration or evaporation rate, h is the pressure head at the soil surface, h_A is the minimum allowable pressure head (related to vapor equilibrium), h_S is the maximum allowable pressure head, often set to zero to trigger runoff, or adjusted based on water accumulation during excess irrigation or rainfall.

If h reaches either limit, the model switches to a Dirichlet boundary (fixed pressure head) to compute the actual flux. Feddes et al. (1974) provided methods to estimate E and h_A based on weather and soil data.

Another system-dependent case is the seepage face, where water leaves the domain only if the pressure head becomes positive:

$$q_0(z,t) = 0 \quad \text{for} \quad h(z,t) < 0, \quad h(z,t) = 0 \quad \text{for} \quad h(z,t) \geq 0 \tag{3.12}$$

Table 3.1 summarizes typical boundary conditions used in soil–water models. At the soil surface, water can enter through rainfall or irrigation, which is usually described as a flux (Neumann condition). If too much water causes ponding, the surface is treated as saturated using a pressure head (Dirichlet condition). Water can also leave the soil surface through evaporation, represented as a negative flux, or through surface runoff when rainfall exceeds infiltration capacity.

At the bottom boundary, different conditions are used depending on the situation. Free drainage assumes water moves out of the soil freely under gravity. If a water table is present, the pressure head is fixed to represent a constant saturated zone. In contrast, if there is an impermeable layer such as bedrock or dense clay, a zero-flux condition is applied to prevent downward water movement.

Table 3.1 Common Boundary Conditions for Soil–Water Models.

Boundary Location	Process / Scenario	Boundary Condition Type	Mathematical Expression
Soil Surface	Rainfall / Irrigation Input	Neumann (Flux)	$-K(h)\left(\frac{\partial h}{\partial z}+1\right)=q_0(t)$
	Ponding (excess rainfall)	Dirichlet (Pressure Head)	$h(z,t)=h_0$
	Evaporation	Neumann (Negative Flux)	$-K(h)\left(\frac{\partial h}{\partial z}+1\right)=-E(t)$
	Surface Runoff	Limited Flux (conditional)	$K(h)\left(\frac{\partial h}{\partial z}+1\right)\leq P(t)$
Bottom Boundary	Free Drainage	Neumann (Zero Flux Gradient)	$\frac{\partial h}{\partial z}+1=0$
	Water Table Present	Dirichlet (Fixed Pressure Head)	$h(z,t) = 0$
	Impermeable Layer	Neumann (Zero Flux)	$-K(h)\left(\frac{\partial h}{\partial z}+1\right)=0$

3.3 Soil Water Retention Curve (SWRC)

The SWRC, also known as the soil moisture characteristic curve, illustrates the relationship between volumetric water content (θ) and matric potential (h), which reflects the suction force by which soil holds water. Matric potential is negative in unsaturated soils and becomes more negative as the soil dries. The SWRC typically has a nonlinear shape and can be divided into three key regions (Jury & Horton, 2004):

- Air-Entry Region: Near saturation, water content remains nearly constant until a threshold tension —called the air-entry value (h_a)—is reached. Beyond this point, air enters the largest pores.

- Capillary Region: As tension increases, water is progressively removed from smaller pores. The slope of this section indicates the soil's pore-size distribution. Intact soil cores are essential here for accurate results.
- Adsorption Region: At very negative pressures, water exists as thin films bound to soil particles, especially in clays. Water in this zone is generally unavailable to plants.

Key Parameters of SWRC

1. θ_s (Saturated Water Content): Maximum water held at zero matric potential.
2. θ_{fc} (Field Capacity): Water content after gravitational drainage (~ -10 to -33 kPa).
3. θ_{wp} (Permanent Wilting Point): Water content at which plants can no longer extract water (~ -1500 kPa).
4. θ_r (Residual Water Content): Water bound too tightly to soil particles to be plant available.

Table 3.2 Default initial estimates of selected parameters in models for unsaturated hydraulic functions [after Carsel and Parrish, 1988]

Soil Texture	$\theta_r(cm^3/cm^3)$	$\theta_s(cm^3/cm^3)$	$\alpha\ (cm^{-1})$	n	K_s
Sand	0.045	0.43	0.145	2.68	712.80
Loamy sand	0.057	0.41	0.124	2.28	350.16
Sandy loam	0.065	0.41	0.075	1.89	106.08
Loam	0.078	0.43	0.036	1.56	24.96
Silt	0.034	0.46	0.016	1.37	6.00
Silt loam	0.067	0.45	0.02	1.41	10.80
Sandy clay loam	0.1	0.39	0.059	1.48	31.44
Clay loam	0.095	0.41	0.019	1.31	6.24
Silty clay loam	0.089	0.43	0.01	1.23	1.68
Sandy clay	0.1	0.38	0.027	1.23	2.88
Silty clay	0.07	0.36	0.005	1.09	0.48
Clay	0.068	0.38	0.008	1.09	4.80

Plant Available Water (PAW)

It is the amount of water in the soil that can be extracted by plant roots, existing between field capacity $(\theta_{fc})$and wilting point (θ_{wp}). This range represents the water that is easily accessible to plants for uptake, not too tightly bound by soil particles nor too loosely held to be lost by drainage:

$$PAW = \theta_{fc} - \theta_{wp} \tag{3.13}$$

This value is critical for irrigation planning, crop health management, and assessing drought resilience.

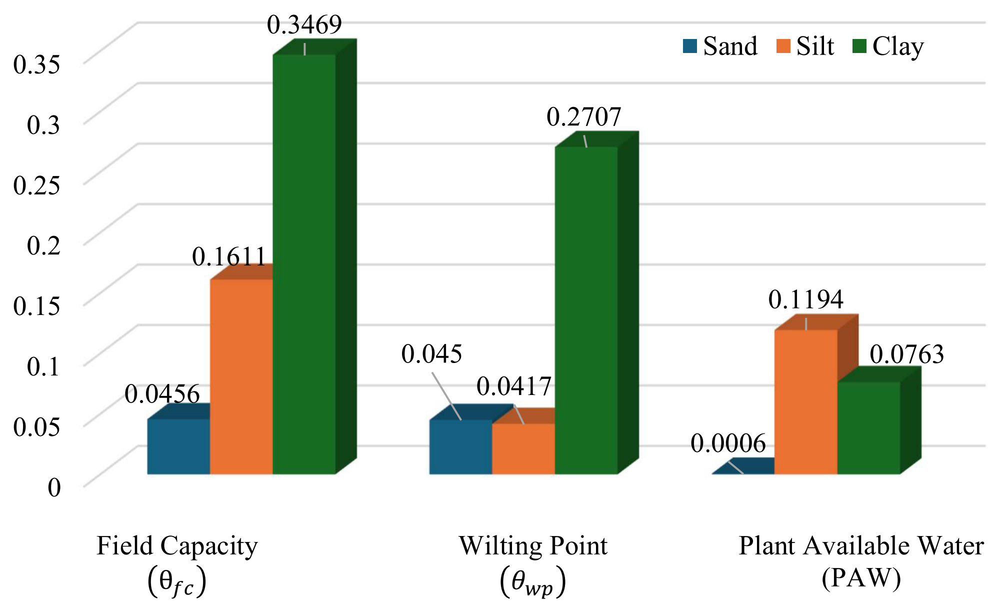

Figure 3.2 Plant-Available Water (cm^3cm^{-3}) for typical soil types: sand, silt, and clay

Factors Influencing SWRC Shape

The shape of the Soil Water Retention Curve (SWRC) is influenced by several factors. Soil texture plays a major role—sandy soils, with large pores, drain quickly and lose water at low tensions, while clayey soils retain water longer due to finer pores. Soil structure enhances water retention when well-aggregated, increasing porosity and improving water availability in the mid-range. Organic matter contributes to higher retention, especially in the capillary region, because of its ability to hold water. In contrast, compaction decreases macroporosity, steepens the initial slope of the curve, and reduces the soil's overall capacity to retain water.

Models for Describing the Soil Water Retention Curve

To accurately simulate water movement in unsaturated soils, smooth mathematical models are used to represent the nonlinear relationship between soil water content (θ) and pressure head (h). Rather than fitting the curve through every data point, these models aim to capture the overall trend, reducing the influence of experimental errors and enabling stable solutions in numerical simulations. Two widely used models are the van Genuchten model and the Brooks–Corey model.

1. van Genuchten Model:

The van Genuchten model (1980) is an empirical model that describes the soil water retention curve using flexible fitting parameters. It is expressed as:

$$\theta(h) = \theta_r + \frac{\theta_s - \theta_r}{[1 + (-\alpha h)^n]^m}, \quad \text{where } m = 1 - \frac{1}{n} \tag{3.14}$$

Here, θ_s and θ_r are the saturated and residual water contents, respectively, while α, n, and m are fitting parameters controlling the curve shape. The van Genuchten model produces a smooth, continuous curve suitable for a wide range of soil types and is commonly used in numerical hydrological models. However, it does not explicitly represent the air-entry point, which may limit its accuracy in coarse-textured soils.

2. Brooks-Corey Model

The Brooks–Corey model (1964) provides a piecewise description of the SWRC, distinguishing between the saturated and unsaturated regions. It defines effective saturation (S_e) as:

For the Air-Entry Region (Saturated Zone):

$$S_e(h) = \frac{\theta - \theta_r}{\theta_s - \theta_r} = 1, 0 > h > h_a \tag{3.15}$$

For the Unsaturated Region (Beyond Air Entry):

$$S_e(h) = \frac{\theta - \theta_r}{\theta_s - \theta_r} = \left(\frac{h_a}{h}\right)^{\lambda}, h < h_a \tag{3.16}$$

Here, h_a is the air-entry pressure head and λ is the pore size distribution index. This model is particularly effective for sandy soils, where the air-entry point is pronounced, and offers simplicity and computational efficiency. However, it may be less accurate for fine-textured soil due to its discontinuous shape at air entry and limited ability to describe gradual water release at low moisture contents.

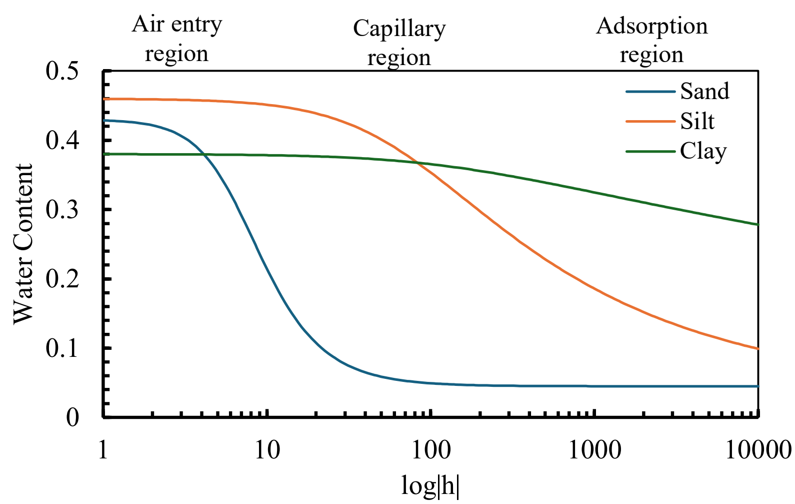

Figure 3.3 Soil moisture characteristic curves for typical soil types: sand, silt, and clay

3.4 Hydraulic Conductivity Function

Hydraulic conductivity describes how easily water moves through soil. It is influenced by the soil's water content and matric potential, especially under unsaturated conditions.

Saturated Hydraulic Conductivity (K_s):

When the soil is fully saturated, saturated hydraulic conductivity (K_s) represents the maximum rate of water flow, as all pores are filled with water.

Unsaturated Hydraulic Conductivity $K(\theta)$:

As the soil dries, unsaturated hydraulic conductivity ($K(\theta)$ decreases significantly because water is held in smaller pores by capillary forces, and the larger pores, which typically allow easier flow, become air-filled. This relationship between water content and conductivity is highly nonlinear and is a key factor in modeling water movement through unsaturated soils.

Models for Representing the Hydraulic Conductivity Function

Accurately modeling unsaturated water flow in soils requires reliable estimates of hydraulic conductivity, which varies with soil water content or pressure head. Several models have been developed to describe the hydraulic conductivity function, enabling better prediction of water movement through soils under changing moisture conditions.

1. Gardner Model (1958): This is a simple exponential model where hydraulic conductivity decreases with increasing suction:

$$K(h) = K_S\, e^{\alpha h} \tag{3.17}$$

where K_s is the saturated hydraulic conductivity and α is the soil-dependent parameter. This model is useful for coarse soils and highlights rapid declines in conductivity as suction increases.

2. Campbell Model (1974): Based on a power-law relationship, it expresses conductivity as a function of volumetric water content:

$$K(\theta) = K_S \left(\frac{\theta}{\theta_S}\right)^m \tag{3.18}$$

where m is a fitting parameter.

3. Haverkamp Model (1977): This model introduces a rational function of pressure head:

$$K(h) = \frac{K_S}{1 + \left(\frac{h}{a}\right)^N} \tag{3.19}$$

where a and N are fitting parameters.

4. Burdine Model (1953): This model is derived from capillary theory and pore-size distribution:

$$K(S_e) = K_S\, S_e^l \frac{\int_0^{S_e} \frac{dS_e}{h^2(S_e)}}{\int_0^1 \frac{dS_e}{h^2(S_e)}} \tag{3.20}$$

where K_S is the saturated hydraulic conductivity, l is a fitting parameter (typically between 0.5 and 2), known as the pore connectivity parameter, which describes the tortuosity of the flow paths, S_e is effective saturation, and $h(S_e)$ is the water retention curve relationship.

5. Mualem Model (1976): Extending Burdine's approach, Mualem modeled soil as capillaries in series:

$$K(S_e) = K_S\, S_e^l \frac{\left[\int_0^{S_e} \frac{dS_e}{h(S_e)}\right]^2}{\left[\int_0^1 \frac{dS_e}{h(S_e)}\right]^2} \tag{3.21}$$

It is often used in combination with the van Genuchten retention function for improved accuracy.

6. Brooks–Corey Model (1964): Used with the Burdine approach, this model incorporates a defined air-entry value:

$$K(S_e) = K_S\, S_e^{1+l+2/\lambda} \tag{3.22}$$

In the original study by Brooks and Corey in 1964, the parameter l was assumed to be 2.0.

7. van Genuchten–Mualem Model: This widely used model integrates the van Genuchten water retention function with Mualem's hydraulic conductivity theory:

$$K(S_e) = K_s S_e^l \left[1 - \left(1 - S_e^{1/m}\right)^m\right]^2 \tag{3.23}$$

where $S_e = \frac{\theta - \theta_r}{\theta_s - \theta_r}$ is the effective saturation, $m = 1 - \frac{1}{n}$ from the van Genuchten model, l is usually taken as 0.5 (Mualem, 1976)

This formulation enables the hydraulic conductivity to be directly estimated from the water retention curve, providing a smooth, continuous, and accurate representation of unsaturated conductivity. It is well-suited for numerical simulation tools like HYDRUS and is widely used in modeling flow through variably saturated soils.

Measurement and Estimation of Hydraulic Properties

Table 3.4 summarizes the main techniques used to obtain soil hydraulic properties. Laboratory methods, such as pressure plate apparatus, permeameters, and Tempe cells, provide direct measurements of soil water retention and conductivity under controlled conditions. Field methods, including tension and double-ring infiltrometers, allow in-situ determination of saturated and unsaturated conductivity. Estimation approaches, mainly pedotransfer functions (Rosetta, HYPRES, and Saxton & Rawls), use soil texture, organic matter, or regional datasets to predict hydraulic parameters when direct measurements are unavailable.

Table 3.3 Soil Hydraulic Properties Measurement & Estimation

Method Type	Technique / Model	Key Features / Use	Reference
Laboratory Method	Pressure Plate Apparatus	Measures soil water retention curve under known pressures.	Klute, A. (1986)
	Constant/Falling Head Permeameters	Measures saturated hydraulic conductivity in controlled conditions.	Klute, A. (1986)
	Tempe Cells	Measures unsaturated conductivity and retention simultaneously.	Dane & Topp (2002)
Field Method	Tension Infiltrometer	Measures unsaturated conductivity in field under tension.	Ankeny et al. (1991)
	Double-Ring Infiltrometer	Estimates saturated conductivity using infiltration rings.	Bouwer (1986)
Estimation Method	Pedotransfer Function - Rosetta	Estimates hydraulic properties using soil texture and neural networks.	Schaap et al. (2001)
	Pedotransfer Function - HYPRES	Estimates soil hydraulic parameters from European soil data.	Wösten et al. (1999)
	Pedotransfer Function - Saxton & Rawls	Estimates field capacity, wilting point, and K_s using texture and OM.	Saxton & Rawls (2006)

3.5 Root Water Uptake Models

Root water uptake models are essential tools for simulating how plants absorb water from the soil, which significantly influences soil moisture dynamics and plant growth. These models typically use a macroscopic approach, representing water uptake as a sink term $S(h)$ in Richards' equation, which governs water flow in unsaturated soils. The sink term depends on the soil water potential h, root distribution, and plant demand. The modified form of Richards' equation for unsaturated flow is expressed as:

$$\frac{\partial\theta(h)}{\partial t} = \frac{\partial}{\partial z}\left(K(h)\frac{\partial h}{\partial z}\right) + \frac{\partial K(h)}{\partial z} - S(h) \tag{3.24}$$

where θ is the volumetric water content, t is time, $K(h)$ is the hydraulic conductivity, which depends on the soil water potential (h), h is the soil water potential or pressure head, $S(h)$ is the sink term representing root water uptake.

The sink term $S(h)$ at a given soil depth z is commonly expressed as:

$$S(h,z) = \alpha(h) \cdot \beta(z) \cdot Tr \tag{3.25}$$

where $\alpha(h)$ is the water stress response function, $\beta(z)$ is the root density distribution function describing the proportion of roots at different soil depths (van Genuchten, 1987) and T_r is the Potential transpiration rate.

The total uptake of root water is calculated by integrating $S(z)$ over the root zone: $S_{total} = \int_0^{z_{max}} S(z)dz$, where z_{max} is the maximum rooting depth.

Two widely used models are the Feddes model and the van Genuchten model.

1. Feddes Model

The Feddes model simulates plant root water uptake under varying soil moisture conditions by introducing a piecewise linear stress function $\alpha(h)$, which adjusts the uptake rate based on the soil water potential h. It identifies three main zones:

- Optimal Uptake Range (h_{opt}) : Maximum uptake occurs between approximately –10 to –25 kPa, depending on plant and soil type.

- Dry Conditions (h_{low}): Below this threshold (often around –1500 kPa), uptake ceases due to permanent wilting.
- Wet Conditions (h_{high}): Near-saturation conditions (close to 0 kPa) reduce uptake due to waterlogging effects on roots.

The stress response function $\alpha(h)$ is defined as:

$$\alpha(h) = \begin{cases} 1 & , h_{low} < h < h_{opt} \\ \dfrac{h - h_{low}}{h_{opt} - h_{low}} & , h < h_{opt} \\ 0 & , h \leq h_{low} \ or \ h \geq h_{high} \end{cases} \tag{3.26}$$

This function captures reduced water uptake under both drought and saturated conditions, making the model widely applicable in soil-plant water flow simulations.

2. van Genuchten Model (with Mualem Approach)

The van Genuchten model couples water uptake with soil hydraulic properties such as the soil water retention curve and unsaturated hydraulic conductivity. The effective saturation S_e is defined as:

$$S_e(h) = \frac{\theta(h) - \theta_r}{\theta_s - \theta_r} = [1 + (\alpha|h|)^n]^{-m} \tag{3.27}$$

where θ_s is the saturated water content, θ_r is the residual water content and α, n, m are empirical parameters with $m = 1 - \frac{1}{n}$.

Using the Mualem conductivity function, the unsaturated hydraulic conductivity is:

$$K(S_e) = K_s \cdot S_e^l \cdot \left[1 - \left(1 - S_e^{1/m}\right)^m\right]^2 \tag{3.28}$$

This formulation allows detailed simulation of how root uptake varies with soil texture, water content, and hydraulic conductivity. The model is useful for crops in sandy and clayey soils, making it ideal for inclusion in tools like HYDRUS.

3.6 Mechanisms of Water Uptake

Water uptake in plants is governed by differences in water potential and involves coordinated physical and physiological processes.

- **Absorption**: Water enters roots primarily through osmosis, moving from higher water potential in the soil to lower potential within root cells. Root hairs enhance this process by increasing the absorption surface area, especially in dry or heterogeneous soils.
- **Transport**: Once inside the root, water travels radially to the xylem, where it moves upward to aerial parts of the plant. This ascent is mainly driven by transpirational pull—a tension generated by water evaporation from leaves. Additionally, root pressure, arising from active ion accumulation in the xylem during low transpiration (e.g., at night), contributes to upward water movement and is often visible as guttation.
- **Regulation**: Water uptake is regulated by aquaporins, membrane proteins that control water permeability in root cells. Plants also use feedback mechanisms, adjusting stomatal conductance and root activity in response to environmental factors such as soil moisture, humidity, and temperature.

Both the Feddes and van Genuchten models incorporate these dynamics by using root distribution functions (e.g., Root Length Density, RLD) to simulate the spatial patterns of water uptake in soil.

3.7 Root Length Density (RLD) function

The Root Length Density (RLD) function quantifies root distribution within soil, defined as root length per unit soil volume:

$$\beta(z) = \frac{L}{V} \tag{3.29}$$

where L is the total length of roots (cm) in a given soil volume and V is the volume of soil. RLD typically decreases with depth and directly influences the plant's ability to absorb water and nutrients.

Common RLD Representations:

1. Exponential Decay:

$$\beta(z) = \beta_0 e^{\{-\lambda z\}} \tag{3.30}$$

where β_0 is the root length density at the soil surface $(z = 0)$, λ is the root decay coefficient (rate of decrease with depth) and z is depth (cm). This function assumes that roots are most concentrated near the soil surface and decrease gradually with depth.

2. Piecewise Linear Function:

For some plants, RLD may be described as different linear segments across soil layers:

$$\beta(z) = \begin{cases} \beta_1 & 0 \leq z < z_1 \\ \beta_2 & z_1 \leq z < z_2 \\ \dots & \dots \end{cases} \tag{3.31}$$

3. Normalized Distribution:

To normalize the RLD function across the total root zone:

$$\int_0^{z_{\max}} \beta(z)\,, dz = 1 \tag{3.32}$$

where $z_{\max}$ is the maximum rooting depth.

In root water uptake models (e.g., Feddes model), RLD function $\beta(z)$ determines uptake efficiency at different depths through the sink term:

$$S(h, z) = \beta(z) \cdot \alpha(h) \cdot T_r \tag{3.33}$$

where $S(z)$ is the water uptake rate, $\alpha(h)$ is the stress response function, and T_r is the potential transpiration.

3.8 Numerical Methods for Solving Water Flow and Root Uptake

Numerical methods are essential for solving the complex, nonlinear equations that govern water flow and root uptake in soil-plant systems, particularly Richards' equation.

Due to its nonlinear dependence on soil properties and time-varying boundary conditions, analytical solutions are rarely feasible. Instead, numerical approaches such as the Finite Difference Method (FDM) and Finite Element Method (FEM) are employed to discretize the equations over space and time, allowing for accurate and stable simulations of unsaturated flow and root water uptake. These methods form the foundation of most modern hydrological models used in soil–plant–atmosphere studies.

3.8.1 Finite Difference Method (FDM)

The Finite Difference Method (FDM) is a widely used numerical technique for solving partial differential equations, such as Richards' equation, which governs unsaturated water flow in soils. This method discretizes both space and time domains and approximates derivatives using finite differences, enabling the simulation of water movement and root water uptake.

Richards' Equation with Root Uptake

The one-dimensional form of Richards' equation, incorporating a sink term for root water uptake, is given by:

$$\frac{\partial \theta}{\partial t} = \frac{\partial}{\partial z} K(h) \frac{\partial h}{\partial z} + \frac{\partial}{\partial z} K(h) - S(z) \tag{3.34}$$

Or in its head-based form:

$$C(h) \frac{\partial h}{\partial t} = \frac{\partial}{\partial z} K(h) \frac{\partial h}{\partial z} + \frac{\partial}{\partial z} K(h) - S(z) \tag{3.35}$$

where θ is the volumetric water content, h is the soil water pressure head, $K(h)$ is the unsaturated hydraulic conductivity, $C(h)$ is the specific moisture capacity = $d\theta/dh$, $S(z)$ is sink term representing root water uptake, z is spatial coordinate (depth) and t is time.

Spatial and Temporal Discretization

Discretize Space: Dividing the soil profile into N equally spaced nodes, each separated by a spacing of Δz. The position of the $i-th$ node is represented by z_i, which corresponds to the depth at that point in the soil.

Discretize Time: Dividing it into intervals of length Δt, where t^n denotes the time at the n^{th} time step.

Finite Difference Approximations

1. Time Derivative: Use a first-order forward difference for $\frac{\partial\theta}{\partial t}$

$$\frac{\partial\theta}{\partial t} \approx \frac{\theta_i^{n+1} - \theta_i^n}{\Delta t} \tag{3.36}$$

where θ_i^n is the volumetric water content at node i and time step n.

2. Spatial Derivative: For $\frac{\partial}{\partial z}\left(K(\theta)\frac{\partial h}{\partial z}\right)$, we use central differences:

Approximate the flux term at node (i) as:

$$\left.\frac{\partial h}{\partial z}\right|_i \approx \frac{h_{i+1}^n - h_i^n}{\Delta z} \tag{3.37}$$

The hydraulic conductivity $K(h)$ is calculated halfway between adjacent node points, i.e. $K_{i+1/2}$ is approximated as:

$$K_{i+1/2}^n = \frac{K(h_i^n) + K(h_{i+1}^n)}{2} \tag{3.38}$$

The flux gradient is then:

$$\left.\frac{\partial}{\partial z}\left(K\,\frac{\partial h}{\partial z}\right)\right|_i \approx \frac{K_{i+1/2}\,\frac{h_{i+1}^n - h_i^n}{\Delta z} - K_{i-1/2}\,\frac{h_i^n - h_{i-1}^n}{\Delta z}}{\Delta z} \tag{3.39}$$

3. Sink Term: The sink term $S(z)$ is evaluated at each node i, based on root water uptake models:

$$S_i^n = \beta_i \cdot \alpha(H_i^n) \cdot T_r \tag{3.40}$$

Substitute the finite difference approximations into the Richards equation, we get

$$\frac{\theta_i^{n+1} - \theta_i^n}{\Delta t} = \frac{1}{\Delta z}\left[K_{i+1/2}\frac{H_{i+1}^n - H_i^n}{\Delta z} - K_{i-1/2}\frac{H_i^n - H_{i-1}^n}{\Delta z}\right] - S_i^n \tag{3.41}$$

Rearranging for θ_i^{n+1}:

$$\theta_i^{n+1} = \theta_i^n + \Delta t\left[\frac{1}{\Delta z}\left(K_{i+1/2}\frac{H_{i+1}^n - H_i^n}{\Delta z} - K_{i-1/2}\frac{H_i^n - H_{i-1}^n}{\Delta z}\right) - S_i^n\right] \tag{3.42}$$

Solution Procedure

The solution procedure for applying the finite difference method begins with initialization. Initially, the values of the volumetric water content θ_i^0 are assigned at all spatial nodes (i), based on the initial soil moisture conditions. Additionally, boundary conditions for the soil water potential (ψ) or the water content (θ) are set at the soil surface and at the bottom of the profile, ensuring the model has the necessary starting and boundary values.

Next, the process iterates over time. At each time step (n), the hydraulic conductivities $K_{i+1/2}$ and $K_{i-1/2}$ are computed, based on the current water content θ_i^n at each node. The discretized form of Richards' equation is solved to update the pressure head and water content across the profile. Because the equation is nonlinear, iterative numerical techniques such as Newton-Raphson or Picard iteration are employed to achieve convergence at each time level. Finally, once the values of θ_i^{n+1} are updated, the model proceeds to the next time step. This process continues until the desired final time is reached, providing a time series of soil moisture values and water potential profiles across the soil domain.

However, this method also has some difficulties. The equation is highly nonlinear, so it needs repeated calculations (iterations), which can take a lot of computing time. If we use explicit methods, we must take very small time steps to keep the solution stable. On the other hand, implicit methods are more stable but involve solving complex equations at each step. Also, applying correct boundary conditions, like infiltration or evaporation, is very important to get accurate results. All these factors need to be carefully handled to make sure the simulation of water flow and root water uptake in soil is both accurate and efficient.

3.8.2 Finite Element Method (FEM)

The finite element method (FEM) is a numerical technique used to solve the Richards equation by dividing the soil domain into smaller elements and approximating the solution using basis (shape) functions. The one-dimensional Richards equation for unsaturated flow is given by:

$$\frac{\partial \theta}{\partial t} = \frac{\partial}{\partial z}\left(K(\theta)\frac{\partial \psi}{\partial z}\right) - S(z) \tag{3.43}$$

The equation is nonlinear because θ and $K(\theta)$ are functions of ψ.

Weak Formulation

1. Multiply by a Test Function: Multiply the entire equation by a test function $w(z)$ (which belongs to the same function space as $\psi(z)$:

$$w(z)\frac{\partial \theta}{\partial t} = w(z)\frac{\partial}{\partial z}\left(K(\theta)\frac{\partial \psi}{\partial z}\right) - w(z)S(z) \tag{3.44}$$

2. Integrate Over the Domain: Integrate both sides over the domain $[0, L]$:

$$\int_0^{\mathrm{L}} w\frac{\partial \theta}{\partial t}, dz = \int_0^L w\frac{\partial}{\partial z}\left(K(\theta)\frac{\partial \psi}{\partial z}\right), dz - \int_0^L w\, S(z), dz \tag{3.45}$$

3. Apply Integration by Parts: Use integration by parts on the second term to move the derivative off ($\frac{\partial \psi}{\partial z}$):

$$\int_0^L w\frac{\partial \theta}{\partial t}, dz = -\int_0^L \frac{\partial w}{\partial z}K(\theta)\frac{\partial \psi}{\partial z}, dz + \left[wK(\theta)\frac{\partial \psi}{\partial z}\right]_0^L - \int_0^L w\, S(z), dz \tag{3.46}$$

   Here, the boundary term

$$\left[wK(\theta)\frac{\partial \psi}{\partial z}\right]_0^L \tag{3.47}$$

   represents fluxes at the boundaries.

4. Weak Form: The equation becomes:

$$\int_0^L w\frac{\partial\theta}{\partial t},dz+\int_0^L\frac{\partial w}{\partial z}K(\theta)\frac{\partial\psi}{\partial z},dz=\int_0^L w\,S(z),dz+\left[wK(\theta)\frac{\partial\psi}{\partial z}\right]_0^L \quad (3.48)$$

Finite Element Approximation

1. Discretize the Domain: Divide the domain $[0, L]$ into N finite elements. Each element (e) spans $([z_e, z_{e+1}])$.
2. Basis Functions: Approximate $\psi(z)$ using a linear combination of basis function $N_i(z)$ over the nodes:

$$\psi(z)\approx\sum_{i=1}^{M}\psi_i N_i(z) \quad (3.49)$$

where ψ_i is the value of ψ at node (i) and $N_i(z)$ is the Shape function (e.g., linear or quadratic).
3. Test Functions: Choose the test functions $w(z)$ to be the same as the basis functions (Galerkin method): [$w(z) = N_j(z)$]
4. Substitute into the Weak Form: Substitute the approximations for (ψ) and (w) into the weak form:

$$\int_0^L N_j\frac{\partial\theta}{\partial t},dz+\int_0^L\frac{\partial N_j}{\partial z}K(\theta)\frac{\partial\psi}{\partial z},dz=\int_0^L N_jS(z),dz+\left[N_jK(\theta)\frac{\partial\psi}{\partial z}\right]_0^L \quad (3.50)$$

5. Matrix Formulation: After discretizing the domain, the equation is written in matrix form:

$$C\frac{\partial\psi}{\partial t}+K\psi=F \quad (3.51)$$

where C is the capacitance matrix, representing $\int_0^L N_j\frac{\partial\theta}{\partial t}dz$, K is the stiffness matrix, representing $\int_0^L\frac{\partial N_j}{\partial z}K(\theta)\frac{\partial N_i}{\partial z}dz$, F is the force vector, representing $\int_0^L N_jS(z)\,dz$ and the boundary fluxes.

Solution Procedure

1. Assemble Matrices: Compute the global C, K and F by summing contributions from all elements.

2. Time Discretization: Use a time-stepping method, such as backward Euler, to discretize the time derivative:

$$\frac{\partial \psi}{\partial t} \approx \frac{\psi^{n+1} - \psi^{n}}{\Delta t} \tag{3.52}$$

Substituting into the matrix form gives:

$$C \frac{\psi^{n+1} - \psi^{n}}{\Delta t} + K\psi^{n+1} = F \tag{3.53}$$

3. Iterative Solution: Solve the resulting nonlinear system iteratively (e.g., Newton-Raphson or Picard iteration) at each time step.

Boundary Conditions

Apply Dirichlet or Neumann boundary conditions by modifying K and F:

- Dirichlet (fixed ψ): Replace rows corresponding to boundary nodes.
- Neumann (flux): Include boundary fluxes in F.

The Finite Element Method (FEM) is a powerful and commonly used technique in soil studies to simulate how water moves through the soil and is taken up by plant roots. It works well with different soil types and shapes, even when the soil layers are uneven or complex. FEM is accurate because it carefully tracks water movement and lets us choose different calculation methods for better results. Overall, it helps turn a difficult water flow equation into a simpler form that computers can solve, making it useful for studying water behavior in many types of soil and landscapes.

Software Tools for Numerical Modeling

Table 3.5 provides a comparative overview of widely used software tools for simulating soil-plant-water interactions, including soil water flow, root water uptake, nutrient dynamics, and solute transport. Each tool is built upon either the Finite Element Method (FEM), Finite Difference Method (FDM), or a hybrid scheme, and is selected based on its capabilities and intended applications.

Table 3.4 Common numerical modeling tools used for simulating soil water flow, root water uptake, nutrient uptake, and solute transport

Software Tool	Numerical Method	Key Features	Reference
HYDRUS (1D/2D/3D)	FEM	Simulates water, solute, and root uptake; versatile boundary conditions	Šimůnek et al., 2016
SWAP	FDM	Soil-water-plant-atmosphere interactions; nitrogen and crop models	Kroes et al., 2017
VS2DT/ VS2DRT	FDM	Solute transport in variably saturated media; groundwater focus	Healy, 1990
SUTRA	FEM	Multispecies reactive transport in porous media; geothermal/hydrothermal	Voss & Provost, 2010
FEFLOW	FEM	3D variably saturated flow and transport; strong GUI support	Diersch, 2014
COMSOL Multiphysics	FEM	Custom multiphysics; advanced coupled flow-uptake models	COMSOL AB, 2020
OpenFOAM	FVM	Open-source CFD with porous media solvers; flexible scripting	Weller et al., 1998
MODFLOW (UZF/NWT)	FDM	Groundwater-surface interaction; recharge and nutrient leaching	Harbaugh, 2005
RootBox	Geometry-based + Coupled	Realistic root architecture; usable with HYDRUS/COMSOL	Schnepf et al., 2018
DUFLOW-NUTRIENT	FDM	Water and nutrient dynamics in furrow irrigation	De Jong van Lier et al., 2008

3.9 Influence of Transient Environmental Factors

Environmental factors such as rainfall and irrigation play a significant role in soil moisture dynamics and root water uptake. Since these factors change over time, they directly affect water availability in the root zone and influence plant water absorption. The incorporation of these transient conditions into the modeling of water flow and root uptake is essential for realistic simulation of soil-plant interactions.

3.9.1 Rainfall and Irrigation:

Rainfall and irrigation are the two primary sources of water input in agricultural systems. Both contribute to increase soil moisture and directly affect how much water plants can absorb through their roots. Rainfall is unpredictable and often comes in short bursts, which can quickly wet the upper soil layers and then dry out again. This may lead to surface runoff or deep-water movement depending on the soil type and how hard it rains. On the other hand, irrigation is planned and can be applied in specific amounts and at regular times, which helps ensure that plants get the water they need. Some irrigation methods, like drip irrigation, deliver water directly to the root zone, making water use more efficient but sometimes leaving other parts of the soil dry.

These changing water conditions affect how much water roots can take up. Right after rain or irrigation, water is easily available, and plants can absorb it well. But during dry periods, the soil loses water through evaporation, especially near the surface, and it becomes harder for roots to absorb water. If dry conditions last too long, plants may suffer from water stress, slow growth, or even reduced crop yield.

To model these changes in soil water properly, we include rainfall and irrigation as time-based boundary conditions in the equations. Rainfall is treated as a changing water input over time:

$$q_{\text{rainfall}}(t) = P(t) - E(t) \tag{3.54}$$

where $P(t)$ is rainfall and $E(t)$ is evaporation. For irrigation, we use:

$$q_{\text{irrigation}}(t) = \text{Irrigation Rate} \times f(\text{Spatial Distribution}) \tag{3.55}$$

Here, the irrigation rate and how the water is spread over the soil depend on the method used.

3.9.2 Infiltration

Infiltration is the process by which water enters the soil from the surface and moves downward through the soil layers. This movement is controlled by both gravity and capillary forces. Initially, water fills the large pores (macropores), and then it continues downward through the smaller pores (micropores). The rate at which this water enters the soil is called the infiltration rate, usually measured in mm/hr and denoted by $f(t)$. This rate is influenced by many factors such as soil texture, structure, moisture level, vegetation, land slope, and land management. For example, sandy soils have larger pores and allow faster infiltration, while clay soils infiltrate water more slowly due to smaller pore spaces. Vegetation improves infiltration by reducing runoff and maintaining good soil structure, whereas compacted soils slow it down.

In mathematical modeling, the infiltration rate at the surface can be represented using the Buckingham-Darcy equation:

$$f(t) = -q(t)|_{z=0} = \left[K(h)\frac{\partial h(z,t)}{\partial z} + K(h)\right]\Bigg|_{z=0} \tag{3.56}$$

Here, $K(h)$ is the unsaturated hydraulic conductivity, and $h(z,t)$ is the soil water pressure head. The total infiltration over time, known as cumulative infiltration $I(t)$, is given by:

$$I(t) = \int_0^t f(t)\ dt \tag{3.57}$$

Several models are commonly used to simulate infiltration:

1. Horton's Equation: Describes how the infiltration rate decreases over time:

$$f(t) = f_c + (f_0 - f_c)e^{-kt} \tag{3.58}$$

where f_0 is the initial rate, f_c is the steady rate, and kk is a decay constant.

2. Green-Ampt Model: A physically based model suitable for infiltration into dry soil:

$$I(t) = K(h_0)t + \Delta h\Delta\theta\ \ln\left(1 + \frac{I(t)}{\Delta h\Delta\theta}\right) \tag{3.59}$$

where $K(h_0)$ is the hydraulic conductivity at the surface, $\Delta\theta = \theta_0 - \theta_i$ is the change in water content across the wetting front, $\Delta h = h_0 - h_f$ is the difference in pressure head from surface to wetting front, h_0, θ_0 are the pressure head and water content at the surface and h_f, θ_i are the pressure head and water content at the wetting front (initial conditions).

Special Considerations:

- When ponding occurs (rainfall rate ≥ infiltration rate), h_0 can be taken as the ponding depth or zero.
- Under ponded conditions, surface values are approximated using saturated parameters: $\theta_0 \approx \theta_s$, $K(h_0) \approx K_s$.
- The pressure head at the wetting front h_f is often estimated using capillary length:

$$h_f = -\frac{\lambda_c}{2b} \tag{3.60}$$

where λ_c is the macroscopic capillary length and $b \approx 0.55$ (empirical constant).

3. Philip's Equation: A semi-empirical model that separates early infiltration driven by capillary action and later stages influenced by gravity:

$$f(t) = St^{-1/2} + A \tag{3.61}$$

where S is sorptivity and A is the steady-state infiltration rate.

4. Modified Kostiakov Equation: Used widely in surface irrigation:

$$F(t) = at^b + Kt \tag{3.62}$$

where a, b, and K are empirical parameters.

Each of these models helps to estimate how water moves into the soil under different conditions. Understanding infiltration is important for managing irrigation, predicting runoff, and designing water conservation practices in agriculture.

3.9.3 Soil Water Redistribution

Soil water redistribution is the internal movement of water within the soil profile after infiltration stops. It occurs due to gradients in soil water potential —comprising both matric (capillary) and gravitational components. Following infiltration, surface soil becomes wetter than deeper layers, creating a moisture gradient. Water then moves downward under gravity and laterally upward due to matric potential, redistributing toward drier regions. Over time, the gradient reduces, and the soil approaches hydrostatic equilibrium.

The rate and direction of soil water redistribution are affected by several factors: soil texture, where sandy soils allow faster redistribution due to higher permeability, while clay soils slow the process; initial moisture content, as wetter soils with steeper gradients promote quicker movement; soil structure, since well-aggregated soils with macropores enhance water flow compared to compacted soils; and external conditions, such as temperature-driven evaporation at the surface, which can pull water upward and influence vertical moisture movement. This process is essential for understanding plant water availability, groundwater recharge, and moisture dynamics in unsaturated soils.

3.9.4 Evaporation and Evapotranspiration

Evaporation and evapotranspiration (ET) are two essential processes that govern water loss from the soil-plant system to the atmosphere, significantly affecting the availability of soil moisture for plant uptake and must be carefully incorporated in any transient soil water balance model.

Evaporation

Evaporation refers to the direct loss of water from the soil surface to the atmosphere, occurring in three stages:

1. Stage I (Energy-limited): High evaporation rates when the surface is wet, controlled mainly by atmospheric conditions.
2. Stage II (Soil-limited): Evaporation slows as water must move from deeper layers; governed by soil hydraulic properties.
3. Stage III (Diffusion-limited): Very slow rates when the surface is dry, and vapor diffusion becomes dominant.

Evaporation is commonly modeled as a time-dependent flux at the soil surface:

$$E(t) = \frac{\Delta Q_{\text{evap}}}{\Delta t} \tag{3.63}$$

where $E(t)$ is the evaporation rate at time t, ΔQ_{evap} represents the amount of water lost through evaporation, Δt is the time step over which evaporation occurs.

Transpiration

Transpiration is a biological process in which water absorbed by plant roots is transported through the vascular system and released as vapor from stomata on leaf surfaces. This process is influenced by environmental factors such as temperature, humidity, wind, and light, as well as plant-specific factors including leaf area, stomatal density, and cuticle thickness. Transpiration occurs in three forms: stomatal transpiration, which accounts for about 90% of total water loss; cuticular transpiration, which involves water loss through the leaf cuticle; and lenticular transpiration, which occurs through small openings in woody stems. In soil-plant models, transpiration is typically represented as a sink term that reflects water uptake and loss by plants.

Evapotranspiration (ET)

Evapotranspiration (ET) represents the combined water loss from soil evaporation and plant transpiration, acting as a sink term in soil water balance models. It significantly influences soil moisture dynamics, particularly under semi-arid conditions like those in Jaipur. The most comprehensive FAO Penman–Monteith Equation for estimating daily reference evapotranspiration is given by:

$$ET_0 = \frac{0.408\,\Delta(R_n - G) + \gamma\,\frac{900}{T + 273}\,u_2(e_s - e_a)}{\Delta + \gamma(1 + 0.34u_2)} \tag{3.64}$$

where ET_0 is the reference evapotranspiration (mm/day), Δ is the slope of saturation vapor pressure curve (kPa/°C), R_n is the net radiation (MJ/m²/day), G is the soil heat flux (MJ/m²/day), T is the mean daily air temperature (°C), u_2 is the wind speed at 2 m height (m/s), $e_s - e_a$ is the vapor pressure deficit (kPa) and γ is the psychrometric constant (kPa/°C).

Reference ET_0 values were adjusted using crop coefficients (Kc) to obtain actual crop evapotranspiration:

$$ET_c = K_c \cdot ET_0 \tag{3.65}$$

These ET_c values were used as atmospheric boundary conditions in HYDRUS-1D simulations under different irrigation regimes.

Evapotranspiration is incorporated as a sink term in the modified Richards equation:

$$\frac{\partial \theta}{\partial t} = \frac{\partial}{\partial z} K(h) \frac{\partial h}{\partial z} + \frac{\partial}{\partial z} K(h) - S(h) - ET \tag{3.66}$$

where θ is the volumetric water content, h is the soil water pressure head, $K(\theta)$ is the hydraulic conductivity as a function of θ, $S(h)$ is the root water uptake sink term, ET is the evapotranspiration.

Modeling evapotranspiration (ET) is difficult because it changes quickly with the weather and as plants grow. It also varies from place to place depending on the type of soil, the kind of plants, and small local differences in conditions. Another challenge is that plants respond to stress, like closing their stomata during dry periods, which affects how much water they lose. To make ET models more accurate, they need to include these changing and uneven conditions in both time and space.

3.10 Model Result and Discussion

To assess soil water movement and root water uptake, the HYDRUS-1D model was applied to simulate a 120-day wheat growing season (*Triticum aestivum L.*, variety Raj 4037) in four distinct agro-economic zones of Jaipur. Twelve representative study sites were selected across four agro-economic zones of Jaipur district, with three chosen from each zone to capture spatial variability in soil and climatic conditions. Each site was assigned a unique Site ID to ensure consistent referencing throughout the modeling and analysis. The selected sites and their corresponding IDs are as follows: Amer (AM01), Kotputli (KT02), Govindgarh (GV03), Shahpura (SH04), Virat Nagar (VR05), Kalwad (KL06), Dudu (DD07), Phagi (PH08), Chaksu (CH09), Sambhar Lake (SL10), Bassi (BS11), and Jobner (JB12). These IDs were used systematically in HYDRUS-1D simulations to track model inputs and outputs across the different zones. Each simulation was conducted over a 100 cm soil profile discretized into 101 spatial nodes.

The initial condition was set as a uniform pressure head of –100 cm. The upper boundary was defined as an atmospheric boundary condition with surface run-off, allowing realistic representation of rainfall and irrigation inputs. The lower boundary was set as free drainage to permit gravity-driven outflow.

Table 3.5 Summary of Model Setup and Parameters for Water Flow and Root Water Uptake Simulation Using HYDRUS-1D

Category	Description / Value
Crop	Wheat (Triticum aestivum L., Variety Raj 4037)
Simulation Period	120 days
Soil Profile Depth	100 cm
Spatial Discretization	101 nodes
Initial Condition	Uniform pressure head = –100 cm
Upper Boundary Condition	Atmospheric BC with surface run-off
Lower Boundary Condition	Free drainage
Soil Hydraulic Model	van Genuchten–Mualem model (no hysteresis)
Crop Growth Stages	T_0 (5 d), T_1 (30 d), T_2 (60 d), T_3 (90 d), T_4 (120 d)
Observation Nodes	0 cm, 30 cm, 60 cm, 90 cm, 100 cm
Root Water Uptake Model	Feddes model
Feddes Parameters (Wesseling, 1991)	P_0 = 0 cm (anaerobiosis point)
	P_{opt} = –1 cm (optimal pressure head)
	P_2H = –500 cm (upper limit for reduced uptake)
	P_2L = –900 cm (lower limit for reduced uptake)
	P_3 = –16000 cm (wilting point)
	r_2H = 12 cm/day (maximum uptake at P_2H)
	r_2L = 2.4 cm/day (maximum uptake at P_2L)

Soil water movement was governed by the Richards equation, using the van Genuchten–Mualem model (without hysteresis) to define soil hydraulic properties. Root water uptake was incorporated using the Feddes uptake model, which considers pressure head-dependent water extraction by plant roots.

The simulation period included five crop growth stages, identified as T_0, T_1, T_2, T_3, and T_4 at 5, 30, 60, 90, and 120 days, respectively. Model outputs—such as pressure head, volumetric water content, and root water uptake—were monitored at observation nodes located at 0, 30, 60, 90, and 100 cm depths. This setup enabled evaluation of dynamic soil moisture conditions and root uptake behavior across varied soils and climates in the Jaipur region. Table 3.6 summarizes the model setup and parameters for water flow and root water uptake simulation using HYDRUS-1D model.

Table 3.6 Soil textural properties and bulk density for selected sites in the Jaipur region

Soil Type	Site ID	Sand (%)	Silt (%)	Clay (%)	Bulk Density (g/cm^3)	Vol. water content at -33 kPa in (cm^3/cm^3)	Vol. water content at -1500 kPa in (cm^3/cm^3)
Sandy Loam (Zone 1)	AM01	57.37	22.65	19.97	1.55	0.3301	0.1053
	KT02	41.91	30.70	27.41	1.56	0.3169	0.1463
	GV03	44.71	25.60	29.68	1.58	0.3179	0.1371
Loamy Soil (Zone 2)	SH04	42.92	30.13	26.95	1.58	0.3227	0.1441
	VR05	51.74	25.72	22.50	1.58	0.3420	0.1342
	KL06	46.49	26.68	26.84	1.57	0.3447	0.1337
Clay Loam (Zone 3)	DD07	35.33	39.54	25.08	1.53	0.3392	0.1396
	PH08	46.14	28.94	24.92	1.55	0.3249	0.1388
	CH09	49.56	28.66	21.93	1.58	0.3349	0.1185
Problematic Soil (Zone 4)	SL10	44.82	26.93	28.18	1.56	0.2864	0.1208
	BS11	56.82	24.32	18.88	1.54	0.3381	0.1111
	JB12	36.73	36.98	26.31	1.56	0.3153	0.1363

Source: *SoilGrids, ISRIC – World Soil Information (Hengl et al., 2017)*

Soil Water Retention Characteristics Curve

The soil water retention curves (Fig. 3.4) showed that Zone 3 had the highest water-holding capacity, while Zone 4 held the least. Zone 1 provided slightly better availability during moderate drying, but Zone 3 retained the most water under arid conditions. These differences highlight finer soils in Zone 3 and coarser, fast-draining soils in Zone 4, which help guide irrigation planning with HYDRUS-1D.

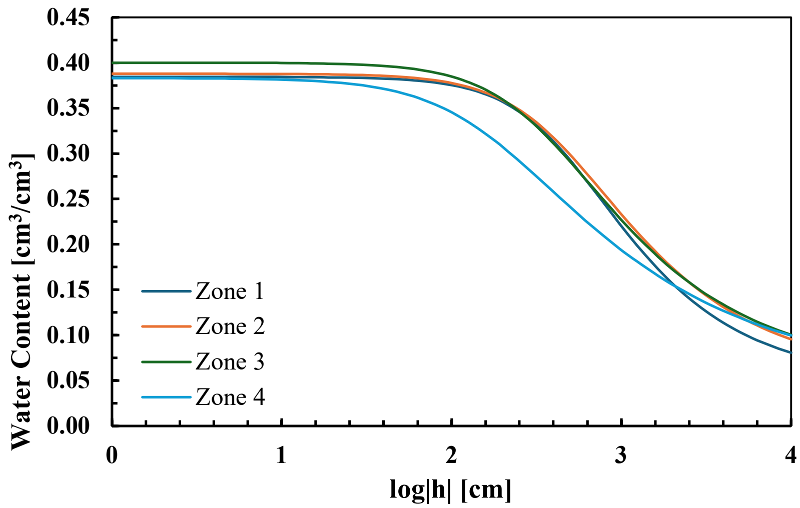

Figure 3.4 Soil water retention curves for four agro-economic zones in Jaipur, showing the relationship between volumetric water content and pressure head ($log|h|$)

Table 3.7 Default initial estimates of van Genuchten parameters for different soil types across selected sites in the Jaipur region using HYDRUS-1D.

Soil Type	Site ID	θ_r (cm^3/cm^3)	θ_s (cm^3/cm^3)	α (cm^{-1})	n (-)	K_s (cm/hr)
Sandy Loam (Zone 1)	AM01	0.0471	0.3844	0.0021	1.7593	5.66
	KT02	0.0523	0.3916	0.0048	1.4556	4.99
	GV03	0.0510	0.3884	0.0038	1.5077	5.28
Loamy Soil (Zone 2)	SH04	0.0519	0.3881	0.0039	1.4958	4.13
	VR05	0.0519	0.3878	0.0022	1.6613	3.66
	KL06	0.0543	0.3933	0.0021	1.6812	3.58
Clay Loam (Zone 3)	DD07	0.0564	0.4001	0.0028	1.6164	4.29
	PH08	0.0515	0.3921	0.0036	1.5322	5.04
	CH09	0.0507	0.3834	0.0021	1.7324	3.78
Problematic Soil (Zone 4)	SL10	0.0463	0.3829	0.0059	1.4523	9.17
	BS11	0.0490	0.3879	0.0020	1.7749	5.50
	JB12	0.0519	0.3887	0.0041	1.5078	4.53

Temporal Variation of Pressure Head at Different Soil Depths

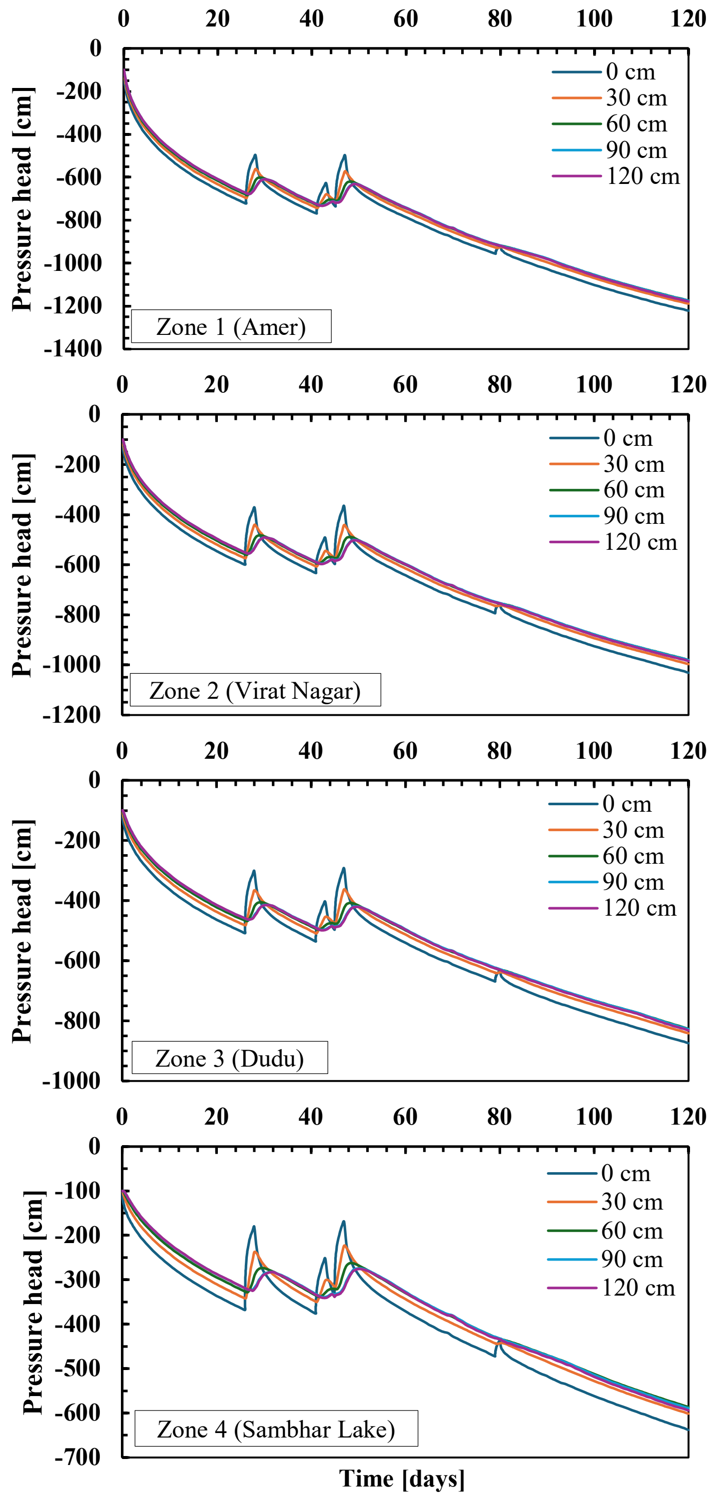

Figure 3.5 Temporal variation of soil pressure head at multiple depths (0–120 cm) over a 120-day wheat growth period in Zones 1–4 (Amer, Virat Nagar, Dudu, Sambhar Lake).

Across all zones, HYDRUS-1D showed a clear top-down drying trend during the wheat season. Surface layers dried quickly, while deeper layers dried more gradually, but by day 120, all depths converged to uniform low-pressure head values. This demonstrates strong plant water uptake and validates the model's ability to simulate realistic soil-water dynamics.

Temporal Variation of Soil Water Content at Different Depths

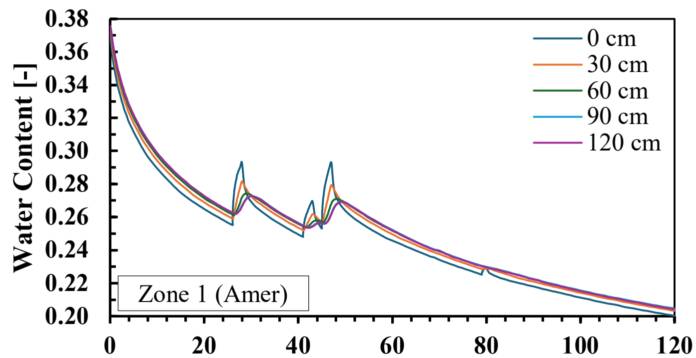

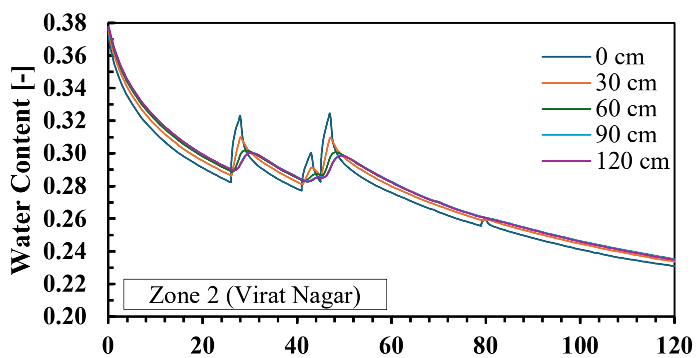

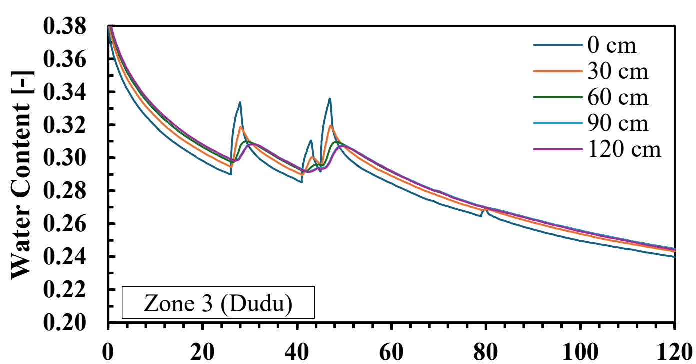

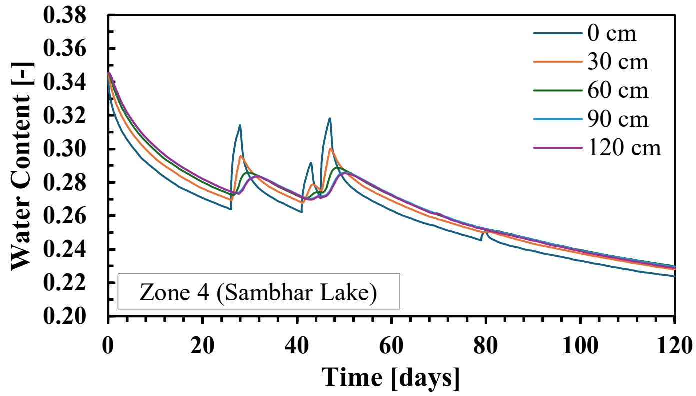

Figure 3.6 Temporal variation of Water content at multiple depths (0–120 cm) over a 120-day wheat growth period in Zones 1–4 (Amer, Virat Nagar, Dudu, Sambhar Lake).

Across all zones, soil moisture decreased from the surface downward, with the upper 30–40 cm showing the most significant changes due to roots and evaporation. By day 120, profiles in all zones dried to nearly uniform values, with Zone 3 retaining slightly more water.

Temporal Variation of Pressure Head with Depth

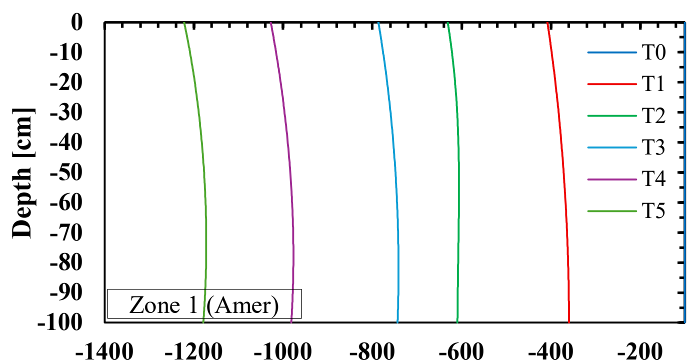

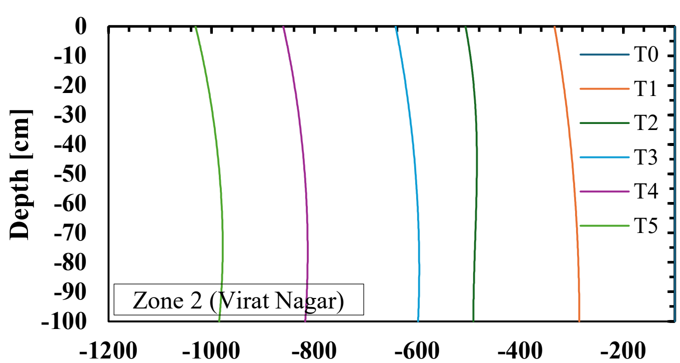

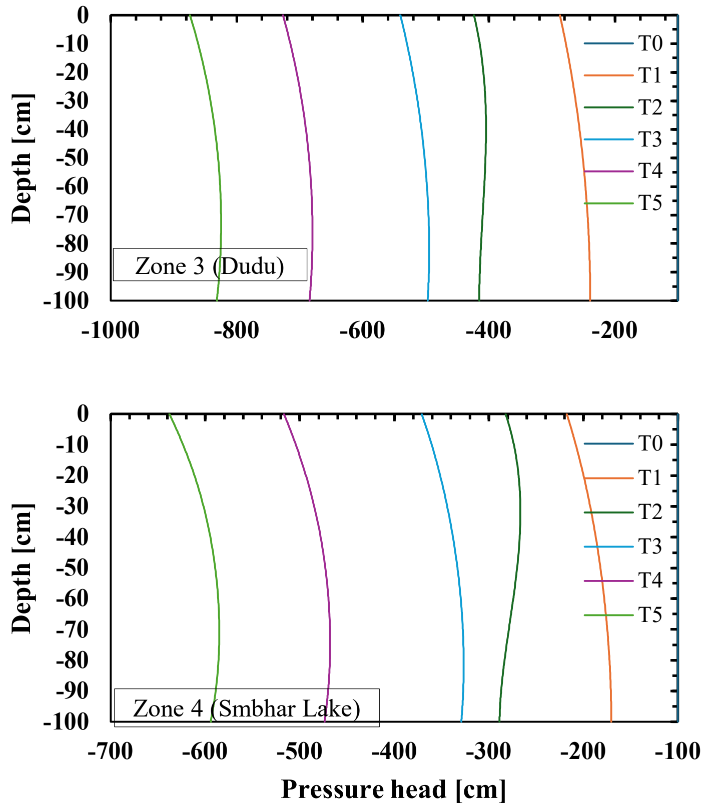

Figure 3.7 Temporal variation of soil pressure head with depth over a 120-day wheat growing season in four zones (Amer, Virat Nagar, Dudu, and Sambhar Lake.

Across all zones, soil pressure head declined from top to bottom during the wheat season, with surface layers drying fastest and deeper layers drying more slowly. By day 120, the soil profile was uniformly dry, especially within the active root zone. These results confirm that HYDRUS-1D accurately captured soil drying patterns under semi-arid conditions.

Temporal Variation of Water Content with Depth

Soil moisture declined from the surface downward in all zones, with the top 40–60 cm showing the largest changes due to roots and evaporation. Deeper layers stayed wetter, confirming limited root activity at depth. These patterns match wheat behavior in semi-arid soils and validate HYDRUS-1D's accuracy.

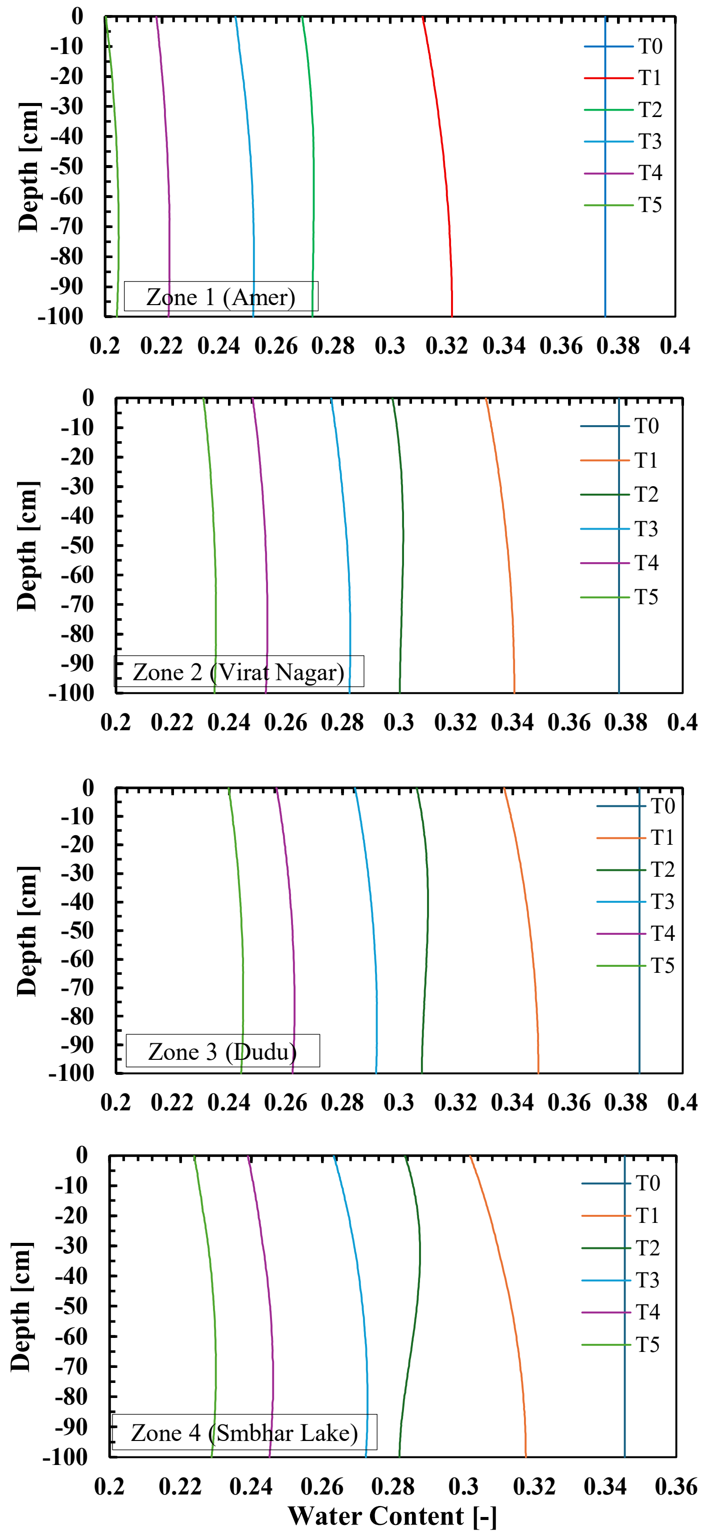

Figure 3.8 Temporal variation of Soil Water Content with depth over a 120-day wheat growing season in four zones (Amer, Virat Nagar, Dudu, and Sambhar Lake).

Hydraulic Conductivity

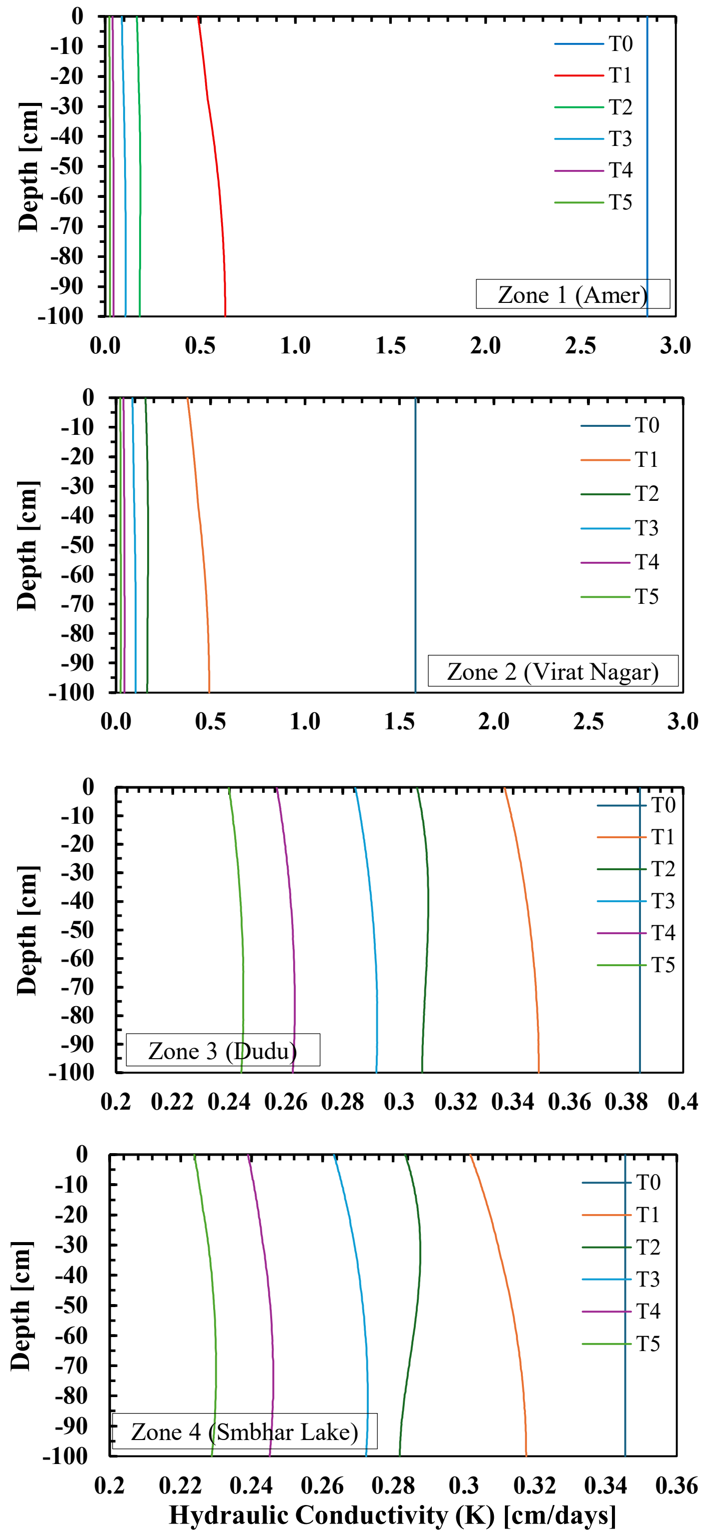

Figure 3.9 Temporal variation of Hydraulic Conductivity with depth over a 120-day wheat growing season in four zones (Amer, Virat Nagar, Dudu, and Sambhar Lake) simulated using HYDRUS-1D.

Hydraulic conductivity declined in all zones, with sharp reductions in the surface layers and slower changes deeper in the soil. Most water loss occurred within the top 40–60 cm due to root uptake and evaporation, while deeper layers stayed wetter for longer.

Root Water Uptake

The HYDRUS-1D simulations showed that soil depth and crop growth stage strongly influenced root water uptake in all four Jaipur zones. Across all sites, uptake occurred almost entirely from the deepest layer (around –99.5 cm), with little to no contribution from the upper 0–90 cm. This reliance on deeper moisture reflects the semi-arid conditions, where surface layers dried quickly due to evaporation and were less reliable as a water source.

Temporally, uptake followed the wheat growth cycle: it was deficient during the early seedling stage (first 20–25 days), rose sharply during mid-season when crop demand peaked (days 30–60), and gradually declined as the crop matured (days 70–120). Maximum uptake (~0.0644 $cm^3/cm^3/day$) was recorded around day 45 across zones, confirming this mid-season peak. Afterward, uptake steadily decreased to ~0.013–0.017 $cm^3/cm^3/day$ by day 120, indicating reduced plant demand.

Taken together, the results highlight two key insights: (i) water absorption was concentrated at the bottom of the root zone, suggesting that deeper roots play a vital role in sustaining wheat under semi-arid stress, and (ii) uptake varied over time in line with the crop's growth stages, with the highest demand during rapid vegetative growth and a tapering off at maturity. These findings confirm that HYDRUS-1D can effectively capture root water uptake's combined depth- and time-dependent dynamics in semi-arid wheat systems.

Cumulative Fluxes

The HYDRUS-1D simulations showed a clear pattern of cumulative fluxes across all four zones. Surface flux shifted from positive (rainfall/irrigation) early in the season to negative later due to evaporation, with maximum loss around days 45–49. Root uptake increased steadily, peaking mid-season, while bottom flux stayed negative across all zones, showing continuous deep drainage. The results highlight the importance of adjusting irrigation to crop demand to reduce water loss in semi-arid soils.

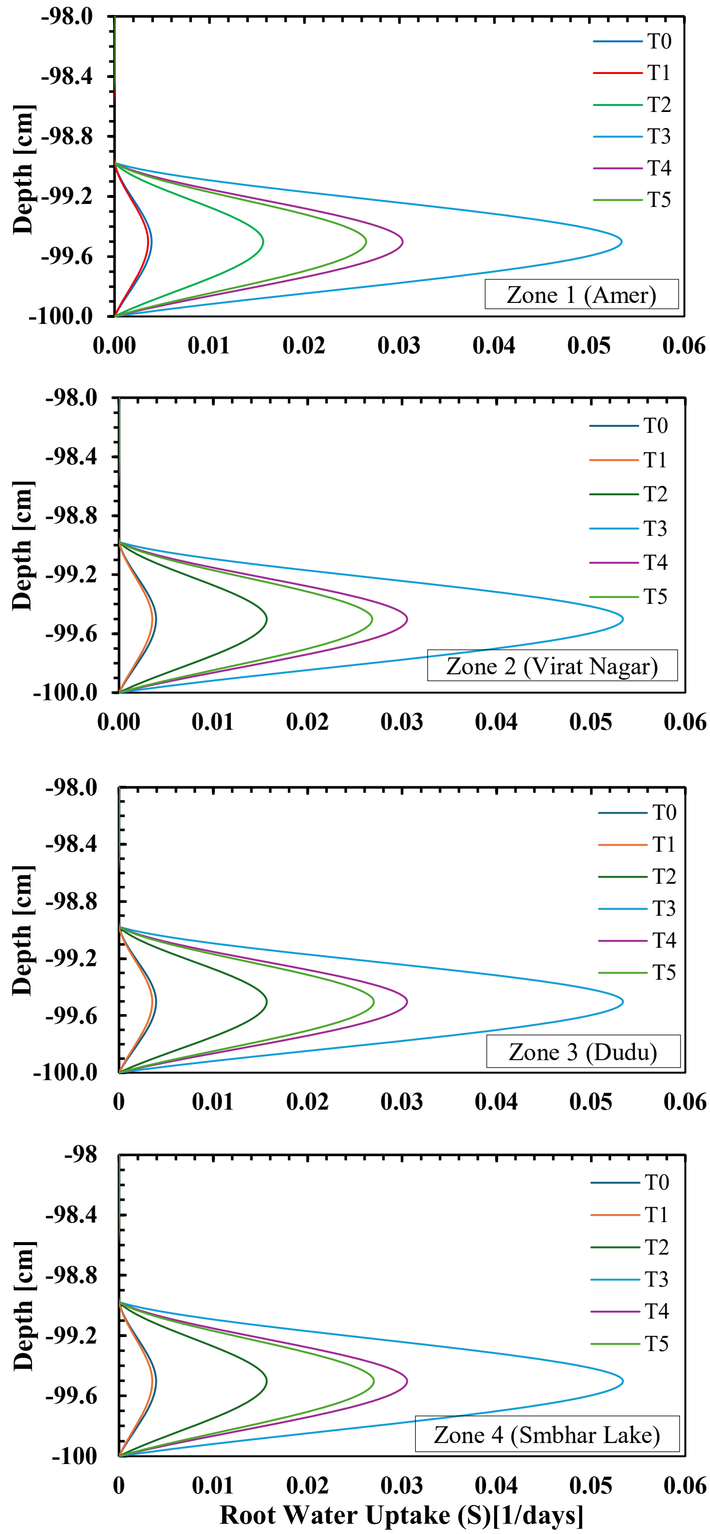

Figure 3.10 Temporal variation of Root Water Uptake with depth over a 120-day wheat growing season in four zones (Amer, Virat Nagar, Dudu, and Sambhar Lake) simulated using HYDRUS-1D.

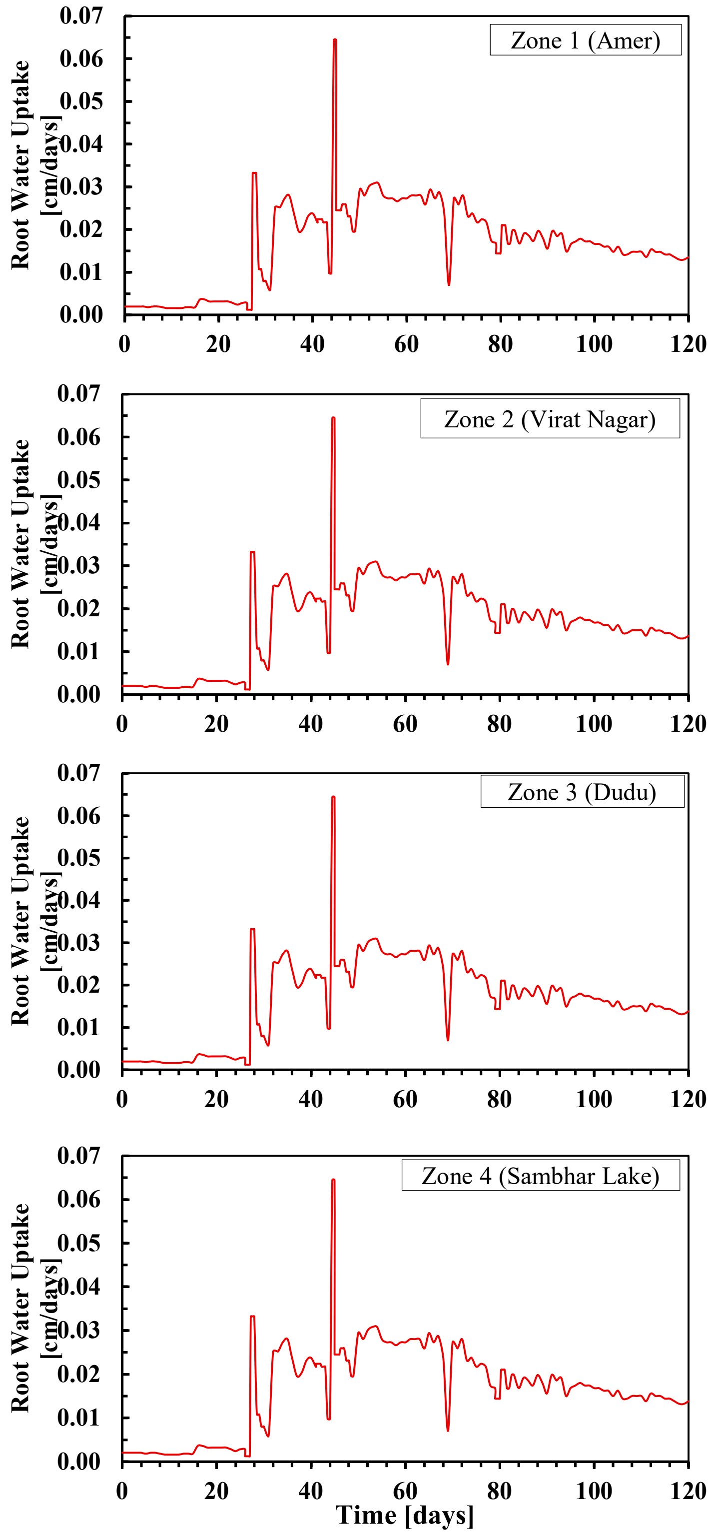

Figure 3.11 Root Water Uptake over a 120-day wheat growing season in four zones (Amer, Virat Nagar, Dudu, and Sambhar Lake) simulated using HYDRUS-1D.

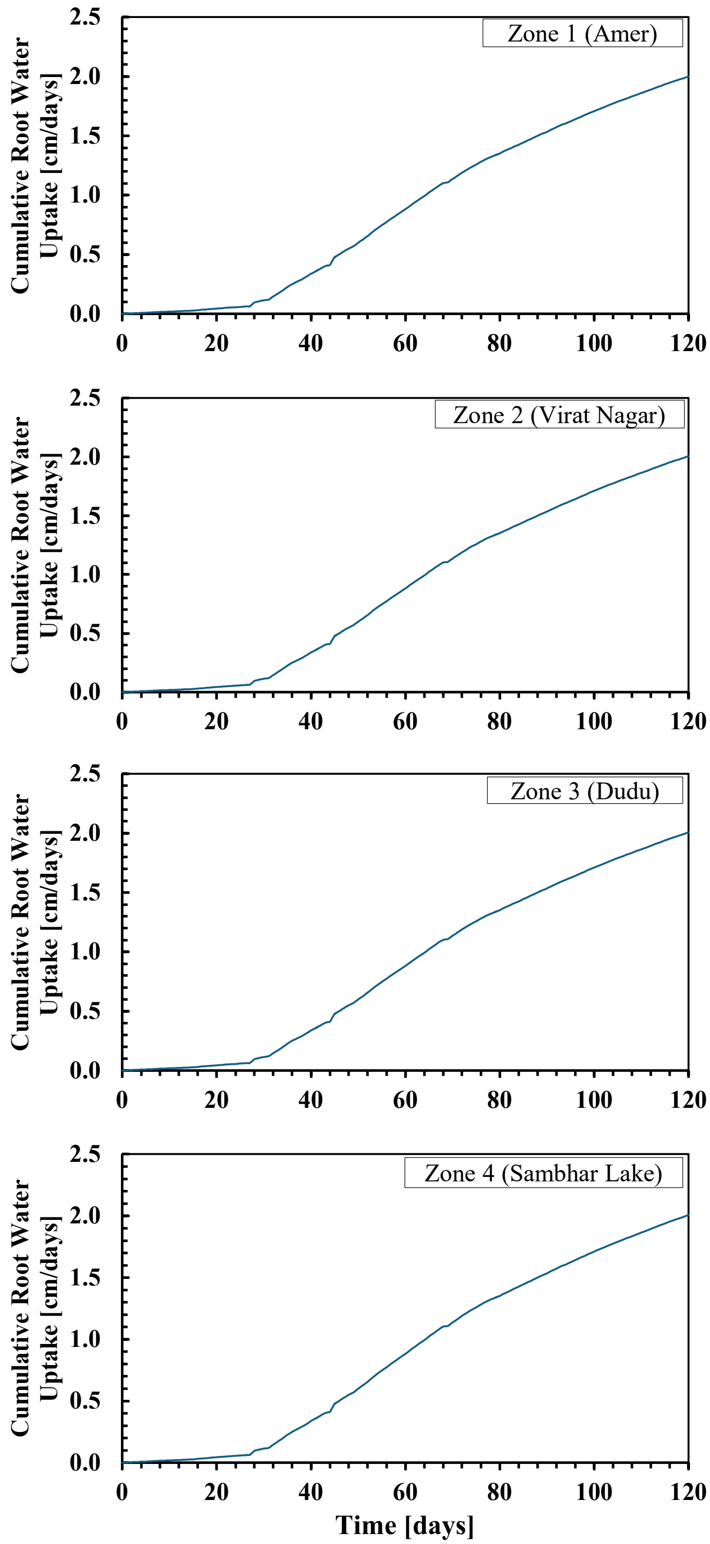

Figure 3.12 Cumulative Root Water Uptake over a 120-day wheat growing season in four zones (Amer, Virat Nagar, Dudu, and Sambhar Lake) simulated using HYDRUS-1D.

Soil Water Storage

Soil water storage declined steadily in all zones, with Zone 3 starting highest (~38.5 cm) and Zone 4 lowest (~34.5 cm). By day 120, storage fell to ~20–24 cm, with Zone 1 depleting fastest and Zone 3 retaining the most. These patterns highlight the influence of soil type on water retention under wheat in semi-arid conditions.

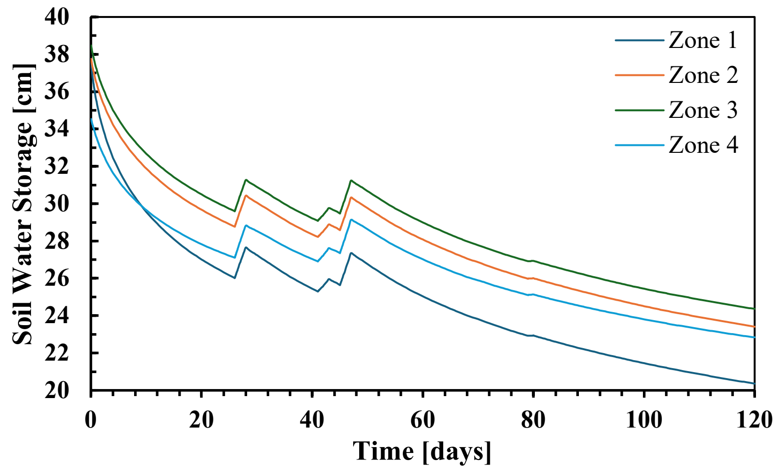

Figure 3.13 Temporal variation of soil water storage over 120 days across all four zones (Amer, Virat Nagar, Dudu, and Sambhar Lake) as simulated by HYDRUS-1D.

Cumulative Infiltration

Infiltration was absent for the first 25 days, rose sharply to ~5 cm between days 26–47, and then stabilized at ~5.1 cm through day 120. This pattern was consistent across zones, likely reflecting rainfall/irrigation followed by field capacity conditions.

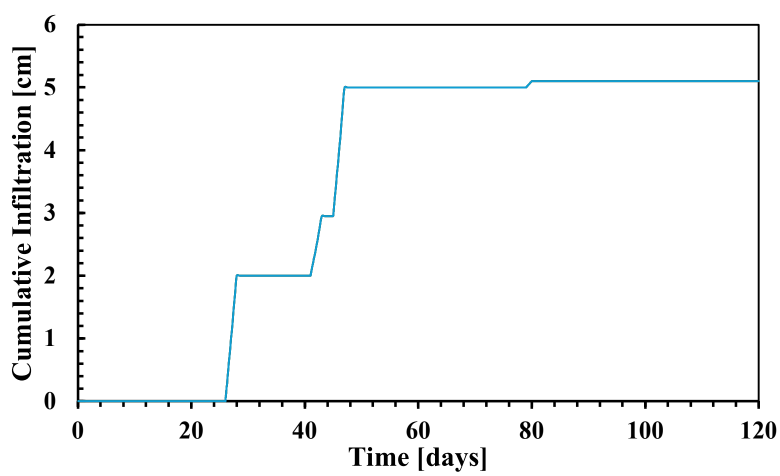

Figure 3.14 Cumulative Infiltration over a 120-day wheat growth period in Zones 1–4 (Amer, Virat Nagar, Dudu, Sambhar Lake) as simulated by HYDRUS-1D.

Cumulative Evaporation Trends

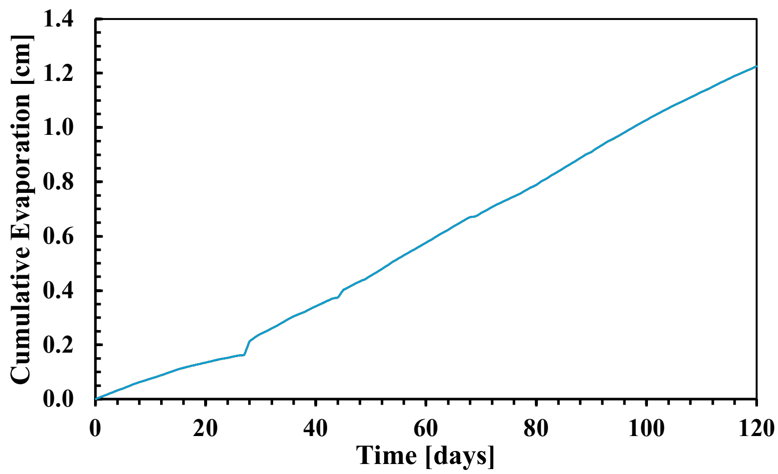

Figure 3.15 Cumulative evaporation over a 120-day wheat growth period in Zones 1–4 (Amer, Virat Nagar, Dudu, Sambhar Lake) as simulated by HYDRUS-1D

Starting from a negligible value initially, Cumulative evaporation rose gradually to ~0.16 cm by day 25, reflecting modest surface drying and low atmospheric demand. It increased sharply to ~0.45 cm by day 50 and then continued steadily to ~1.23 cm by day 120. Nearly identical trends across all zones suggest similar soil surface and climate conditions.

3.11 Conclusion

This chapter presented a detailed analysis of soil water flow and root water uptake under transient conditions using the HYDRUS-1D model across four agro-climatic zones of Jaipur—Amer, Virat Nagar, Dudu, and Sambhar Lake. The model successfully simulated the temporal and spatial distribution of key soil hydraulic parameters, including pressure head, water content, hydraulic conductivity, root water uptake, cumulative water fluxes, and soil water storage during a 120-day wheat growing period.

Results revealed a consistent top-down drying trend in all zones, driven by atmospheric demand and root water uptake. Pressure heads became increasingly negative over time, with the surface layers responding first and most intensely. Correspondingly, soil moisture decreased progressively, especially in the top 40–60 cm, confirming that most root activity was concentrated within this depth range. Deeper layers remained relatively wetter, indicating limited root penetration and slower water dynamics.

Hydraulic conductivity declined significantly in the upper profile due to drying, while root water uptake patterns aligned closely with crop phenology—low in the initial stage, peaking during active growth (around 60 days), and declining thereafter. Cumulative flux analysis demonstrated initial infiltration followed by surface evaporation, consistent root uptake, and substantial deep percolation, which raises concerns regarding potential nutrient leaching. Soil water storage decreased steadily in all zones, with zone-specific differences reflecting variations in soil texture and water retention capacity.

After studying how water moves through soil and how roots absorb it (Chapter 3), the focus now shifts to how this water movement affects plant transport and uptake of nutrients. Chapter 4 builds on this by developing a mathematical model that includes multiple root branches to better understand how root structure, soil moisture, and nutrient availability influence plant growth. It will cover the equations, boundary conditions, and nutrient uptake mechanisms (like Michaelis-Menten kinetics) involved in this process.

Chapter 4

Mathematical Model for Nutrient Uptake in Plants with Multiple Root Branching Structures

Chapter 4

Mathematical Model for Nutrient Uptake in Plants with Multiple Root Branching Structures

4.1 Introduction

To predict crop yields accurately, understanding nutrient uptake through complex root systems is crucial. Just as a child's growth depends not only on the amount of food they eat but also on how effectively their body absorbs nutrients, plants rely on their root systems to extract essential nutrients from the soil. These roots function like a network of straws, extending in various directions to access nutrients distributed unevenly in the soil.

Traditional models often oversimplify root architecture by focusing on single roots or general patterns, which can miss the nuances of real-world nutrient uptake. In reality, plants have intricate root systems with numerous branches of varying lengths and diameters. This complexity affects how efficiently they can absorb nutrients and, consequently, how well they grow (Gregory & Kirkegaard, 2016).

To improve crop yield predictions, we need a model that accurately reflects this complex root structure. By incorporating detailed representations of root branching and nutrient absorption dynamics, we can better understand how plants interact with their environment. This enhanced understanding allows for more precise predictions of how different environmental conditions and management practices impact crop yields (Wasaya et al., 2018).

Such a model can guide decisions on fertilizer application, irrigation, and other agronomic practices, leading to better resource use and increased agricultural productivity. In summary, by advancing our models to capture the complexity of root systems, we can optimize farming practices, reduce waste, and promote more sustainable agriculture.

While numerous models have been developed to understand nutrient uptake in plants, most fall short in representing the true complexity of root systems. These models often rely on significant simplifications:

Oversimplified Root Architecture: Many models assume a simple, uniform root structure, neglecting the intricate branching patterns and variations in root length and diameter that characterize real plant roots. This oversimplification can lead to inaccurate predictions of nutrient uptake, especially in heterogeneous soil environments where nutrient distribution is uneven.

Single Root Focus: Some models focus solely on a single root or a small portion of the root system. While this approach may provide insights into localized nutrient uptake processes, it fails to capture the interactions and competition that occur among multiple roots within a complex root system.

Neglecting Root Dynamics: Roots are not static structures; they grow, branch, and senesce in response to various environmental cues. However, many models assume a fixed root architecture, ignoring the dynamic nature of root growth and its impact on nutrient acquisition.

These limitations hinder our ability to accurately predict nutrient uptake and crop yield responses, particularly under conditions where root architecture and soil heterogeneity play significant roles. Addressing these research gaps by developing models that account for the complexity and dynamics of root systems is essential for advancing our understanding of plant nutrient acquisition and its implications for sustainable agriculture.

The primary objectives of this chapter are:

1. Develop a mathematical model that accurately simulates nutrient uptake in plants by incorporating the complex branching structure of their root systems.
2. Integrate the root uptake model with the water flow model presented in Chapter 3 to capture the interdependence of water and nutrient transport in the soil-plant system.
3. Evaluate the model's performance by comparing its predictions against experimental data or observations, assessing its sensitivity to key parameters, and exploring its behavior under different scenarios.

4. Explore the implications of the model's findings for understanding nutrient uptake mechanisms, predicting crop yields, and informing sustainable agricultural practices.

4.2 Root System Architecture (RSA)

The root system of a plant is a complex and highly organized structure, essential for its survival, growth, and productivity. Each component of the root system has a specific role in absorbing water and nutrients from the soil. The root system architecture is the arrangement of different roots in solid space (Gregory & Kirkegaard, 2016). Just like a building that has walls, roof, and floors, plant root systems also contain different structures including root types (primary, lateral, adventitious), root hairs, and specialized features such as nodules and cluster roots. To understand root architecture, it is important to understand the different structures that make up the root system.

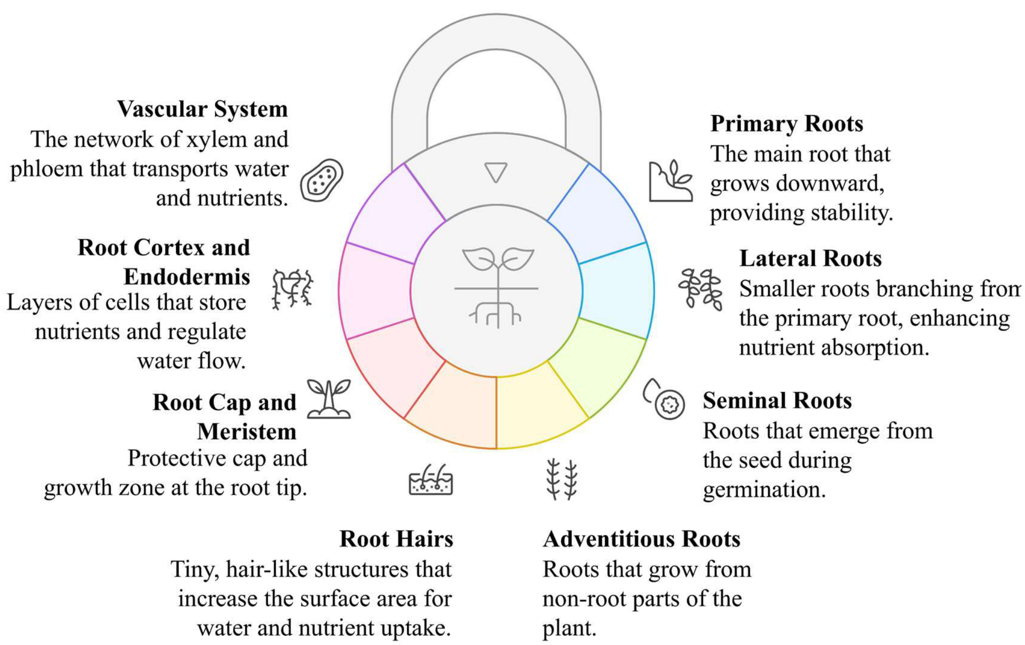

Figure 4.4.1 Root System Architecture

Primary Roots (Taproots)

The primary root, also called the taproot, is the first root to emerge from a seed and originates from the embryo (radicle). It grows vertically downward, anchoring the plant firmly in the soil and accessing deep water and nutrients, which is vital during droughts.

In some plants like carrots and beets, it also functions as a storage organ for nutrients and starches, supporting the plant during dormancy or stress.

Lateral Roots

Lateral roots, which are post-embryonic, branch out from the primary root as first-order roots and form a complex network with higher-order branches. They spread horizontally, increasing the root system's surface area and enhancing nutrient absorption, especially from the upper soil layers. These roots are vital in nutrient-poor soils, often forming symbiotic relationships with mycorrhizal fungi to access distant nutrients like phosphorus. Their growth is highly adaptive, becoming denser in nutrient-rich zones and sparser in poor areas, ensuring efficient resource use.

Seminal Roots

Seminal roots are an essential component of the root system in monocotyledonous plants, forming during the early stages of development. These roots emerge adjacent to the radicle, the embryonic root that first protrudes during germination. They ensure seedling establishment by anchoring the plant and absorbing water and nutrients. Seminal roots are crucial for initial growth, later complemented by adventitious roots for expanded resource uptake and long-term support.

Adventitious Roots

Adventitious roots are roots that develop from non-root tissues, such as stems, leaves, or nodes, rather than originating from another root. They can form at the base of stem cuttings, from leaf explants, in stems of flooded plants, or from nodes in cereal crops (commonly referred to as crown roots). These roots are highly diverse and encompass both embryonic and post-embryonic origins.

Root Hairs

Root hairs are tiny extensions from the root's epidermis near the tips, greatly increasing the root's surface area. They play a crucial role in absorbing water and nutrients, particularly essential minerals like nitrogen, phosphorus, and potassium. Located in nutrient-rich zones, root hairs maximize soil contact and are key to efficient moisture uptake. They also interact with beneficial microbes—such as Rhizobium in legumes—to aid in nutrient acquisition, especially nitrogen through symbiotic nodules (Teng et al., 2015).

Root Cap and Meristem (Root Growth Zone)

Root Cap: Located at the very tip of the root, the root cap is a protective structure that shields the growing tip (meristem) as the root pushes through the soil. It secretes a mucilage that lubricates the root's passage through the soil, reducing friction.

Meristematic Zone (Growth Zone): Just behind the root cap lies the meristematic zone, where cells rapidly divide and grow, enabling root elongation. This zone is responsible for the continuous growth of the root system, allowing the plant to explore new areas of soil for resources.

Root Cortex and Endodermis

Cortex: The cortex is a layer of parenchyma cells just beneath the root's outer layer (epidermis). It serves as a conduit for water and nutrients as they move toward the center of the root, where the vascular system (xylem and phloem) is located.

Endodermis: The endodermis is an inner layer of cells surrounding the vascular tissues. This layer acts as a selective barrier, regulating the movement of water and nutrients into the plant's vascular system. The endodermis contains a waxy layer known as the Casparian strip, which forces water and nutrients to pass through cell membranes, ensuring that harmful substances are filtered out before entering the plant's vascular tissues.

Vascular System (Xylem and Phloem)

Xylem: The xylem is responsible for transporting water and dissolved minerals from the roots to the rest of the plant. It acts as a highway for water and nutrients to move upward through the plant, driven by transpiration (water loss through the leaves).

Phloem: The phloem transports the products of photosynthesis (mainly sugars) from the leaves to the roots, where they are stored or used to fuel further growth. This bidirectional movement ensures that the roots are supplied with energy while also storing excess sugars for future use.

Water Uptake: Root hairs and first order lateral roots are primarily responsible for absorbing water from the soil. Once absorbed, water moves through the cortex and endodermis, entering the xylem where it is transported to the rest of the plant. The deeper primary roots tap into more secure water reserves, especially during periods of drought.

4.3 Nutrient Uptake Mechanisms

Plants take up important nutrients from the soil through their roots to grow and stay healthy. This process happens in different ways, depending on how much of the nutrient is in the soil, the structure of the roots, and the plant's energy levels (Goss et al., 1993). Nutrient uptake can happen in two main ways:

- **Passive uptake**, which doesn't need energy
- **Active uptake**, which uses energy from the plant

Each method helps the plant get the minerals it needs for proper growth and function.

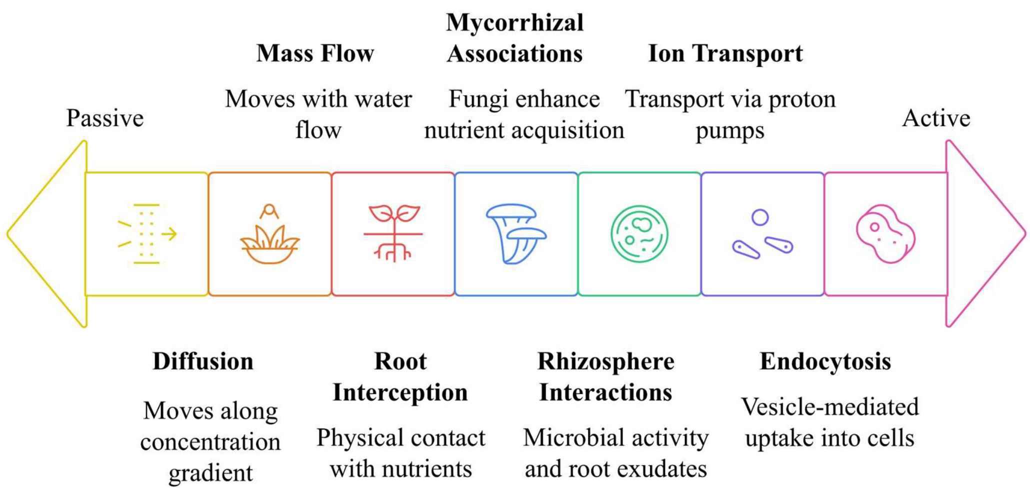

Figure 4.2 Plant nutrient uptake ranges from passive to active

4.3.1 Passive Nutrient Uptake

Passive nutrient uptake means that the plant absorbs nutrients from the soil without using its own energy (ATP). Instead, it depends on natural processes to move nutrients to the root surface. These processes include diffusion, mass flow, and root interception.

Diffusion

Diffusion is the passive movement of nutrient ions from an area of higher concentration (bulk soil) to an area of lower concentration (near root surface), driven by a concentration gradient created when plants absorb nutrients, lowering the ion concentration around the roots. As a result, nutrients naturally flow toward the roots until balance is achieved. (Jungk & Claassen, 1997). This process is described by Fick's First Law of Diffusion:

$$J_d = -D_s \frac{\partial C}{\partial r} \tag{4.1}$$

where J_d is the diffusion flux ($\mathrm{mg/cm^2/sec}$), D_s is the diffusion coefficient of the nutrient in the soil ($\mathrm{cm^2/sec}$), $\frac{\partial C}{\partial r}$ is the nutrient concentration gradient ($\mathrm{mg/cm^3/cm}$). Here D_s depends on soil tortuosity, soil porosity, moisture content, and temperature.

Diffusion plays a key role in transporting moderately mobile nutrients like potassium (K^+) and phosphate ions ($H_2PO_4^-$, HPO_4^{2-}) to the root surface. Several conditions affect its efficiency: higher nutrient concentrations in the soil enhance diffusion rates; sufficient soil moisture acts as a transport medium; and soil texture impacts the speed and retention of nutrients—sandy soils allow quicker diffusion due to larger pores but hold fewer nutrients, while clay soils retain more nutrients but slow diffusion due to smaller pores. Additionally, plants with larger root systems and more root hairs have greater surface area to absorb diffused nutrients effectively. Overall, diffusion is a crucial, energy-free method by which plants absorb essential nutrients from the surrounding soil environment.

Mass Flow

Mass flow refers to the transport of nutrients dissolved in water as the plant absorbs water through its roots. This process is driven by the plant's water uptake, primarily facilitated by transpiration. Transpiration creates a negative pressure gradient, pulling water from the soil into the root system. As water flows toward the roots, it carries dissolved nutrients in the soil solution, which are absorbed by the roots along with the water (Olsen & Kemper, 1968). The flux due to mass flow is given by

$$J_m = C \cdot q \tag{4.2}$$

where J_m is the mass flow flux (($\mathrm{mg/cm^2/sec}$)), C is the nutrient concentration in the soil solution ($\mathrm{mg/cm^3}$), q is the volume of water flux towards the root ($\mathrm{cm^3/sec}$).

Mass flow is particularly important for nutrients that are highly soluble and mobile in the soil, such as nitrogen NO_3^-, NH_4^+ for protein and chlorophyll synthesis, calcium Ca^{2+} for cell wall structure and signaling, and magnesium Mg^{2+} as a critical component of chlorophyll and enzyme activation. Several factors influence the effectiveness of mass flow. Higher transpiration rates enhance water and nutrient uptake by increasing the water flow from the soil to the plant. Sufficient soil moisture is essential to dissolve and transport nutrients effectively, while the solubility of nutrients in water determines their availability for mass flow. For instance, in arid conditions, reduced soil moisture and lower transpiration rates can significantly limit mass flow, often leading to nutrient deficiencies in plants.

Root interception

Root interception is the process by which roots physically grow into new soil regions and directly contact nutrients in the soil matrix. Unlike diffusion or mass flow, this mechanism relies on root growth and expansion to access untapped nutrient pools. As roots elongate and branch into new zones, they increase their surface area for nutrient uptake, a process further enhanced by root hairs and lateral roots (Tomobe et al., 2023). The flux due to root interception can be expressed as

$$J_r = \rho \cdot R \cdot \Delta r \tag{4.3}$$

where J_r is the nutrient uptake by root interception $(\mathrm{mg/cm^2/sec})$, ρ is the nutrient concentration in the soil solid phase (mg/g), R is the root density $(\mathrm{cm/cm^3})$, Δr is the root elongation or growth rate $(\mathrm{cm/sec})$.

Nutrients absorbed through root interception are typically immobile in the soil, requiring direct root contact for uptake. Key nutrients include phosphorus (P), which is often bound to soil particles, and zinc (Zn), a micronutrient critical for enzyme function and protein synthesis. The efficiency of root interception is influenced by several factors. Faster root growth increases the rate of interception, while compacted soils can hinder root penetration and reduce nutrient access. Plants with extensive lateral roots and well-developed root hairs are better equipped for interception. In nutrient-poor soils, plants like legumes often form symbiotic relationships with mycorrhizal fungi to extend their effective root network and improve nutrient interception, especially for immobile nutrients.

Combined Nutrient Uptake

In most scenarios, nutrient uptake is governed by the combined effects of diffusion, mass flow, and root interception. The total nutrient flux (J_t) can be expressed as:

$$J_t = J_d + J_m + J_r \tag{4.4}$$

where J_t represents the total nutrient flux towards the root surface due to all three mechanisms, J_d represents the contribution from diffusion, J_m represents the contribution from mass flow and J_r represents the contribution from root interception.

The relative contributions of each mechanism depend on the specific nutrient, soil properties, and environmental conditions. For example, diffusion dominates for immobile nutrients like phosphorus (P) and potassium (K^+), mass Flow is significant for mobile nutrients like nitrogen (NO_3^-) and calcium (Ca^{2+}) and root Interception plays a role in less mobile nutrients, especially when diffusion and mass flow are limited.

Table 4.1 Equations for Nutrient Uptake Mechanisms

Mechanism	Equation	Key Nutrients	Dominant Factors
Diffusion	$J_d = -D_s \frac{\partial C}{\partial r}$	Phosphorus (P), Potassium (K^+)	Soil moisture, nutrient gradient, soil texture.
Mass Flow	$J_m = C \cdot q$	Nitrogen (NO_3^-, NH_4^+), Calcium (Ca^{2+})	Transpiration, nutrient solubility, water flux.
Root Interception	$J_r = \rho \cdot R \cdot \Delta r$	Phosphorus (P), Zinc (Zn)	Root growth rate, root density, soil contact.

4.3.2 Active Nutrient Uptake

Active nutrient uptake is how plants absorb nutrients using energy (usually ATP), even when the nutrients are more concentrated inside the root than in the soil. This process moves nutrients against their natural flow. It includes methods like ion transport through cell membranes, endocytosis, symbiotic interactions, and other specific processes that help the plant get the nutrients it needs (Chapman et al., 2012).

Ion Transport Across Membrane

Ion transport across membranes is an active process where plant roots use energy (ATP) to take in nutrients like potassium (K^+), nitrate (NO_3^-), and phosphate ($H_2PO_4^-$), even when these are more concentrated inside the plant than in the soil. Special proteins in the root cell membrane help move these ions. Proton pumps (H^+-ATPase) push hydrogen ions (H^+) out of the cell, creating a charge difference. This helps pull positive ions like K^+ and Ca^{2+} into the cell, and negative ions like NO_3^- and Cl^- are absorbed using special carriers. This process is very important for getting key nutrients that plants need to grow and stay healthy (Reid & Hayes, 2003).

Endocytosis

Endocytosis is an active process where root cells use energy (ATP) to take in large nutrient particles or organic molecules. The cell membrane folds inward, wraps around the nutrient, and forms a vesicle that carries it inside the cell. These nutrients are then used, stored, or processed. Though not as common as other methods, endocytosis is important for taking in micronutrients and organic substances, especially from helpful soil microbes (Silverstein et al., 1977).

Mycorrhizal Associations

Mycorrhizal associations are helpful partnerships between plant roots and special fungi. These fungi grow on and around the roots and send out tiny threads (hyphae) into the soil, which increases the area for taking in nutrients. They help the plant absorb hard-to-reach nutrients like phosphorus (P), zinc (Zn), and copper (Cu), especially when these are low or stuck to soil particles. In return, the plant gives the fungi carbohydrates made during photosynthesis. This relationship is very important for nutrient uptake and healthy plant growth (Shi et al., 2023).

Rhizosphere Interactions

The rhizosphere is the area of soil right around plant roots, where important interactions happen to help plants absorb nutrients. Plant roots release organic acids, enzymes, and chemicals that make hard-to-get nutrients like phosphorus and iron easier to absorb. Helpful microbes in this zone also play a big role. For example, Rhizobium bacteria form nodules on legume roots and turn nitrogen from the air into usable form (ammonium, NH_4^+). Other bacteria like Azospirillum and Azotobacter increase nitrogen in the soil, and some microbes make siderophores, which help plants absorb iron. These interactions help plants take up more nitrogen, phosphorus, and iron, improving both plant growth and soil health (Souza et al., 2015).

Nutrient-Specific Mechanisms

Some nutrients like iron (Fe) and phosphorus (P) are hard for plants to absorb because they are not easily dissolved in the soil. To get iron, plants release special chemicals called siderophores that attach to iron and form a form the plant can absorb through its roots. For phosphorus, which is often stuck to soil particles, plant roots release organic acids like citric acid and malic acid to loosen and dissolve it. These special methods help plants absorb these important nutrients, which are needed for healthy growth and proper functioning (Goss et al., 1993).

Table 4.2 Summary of Nutrient Uptake Mechanisms in Plants

Mechanism	Energy Requirement	Key Nutrients	Process Description
Diffusion	Passive	$K^+, H_2PO_4^-$	Movement along a concentration gradient.
Mass Flow	Passive	$NO_3^-, NH_4^+, Ca^{2+}, Mg^{2+}$	Nutrients move with water flow towards roots.
Root Interception	Passive	P, Zn	Physical contact of roots with nutrients.
Ion Transport	Active	$NO_3^-, K^+, H_2PO_4^-$	Transport via proton pumps and carriers.
Endocytosis	Active	Micronutrients, organic molecules	Vesicle-mediated uptake into root cells.
Mycorrhizal Associations	Passive (Symbiotic)	P, Zn, Cu	Fungi enhance nutrient acquisition.
Rhizosphere Interactions	Both	N, P, Fe	Microbial activity and root exudates.

4.4 Nutrient Uptake Models

Nutrient uptake models have been extensively studied to understand the dynamics of plant nutrient absorption and optimize agricultural practices. Over the years, research has evolved from simplified single-branch models to sophisticated multi-branched models that account for the complexities of root architecture and soil heterogeneity. This section reviews the key developments, methodologies, and applications of both model types.

4.4.1 Single-Branch Nutrient Uptake Models

Single-branch nutrient uptake models have served as the foundation for studying nutrient transport and absorption mechanisms, with early contributions like Barber's Nutrient Uptake Model (1984), which focused on the radial movement of nutrients through diffusion and mass flow, relying on Fick's law of diffusion and Michaelis-Menten kinetics to describe uptake rates based on soil nutrient concentration and root absorption capacity. Nye and Tinker (1977) expanded on this by exploring the effects of root radius, nutrient depletion zones, and soil properties, while Clarkson (1985) integrated the impact of soil moisture and its interaction with nutrient availability (Roose et al., 2001). These models, characterized by their simplicity and computational efficiency, are ideal for investigating fundamental nutrient dynamics under uniform soil conditions. However, their limitations include an inability to account for the complexity of real-world root systems, heterogeneous nutrient distributions, root branching, and inter-root competition, making them less applicable for modeling complex agricultural or environmental scenarios.

4.4.2 Multi-Branched Nutrient Uptake Models

The limitations of single-branch models led to the development of multi-branched nutrient uptake models, which incorporate the hierarchical structure of root systems and account for spatial variations in soil properties. Emerging in the late 1990s, these models gained traction with advancements in computational power and imaging technologies. Notable contributions include (Dunbabin et al., 2003) who combined detailed root architecture with dynamic soil nutrient profiles to explore the impact of root branching on nutrient uptake, and Roose and Fowler (2004), who introduced mathematical models with 3D root structures for simulating uptake in heterogeneous soils. (Postma et al., 2014) integrated dynamic root growth into models to simulate nutrient uptake over time, while Pagès et al. (2010) emphasized root plasticity and the adaptive role of lateral roots and root hairs. Multi-branched models offer realistic simulations of nutrient uptake by accounting for root competition, synergistic interactions, and dynamic soil changes, making them invaluable for studying nutrient acquisition and plant performance. However, their high computational demand and the need for detailed input data, such as root growth patterns and soil nutrient distributions, present significant challenges.

Table 4.3 Comparison of Existing Nutrient Uptake Models

Model	**Type**	**Root Architecture**	**Nutrient Transport Mechanisms**	**Strengths**
Barber™s Model (1984)	Single-branch	Single cylindrical root	Diffusion, mass flow, Michaelis-Menten uptake	Analytical simplicity, widely used for nutrient depletion analysis
Nye & Tinker (1977)	Single-branch	Single root model	Diffusion, convection, soil buffering effects	Includes soil nutrient buffering
Clarkson Model (1985)	Single-branch	Single cylindrical root	Diffusion, mass flow, root absorption kinetics	Accounts for soil moisture influence on nutrient uptake
Dunbabin et al. (2002)	Multi-branched	Branched root network	Diffusion, mass flow, root plasticity response	Includes realistic RSA and environmental interactions
Roose & Fowler (2004)	Multi-branched	3D RSA model	Convection-diffusion equations, root competition	Realistic 3D simulation of nutrient uptake dynamics
Postma et al. (2014)	Multi-branched	Dynamic root growth	Root growth kinetics, nutrient availability feedback	Simulates root plasticity, adaptation to soil heterogeneity
Pag¨s et al. (2010)	Multi-branched	Root plasticity models	Dynamic uptake based on soil conditions	Captures adaptive RSA behavior in response to nutrient availability
Machine Learning Models (Recent Advances)	AI-based	Data-driven RSA reconstruction	Uses big data, ML, and real-time soil-plant interactions	Can optimize predictions based on experimental data

4.5 Development of a Multiple Root Branching Model

The soil volume surrounding a root is partitioned into three fractions: solid (ϕ_s), liquid (ϕ_l), and gas (ϕ_g). Assuming the absence of additional phases such as microbes or mucigel, the conservation of soil volume is expressed as:

$$\phi_s + \phi_l + \phi_g = 1 \tag{4.5}$$

The soil porosity (ϕ) is defined as $\phi = \phi_l + \phi_g$. For fully saturated soil, where no air is present, $\phi = \phi_l$.

Nutrient transport in soil involves exchanges between the solid and liquid phases, as well as diffusion and convection within the liquid phase. Diffusion in the solid phase is negligible due to its slow rate. Thus, the conservation equation for ions in the solid phase, assuming no diffusion within this phase, is:

$$\frac{\partial c_s}{\partial t} = d_s \tag{4.6}$$

where c_s represents the concentration of ions in the solid phase (mass per unit volume of soil) and d_s is the rate of interfacial ion transport between the solid and liquid phases.

Nutrient ions in the liquid phase are transported to the root surface by water flow (convection) and by diffusion through the soil's pore water. The conservation equation for ions in the liquid phase is:

$$\frac{\partial}{\partial t}(\phi_l c_l) + \nabla \cdot (c_l u) = \nabla \cdot (\phi_l D \nabla c_l) + d_l \tag{4.7}$$

Here c_l is the nutrient concentration in the liquid phase, $d_l$is the rate of solid-liquid interfacial ion transport, u is the Darcy flux of water (volume flux) and D is the diffusion coefficient in the liquid phase.

According to Nye and Tinker and Barber, the diffusion coefficient (D) in the soil is modeled as $D = D_f f$, where D_f is the diffusion coefficient in free liquid and f is the tortuosity factor. The tortuosity factor f is often approximated as $f \approx \phi_l^d$ with $1 \leq d < 2$, although its exact value is typically determined experimentally under different soil moisture conditions.

Combining the equations for ions in the solid and liquid phases gives the overall nutrient conservation equation:

$$\frac{\partial}{\partial t}(\phi_l c_l + c_s) + \nabla \cdot (c_l u) = \nabla \cdot (\phi_l D \nabla c_l) + d_l + d_s \tag{4.8}$$

Assuming mass conservation during interfacial transport $(d_l + d_s = 0)$, we define: Adsorption: attachment of ions to solid particles, Desorption: detachment of ions from solid particles to water.

If k_a is the adsorption rate and k_d the desorption rate, the interfacial transport rate is:

$$d_s = k_a c_l - k_d c_s = \frac{(k_a/k_d)c_l - c_s}{1/k_d} \tag{4.9}$$

Assuming rapid desorption $1/k_d \to 0$, we obtain:

$$c_s = \frac{k_a}{k_d} c_l = b c_l \tag{4.10}$$

where $b = k_a/k_d$ is the soil buffer power.

Substituting $c_s = bc_l$ into the conservation equation for c_l:

$$(b + \phi_l)\frac{\partial c_l}{\partial t} + \nabla \cdot (c_l u) = \nabla \cdot (\phi_l D \nabla c_l) \tag{4.11}$$

Denoting $c_l = c$ and transforming to radial coordinates, the equation becomes:

$$(b + \phi_l)\frac{\partial c}{\partial t} - \frac{aV}{r}\frac{\partial c}{\partial r} = D\phi_l \frac{1}{r}\frac{\partial}{\partial r}\left(r\frac{\partial c}{\partial r}\right) \tag{4.12}$$

Here a is the root radius, $V\ is\ the$ Darcy flux of water into the root, derived from mass conservation $\nabla \cdot u = 0$ with $u = -a\,V\,/\,r$.

The effective diffusion coefficient is defined as:

$$D_{\text{eff}} = \frac{D_f f \phi_l}{\phi_l + b} \tag{4.13}$$

For $b \gg 1, D_{\text{eff}} \approx \frac{D_f f \phi_l}{b}$.

4.5.1 Initial and Boundary Conditions

Boundary Condition at the Root Surface

Experimental data suggest that nutrient uptake at the root surface is subject to a saturation effect, whereby increasing the concentration indefinitely does not increase the uptake proportionally. Additionally, a critical concentration threshold exists below which nutrient flux into the root ceases, and instead, nutrients may be expelled from the root back into the soil. The boundary condition at the root surface, described by a heuristic Michaelis-Menten type equation, is expressed as:

$$\phi_l D \frac{\partial c}{\partial r} + Vc = \frac{F_m c}{K_m + c} - E \quad \text{at} \quad r = a \tag{4.14}$$

Here c is the nutrient concentration in the liquid phase at the root surface, F_m is the Maximum nutrient flux into the root, K_m is the Michaelis-Menten constant, representing the concentration at which the nutrient flux is half of F_m, E is the rate at which nutrients are expelled from the root, calculated as $E = \frac{F_m c_{min}}{K_m + c_{min}}$, where c_{min} is the minimum concentration at which nutrient uptake ceases, a : Radius of the root.

Initial Condition and Boundary Condition Away from the Root

Initially, at time $t = 0$, it is assumed that the nutrient concentration is uniformly distributed throughout the soil's liquid phase. Therefore, the initial condition is set as:

$$c = c_0 \quad \text{at} \quad t = 0 \quad \text{for} \quad a < r < \infty \tag{4.15}$$

As time progresses, the nutrient concentration far from the root is assumed to remain at this initial level, effectively establishing a far-field boundary condition:

$$c \to c_0 \quad \text{as} \quad r \to \infty \quad \text{for} \quad t > 0 \tag{4.16}$$

This condition is referred to as the nutrient far-field boundary condition, ensuring that the influence of the root on the soil's nutrient concentration diminishes with distance.

4.5.2 Non-Dimensionalisation and Parameter Estimation

The Nye-Tinker-Barber model, as described earlier, is a diffusion-convection equation with a non-linear boundary condition. This non-linearity necessitated numerical solutions, as carried out by Nye and Tinker and Barber. Numerical solutions, while straightforward using methods such as implicit finite difference schemes (Chakraborty & Kadoli, 2014), require separate computations for each set of parameter configurations. This process is not only time-consuming but also limits the model's scalability to incorporate more realistic root structures, such as root branching.

In this chapter, we first non-dimensionalise the model to identify parameter combinations influencing the solution. Subsequently, we derive analytical approximations to the solution under various parameter limits. These analytical solutions will serve as a foundation for scaling the model from a single cylindrical root to a root branching structure in the subsequent chapters.

Non-Dimensionalisation

To simplify the model, we introduce non-dimensional variables by scaling time, space, and concentration as follows:

$$t = \frac{a^2(\phi_l + b)}{D\phi_l} t^*, \quad r = ar^*, \quad c = K_m c^* \tag{4.17}$$

Here t^* , r^* and c^* are dimensionless time, radial, and concentration variables, respectively. Substituting these scales into the model and omitting the * notation for simplicity, the dimensionless model is given by:

$$\frac{\partial c}{\partial t} - P_e \frac{1}{r}\frac{\partial c}{\partial r} = \frac{1}{r}\frac{\partial}{\partial r}\left(r\frac{\partial c}{\partial r}\right) \tag{4.18}$$

with the following boundary conditions:

$$\frac{\partial c}{\partial r} + P_e c = \lambda \frac{c}{1 + c} - \epsilon \quad \text{at} \quad r = 1, \tag{4.19}$$

$$c \to c_\infty \quad \text{as} \quad r \to \infty \quad \text{for} \quad t > 0 \tag{4.20}$$

and the initial condition:

$$c = c_\infty \quad \text{at} \quad t = 0 \quad \text{for} \quad 1 < r < \infty \tag{4.21}$$

The dimensionless parameters introduced are defined as:

$$P_e = \frac{aV}{D\phi_l}, \quad \lambda = \frac{F_m a}{DK_m\phi_l}, \quad \epsilon = \frac{Ea}{DK_m\phi_l}, \quad c_\infty = \frac{c_0}{K_m} \tag{4.22}$$

By this process, the original model with eight dimensional parameters is reduced to a model with four dimensionless parameters. These parameters include:

P_e (Péclet number): Represents the balance between water movement (V) and diffusion $(D\phi_l)$ over the characteristic length scale a, λ : Dimensionless nutrient uptake parameter, c_∞ : Dimensionless far-field nutrient concentration and ϵ : Represents the minimum concentration below which nutrient uptake ceases.

This reduction not only simplifies the analysis of the model but also highlights the dominant factors influencing nutrient transport and uptake, making it more adaptable for extending the model to complex root architectures.

Parameter Estimation

The diffusion coefficient for nutrient ions in free water, D, and the Darcy flux of water, V, are relatively constant across most nutrients. Consequently, the Péclet number, P_e, varies primarily with the root radius, a, under a given soil moisture condition ϕ_l.

If $a \ll D\phi_l/V$, the convection term is negligible, and nutrient transport is dominated by diffusion. Conversely, if $a \gg D\phi_l/V$, diffusion becomes negligible, and mass flow primarily governs nutrient transport. Typical values for D are around $10^{-5}\,\mathrm{cm^2s^{-1}}$, while V is approximately $10^{-7}\,\mathrm{cms^{-1}}$. The Péclet number is defined as:

$$P_e = \frac{aV}{D_f f \phi_l}, \tag{4.23}$$

where f is the diffusion impedance factor, and ϕ_l typically ranges from 0.1 to 0.5 for crop-suitable soils. For root radii typical of agricultural plants $(0.0005\,\mathrm{cm} \le a \le 0.06\,\mathrm{cm})$, P_e is very small, on the order of 10^{-5} to 10^{-2}, indicating diffusion dominance.

In most cases, P_e -related terms are negligible compared to λ-related terms, as λ depends linearly on a. For typical plants, $V < F_m/K_m$, ensuring $P_e <$. An exception is calcium, where $\lambda \approx P_e$, requiring inclusion of $O(P_e)$ terms in the boundary condition.

Key Cases and Solutions

Now, we explore different cases in the mathematical model of nutrient uptake, specifically focusing on how nutrient concentration at the far-field (c_∞) affects the model's behavior under different conditions, starting from the small far-field concentration limit and progressing through the other regimes. These cases describe different regimes of nutrient transport in the soil based on the relative magnitudes of

c_∞ and λ. The main takeaway is that nutrient accumulation or depletion around the root, and the concentration gradient, depends strongly on both the soil nutrient concentration and the root's uptake efficiency. Each of the cases introduces a different approximation or scaling for the concentration profile, leading to a diverse set of behaviors for nutrient dynamics in the root zone.

1. The Limit $c_\infty \ll 1$

This limit corresponds to a scenario where the soil is nutrient-depleted or the nutrient concentration is very low in the far field. When c_∞ (the far-field concentration of nutrients) is very small, it indicates a situation where nutrient availability in the soil is low. This typically corresponds to nutrient-limited conditions, such as in semi-arid regions or where soil fertility is poor.

Approximate Solution for $\lambda \gg 1$

In this case, the root uptake capacity is much greater than the nutrient concentration in the soil. The root will absorb nutrients very efficiently, and there will be little to no accumulation of nutrients near the root. The concentration profile will be primarily determined by diffusion to the root, with a very steep gradient.

Assumption: Since $\lambda \gg 1$, the concentration gradient near the root will be very steep because the root absorbs nutrients faster than they can diffuse toward it. Essentially, the nutrient concentration at the root surface will be close to zero.

Solution: For $\lambda \gg 1$, we approximate the nutrient concentration near the root as being very small. In this case, the diffusion term dominates in the far field, and the solution to the equation is dominated by a boundary condition that effectively has no nutrient accumulation at the root surface.

$$\frac{d^2c(r)}{dr^2} = \frac{\lambda}{D}c(r) \tag{4.24}$$

The general solution is:

$$c(r) = Ae^{-\sqrt{\frac{\lambda}{D}}r} \tag{4.25}$$

Where A is a constant determined by the boundary conditions. At the root surface $(r = a)$:

$$-D\frac{dc}{dr}\bigg|_{r=a} = \lambda c(a) \tag{4.26}$$

This leads to the zero-sink model, where the nutrient concentration at the root surface is negligibly small compared to the concentration in the soil.

Physical Interpretation: The plant's root system absorbs nutrients so efficiently that there is no accumulation near the root, and the nutrient concentration at the root surface remains essentially zero.

Zero-sink Model

The zero-sink approximation arises when the nutrient uptake is so efficient that nutrients do not accumulate near the root surface. Essentially, the plant's root capacity is large enough to prevent any significant concentration build-up at the root interface. Therefore, the root surface is not a "sink" for the nutrients, and the nutrients are absorbed nearly instantaneously.

Mathematical Implications: The nutrient concentration at the root surface will remain very low, and the nutrient flux at the root is set by the diffusion of nutrients from the surrounding soil to the root surface.

Solution Approach: The nutrient transport equation will be dominated by diffusion with minimal interference from the root's uptake. The boundary condition at the root will be simplified, and nutrient concentration will decay smoothly from the root surface to the far field.

$$\frac{\partial c}{\partial r}\bigg|_{r=a} = 0 \tag{4.27}$$

Physical Interpretation: The concentration of nutrients near the root will be nearly uniform, and there will be no substantial nutrient gradient between the root and the soil.

Approximate Solution for $\boldsymbol{\lambda \ll 1}$

In this case, the root’s uptake capacity is much lower than the nutrient concentration in the soil. The root is inefficient at absorbing nutrients, leading to a significant accumulation of nutrients around the root surface. Nutrient diffusion from the soil is slower than the root's absorption rate, causing a steep concentration gradient near the root.

Assumption: Since $\lambda \ll 1$, the concentration at the root surface will be much larger than in the far field because the root uptake is weak, and nutrients accumulate at the root interface.

Solution: For $\lambda \ll 1$, the concentration at the root surface will be large, and the nutrient flux will be dominated by diffusion from the surrounding soil to the root. The concentration profile near the root is governed by the following equation:

$$\frac{d^2c(r)}{dr^2} = -\frac{\lambda}{D}c(r) \tag{4.28}$$

The general solution to this equation is:

$$c(r) = Ae^{\sqrt{\frac{\lambda}{D}}r} \tag{4.29}$$

This is an exponential solution, indicating that the concentration at the root surface increases significantly compared to the concentration in the far field. At the root surface ($r = a$):

$$\left.\frac{\partial c}{\partial r}\right|_{r=a} = -\lambda c(a) \tag{4.30}$$

Physical Interpretation: In this scenario, nutrient concentration builds up near the root surface because the root cannot absorb nutrients fast enough, leading to a high concentration at the root and a large concentration gradient in the soil.

2. The Limit $c_\infty \gg 1$

This limit corresponds to a scenario where the soil is nutrient-rich, and the concentration of nutrients in the far field is high. This is a situation where the soil is well-fertilized or inherently nutrient-rich, and the model will describe nutrient transport from this abundant supply to the plant roots.

Approximate Solution for $\lambda \gg 1$

Here, the root's uptake capacity is much larger than the nutrient concentration in the soil. Since c_∞ is high, the root absorbs nutrients quickly, and there will be a steep concentration gradient near the root surface. The concentration at the root surface will approach the saturation level.

Solution: In this case, the nutrient concentration at the root surface will approach a maximum value, often described by the Michaelis-Menten constant K_m. This constant is the nutrient concentration at which the root reaches half of its maximum uptake capacity. The nutrient uptake becomes saturated when $c(a) \sim K_m$, and the system behaves according to the Michaelis-Menten kinetics.

The governing equation becomes:

$$-D\frac{dc}{dr}\bigg|_{r=a} = \lambda c(a) \tag{4.31}$$

where $c(a)$ saturates at the maximum uptake rate.

As the concentration approaches saturation, the equation can be written as:

$$\phi_l D\frac{\partial c}{\partial r} + Vc = \frac{F_m c}{K_m + c} - E \quad \text{at} \quad r = a \tag{4.32}$$

Physical Interpretation: Nutrient uptake at the root becomes constrained by the root's maximum capacity to absorb, and the concentration at the root surface approaches a saturation point. The concentration gradient near the root will be steep, with rapid nutrient uptake near the root surface and slower movement further out into the soil.

Approximate Solution for $\boldsymbol{\lambda \ll 1}$

In this case, λ is small, so the root's uptake capacity is weak compared to the available nutrient supply. The concentration at the root surface remains near c_∞, and there is a small gradient near the root.

Solution: The solution for $\lambda \ll 1$ is nearly constant throughout the root zone, with the concentration at the root surface approaching c_∞ (the concentration in the soil far away from the root). The nutrient gradient is shallow and primarily driven by diffusion.

$$\frac{\partial c}{\partial r}\bigg|_{r=a} = -\lambda c(a) \tag{4.33}$$

Here, the nutrient uptake does not significantly affect the concentration in the soil around the root, and the concentration near the root will remain close to c_∞.

Physical Interpretation: The root will be able to absorb nutrients at a slower rate, and the system behaves more like a passive diffusion system with a low nutrient uptake rate.

3. The Regime $c_\infty = O(1)$

In this regime, the nutrient concentration at the far-field is moderate, neither very low nor very high. This represents a balanced scenario where the root's uptake capacity is comparable to the nutrient supply.

Approximation for $\lambda \ll 1$

In this case, the root's uptake is weak, and there will be significant nutrient accumulation near the root surface. The concentration near the root will be much higher than the concentration in the far field. Since the root cannot absorb nutrients as efficiently as they are supplied, a substantial nutrient gradient forms between the root and the surrounding soil.

Solution: The concentration profile will be dominated by diffusion, and the concentration at the root will be governed by:

$$\frac{d^2c(r)}{dr^2} = -\frac{\lambda}{D}c(r) \tag{4.34}$$

This equation leads to an exponential profile of the form:

$$c(r) = Ae^{\sqrt{\frac{\lambda}{D}}r} \tag{4.35}$$

The concentration at the root surface will be higher than \(c_\infty\), and the nutrient gradient will drive diffusion toward the root. The concentration profile near the root will exhibit a typical diffusion-dominated behavior, with the root acting as a weak sink for the nutrients.

$$\left.\frac{\partial c}{\partial r}\right|_{r=a} = -\lambda c(a) \tag{4.36}$$

Physical Interpretation: Nutrient concentration at the root will be higher than in the far field but will not saturate the root. Nutrient uptake will be limited, and diffusion will dominate in transporting nutrients to the root.

Approximation for $\lambda \gg 1$

In this case, the root's uptake capacity is strong, and the nutrient concentration at the root surface will quickly reach a value close to K_m, the maximum rate of uptake. This saturation at the root surface limits further nutrient uptake, as the root can only absorb nutrients up to a certain level.

Solution: The nutrient profile near the root will resemble a zero-sink model, and the concentration at the root will decrease exponentially:

$$c(r) = Ae^{-\sqrt{\frac{\lambda}{D}}r} \tag{4.37}$$

The concentration at the root surface will be controlled by the Michaelis-Menten kinetics, with the nutrient concentration near the root surface approaching the saturation level, K_m. The nutrient gradient between the root and the soil will be steep, especially near the root.

$$\phi_l D \frac{\partial c}{\partial r} + Vc = \frac{F_m c}{K_m + c} - E \quad \text{at} \quad r = a \tag{4.38}$$

Physical Interpretation: The root absorbs nutrients quickly until it reaches the saturation point. The concentration at the root surface will be near K_m, and nutrient uptake is controlled by the Michaelis-Menten constant.

Regime $\boldsymbol{\lambda = O(1)}$

In the case, the root's uptake capacity is comparable to the nutrient diffusion, and the concentration gradient around the root will be moderate. The nutrient concentration at the root surface will be determined by a balance between diffusion, convection, and uptake.

Solution: This scenario leads to a solution where the nutrient concentration at the root surface is balanced by both diffusion and uptake, and the concentration profile near the root is neither steep nor flat. In this regime, the nutrient concentration at the root surface is determined by the interaction between the root's ability to uptake nutrients and the nutrient flux coming from the surrounding soil. The nutrient concentration profile will reflect both the supply of nutrients and the root's uptake ability, without completely dominating.

$$\left.\frac{\partial c}{\partial r}\right|_{r=a} = -\lambda c(a) \tag{4.39}$$

Physical Interpretation: The root efficiently absorbs nutrients, but the concentration at the root surface remains balanced with the supply in the soil. The system is in equilibrium, with nutrients moving toward the root at a rate that matches the uptake.

Table 4.4 Summary of Regimes and Approximations

Regime	$\lambda \gg 1$	$\lambda \ll 1$
$c_\infty \ll 1$	Zero-sink model: Nutrient uptake dominates, No significant nutrient build-up at the root.	Weak uptake: Nutrient accumulates near the root, Slow root absorption leads to high gradients.
$c_\infty \gg 1$	Saturation at root surface: Michaelis-Menten kinetics dominate, Steep gradients near the root.	Passive uptake: Concentration near the root remains close to c_∞.
$c_\infty = O(1)$	Efficient uptake: Root uptake balances diffusion, Moderate gradients near the root.	Diffusion-dominated: Weak root uptake causes accumulation near the root surface.

4.6 Model Results and Discussion

The HYDRUS-1D model was utilized to simulate one-dimensional water and nitrate uptake in a 100 cm soil profile across four representative soil profiles in Jaipur—Amer, Virat Nagar, Dudu, and Sambhar Lake from each Agro economic zone. The crop selected for 120 days simulation was wheat (*Triticum aestivum* L., variety Raj 4037), which is predominant in this region. The model domain was discretized into 101 spatial nodes with soil hydraulic properties defined using zone-specific van Genuchten parameters. The simulations integrate site-specific soil hydraulic properties, nitrate transport parameters, and variable rainfall and fertigation schedules.

Initial conditions included a uniform pressure head of -100 cm and a uniform nitrate concentration of 5 mg/L throughout the profile. Boundary conditions for water flow included a constant surface flux (representing irrigation or rainfall) at the top and a free drainage boundary at the bottom. Solute (nitrate) transport was governed by a concentration flux boundary at the surface and a zero-concentration gradient at the lower boundary.

Root water uptake was simulated using the Feddes model, while nitrate uptake by roots was implemented using a Michaelis–Menten-type approach. The simulations covered multiple crop growth stages (T0–T5) and outputs included nitrate concentration profiles, nitrate uptake rates, and cumulative uptake for all zones.

Surface Nitrate Concentration over Time

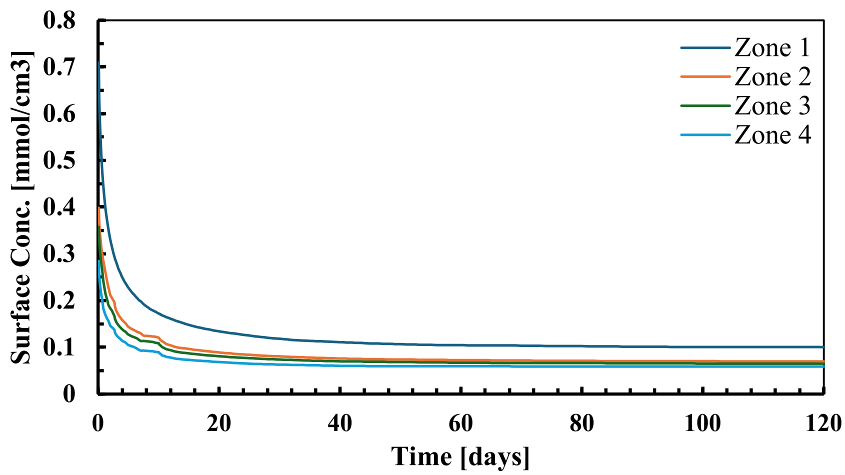

Figure 4.3 Temporal variation of surface nitrate concentration across Jaipur's agro-ecological zones.

Over the 120-day wheat season, nitrate concentrations showed clear zone-wise differences. Zone 1 (Amer) began with the highest level (~0.72 mmol/cm³) and remained higher throughout due to rapid drainage and low retention. All zones experienced a sharp decline in the first 10 days from uptake and leaching, after which values stabilized. By Day 100, surface nitrate settled at ~0.12 mmol/cm³ (Zone 1), 0.09 (Zone 2), 0.08 (Zone 3), and 0.075 (Zone 4). Finer soils, such as in Sambhar Lake (Zone 4), retained less nitrate at the surface, reflecting stronger leaching or uptake. These results emphasize the need for site-specific nitrogen strategies—split applications in Amer and leaching control in Sambhar.

Root Zone Nitrate Concentration

HYDRUS-1D simulations over 120 days demonstrated clear spatial variability in nitrate accumulation within the 0–100 cm root zone across the four sites. Zone 1 (Amer) recorded the highest buildup, exceeding ~0.006 mmol/cm³ by Day 120, followed by Zone 2 (Virat Nagar) at ~0.003 mmol/cm³, Zone 3 (Dudu) with slightly lower levels, and Zone 4 (Sambhar Lake) stabilizing near ~0.002 mmol/cm³. These differences reflect soil texture effects: the coarser soil of Amer slowed leaching and allowed greater surface retention, while the finer soils of Sambhar promoted deeper nitrate movement or enhanced uptake. The results underscore the need for site-specific nitrogen strategies, with slow-release fertilizers more effective in Amer and frequent, low-dose applications better suited for Sambhar.

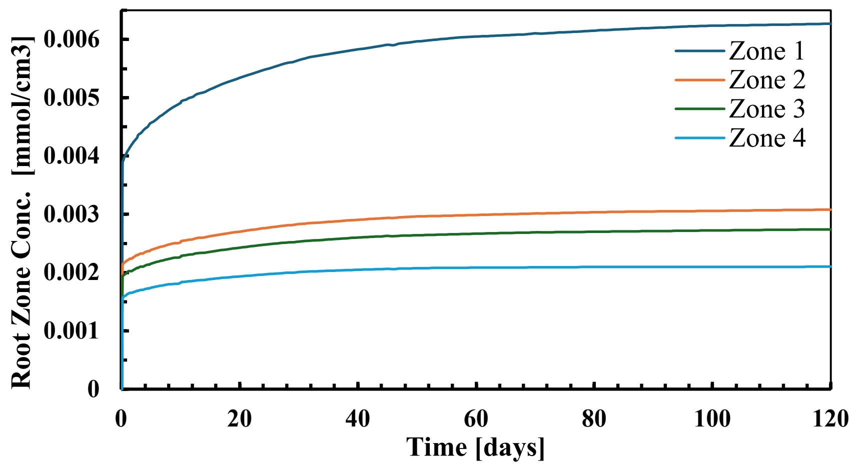

Figure 4.3 Temporal variation in root zone nitrate concentration across Jaipur's agro-ecological zones.

Bottom Nitrate Concentration

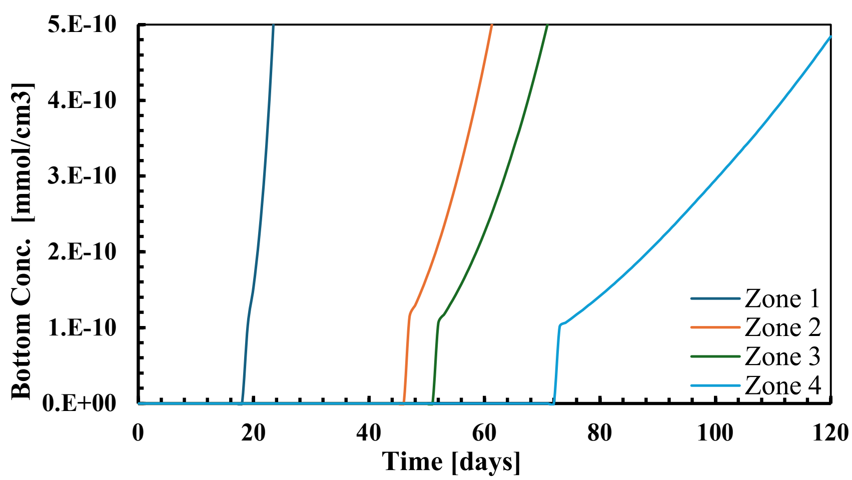

Figure 4.4 Temporal evolution of nitrate concentration at the bottom boundary of the soil profile across Jaipur's agro-ecological zones

HYDRUS-1D simulations over 120 days revealed zone-specific nitrate breakthrough patterns at the 100 cm soil profile bottom. Zone 1 (Amer) exhibited the earliest breakthrough (~Day 20), followed by Zone 2 (Virat Nagar, ~Day 40), Zone 3 (Dudu, ~Day 50), and Zone 4 (Sambhar Lake, ~Day 75). The early onset in Zone 1 reflects rapid leaching due to sandy texture and low water retention, while delayed movement in Zone 4 is consistent with its higher clay content and stronger nitrate retention. These results suggest Zone 1 poses higher risk for groundwater contamination, whereas Zone 4 offers greater nitrate retention but may still require careful fertilizer management under heavy irrigation.

Nitrate Concentration Profile with Depth

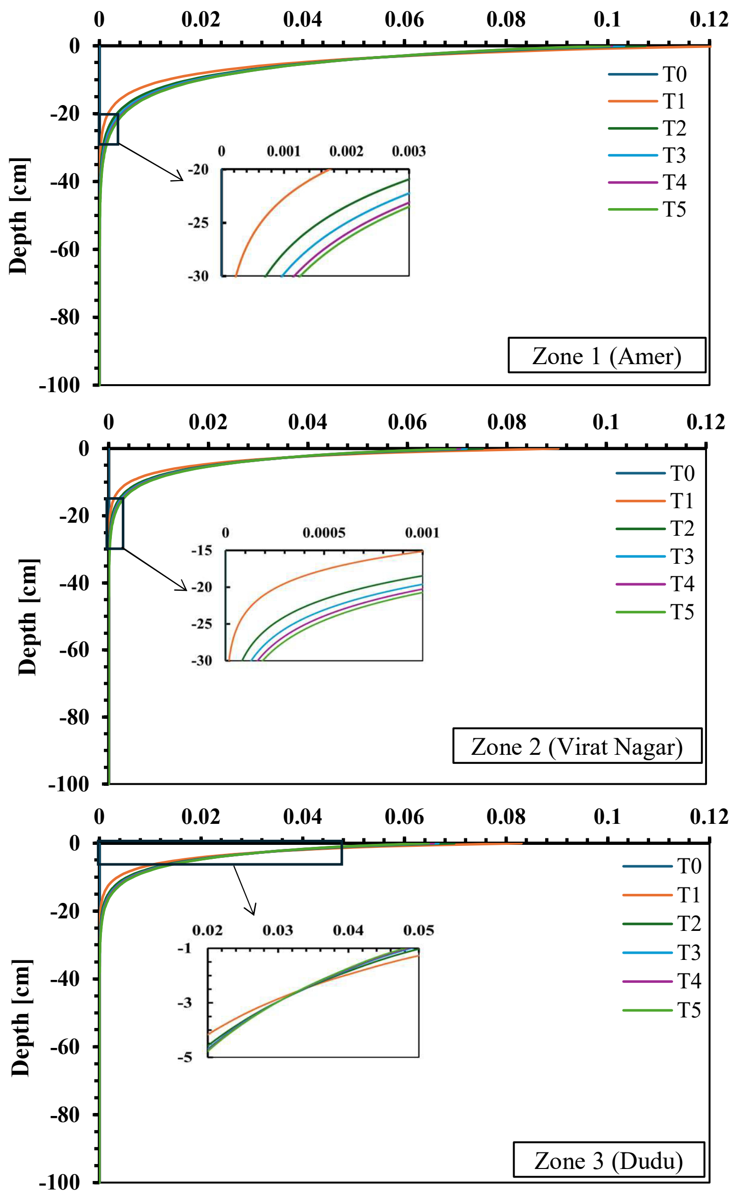

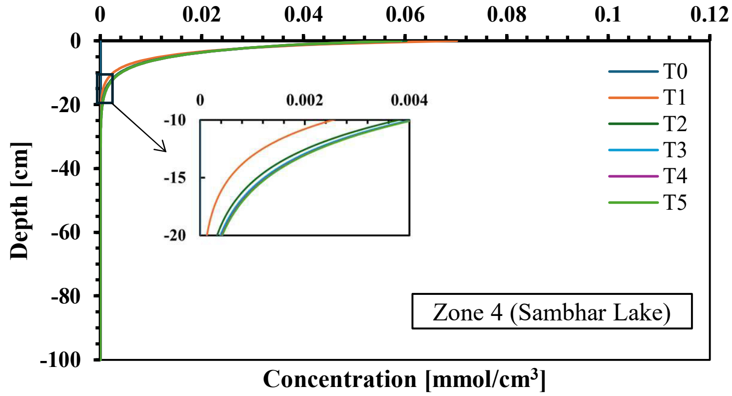

Figure 4.5 Nitrate concentration profiles at time steps T1–T5 as a function of soil depth.

HYDRUS-1D simulations of nitrate distribution across the 0–100 cm soil profile in Jaipur revealed distinct zone-specific leaching behaviors shaped by soil texture. In Zone 1 (Amer), surface nitrate was initially highest (0.1268 mmol/cm³ at T1) but declined rapidly as leaching progressed, with concentrations above 0.05 mmol/cm³ still present in the top 10 cm by T5 and measurable amounts reaching 100 cm, highlighting the high mobility of sandy loam soils. Zone 2 (Virat Nagar) showed a lower initial peak (0.09034 mmol/cm³) that decreased to 0.06963 mmol/cm³ by T5, with nitrate persisting in the top 20 cm and trace levels detectable at 100 cm, reflecting moderate vulnerability of loamy soils. Zone 3 (Dudu) followed a similar pattern, with surface concentrations falling from 0.083 to 0.0648 mmol/cm³, nitrate remaining between 0.048–0.029 mmol/cm³ in the upper 20 cm, and faint traces observed at 100 cm, suggesting intermediate retention that requires careful nutrient scheduling. Zone 4 (Sambhar Lake) displayed the slowest nitrate migration, with surface levels reducing from 0.07019 to 0.05909 mmol/cm³ and most nitrate confined to the top 40 cm due to finer soil texture and higher water-holding capacity, though trace amounts still leached beyond 90 cm under irrigation. Collectively, the results show that Amer soils are most prone to rapid nitrate loss, while Sambhar soils retain nitrate longer in the root zone, underscoring the need for site-specific nitrogen management strategies such as split applications in sandy soils and irrigation-synchronized fertilization in finer-textured soils.

Root Solute Uptake

HYDRUS-1D simulations over the 120-day wheat season showed clear differences in how roots absorbed nitrate across the four zones. Zone 1 (Amer) recorded the highest uptake rates, with a sharp peak of about 0.00075 mmol/cm²/day between Days 35 and

45, reflecting greater nitrate availability in its sandy soils. Zones 2 (Virat Nagar) and 3 (Dudu) displayed more moderate and smoother uptake patterns, peaking near 0.0003 mmol/cm²/day, while Zone 4 (Sambhar Lake) consistently remained the lowest, with uptake stabilizing at much smaller values. These patterns underline how soil texture influences nitrate supply to roots, reinforcing the need for location-specific fertilizer scheduling and placement.

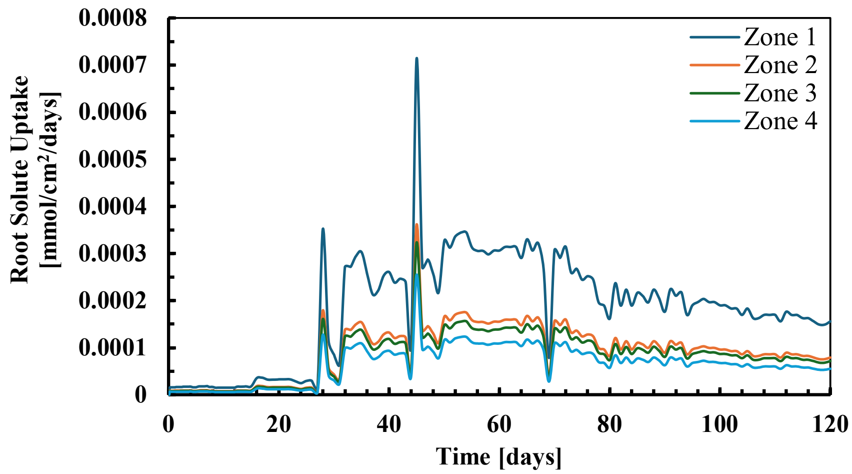

Figure 4.6 Temporal dynamics of root nitrate uptake rate in Jaipur's agro-ecological zones

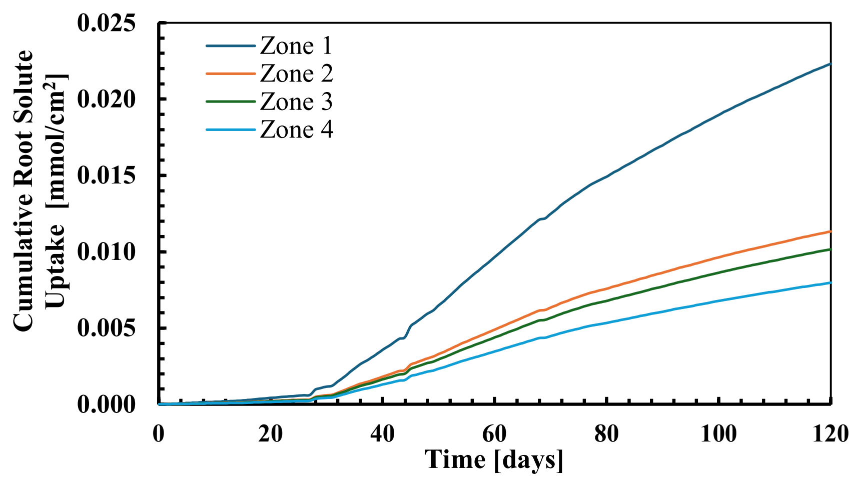

Figure 4.7 Cumulative root solute uptake over time for different zones of Jaipur

Cumulative Root Solute Uptake

When cumulative uptake was considered, Zone 1 again stood out, surpassing 0.022 mmol/cm² by Day 120 due to both higher availability and faster uptake rates. Virat Nagar and Dudu followed with totals of about 0.014–0.015 mmol/cm², suggesting soils that support steady nutrient absorption. In contrast, Sambhar Lake showed the lowest cumulative uptake (~0.012 mmol/cm²), likely because finer-textured soils allowed greater leaching or reduced retention. Together, these findings highlight the importance of adopting site-tailored fertilizer strategies—for example, using split or slow-release applications in sandy soils and careful timing in finer soils—to improve nitrogen use efficiency while reducing losses.

Root Nitrate Uptake with Soil Depth

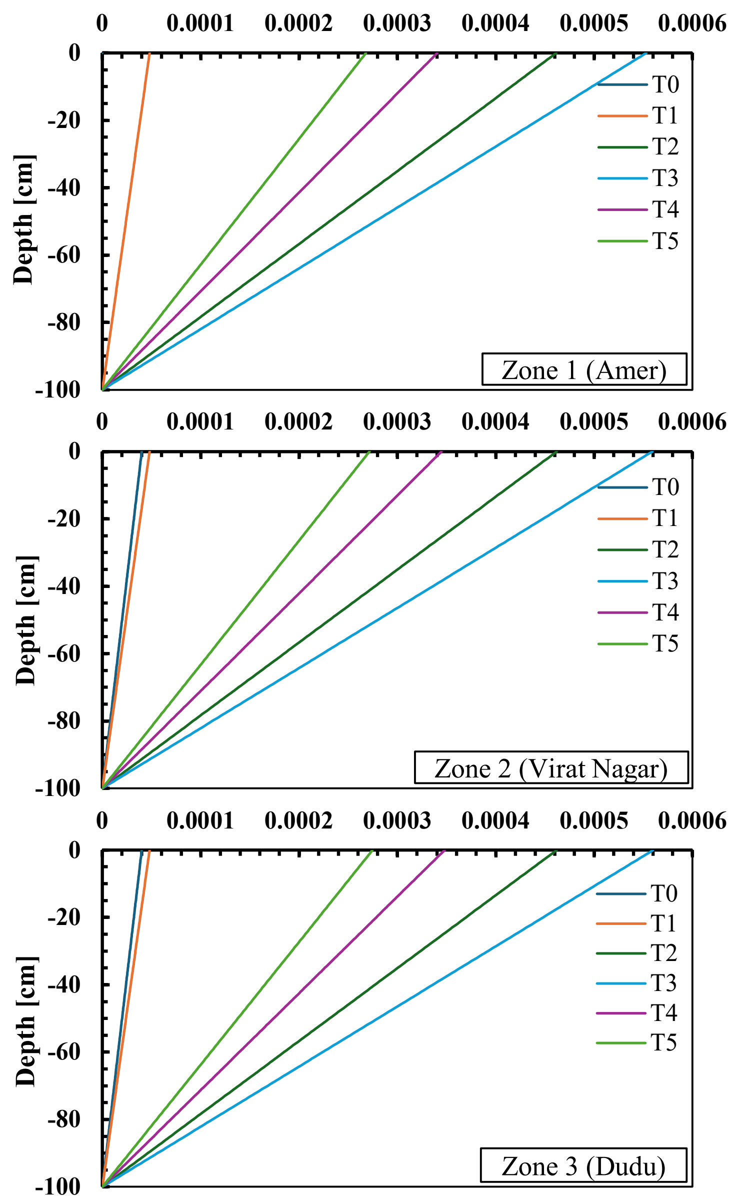

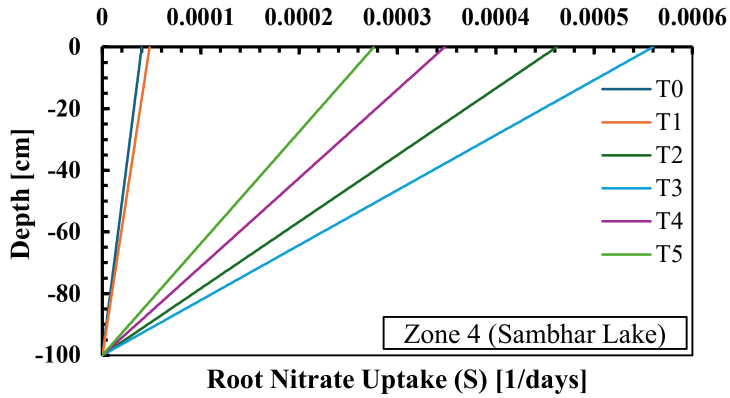

Figure 4.8 Simulated root nitrate uptake profiles (mmol/cm³/day) with soil depth (0–100 cm) at six growth stages (T0–T5).

HYDRUS-1D simulations over the wheat-growing season highlighted clear zone-wise differences in root nitrate uptake across the 0–100 cm soil profile, strongly influenced by soil texture and nitrate mobility. In Amer (Zone 1), uptake was initially low but intensified as the crop developed, peaking during mid-growth (T3) at ~5.55×10^{-4} mmol/cm³/day at the surface and extending to about 80 cm. The uptake followed a bell-shaped pattern, with the top 60 cm consistently acting as the active root zone, underscoring the importance of surface-oriented and split fertilizer applications in sandy loam soils. Virat Nagar (Zone 2) showed a similar trend but with slightly lower maximum uptake and stronger retention in mid-depth layers (30–60 cm). Uptake peaked at ~5.59×10^{-4} mmol/cm³/day during T2–T3, with most absorption confined to the upper 60 cm. This suggests a balanced rooting environment, where split surface applications are effective while deeper placement offers little benefit. Dudu (Zone 3) displayed a more uniform vertical uptake profile, with peak activity (~5.60×10^{-4} mmol/cm³/day) again during T3. While most uptake occurred in the top 30 cm, roots continued to absorb nutrients efficiently down to 70 cm, indicating suitability for both surface and moderate subsurface fertilization, with limited leaching risk below 80 cm. In contrast, Sambhar Lake (Zone 4) showed uptake strongly restricted to the top 30 cm, with peak values (~4.62×10^{-4} mmol/cm³/day) during T2 and a rapid decline with depth. Root activity below 60 cm was minimal, and uptake was negligible beyond 80 cm, highlighting a strong dependence on topsoil nutrients and the potential for nitrate leaching losses below the root zone.

Overall, these results demonstrate that wheat nitrate uptake in Jaipur soils is shaped by both depth and time, with Amer soils showing rapid uptake and leaching risks, Virat

Nagar and Dudu maintaining moderate, sustained uptake across mid-depths, and Sambhar soils relying almost entirely on the surface layer. Such patterns emphasize the need for site-specific nutrient strategies—split or controlled-release fertilizers for sandy zones, balanced mid-depth applications in loamy soils, and shallow placement with careful irrigation in finer soils—to maximize nutrient use efficiency and reduce environmental impacts.

4.7 Conclusion

In this chapter, we used HYDRUS-1D to simulate how nitrate moves through soil and is taken up by plant roots in four areas of Jaipur: Amer, Virat Nagar, Dudu, and Sambhar Lake. Each location has different soil types, which affected how nitrate behaves in the soil. We studied how nitrate concentration changed at the surface, in the root zone, at the bottom of the soil profile, and how much was taken up by roots over time and depth.

In Zone 1 (Amer), the sandy soil caused nitrate to move quickly downwards, leading to early root uptake but also a higher chance of nutrient loss through deep leaching. Zones 2 (Virat Nagar) and 3 (Dudu) showed more balanced conditions where nitrate remained in the root zone longer, helping plants absorb nutrients more effectively. Zone 4 (Sambhar Lake) had fine-textured soil that held nitrate in the upper layers, but root uptake below 60 cm was very low, which means unused nitrate could still move down and pollute groundwater.

We found that most root uptake happened during the middle growth stages (T2–T3), especially in the top 20–30 cm of soil. These results show the importance of applying fertilizers at the right time and in the right way—like in split doses or using slow-release forms—to match plant needs and avoid nutrient waste.

Now that we've seen how nitrate moves and is taken up by roots, the next step is to understand how this affects crop yield. In Chapter 5, we will build a model that connects the amount of nitrate (and other pollutants) in the soil to how much crop is produced. We will study how too little, or too much nitrate affects growth and use real data from Jaipur to check if the model works in actual farming conditions. This will help us see how managing nutrients can improve crop production and protect the environment at the same time.

Chapter 5

Model for Nutrient/ Pollutant Load and Its Impact on Crop Yield

Chapter 5

Model for Nutrient/Pollutant Load and Its Impact on Crop Yield

5.1 Introduction

The relationship between solute transport, nutrient/pollutant load, and crop yield is a critical aspect of agricultural productivity and environmental sustainability. Solute transport refers to the movement of dissolved substances, such as nutrients and pollutants, through soil and into plant systems. This process significantly influences the availability of essential nutrients for crop growth and the accumulation of potentially harmful pollutants, both of which have direct and indirect effects on crop yields.

Nutrients, such as nitrogen, phosphorus, and potassium, are vital for plant growth and productivity. They support key physiological processes, including photosynthesis, protein synthesis, and cell development. Insufficient or imbalanced nutrient levels can lead to suboptimal crop performance, reduced yields, and economic losses for farmers. Conversely, pollutants, which may originate from industrial waste, excessive fertilizer use, or pesticide applications, can degrade soil health, disrupt microbial communities, and introduce toxic elements into the plant-soil system. These factors not only reduce crop yields but also pose risks to human health and the environment.

Existing models in agricultural science often address nutrient dynamics and pollutant dynamics separately. This compartmental approach overlooks the complex interactions that can occur between the two, leading to gaps in our understanding of how they collectively influence crop performance. For example, high pollutant levels may impair a plant's ability to uptake essential nutrients, while nutrient availability can affect the bioavailability and toxicity of certain pollutants. Moreover, many existing models rely on simplifying assumptions that fail to capture the variability and complexity of real-world agricultural systems, leading to inadequate predictions of crop yield responses under varying nutrient and pollutant loads.

This chapter aims to develop a mathematical model that captures the dynamics of nutrient and pollutant loads in the soil-plant system. The model seeks to quantify their respective impacts on crop yields by incorporating key factors such as transport mechanisms, nutrient uptake by roots, and the effects of pollutant toxicity. By simulating various scenarios, the model will provide insights into optimizing nutrient management strategies and mitigating pollutant effects to achieve sustainable agricultural practices.

5.2 Mathematical Modeling of Nutrient/Pollutant Load

To model the behavior of nutrient and pollutant dynamics, we consider an integrated soil-plant system where solutes, such as nutrients and pollutants, undergo transport, transformation, and uptake. The system incorporates the following components:

Soil Domain Representation

The soil is represented as a homogeneous and isotropic medium, simplifying its complex structure for modeling purposes. This assumption allows us to focus on the overall behavior of solute transport without accounting for localized heterogeneities, such as preferential flow paths or micro-scale variability. Within this domain, the following processes govern solute behavior:

Solute Transport: Movement of nutrients and pollutants through soil pores via processes like advection and diffusion.

Environmental Interactions: External factors, including rainfall, irrigation, and evaporation, that influence water content and solute mobility.

Plant System Dynamics

The plant system is modeled as a network of root structures that interact dynamically with the soil to uptake nutrients and, in some cases, pollutants. The key processes include:

Nutrient Uptake: Active and passive transport mechanisms within roots.

Pollutant Interaction: Accumulation or toxicity effects caused by pollutants reaching critical concentrations.

Key Modeling Assumptions

To maintain model tractability while preserving essential system dynamics, the following simplifying assumptions are adopted:

(i) Uniform Soil Properties

The soil properties, such as texture, porosity, and hydraulic conductivity, are spatially consistent throughout the modeled domain. This ensures that solute transport equations can use constant parameters.

(ii) Initial Solute Distribution

Initial concentrations of nutrients and pollutants are determined by fertilizer or chemical application techniques and pre-existing contamination from past land use or industrial discharge.

(iii) Transport Mechanisms

- Advection: Solutes move with the bulk flow of water driven by gravity and pressure gradients.
- Diffusion: Solutes spread from areas of higher concentration to lower concentration, driven by molecular motion.
- Root Uptake: Solutes are absorbed by plant roots according to concentration gradients and plant demand.

(iv) Environmental Boundary Inputs

- Rainfall and irrigation affect the soil water content and, consequently, the mobility of solutes.
- Temperature and pH impact nutrient availability and pollutant reactivity, influencing the dynamics of solute transport.

(v) Transformation and Decay

- Nutrient Uptake: Nutrients are depleted due to plant absorption.
- Pollutant Decay: Pollutants may undergo transformation or degradation (e.g., microbial activity), reducing their concentration over time.

Model Framework and Implementation

The complete system is mathematically formulated by integrating:

- Richards' equation for unsaturated water flow,
- Advection-dispersion-reaction (ADR) equation for solute transport, and

- Root uptake models (e.g., Michaelis-Menten or Feddes-type functions) to simulate nutrient absorption.

Boundary conditions, source terms, and time-dependent environmental drivers are explicitly incorporated to reflect realistic field scenarios.

5.3 Solute Transport Equations

Transport equations provide the mathematical basis to understand how nutrients and pollutants move and transform within soil and plant systems. These equations capture critical physical and chemical processes, including the movement of solutes with water (advection), spreading due to concentration differences (diffusion and dispersion), uptake by plant roots, and transformations due to chemical and biological reactions. By accurately modeling these processes, we can predict the fate of nutrients and pollutants and their impact on crop productivity and environmental quality.

5.3.1 Conservation of Mass

The fundamental equation governing solute transport is derived from the principle of mass conservation. It asserts that the rate of change of solute mass per unit volume of soil is equal to the net flux divergence minus any internal sources or sinks. Mathematically, the one-dimensional solute conservation equation is expressed as:

$$\frac{\partial C_T}{\partial t} = -\frac{\partial J_s}{\partial z} - S \tag{5.1}$$

where C_T is the total solute concentration [ML^{-3}], J_s is the solute flux [ML^{-2}T^{-1}], z is the vertical coordinate (positive upward), S is the sink/source term [ML^{-3}T^{-1}], accounting for plant uptake or chemical reactions.

The total solute concentration C_T includes both: the liquid-phase concentration c [ML^{-3}] — mass of solute per unit volume of soil water, and the adsorbed-phase concentration s [MM^{-1}] — mass of solute adsorbed onto soil particles per unit mass of soil. To express both components on a per-unit-volume-of-soil basis, the following relationship is used:

$$C_T = \theta c + \rho_b s \tag{5.2}$$

where θ is the volumetric water content [L^3L^{-3}] and ρ_b is the bulk density of the soil [ML^{-3}]. This equation ensures conservation of total solute mass by accounting for both dissolved and adsorbed forms.

5.3.2 Transport processes

Solute transport in soil is governed by the combined effects of multiple physical mechanisms that dictate how nutrients and pollutants move through the soil-water-plant continuum. In the liquid phase, the total solute flux J_s consists of three primary components: Advective flux J_{lc}, Diffusive flux J_{ld} and Hydrodynamic dispersive flux J_{lh}. Thus, the total solute flux is expressed as:

$$J_s = J_{lc} + J_{ld} + J_{lh} \tag{5.3}$$

Advection

Advection refers to the transport of solute carried by the bulk flow of water, driven by pressure and gravity gradients. The advective solute flux is given by:

$$J_{lc} = q \cdot c \tag{5.4}$$

where q is the Darcy water flux $[L^3/L^2T] = [L/T]$, c is the solute concentration in the liquid phase $[M/L^3]$. The product $q \cdot c$ yields units of solute flux $[M/L^2T]$.

If advection were the only transport mechanism, solute molecules would move uniformly at the average water velocity. For constant surface concentration c_0, this would lead to a piston flow or square wave solute distribution in the soil profile. In such scenarios, the solute front moves with the pore water velocity v, which is related to the Darcy flux and volumetric water content θ as:

$$v = \frac{q}{\theta} \tag{5.5}$$

This velocity accounts for the fact that water flow occurs only through the pore space (i.e., wetted cross-sectional area), and not through the entire bulk soil.

Diffusion

Diffusion is the result of random molecular motion, driving solutes from regions of higher concentration to lower concentration. In free water, this process is described by Fick's First Law:

$$J_{ld} = -D_l^w \frac{\partial c}{\partial z} \tag{5.6}$$

where D_l^w is the diffusion coefficient in free water $[L^2/T]$, $\partial c/\partial z$ is the concentration gradient in the vertical direction.

In soil, diffusion is hindered due to reduced cross-sectional area and tortuous flow paths caused by soil particles and air pockets. To account for this, an effective diffusion coefficient in soil, D_l^s, is used:

$$J_{ld} = -\theta D_l^s \frac{\partial c}{\partial z} \tag{5.7}$$

where

$$D_l^s = \xi_l(\theta) D_l^w \quad \text{and} \quad \xi_l(\theta) = \frac{\theta^{7/3}}{\theta_s^2} \tag{5.8}$$

Here, $\xi_l(\theta)$ is the tortuosity factor as proposed by Millington and Quirk (1961), and θ_s is the saturated water content. Because $\xi_l(\theta) < 1$, the effective diffusion coefficient in soil is typically much smaller than in water (often < 1 cm^2/day), which slows down the diffusion rate.

Hydrodynamic Dispersion

Hydrodynamic dispersion arises from microscopic-scale velocity variations in soil water due to differences in pore size and pore water velocity, non-parallel flow paths (streamlines), mixing between pores and velocity gradients within individual pores (e.g., parabolic flow profile). These effects cause spreading of the solute front beyond what is predicted by diffusion alone. Hydrodynamic dispersion is described using Fick's law type equation:

$$J_{lh} = -\theta D_{lh} \frac{\partial c}{\partial z} \tag{5.9}$$

where D_{lh} is the hydrodynamic dispersion coefficient $[L^2/T]$ and θ is the volumetric water content. Empirical studies have shown that D_{lh} is proportional to the average pore water velocity v (Bresler, 1973):

$$D_{lh} = \lambda v \tag{5.10}$$

where λ is the dispersivity [L], a parameter reflecting the range of pore sizes and heterogeneity of the soil. The value of λ varies with the scale of observation. For Laboratory-scale (packed columns): $\lambda \approx 0.5 - 2$ cm, for Field-scale (intact soil cores): $\lambda \approx 5 - 20$ cm and for Aquifer-scale: $\lambda > 1$ m. This phenomenon is known as scale-dependent dispersivity.

The total solute flux combining all three transport processes can be written as:

$$J_s = qc - \theta D_l^s \frac{\partial c}{\partial z} - \theta D_{lh} \frac{\partial c}{\partial z} \tag{5.11}$$

The diffusion and dispersion terms can be combined into a single effective dispersion coefficient D_e:

$$D_e = D_l^s + D_{lh} \tag{5.12}$$

Thus, the final expression for total solute flux becomes:

$$J_s = qc - \theta D_e \frac{\partial c}{\partial z} \tag{5.13}$$

This formulation is central to the advection–dispersion model for solute transport and provides the basis for numerical simulations of nutrient and pollutant movement in soil.

5.3.3 Advection Dispersion Equation

The Advection–Dispersion Equation (ADE) is the fundamental equation used to describe solute transport in unsaturated or saturated porous media. It is derived by substituting the total solute flux expression into the general conservation of mass equation. Starting from the mass conservation equation:

$$\frac{\partial(\theta c + \rho_b s)}{\partial t} = -\frac{\partial J_s}{\partial z} - S \tag{5.14}$$

and substituting the expression for total solute flux:

$$J_s = qc - \theta D_e \frac{\partial c}{\partial z} \tag{5.15}$$

we obtain the full form of the advection–dispersion–reaction equation:

$$\frac{\partial(\theta c + \rho_b s)}{\partial t} = -\frac{\partial}{\partial z}\left(qc - \theta D_e \frac{\partial c}{\partial z}\right) - S \tag{5.16}$$

This equation accounts for Advection (mass transport due to water flow), Dispersion (spreading due to velocity variations and diffusion), Sorption (adsorption-desorption equilibrium, included in $\rho_b s$) and Source/Sink terms (plant uptake, chemical decay).

ADE Without Sorption or Sources/Sinks

In the absence of sorption ($S = 0$) and sources/sinks ($S = 0$), the equation simplifies to:

$$\frac{\partial(\theta c)}{\partial t} = \frac{\partial}{\partial z}\left(\theta D_e \frac{\partial c}{\partial z}\right) - \frac{\partial(qc)}{\partial z} \tag{5.17}$$

This is a general form of the Advection–Dispersion Equation (ADE), also referred to as the Convection–Dispersion Equation (CDE). The first term on the right-side accounts for dispersion and the second term accounts for mass flow (advection).

ADE Under Steady-State Flow Conditions

For steady-state flow conditions, both the Darcy flux J_w and volumetric water content θ are constant in space and time, the equation further simplifies. Since D_e is proportional to the pore water velocity $v = q/\theta$, it also becomes constant under these assumptions. The ADE then becomes:

$$\theta \frac{\partial c}{\partial t} = \theta D_e \frac{\partial^2 c}{\partial z^2} - q \frac{\partial c}{\partial z} \tag{5.18}$$

Dividing both sides by θ, and recognizing that $v = \frac{q}{\theta}$, we obtain the classical form of the ADE:

$$\frac{\partial c}{\partial t} = D_e \frac{\partial^2 c}{\partial z^2} - v \frac{\partial c}{\partial z} \tag{5.19}$$

The solution to this equation yields the solute concentration as a function of both depth and time, denoted by $c(z,t)$. The specific form of the solution is determined by the initial conditions (i.e., the solute concentration profile at $t = 0$), and the boundary conditions (such as specified concentrations or fluxes at the soil surface and bottom). Additionally, the solution is influenced by the soil structure, particularly whether the profile is homogeneous or consists of multiple stratified layers. Solutions to the ADE can be obtained analytically for simple boundary conditions (e.g., semi-infinite domain with constant concentration at the surface), or numerically for more complex field-scale scenarios.

5.4 Analytical Solution of ADE

Under the assumption of uniform soil properties and steady water flow, the advection–dispersion equation (ADE) can often be solved analytically. Various analytical solutions for different boundary and initial conditions have been provided by Skaggs and Leij (2002) and Jury and Roth (1990). One powerful technique to derive analytical solutions is the Laplace transform method, which converts the partial differential equation into an ordinary differential equation (ODE) that is easier to solve.

The one-dimensional ADE in the vertical direction (z, positive downward) is given by:

$$\frac{\partial c}{\partial t} = D_e \frac{\partial^2 c}{\partial z^2} - v \frac{\partial c}{\partial z} \tag{5.20}$$

where $c(z,t)$ is the solute concentration [M/L³] at position z and time t, D_e is the effective dispersion coefficient [L²/T] (constant) and v is the advection velocity [L/T] (constant). z: is vertical coordinate [L] and t is time [T].

Initial and Boundary Conditions

We consider the following commonly used conditions:

Initial condition (IC):

$$c(z,0) = 0 \quad \text{for all } z > 0 \tag{5.21}$$

Boundary conditions (BC):

At the soil surface $z = 0$: Type-3 (Cauchy) boundary condition, which specifies solute flux:

$$qc(0,t) - \theta D_e \frac{\partial c(0,t)}{\partial z} = qc_0(t) \tag{5.22}$$

For a constant concentration input $c_0(t) = c_0$, this becomes a special case of a Type-1 (Dirichlet) condition:

$$c(0,t) = c_0 \tag{5.23}$$

At depth $z \to \infty$: Type-2 (Neumann) boundary condition:

$$\frac{\partial c(\infty,t)}{\partial z} = 0 \quad \text{(no concentration change at depth)} \tag{5.24}$$

Now, apply the Laplace transform with respect to time t:

$$\mathcal{L}\{c(z,t)\} = \bar{c}(z,s) = \int_0^\infty c(z,t)e^{-st}dt \tag{5.25}$$

Applying this transform to each term of the PDE, assuming zero initial conditions (i.e., $c(z,0) = 0$):

$$\mathcal{L}\left\{\frac{\partial c}{\partial t}\right\} = s\bar{c}(z,s) - c(z,0) = s\bar{c}(z,s) \tag{5.26}$$

$$\mathcal{L}\left\{\frac{\partial^2 c}{\partial z^2}\right\} = \frac{d^2\bar{c}(z,s)}{dz^2} \tag{5.27}$$

$$\mathcal{L}\left\{\frac{\partial c}{\partial z}\right\} = \frac{d\bar{c}(z,s)}{dz} \tag{5.28}$$

Thus, the PDE becomes an ordinary differential equation (ODE):

$$s\bar{c}(z,s) = D_e \frac{d^2\bar{c}(z,s)}{dz^2} - v\frac{d\bar{c}(z,s)}{dz}$$

$$D_e \frac{d^2\bar{c}}{dz^2} - v\frac{d\bar{c}}{dz} - s\bar{c} = 0 \tag{5.29}$$

Assume solution of the form $\bar{c}(z,s) = e^{mz}$. Substitute into the ODE:

$$D_e(m^2)e^{mz} - v(m)e^{mz} - se^{mz} = 0$$

Canceling e^{mz}, we get the characteristic equation:

$$D_e m^2 - vm - s = 0$$

Solve for m:

$$m = \frac{v \pm \sqrt{v^2 + 4D_e s}}{2D_e}$$

Thus, a general solution is given by

$$\bar{c}(z, s) = Ae^{m_1 z} + Be^{m_2 z} \tag{5.30}$$

Where

$$m_1 = \frac{v + \sqrt{v^2 + 4D_e s}}{2D_e}, \quad m_2 = \frac{v - \sqrt{v^2 + 4D_e s}}{2D_e} \tag{5.31}$$

Transforming the boundary conditions into the Laplace domain:

At $z = 0$:

$$\bar{c}(0, s) = \frac{c_0}{s}$$

At $z \rightarrow \infty$:

$$\bar{c}(z \rightarrow \infty, s) = 0$$

From boundary condition at infinity, we must discard exponential terms that grow unbounded as $z \rightarrow \infty$. Since $m_1 > 0$, discard $e^{m_1 z}$. Hence, the solution simplifies to:

$$\bar{c}(z, s) = Be^{m_2 z}$$

Apply boundary at $z = 0$:

$$\bar{c}(0, s) = B = \frac{c_0}{s}$$

Thus, the solution in Laplace domain is:

$$\bar{c}(z, s) = \frac{c_0}{s} \exp\left(\frac{v - \sqrt{v^2 + 4D_e s}}{2D_e} z\right) \tag{5.32}$$

To find the solution in the time domain, we apply the inverse Laplace transform:

$$c(z, t) = \mathcal{L}^{-1}\{\bar{c}(z, s)\}$$

First, rewrite clearly the Laplace-domain solution:

$$\bar{c}(z,s) = \frac{c_0}{s}\exp\left(\frac{vz}{2D_e}\right)\exp\left(-\frac{z}{2D_e}\sqrt{v^2+4D_e s}\right)$$

$$= \frac{c_0}{s}\exp\left(\frac{vz}{2D_e}\right)\exp\left(-\frac{z}{2D_e}.2\sqrt{D_e}\sqrt{s+\frac{v^2}{4D_e}}\right)$$

$$= \frac{c_0}{s}\exp\left(\frac{vz}{2D_e}\right)\exp\left[-\frac{z}{\sqrt{D_e}}\sqrt{s+\frac{v^2}{4D_e}}\right] \tag{5.33}$$

From the Laplace transform tables, we have the following known inverse:

$$\mathcal{L}^{-1}\left\{\frac{1}{s}\exp\left(-x\sqrt{s+k}\right)\right\} = \text{erfc}\left(\frac{x}{2\sqrt{t}} - k\sqrt{t}\right) \tag{5.34}$$

Applying this formula, we identify:

$$x = \frac{z}{\sqrt{D_e}} \quad and \quad k = \frac{v^2}{4D_e} \tag{5.35}$$

Thus, the inverse Laplace transform is directly obtained as:

$$c(z,t) = c_0\exp\left(\frac{vz}{2D_e}\right)\text{erfc}\left(\frac{\frac{z}{\sqrt{D_e}}}{2\sqrt{t}} - \frac{v^2}{4D_e}\sqrt{t}\right)$$

$$= c_0\exp\left(\frac{vz}{2D_e}\right)\text{erfc}\left(\frac{z}{2\sqrt{D_e\,t}} - \frac{v^{2\sqrt{t}}}{4\,D_e}\right) \tag{5.36}$$

Thus, after algebraic simplifications (well-documented in transport literature), the standard known analytical solution for the given PDE is commonly represented as:

$$c(z,t) = \frac{c_0}{2}\left[\text{erfc}\left(\frac{z-vt}{2\sqrt{D_e t}}\right) + \exp\left(\frac{vz}{D_e}\right)\text{erfc}\left(\frac{z+vt}{2\sqrt{D_e t}}\right)\right] \tag{5.37}$$

where $\text{erfc}(x)$ is the complementary error function defined by:

$$\text{erfc}(x) = 1 - \text{erf}(x) = \frac{2}{\sqrt{\pi}}\int_x^{\infty} e^{-u^2}\,du \tag{5.38}$$

This form clearly shows two complementary processes. The first term accounts for solute transport in the direction of flow (advection and dispersion). The second term, modulated by the exponential, accounts for back-diffusion, where solutes spread in the opposite direction. The complementary error function (erfc) represents the effects of dispersion and spreading. The exponential term $\exp\left(\frac{vz}{D_e}\right)$ reflects how advection accelerates solute movement through the soil profile.

This analytical solution is extensively used in environmental modeling, groundwater hydrology, and soil science, particularly for solving advection–dispersion equations under constant concentration boundary conditions.

5.5 Incorporation of Environmental Factors

Environmental factors significantly influence the dynamics of nutrient and pollutant transport in soil, affecting key parameters such as pore water velocity (v), diffusion coefficient (D), and reaction rates ($R_d(C)$). This section describes the incorporation of rainfall, irrigation, evapotranspiration, temperature, and pH into the mathematical model.

Rainfall and Irrigation

Rainfall and irrigation are critical sources of water input to the soil system. These inputs alter soil water content, directly affecting the pore water velocity (v), which governs the advective transport of solutes.

The pore water velocity, $v(t)$, is influenced by both rainfall (Q_r) and irrigation (Q_i) rates, normalized by the soil porosity (ϕ). It is modeled as:

$$v(t) = \frac{Q_r}{\phi} + \frac{Q_i}{\phi}, \tag{5.39}$$

where Q_r is the rainfall rate (e.g., mm/day), Q_i is the irrigation rate (e.g., mm/day), ϕ is the soil porosity, representing the fraction of soil volume available for water and solute transport.

Increased water flow from rainfall or irrigation speeds up solute movement through advection $\left(v\frac{\partial C}{\partial x}\right)$, dilutes solutes near the surface, and can push nutrients or pollutants deeper into the soil. This may reduce nutrient availability to plants or lead to leaching beyond the root zone.

At the soil surface ($x = 0$), rainfall or irrigation creates a flux boundary condition for solutes:

$$J = -D\frac{\partial C}{\partial x} + vC \tag{5.40}$$

where J represents the flux of solutes entering the soil.

Evapotranspiration

Evapotranspiration (ET), which combines water loss through soil evaporation and plant transpiration, plays a significant role in modifying solute transport by reducing soil moisture. This reduction in water content decreases the pore water velocity (v), thereby slowing the advective movement of solutes. It also lowers the effective diffusion coefficient (D), as diminished water pathways restrict solute mobility.

As a result, nutrients and pollutants can build up near the soil surface, which may lead to harmful concentrations. Dry soil conditions also make it harder for plants to absorb nutrients, especially those that do not move easily, like phosphorus. In the model, evapotranspiration is included as a time-based decrease in soil water content using the equation:

$$\theta(t) = \theta_0 - ET(t), \tag{5.41}$$

where θ_0 is the initial soil water content.

Temperature and pH

Temperature and pH significantly affect solute transport and reactions in the soil–plant system. Temperature influences both reaction rates and diffusion. Many transformation processes follow an Arrhenius-type relationship:

$$R_d(C) = R_{d,0} \cdot e^{-\frac{E_a}{RT}} \tag{5.42}$$

where $R_d(C)$ is the temperature-dependent reaction rate, $R_{d,0}$ is the reference rate, E_a is activation energy, R is the gas constant, and T is temperature in Kelvin. Diffusion also increases with temperature as:

$$D(T) = D_0 \cdot \frac{T}{T_0} \tag{5.43}$$

Soil pH affects nutrient solubility and microbial processes. For instance, phosphorus becomes less available at very low or high pH due to precipitation with iron, aluminum, or calcium. To model these effects, nutrient availability can be expressed as a function of pH:

$$A(pH) = \frac{a}{1 + e^{-k(pH - pH_{\text{opt}})}} \tag{5.44}$$

where $A(pH)$ is availability, aa is the maximum value, and pH_{opt} is the optimal pH for uptake. Including temperature and pH dependencies improves model accuracy for nutrient transport and transformation.

In numerical models like HYDRUS, environmental factors are typically implemented as follows:

Table 5.1 Environmental Factors Incorporated in HYDRUS Solute Transport Modeling and Their Influence on Model Parameters and Processes

Environmental Factor	Input Format	Impact on Model
Rainfall/Irrigation	Time-variable BC file	Affects water flow (advection) and leaching
Temperature	Constant or time series	Alters decay rates, uptake kinetics
Soil Moisture	Computed internally	Influences θ, affects advection and diffusion
pH	Static or empirical	Modifies sorption and reaction coefficients
ET	Time-variable function	Controls water extraction, indirectly affects transport

5.6 Numerical Solutions

The equations governing nutrient and pollutant transport in the soil–plant system are often nonlinear, coupled, and influenced by spatial and temporal variability, making analytical solutions impractical. Therefore, numerical methods are essential for solving these complex systems. Two commonly used approaches are the Finite Difference

Method (FDM) and the Finite Element Method (FEM). FDM is well-suited for simple, one-dimensional problems due to its simplicity and computational efficiency, while FEM offers greater flexibility for irregular domains and heterogeneous soils. These methods enable accurate simulation of solute behavior under realistic field conditions.

5.6.1 Finite Difference Method (FDM)

The Finite Difference Method works by discretizing both the spatial and temporal domains into grids. The spatial domain, typically defined as $x \in [0, L]$, is divided into evenly spaced grid points separated by a fixed spatial step Δx. Likewise, the temporal domain $t \in [0, T]$ is divided into time steps of size Δt. Derivatives in the governing equations are then replaced with finite difference approximations. For instance, the first-order time derivative is approximated using a forward difference as:

$$\frac{\partial C}{\partial t} \approx \frac{C_i^{t+1} - C_i^t}{\Delta t} \tag{5.45}$$

and the second-order spatial derivative is represented using a central difference:

$$\frac{\partial^2 C}{\partial x^2} \approx \frac{C_{i+1}^t - 2C_i^t + C_{i-1}^t}{\Delta x^2} \tag{5.46}$$

Using these approximations, the advection–dispersion–reaction equation can be discretized into a solvable algebraic form. The general form of the finite difference equation becomes:

$$\frac{C_i^{t+1} - C_i^t}{\Delta t} + v \cdot \frac{C_{i+1}^t - C_{i-1}^t}{2\Delta x} - D \cdot \frac{C_{i+1}^t - 2C_i^t + C_{i-1}^t}{\Delta x^2} = -R_u(C_i^t) - R_d(C_i^t) \tag{5.47}$$

where v is the pore water velocity, D is the dispersion coefficient, $R_u(C)$ represents nutrient uptake by plant roots, and $R_d(C)$ represents degradation or transformation of solutes.

To improve numerical stability and accuracy, especially for transient problems, the Crank–Nicholson scheme is often employed. This semi-implicit method averages the solution between the current and the next time steps, resulting in the equation:

$$\frac{C_i^{t+1} - C_i^t}{\Delta t} = \frac{1}{2}[f(C^{t+1}) + f(C^t)] \tag{5.48}$$

where $f(C)$ includes the advection, dispersion, and reaction terms. The Crank–Nicholson method is advantageous because it is unconditionally stable for linear problems and provides higher accuracy than purely explicit methods.

The Finite Difference Method offers several advantages. It is conceptually simple, easy to program, and efficient for problems with regular, one-dimensional geometries. However, it also has limitations. Explicit schemes within FDM may face stability issues if the time step is too large relative to the spatial grid size (as governed by the Courant–Friedrichs–Lewy condition). Moreover, FDM is not ideally suited for domains with irregular shapes or highly variable soil properties, where mesh flexibility becomes important.

5.6.2 Finite Element Method (FEM)

FEM offers a highly flexible framework that is well-suited for multidimensional problems and spatially variable soils. Unlike traditional grid-based methods, FEM divides the domain into smaller, interconnected subdomains called elements, over which the governing equations are solved using interpolation techniques.

The FEM process begins with domain discretization, where the physical domain is partitioned into finite elements—such as triangular or quadrilateral shapes in two-dimensional models. Nodes are assigned at the corners or along the edges of these elements, and solute concentrations are calculated at these nodal points. Within each element, the solute concentration $C(x,t)$ is approximated as a weighted sum of predefined shape functions:

$$C(x,t) \approx \sum_{i=1}^{n} N_i(x) \cdot C_i(t) \tag{5.49}$$

where $N_i(x)$ are the shape functions associated with each node of the element, and $C_i(t)$ are the unknown time-dependent nodal concentrations.

To derive the finite element equations, the advection–dispersion–reaction equation is first converted into its weak form. This involves multiplying the equation by a test (or weighting) function and integrating over the domain of the element. The weak formulation ensures that the conservation laws are satisfied in an averaged sense, which enhances numerical stability and allows for better handling of boundary conditions and discontinuities.

Following the weak formulation, each element contributes to the global system of equations. These contributions are assembled into a global matrix equation of the form:

$$[K] \cdot \{C\} = \{F\} \tag{5.50}$$

where $[K]$ is the stiffness matrix, incorporating effects of diffusion, advection, and reaction terms, $\{C\}$ is the vector of unknown nodal concentrations and $\{F\}$ is the load vector that includes source terms and boundary conditions.

This system is solved using appropriate numerical solvers, such as LU decomposition, conjugate gradient methods, or other iterative techniques depending on the size and nature of the matrix.

The Finite Element Method presents several significant advantages. It is highly adaptable to irregular domain shapes, allows for local mesh refinement, and efficiently handles heterogeneous soil properties. Its flexibility makes it ideal for solving complex, real-world problems where soil conditions vary significantly in space and time.

However, FEM also has its limitations. It tends to be computationally intensive, especially for large-scale or three-dimensional models, and it requires specialized knowledge in mesh generation, element selection, and numerical solvers. The setup and execution of FEM simulations often demand more time and resources compared to simpler methods like the Finite Difference Method (FDM).

5.7 Crop Yield as a Function of Nutrient and Pollutant Levels

Crop yield is a complex function of both nutrient availability and the presence of toxic pollutants in the soil-plant system. While essential nutrients like nitrogen, phosphorus, and potassium are necessary for plant growth and productivity, pollutants such as heavy metals and organic contaminants can disrupt physiological processes and reduce crop yields. Understanding and modeling these relationships quantitatively is essential for optimizing agricultural practices and mitigating environmental risks. This section explores these relationships through the development of two key models: the Nutrient Response Function, which describes how crop yield responds to varying nutrient levels, and the Pollutant Stress Function, which quantifies the impact of pollutants on crop productivity.

5.7.1 Nutrient Response Function

The Nutrient Response Function establishes a relationship between the availability of nutrients in the soil and the resulting crop yield. This relationship is influenced by the type of nutrient, the plant species, soil properties, and environmental conditions. This function captures the essential behavior of crop plants, which respond positively to nutrient inputs up to an optimal level, beyond which additional nutrients offer diminishing or negative returns. The relationship between nutrient availability and crop growth is foundational to understanding agricultural productivity. Essential nutrients like nitrogen (N), phosphorus (P), and potassium (K) play critical roles in plant physiological processes. Nitrogen is a key component of chlorophyll, driving photosynthesis, while phosphorus is vital for energy transfer and root development as part of ATP synthesis. Potassium, on the other hand, regulates water balance and enhances stress resistance by maintaining osmotic balance within plant cells. When these nutrients are available in adequate amounts, crops can achieve their full yield potential. However, both deficiencies and excesses can lead to reduced productivity or even toxicity.

Mathematical Representation

The relationship between soil nutrient concentration (N) and crop yield (Y) is often represented using the Michaelis-Menten equation or its variants:

$$Y = Y_{max} \cdot f(N) = Y_{max} \cdot \frac{N}{N + K_N}, \tag{5.51}$$

where Y is the crop yield, Y_{max} is the maximum achievable yield under optimal nutrient conditions, N is the available nutrient concentration in the soil and K_N is the half-saturation constant, representing the nutrient concentration at which yield is 50% of Y_{max}.

Optimal Nutrient Thresholds for Maximum Yield

To understand how different nutrient levels influence crop yield, it is helpful to divide the nutrient availability spectrum into three conceptual zones:

- **Deficiency Zone**: Nutrient levels are below what the plant requires for optimal growth. In this zone, yield increases nearly linearly (or quadratically) with additional nutrients.
- **Sufficiency Zone**: Nutrient levels are within an optimal range. The crop achieves its maximum potential yield and further increases in nutrient concentration do not significantly affect productivity.
- **Toxicity Zone**: Excessive nutrient levels begin to harm the plant, leading to physiological stress, nutrient imbalances, and reduced yield.

Threshold Model

To capture the full nutrient–yield relationship across all zones, a piecewise threshold model is used:

$$Y(N) = \begin{cases} a \cdot N - b \cdot N^2, & \text{if } N \leq N_{opt} \\ Y_{max}, & \text{if } N_{opt} < N \leq N_{toxic} \\ Y_{max} - c \cdot (N - N_{toxic})^2, & \text{if } N > N_{toxic} \end{cases} \tag{5.52}$$

where N is the nutrient concentration in the soil, N_{opt} is the optimal nutrient level for maximum yield, N_{toxic} is the nutrient concentration beyond which toxicity effects occur, Y_{max} is the maximum achievable yield under optimal conditions and a, b, c are the coefficients derived from regression analysis of yield response data, reflecting the sensitivity of the crop to changes in nutrient level. This model allows for a continuous and realistic representation of crop yield under a wide range of nutrient conditions, from deficiency to toxicity.

Explanation of Model Components

- In the Deficiency Zone ($N \leq N_{opt}$), yield increases with nutrient input, but at a decreasing rate due to the quadratic term $-bN^2$, which represents diminishing returns as the crop approaches optimal nutrition.
- In the Sufficiency Zone ($N_{opt} < N \leq N_{toxic}$), yield stabilizes at its maximum Y_{max}, indicating that the plant has adequate nutrients and additional inputs do not increase productivity.
- In the Toxicity Zone ($N > N_{toxic}$), yield declines as excess nutrients begin to interfere with plant metabolism. This is captured by the negative quadratic term $-c(N - N_{\text{toxic}})^2$, which models the yield penalty associated with toxicity.

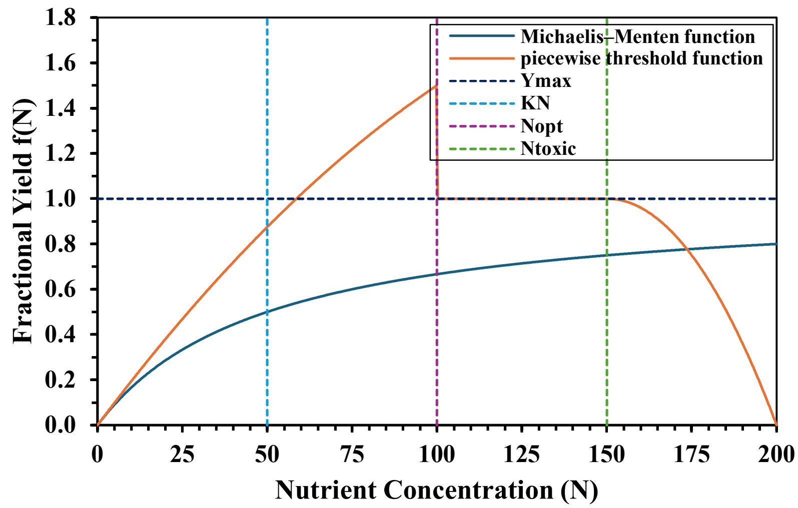

Figure 5.1 Graph of crop yield response as a function of nutrient concentration (N), comparing the Michaelis–Menten model and the piecewise threshold model.

The graph 5.1 presents the relationship between nutrient concentration (N) in soil and the resulting crop yield using two models: the Michaelis–Menten model and a Piecewise Threshold model. The x-axis represents the available nutrient concentration (N), while the y-axis shows the fractional crop yield normalized by the maximum possible yield ($Y_{\max}$). The Michaelis–Menten curve shows a smooth, a saturating yield response based on the equation $\mathrm{Y} = Y_{\max} \cdot \frac{N}{N+K_N}$, where K_N is the half-saturation constant. The piecewise model represents yield behavior across three zones—deficiency, sufficiency, and toxicity—defined by thresholds N_{opt} and N_{toxic}, with quadratic coefficients a, b, and c controlling curvature. Yield reaches a maximum value $Y_{\max}$ in the sufficiency zone.

5.7.2 Pollutant Stress Function

The Pollutant Stress Function models the adverse effects of toxic pollutants on crop yield. Pollutants, such as heavy metals, pesticides, and industrial residues, can disrupt plant physiological processes and reduce productivity.

Mechanisms of Pollutant Toxicity

Heavy Metals: Pollutants such as cadmium (Cd), arsenic (As), and lead (Pb) pose significant risks to plants by disrupting physiological and biochemical processes. These heavy metals:

- Inhibit Enzymatic Activity: Bind to active sites of key enzymes, reducing their efficiency or rendering them inactive.
- Block Nutrient Uptake: Compete with essential ions like calcium (Ca^{2+}), magnesium (Mg^{2+}), and potassium (K^{+}) for uptake, leading to nutrient deficiencies.
- Accumulate in Plant Tissues: Interfere with metabolic pathways, including respiration and protein synthesis, ultimately impairing growth and reproduction.

Organic Pollutants: Persistent organic pollutants (POPs), including pesticides and industrial chemicals, affect plant health through:

- Interference with Photosynthesis: Damage photosynthetic pigments or inhibit the electron transport chain, reducing energy production.
- Induction of Reactive Oxygen Species (ROS): Trigger oxidative stress by generating ROS, which damage cellular components like lipids, proteins, and DNA, leading to cell death and reduced productivity.

Understanding these mechanisms is crucial for developing mitigation strategies to protect plants from pollutant-induced stress and ensure sustainable agricultural productivity.

Yield Reduction Models

The relationship between pollutant concentration (P) and crop yield (Y) can be described using various models:

Sigmoidal Response Curve: The pollutant stress function accounts for yield reduction due to toxic pollutant concentrations. A typical sigmoidal (logistic) function is used:

$$g(P) = 1 - \frac{1}{1 + e^{-(P - T_P)/S}} \tag{5.53}$$

where Y_{max} is the maximum yield in the absence of pollutants, P is the pollutant concentration in the soil, T_P is the critical pollutant concentration at which yield is reduced by 50% and k is the slope parameter, that determines the steepness of the yield reduction curve.

Key features: For $P < T_P$, yield reduction is minimal $g(P) \approx 1$. For $P > T_P$, yield declines rapidly, approaching zero as P becomes excessively high.

Linear Response: For certain pollutants, yield reduction is linear:

$$Y = Y_{max} - r \cdot P \tag{5.54}$$

where r represents the rate of yield loss per unit increase in pollutant concentration.

Threshold Response: Pollutants may have negligible effects until a certain threshold concentration (P_{thresh}) is reached, beyond which yield decreases sharply:

$$Y = \begin{cases} Y_{\max}, & \text{if } P \leq P_{\text{thresh}} \\ Y_{\max} - c \cdot (P - P_{\text{thresh}})^2, & \text{if } P > P_{\text{thresh}} \end{cases} \tag{5.55}$$

5.7.3 Combined Effects of Nutrients and Pollutants

Nutrient and pollutant effects are often interdependent. The combined model accounts for these interactions by integrating $f(N)$ and $g(P)$ multiplicatively:

$$Y = Y_{\max} \cdot f(N) \cdot g(P) \tag{5.56}$$

where $Y_{\max}$ is the maximum potential yield under optimal conditions, $f(N)$ is the nutrient response function and $g(P)$ is the pollutant stress function.

$$Y = Y_{\max} \cdot \frac{N}{K_N + N} \cdot \left(1 - \frac{1}{1 + e^{-(P - T_P)/S}}\right) \tag{5.57}$$

Figure 5.2 illustrates the interaction between nutrient concentration and pollutant stress on crop yield. Each curve represents a different level of pollutant concentration (P), demonstrating how increasing pollutant levels progressively reduce the effectiveness of nutrient uptake and subsequently diminish crop yield. The model behind the graph uses a well-known mathematical approach called the Michaelis–Menten function to describe how plants respond to nutrients, while pollutant stress is incorporated through a sigmoidal function to simulate yield reduction. Although applicable to various nutrients, the parameters used (e.g., $K_N = 50$ mg/kg) align most closely with nitrogen (N) response, making the graph representative of nitrogen dynamics in soil. The graph includes nutrient concentrations ranging from 0–150 mg/kg and corresponding yield values at pollutant levels of 0, 15, 30, 45, and 60 mg/kg.

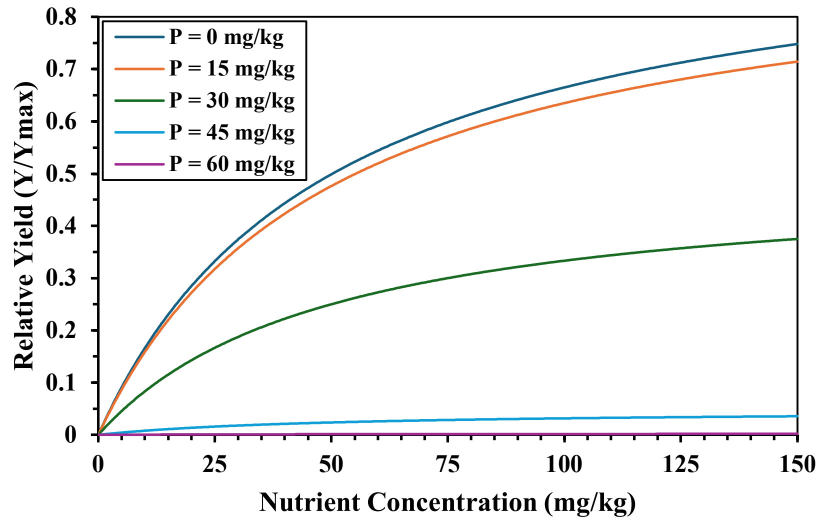

Figure 5.2 Yield response curves showing the combined effects of nutrient concentration (N) and pollutant stress (P) on crop yield.

5.8 Conclusion

In this chapter, a comprehensive modeling framework has been developed to understand the impact of nutrient and pollutant dynamics on crop yield within the soil–plant system. Beginning with the physical principles of solute transport, the chapter presented the governing equations of mass conservation and the Advection-Dispersion Equation (ADE), incorporating critical processes such as advection, diffusion, dispersion, and root uptake. These were further extended to include the influence of environmental factors like rainfall, irrigation, evapotranspiration, temperature, and pH, all of which significantly alter solute behavior in soil.

Both analytical and numerical methods were explored for solving the ADE under varying field conditions. Finite Difference and Finite Element Methods were presented as powerful tools for simulating real-world transport processes, especially in heterogeneous or irregular domains.

Next, we studied how crop yield depends on nutrient availability and pollutant levels. We used well-known mathematical models to describe this. The nutrient response function showed that crops grow better with more nutrients up to a point, after which the benefit levels off. The pollutant stress function showed that higher levels of toxic substances can harm plant growth and reduce yields. Finally, a combined model was presented that considers both nutrients and pollutants together, giving a more realistic picture of how they interact to influence yield.

Graphs and simulations showed that as pollutant levels increase, the positive effect of nutrients on yield starts to decline. While these models can be used for various nutrients, the parameters we used in this chapter are most closely related to nitrogen, making the results especially useful for nitrogen management in crops like wheat.

In summary, this chapter brings together soil science, plant growth, and environmental effects into one model. It helps us understand how to manage fertilizers better while also being aware of the risks of pollution—an important step toward sustainable agriculture.

The deterministic model discussed in this chapter provides a strong foundation for understanding solute transport and crop yield dynamics. The next chapter extends this work by incorporating stochastic elements, addressing the variability and uncertainty inherent in real-world systems. This approach will enhance the model's applicability to diverse agricultural and environmental conditions.

Chapter 6

Stochastic Modeling of Solute Transport and Crop Yield Variability

Chapter 6

Stochastic Modeling of Solute Transport and Crop Yield Variability

6.1 Introduction

Traditional models for crop and soil processes usually assume that an entire field is uniform. They use soil data from a few points, average it, and apply it to the whole area. This makes it easier to calculate, but it raises important questions: Do these averages really represent the actual field? How should soil properties be averaged? Should we also measure the uncertainty in our predictions?

A better approach is stochastic modeling, which accepts that soil properties change from place to place. Here, soil and crop variables like water content, salt concentration, or yield are treated as random variables. Using statistical principles, we can calculate the average values (means) and how much they vary (variances). This way, we can predict how differences in soil affect crop yield, water use, and salinity under given conditions like irrigation rate and water quality (Russo, 1986).

6.2 Water transport problem

Traditional water flow modeling uses partial differential equations like Richards' equation, solved with specific boundary and initial conditions and soil hydraulic data. While accurate, this approach is complex for homogeneous soils due to nonlinear equations and time-consuming property measurements. (Bresler and Dagan,1983a, 1983b). In spatially variable fields, the main goal is often to estimate average water content over time (t) and depth (z), which can be simpler than solving the full homogeneous case. Errors from uncertain soil properties and model approximations can partly cancel during averaging, and natural variability often outweighs modeling errors.

Stochastic modeling takes advantage of this by using simplified flow models to predict key statistics—means and variances—providing realistic results for variable fields. In this section, these ideas are applied to infiltration into soil with uniform starting water content and redistribution of water after infiltration.

6.2.1 Mathematical statement of flow problem

We consider vertical water flow in soil that is horizontally variable but vertically uniform, with z directed downward from the surface. The one-dimensional Richards' equation for soil moisture θ is:

$$\frac{\partial\theta}{\partial t}+\frac{\partial}{\partial z}\left(K\frac{dh}{d\theta}\frac{\partial\theta}{\partial z}\right)+\frac{\partial K}{\partial z}=0 \tag{6.1}$$

Initial condition:

$$\theta=\theta_n, \quad t=0, \quad z>0 \tag{6.2}$$

Surface flux during infiltration:

$$q=q_0, \quad 0<t<t_i, \quad z=0, \quad \theta(0,t)<\theta_s \tag{6.3}$$

Post-infiltration:

$$q=0, \quad t>t_i, \quad z=0 \tag{6.4}$$

If ponding occurs

$$\theta=\theta_s, \quad t_p<t<t_i, \quad z=0 \tag{6.5}$$

where $\theta_n(\geq\theta_r)$ is the initial moisture content, q_0 is the constant flux on the surface and t_i is the infiltration time, t_p is the ponding time.

Soil hydraulic properties follow Brooks & Corey (1964):

$$\frac{K(h)}{K_s}=\left(\frac{h_a}{h}\right)^{\eta}, \quad S_e=\frac{\theta-\theta_r}{\theta_s-\theta_r}=\left(\frac{h_a}{h}\right)^{\lambda} \tag{6.6}$$

where $\theta_s, \theta_r, h_a, K_s, \eta$, are constants. The goal is to solve Richards' equation for fields with spatially varying hydraulic properties, using these constitutive relationships and boundary conditions.

6.2.2 Methodology of Stochastic Flow Problem

In equations (6.6), the parameters $\theta_s, \theta_r, h_a, \eta, \lambda, K_s$ may vary spatially. Here, only K_s is treated as a random variable $K_s(x, y)$, while $\theta_s, \theta_r, h_a, \eta$, are constants, as K_s shows the greatest field variability (Russo & Bresler, 1982a). Flow is assumed vertical and 1-D, neglecting horizontal gradients when the horizontal correlation scale is much larger than the vertical scale (Russo & Bresler, 1982b).

The spatial variability of K_s is described by the joint PDF:

$$f_k(K_{s1}, K_{s2}, \dots, K_{sn}) \tag{6.7}$$

with weak stationarity—$E[K_s]$ constant, and two-point correlation depending only on $r_{12} = |r_1 - r_2|$. This structure is fully described by $f_k(K_s)$ and its auto-covariance. Since θ (or S), Ψ, and K depend on K_s via equations (6.6), they are also random, making equation (6.1), a stochastic PDE with deterministic initial and boundary conditions (Equations (6.2)–(6.5)).

Statement of the problem

In a spatially variable field, we seek the statistical structure of θ (or S), h, and K satisfying equation (6.1) , the constitutive relations (6.5), and boundary/initial conditions (6.2)–(6.5)) for stationary K_s. The unconditional mean and variance of S are:

$$E[S(z,t)] = \int_0^\infty S(z, t; K_s) f_k(K_s)\ dK_s \tag{6.8}$$

$$\sigma_S^2(z,t) = \int_0^\infty \{S(z,t;K_s) - E[S(z,t)]\}^2 f_k(K_s)\ dK_s \tag{6.9}$$

Similar forms hold for h and K. Under stationarity, $E[S(z,t)]$ equals the horizontal average at depth z and time t.

The spatial variability of K_s is modeled via the lognormal distribution of $\delta = d/E[d]$, with:

$$Y = ln\ \delta, \quad f_Y(Y) = \frac{1}{\sqrt{2\pi}\sigma_Y} \exp\left[-\frac{(Y - m_Y)^2}{2\sigma_Y^2}\right] \tag{6.10}$$

From microscopic flow theory

$$\frac{K_s}{K_s^*} = \delta^2, \quad K_s^* = \left[E\left(K_s^{1/2}\right)\right]^2 \tag{6.11}$$

and

$$K_s = K_s^* e^{2Y}, \quad f_k(K_s)\, dK_s = f_Y(Y)\, dY \tag{6.12}$$

Once the deterministic parameters θ_s, θ_s, θ_r, h_a, η, λ, K_s^*, m_Y, σ_Y, (describing the field) and q_0, t_i, θ_n (describing the flow) are specified, the calculation of $E[S(z,t)]$ (Equation (6.8)) and $\sigma_S^2(z,t)$ (Equation (6.9)) involves the following steps:

1. Solving Equations (6.1) – (6.6) to determine $S(z,t;K_s)$ for an arbitrary K_s.

2. Integrating over Y using Equations (6.12).

6.2.3 Approximate Water Flow Model

Under constant surface flux (Equation 6.3), the infiltration–redistribution cycle is approximated by a piston-type wetting front approach (Green & Ampt, 1911; Mein & Larson, 1973; Dagan & Bresler, 1983. The model assumes strictly vertical flow, with soil properties constant along the vertical but varying horizontally according to a probability distribution. The $K(\theta)$ relationship follows Equations (6.6)–(6.7), with variability arising only from the saturated hydraulic conductivity K_s, linked to a lognormally distributed scaling parameter δ $(Y = \ln \delta)$. Water enters the soil at a constant surface rate q_0 for an infiltration period t_i, starting from a uniform initial water content. A piston-type profile is assumed, where $q(z,t)$ and $\theta(z,t)$ are step functions—uniform above the wetting front depth $L(t)$ and equal to initial values below it. Due to spatial variability in K_s, these variables can differ horizontally at the same time and depth.

Model Solution

The steps to solve one infiltration-redistribution cycle in the approximate deterministic problem are as follows:

Step 1 — Dimensionless variables & ponding time: Given the input parameters $K_s, \eta, \lambda, h_a, \theta_r, \theta_s, \theta_n, q_0$, and t_i, calculate the following dimensionless variables:

$$\tilde{t} = \frac{tq_0(\eta - 1)}{h_a(\theta_s - \theta_r)}, \quad \mu = 1 - \frac{1-\lambda}{\eta}, \quad \widetilde{K} = \frac{\overline{K}}{q_0}, \quad \tilde{L} = \frac{L(\eta - 1)}{h_a} \tag{6.13}$$

and the ponding time (t_p)

$$\widetilde{t_p} = \frac{\widetilde{K_s}\left[1 - \left(\frac{\widetilde{K_n}}{\widetilde{K_s}}\right)^{(1-1/\eta)} - S_n + S_n\left(\frac{\widetilde{K_n}}{\widetilde{K_s}}\right)^{(1-1/\eta)}\right]}{\left(1 - \widetilde{K_n}\right)\left(1 - \widetilde{K_s}\right)} \tag{6.14}$$

Step 2 — Infiltration:

If $t_p > t_i$: The value of $K(t)$ during the entire infiltration stage is computed from

$$\overline{S} = \left(\frac{\widetilde{K}}{\widetilde{K_s}}\right)^{\lambda/\eta}, \quad L = \frac{(q_0 - K_n)t}{(\theta_s - \theta_r)\left(\overline{S} - S_n\right)} \tag{6.15}$$

If $t_p < t_i$: The soil becomes saturated during infiltration. The volume of water per unit area of soil, $V(t)$ and the surface flux $q(0,t)$ is calculated as:

$$\tilde{V} - \widetilde{V_p} - \alpha \ln \frac{\alpha + \tilde{V}}{\alpha + \widetilde{V_p}} = \left(\tilde{t} - \widetilde{t_p}\right)\left(\widetilde{K_s} - \widetilde{K_n}\right) \tag{6.16}$$

$$q(0,t) = \frac{d\tilde{V}}{d\tilde{t}} = K_s + K_s h_a \frac{\theta_s - \theta_n}{(\eta - 1)V} \tag{6.17}$$

Step 3 — Redistribution ($t > t_i$):

For $t > t_i$, the values of $K(t)$ are computed by numerically integrating:

$$\frac{d\overline{K}}{dt} = -\frac{\eta}{\lambda} \frac{\overline{K}^{1-\lambda/\eta} K_s^{\lambda/\eta}\left[\left(\overline{K}/K_s\right)^{\lambda/\eta} - S_n\right]}{V_0 - K_n t} \left[\overline{K} - K_n + \frac{h_a}{\eta - 1} \frac{\left(\overline{K}^{(1-1/\eta)} K_s^{1/\eta} - K_n S_n^{-1/\eta}\right)\left(K^{\lambda/\eta} K_s^{-\lambda/\eta} - S_n\right)}{V_0 - K_n t}\right] \tag{6.18}$$

Subsequently, $\overline{S}$ is derived using Equation (21), while L is obtained from:

$$V(t) = V_0 - K_n t, \quad t > 0 \tag{6.19}$$

where V_0 is the water volume in the profile at the end of infiltration ($t = t_i$). For convenience, $t = 0$ is considered as the start of redistribution. This approach conserves mass satisfies Darcy's law on average and captures variability through K_s statistics.

6.2.4 Computations Of Statistical Moments of Flow Variables

The mean and variance of flow variables are computed from equations (6.8)–(6.9). Instead of Monte Carlo simulation, the cumulative PDF division method is used:

$$P(Y) = \int_{-\infty}^{Y} f(Y)\ dY \tag{6.20}$$

The range is divided into N equal classes. For each class i:

$$Y_i = Z_i \sigma_Y + m_Y, \quad K_s^i = K_s^* e^{2Y_i} \tag{6.21}$$

Approximate model steps:

1. Compute Y_i, K_s^i (Equation 6.21).
2. Define dimensionless variables:

$$\tilde{t} = \frac{t q_0 (\eta - 1)}{h_a(\theta_s - \theta_r)}, \quad \mu = 1 - \frac{1-\lambda}{\eta}, \quad \widetilde{K^\iota} = \frac{\overline{K}^i}{q_0} \tag{6.22}$$

3. Compute ponding time $\widetilde{t_p}$ (Equation 6.14).
4. Infiltration: For $\widetilde{t_\iota} > \tilde{t} > \widetilde{t_p}$, set$S_i = 1$, $\widetilde{K^\iota} = \widetilde{K_s^\iota}$, and solve for $\widetilde{V_\iota}$ (Newton's method). Otherwise, compute $K_i(t)$ and derive $S_i(t)$, $L_i(t)$ (Equation 6.15).
5. Redistribution ($t > \widetilde{t_\iota}$): Integrate Equation (6.18) (Runge–Kutta) to update $S_i(t)$, $L_i(t)$.
6. For $L_i(t) > z$:

$$G_i(z,t) = 1 + \frac{\psi_w}{(\eta - 1)L_i(t)}\left[S_i(t)^{-1/\beta} - S_n\right], \tag{6.23}$$

$$q_i(t) = K_i(t) G_i(z,t) \tag{6.24}$$

   If $L_i(t) < z$, set $S_i(z,t) = S_n$, $K_i(z,t) = K_s^i S_n^{\eta/\beta}$, $q_i(z,t) = K_i(z,t)$.

7. Repeat for $i = 1, \ldots, N$ and compute moments:

$$\overline{u}(z,t) = \frac{1}{N}\sum_{i=1}^{N} u_i(z,t) \tag{6.25}$$

$$\sigma_u^2(z,t) = \frac{1}{N}\sum_{i=1}^{N} [u_i - \overline{u}]^2 \tag{6.26}$$

$$\gamma_u(z,t) = \frac{1}{N}\sum_{i=1}^{N} [u_i - \overline{u}]^3 \tag{6.27}$$

8. Repeat over desired $z,\ t$.

6.2.5 Computation of Statistical Moments by Numerical Methods

Statistical moments are obtained by numerically solving Eq. (6.1) with initial condition (6.2) and boundary conditions (6.3)–(6.5) using finite differences. For $t > 0$, the surface boundary is:

$$q(0,t) = -K(0,t)\left[\frac{\partial h(0,t)}{\partial z} - 1\right] \leq q_0 \tag{6.28}$$

$$h_a \leq h \leq h_a S_n^{-1/\lambda} \tag{6.29}$$

During infiltration, q_0 is imposed; during redistribution, $q_0 = 0$. The numerical scheme iteratively switches between flux and pressure head boundary conditions:

1. Prescribed flux: Start with a fraction of q_0; if Eq. (6.23) holds, increase $q(0,t)$.
2. Prescribed head: If h violates Eq. (6.23), set $h = h_a$ until Eq. (6.22) holds.
3. Flux adjustment: If computed q exceeds potential, reset to q_0 and continue until convergence.

Soil hydraulic properties:

- Soil Moisture Retention Curve: Equation (6.6) with $\lambda, h_a, \theta_s, \theta_r$ as in the approximate model; hysteresis ignored.
- Hydraulic Conductivity Function: Equation (6.6) with $m_Y, \eta, K_s^*, \sigma_Y$ as before; use same $K_s^i(i = 1, \dots, Ni = 1, \dots, N)$.

Statistical moments:

Computed $u_i(z,t,Y_i)(i = 1, \dots, Ni = 1, \dots, N)$ are substituted into:

$$\overline{u} = \frac{1}{N}\sum_{i=1}^{N} u_i\,, \quad \sigma_u^2 = \frac{1}{N}\sum_{i=1}^{N}(u_i - \overline{u})^2\,, \quad \gamma_u = \frac{1}{N}\sum_{i=1}^{N}(u_i - \overline{u})^3$$

for $u \in \{S, \psi, K\}$.

6.2.6 Model Results for a Highly Variable Soil

To evaluate the performance of the stochastic infiltration–redistribution model under realistic field conditions, a sandy loam representative of the Jaipur region was selected. Jaipur's soils are characterized by moderate to high permeability, with relatively low organic content and high sand content. Based on local studies and typical soil properties, the distribution parameters σ_Y and m_Y were adapted for a sandy loam representative of Jaipur.

Statistical Description of K_s

The saturated hydraulic conductivity K_s was modelled as a lognormally distributed random variable:

$$Y = \ln\delta \quad \text{with} \quad Y \sim \mathcal{N}(m_Y, \sigma_Y^2)$$

where $\sigma_Y = 0.98, \quad m_Y = -0.45$

This choice reflects field-measured variability from regional studies. The relation between δ and K_s follows:

$$K_s = K_s^* e^{2Y}, \quad K_s^* = 0.45\text{ cm/hr}$$

The mean and variance of K_s are thereby determined entirely by (m_Y, σ_Y, K_s^*).

For hydraulic conductivity $K(h)$ and effective saturation $S(h)$, Brooks–Corey relationships (6.6) were used with parameter values typical of sandy loam:

$$\eta = 2.1, \quad \lambda = 0.31, \quad h_a = 10\text{ cm}, \quad \theta_s = 0.38, \quad \theta_r = 0.04\text{ or }0.02$$

These parameters, combined with m_Y, σ_Y, K_s^*, yield the deterministic property set:

$$(m_Y, \sigma_Y, h_a, \eta, \lambda, K_s^*, \theta_s, \theta_r)$$

With these eight deterministic parameters $(m_Y, \sigma_Y, h_a, \eta, \lambda, K_s^*, \theta_s, \theta_r)$, the statistical moments of the flow variables $\theta(z,t)$ or $S(z,t), \psi(z,t)$, etc., were computed for various combinations of initial and boundary parameters (q_0, t_i, θ_n) characterizing the flow, where q_0 is the constant infiltration flux, t_i is infiltration duration, and θ_n is the uniform initial volumetric water content. For the presented case: $\theta_n = 0.12, q_0 = 0.3\ \text{cm/hr}, t_i = 1.5$ days.

Numerical Computation

Numerical computations (Hanks et al., 1969) were performed using 90 depth increments, with the increment size adjusted based on K_s. For example: for $q_0 = 0.3\ \text{cm/hr}$, the increments ranged from 0.05 to 1.5 cm, for $q_0 = 5.0\ \text{cm/hr}$, the increments ranged from 0.1 to 3.5 cm. The minimum time step (Δt) was set to 0.02 hr. The stochastic ensemble of K_s was generated from the specified (m_Y, σ_Y) distribution, and corresponding infiltration/redistribution solutions were computed for each realization. Statistical moments were then evaluated using:

$$E[S(z,t)] = \frac{1}{N}\sum_{i=1}^{N} S_i(z,t) \tag{6.30}$$

$$\text{CV}(S) = \frac{\sqrt{\frac{1}{N}\sum_{i=1}^{N}(S_i - E[S])^2}}{E[S]} \tag{6.31}$$

6.3 Solute transport

Solute movement in soil is typically modeled by the mass-balance partial differential equation (dispersion–convection form) under specified initial and boundary conditions. In traditional approaches, the field is treated as a homogeneous porous medium, and numerical solutions—often developed for saturated–unsaturated laboratory columns—are applied directly.

In spatially variable fields, however, hydraulic properties such as K_s vary significantly. A more realistic approach is to represent the field as an ensemble of vertical homogeneous columns, each with its own K_s, producing different local solute transport responses. If K_s is random, then θ, $V = q / \theta$, and solute concentration C are also random variables, described by probability density functions (PDFs) rather than single deterministic values.

This stochastic framework captures the statistical behavior of solute transport across the field, offering a more accurate representation than homogeneous models and enabling computation of moments such as $E[C(z,t)]$ and $\sigma_C^2(z,t)$ for variable soils.

6.3.1 Mathematical Statement of Transport Problem

The macroscopic mass balance equation governing noninteracting solute dispersion in one-dimensional flow through a homogeneous soil column is expressed as:

$$\frac{\partial C}{\partial t} + V\frac{\partial C}{\partial z} = D_p\frac{\partial^2 C}{\partial z^2} + \frac{1}{\theta}\frac{\partial}{\partial z}\left(\theta D_h\frac{\partial C}{\partial z}\right) \tag{6.32}$$

where C is the solute concentration (dimensionless, varying between 0 and 1), θ is the volumetric water content, z is the vertical coordinate (positive downward), t is the time, D_h is the mechanical dispersion coefficient, D_p is the effective molecular diffusivity for static fluid in the soil system.

A rough estimate for D_p is $(2/3)D_0$, where D_0 is the diffusivity in the solution phase. It is assumed that $\theta = \theta(z,t)$, and the pore velocity $V(z,t) = q/\theta$ (with q as the specific discharge) are known solutions of the flow equation and are independent of C.

For saturated flow $(\theta = \theta_s = \text{constant})$, it has been demonstrated (Saffman,1959, 1960) that under general conditions:

$$D_h = \lambda V \tag{6.33}$$

where λ is the dispersivity for longitudinal dispersion.

Equation (40) and the relationship in Equation (41) are widely accepted for unsaturated flow as well, albeit with some limitations (Bresler, 1973; Segol, 1977). For most soils, λ typically ranges from 0.1 to 3 cm (Bresler and Laufer, 1974; Biggar and Nielsen, 1976).

Simplifications and Assumptions

Equation (6.40) applies to soil lying in the horizontal x, y plane beneath $z = 0$ (with z positive downward). Water flow is driven by surface recharge q_0, occurring at volumetric water content θ and pore water velocity V. Despite the inherent heterogeneity of soils and potential nonuniform application, it is assumed that flow remains vertical.

This assumption is valid for the upper soil layer, typically 1 to several meters thick, as considered here. Furthermore, studies by Russo and Bresler (1981b) demonstrated that the horizontal length scale characterizing variations in hydraulic properties (x, y) is significantly larger than the soil depth (at least in the Bet Dagan field). Consequently, lateral flow contributions are negligible compared to vertical flow. By adopting this simplification, the solute transport equation (Equation (6.40)) retains only derivatives with respect to t and z, making the problem more tractable while maintaining accuracy for the scenarios considered.

6.3.2 Stochastic Transport in Non-steady Vertical Flow

In the previous section, a stochastic approximate model for water flow in a spatially variable field was developed to analyze infiltration and redistribution processes. This model assumed: vertical flow direction, spatial variability confined to the horizontal plane, variability associated with saturated hydraulic conductivity (K_s), deterministic uniform recharge applied to the soil surface during $t \leq t_i$, uniform initial moisture content $\theta = \theta_n$ and a piston-type water content profile.

This section focuses on modeling inert solute transport under similar flow conditions. It is assumed that the solute concentration in the soil prior to infiltration (C_n) is uniform, while water with a higher concentration ($C_0 > C_n$) is applied to the soil surface during $0 < t < t_i$. The aim is to compute the expectation $E(C)$ and variance σ_C^2 as functions of depth (z) and time (t) under these conditions, which are relevant for leaching and pollution problems. Both a simplified salt transport model and a more accurate computer model are used to calculate mean concentration and its variance in a spatially variable field.

6.3.3 Derivation of Approximate Solution for Salt Transport

For vertical, one-dimensional flow with a deterministic pore velocity $V(z,t)$, the transport of an inert solute can be described by the following equations:

$$\frac{\partial C}{\partial t} + V\frac{\partial C}{\partial z} = \frac{\partial}{\partial z}\left(D\frac{\partial C}{\partial z}\right) \tag{6.34}$$

$$C = 0, \quad t = 0, \quad z > 0 \tag{6.35}$$

$$C = 1, \quad 0 < t < t_i, \quad z = 0 \tag{6.36}$$

$$\frac{\partial C}{\partial z} = 0, \quad t > t_i, \quad z = 0 \tag{6.37}$$

Using the approximate solution for water flow developed in Section I, the actual moisture content profile is replaced with a uniform profile ($\theta = \overline{\theta}$), or equivalently ($\overline{S} = (\overline{\theta} - \theta_r)/(\theta_s - \theta_r)$), extending from the soil surface ($z = 0$) to an equivalent front ($z = L$). Beyond this front ($z > L$), the moisture content remains at its initial value (θ_n).

During infiltration with constant recharge (q_0) applied at $z = 0$, as well as during redistribution, the average pore velocity is given by:

$$\overline{V} = \frac{\overline{q}}{\overline{\theta}} = \frac{\overline{q}}{\overline{S}(\theta_s - \theta_r) + \theta_r} \tag{6.38}$$

This velocity is constant within the profile and depends solely on time t.

Under the piston flow approximation, the transport equation becomes:

$$\frac{\partial C}{\partial t} + \overline{V}(t)\frac{\partial C}{\partial z} = \frac{\partial}{\partial z}\left(D\frac{\partial C}{\partial z}\right), \quad 0 < z < L \tag{6.39}$$

Relating $\overline{V}\ to\ L$:

$$\overline{V}(t) = \frac{dL}{dt} \tag{6.40}$$

which is accurate for gravitational infiltration and redistribution. Neglecting the molecular diffusivity term simplifies Equation [92] to:

$$\frac{\partial C}{\partial t} + \frac{dL}{dt}\frac{\partial C}{\partial z} = \lambda\frac{dL}{dt}\frac{\partial^2 C}{\partial z^2}, \quad 0 < z < L \tag{6.41}$$

where λ represents dispersivity.

Using the transformations:

$$\zeta = z - L(t), \quad \tau = \int_0^t \frac{\lambda}{\lambda_{\max}}\frac{dL}{dt'}dt' \tag{6.42}$$

The equation becomes

$$\frac{\partial C}{\partial \tau} = \lambda_{\max}\frac{\partial^2 C}{\partial \zeta^2}, \quad -L < \zeta < 0 \tag{6.43}$$

The initial and boundary conditions transform as follows:

$$C = 0, \quad \tau = 0, \quad \zeta > 0 \tag{6.44}$$

$$C = 1, \quad \zeta = -L(\tau) \tag{6.45}$$

$$\frac{\partial C}{\partial \zeta} = 0, \quad t > t_i, \quad \zeta = -L \tag{6.46}$$

Solution for Concentration Profile

In the moving frame (ζ), the problem simplifies to one of heat conduction with boundary conditions. For large L, where the boundaries at $\zeta = -L$ can be effectively removed, the solution is given by (Carslaw and Jaeger, 1959):

$$C(\zeta, \tau) = \operatorname{erf}\left(-\frac{\zeta}{2\sqrt{\lambda_{\max}\tau}}\right), \quad 0 > \zeta > -L \tag{6.47}$$

Substituting variations in λ between $\lambda = 0$ and $\lambda = \lambda_{\max}$ (Bresler and Dagan, 1983b), τ becomes:

$$\tau = \frac{L^2}{26\lambda_{\max}}, \quad \text{for } \frac{L}{\lambda_{\max}} < 13 \tag{6.48}$$

$$\tau = L - \frac{13}{2}\lambda_{\max}, \quad \text{for } \frac{L}{\lambda_{\max}} > 13 \tag{6.49}$$

Consequently, $C(\zeta, \tau)$ becomes:

$$C(z, t; Y) = \operatorname{erf}\left(\frac{L(t; Y) - z}{\left(\frac{2}{26}\right)^{1/2} L(t; Y)}\right), \quad L < 13\lambda_{\max} \tag{6.50}$$

$$C(z, t; Y) = \operatorname{erf}\left(\frac{L(t; Y) - z}{2\sqrt{\lambda_{\max}\sqrt{L - 6.5}}}\right), \quad L > 13\lambda_{\max} \tag{6.51}$$

The expectation ($E[C]$) and variance (σ_C^2) of solute concentration are computed as:

$$E[C(z, t)] = \int_{-\infty}^{\infty} C(z, t; Y) f_Y(Y) dY \tag{6.52}$$

$$\sigma_C^2(z, t) = \int_{-\infty}^{\infty} (C - E[C])^2 f_Y(Y) dY \tag{6.53}$$

Here, $f_Y(Y)$ is the normal PDF as defined in Equation [6.10].

PDF of Solute Concentration

The probability density function $f_C(z, t; C)$ can be derived using:

$$f_C dC = f_Y dY, \quad P_C = \int_0^C f_C dC = \int_{-\infty}^{Y(z,t;C)} f_Y dY \tag{6.54}$$

which allows for evaluating the fractional area of the field where C is below a specified value. By leveraging the integration of $f_Y dY$ (similar to the statistical moments of $(\overline{S})$ in Section I), this approach seamlessly incorporates solute transport calculations.

Statistical Moments of Solute Concentration

The mean ($E[C]$) and variance (σ_C^2) of solute concentration are computed by:

$$E[C(z,t)] = \int_{-\infty}^{\infty} C(z,t;Y) f_Y(Y) dY \tag{6.55}$$

$$\sigma_C^2(z,t) = \int_{-\infty}^{\infty} (C - E[C])^2 f_Y(Y) dY \tag{6.56}$$

where f_Y is the PDF of Y (Equation [13]).

Computation Procedure for Approximate Model

1. Initialization: Define t, calculate $L(t; Y)$ using Equation [6.15]

$$L_i(t) = \frac{V_i(t)}{(\theta_s - \theta_r)\left(\overline{S} - S_n\right)} \tag{6.57}$$

2. Depth Comparison: Compare $L_i(t)$ with z. If $L_i(t) \geq z$, compute $C_i(z, t; Y_i)$ using Equations [6.49] or [6.50]. Otherwise, set $C_i(z, t; Y_i) = 0$.

3. Iteration: Repeat for $i = 1, 2, \ldots, N$.

4. Statistical Moments: Compute the moments:

$$E[C(z,t)] = \frac{1}{N} \sum_{i=1}^{N} C_i(z,t) \tag{6.58}$$

$$\sigma_C^2(z,t) = \frac{1}{N} \sum_{i=1}^{N} (C_i(z,t) - E[C(z,t)])^2 \tag{6.59}$$

Computation Procedure for Numerical Model

Using finite difference equations to solve the transport equation (6.33) with the boundary condition

$$-D\frac{\partial C}{\partial z}+V(0,t)C(0,t)-\frac{q_0}{\theta(0,t)}=0 \tag{6.60}$$

Dispersivity (λ) and diffusion coefficient (D_m) are calculated using:

$$\lambda=\begin{cases}\lambda_{\text{pore}}+\dfrac{L(t)\left(\lambda_{\max}-\lambda_{\text{pore}}\right)}{13\lambda_{\max}}, & L(t)<13\lambda_{\max},\\ \lambda_{\max}, & L(t)\geq 13\lambda_{\max}\end{cases} \tag{6.61}$$

This yields the final numerical solutions for $E[C]$ and σ_C^2.

6.3.4 Computation of Statistical Moments of C

The statistical moments of solute concentration $C(z,t)$, such as the mean ($E[C]$) and variance (σ_C^2), are computed using known values of m_Y, σ_Y, and six deterministic parameters $(\eta,\beta,\theta_s,\theta_r,K_s^*,\psi_w)$ that characterize the soil field. The initial and boundary conditions, defined by parameters $(R=q_0,t_i,\theta_n)$, characterize the flow. Two computational methods are employed to analyze solute concentration.

Approximate Model

This model computes the equivalent wetting front depth $L(t;Y)$ from Equation [6.15] and substitutes it into Equations [103] or [104] to determine the solute concentration $C(z,t;Y)$. It involves the following steps:

1. Initialization: Set $i\ =\ 1$, define t, and compute $L_i(t)$ using Equation [6.15]:

$$L_i(t)=\frac{V_i(t)}{(\theta_s-\theta_r)\left(\overline{S}-S_n\right)}$$

2. Depth Values: Define and list several values of z.

3. Comparison and Calculation: Compare $L_i(t)$ with the input values of z. If $L_i(t)\geq z$, compute $C_i(z,t)=C(z,t;Y_i)$ from Equations [103] and [104]. Otherwise, set $C_i(z,t)=0$.

4. Iteration: Increment i $(i=2,3,\dots,N)$ and repeat steps 1–3.

5. Statistical Moments: Once $C_i(z,t)$ is determined for all N values, compute the following moments:

Mean:

$$E[C(z,t)] = \frac{1}{N}\sum_{i=1}^{N} C_i(z,t) \tag{6.62}$$

Variance:

$$\sigma_C^2(z,t) = \frac{1}{N}\sum_{i=1}^{N}(C_i(z,t) - E[C(z,t)])^2 \tag{6.63}$$

Skewness:

$$\gamma_C(z,t) = \frac{1}{N}\sum_{i=1}^{N}(C_i(z,t) - E[C(z,t)])^3 \tag{6.64}$$

6. Time Iteration: Change t and repeat steps 1–5.

Numerical Model

For the numerical model, finite difference equations approximate the partial differential equation of water flow problem (Equation [88]), the initial conditions (Equation [89]), and the boundary conditions (Equation [91]). These equations are then solved numerically.

The boundary condition at the soil surface ($z = 0$) for $0 < t \leq t_i$ (Equation [90]) is replaced by the flux condition:

$$-D(\zeta,t)\frac{\partial C}{\partial z} + V(0,t)C(0,t) - \frac{q_0}{\theta(0,t)} = 0 \tag{6.65}$$

Here, $D(\zeta,t) = D_m[\theta(0,t)] + \lambda[L(t)]V(0,t)$, where λ is calculated as:

For $L(t) < 13\lambda_{\max}$:

$$\lambda = \lambda_{\text{pore}} + \frac{L(t)\left(\lambda_{\max} - \lambda_{\text{pore}}\right)}{13\lambda_{\max}} \tag{6.66}$$

For $L(t) \geq 13\lambda_{\max}$:

$$\lambda = \lambda_{\max}$$

Here, $\lambda_{\max} = 3cm$ (Biggar and Nielsen, 1976) and $\lambda_{\text{pore}} = 0.1cm$ (Bresler and Laufer, 1974). The molecular diffusivity is given by:

$$D_m[\theta(0,t)] = D_0 a e^{b\theta(0,t)}$$

with $D_0 = 0.04\,\text{cm}^2/\text{hr}$, $a = 0.002$, and $b = 10$ (Bresler, 1973).

Soil Properties for Numerical Computations

The soil moisture retention curves follow Equation [6.6], with parameters $\beta, \psi, \theta_s, \theta_r$ identical to those used in the approximate model. Hysteresis in the $\theta(\psi)$ relationship is not considered. Hydraulic conductivity (Equation [6.6]) is computed using the same deterministic $\eta, K_s^*, m_Y, \sigma_Y$ values and K_s^i for $i = 1, 2, \ldots, N$.

The calculated values of $C_i(z, t; Y_i)$ are substituted into Equations [6.61], [6.62], and [6.63] to compute the statistical moments of solute concentration. Numerical computations were conducted under the following conditions: 90 depth increments were used, with the increment size varying between 0.05 and 2 cm for $q_0 = 0.5\,\text{cm/hr}$, 0.02 hr to ensure computational accuracy.

6.4 Crop Yield variability

In a field with a spatially variable soil parameter (such as $K_s, \eta, \beta, \theta_s, \theta_r$, etc.) and boundary and initial conditions (R or q_0, θ_n, C_n), crop yield Y (not to be confused with $Y = \ln\delta$ in Equation [12]) is regarded as a random function of the spatial coordinates of the field domain. The dependence of Y on the space coordinates (x, y) is indirect because crop yield depends generally on a set (vector) $\vec{R}$ of boundary and initial conditions (man-controlled variables) and on another set (or a vector) of spatial random functions a. Hence, Y is a functional depending on a set of random variables $\vec{\alpha} = \alpha^{(1)}, \alpha^{(2)}, \cdots, \alpha^{(n)}$, which are generally random functions of $\vec{x}(z, y)$ and the parameters a) are characterized by their unconditional PDF. For any point in the field with area A (i.e., $\vec{x} \in A$), crop yield depends on $\vec{R}(\vec{x})$ and $\vec{\alpha}(\vec{x})$

$$Y(\vec{x}) = f\left[\vec{R}(\vec{x}), \vec{\alpha}(\vec{x})\right] = f\left[R^{(1)}(\vec{x}), \cdots R^{(L)}(\vec{x}), \alpha^{(1)}(\vec{x}), \cdots \alpha^{(n)}(\vec{x})\right] \qquad (6.67)$$

The quantity of general interest to the farmer is the space average yield over the field given by

$$\overline{Y} = \frac{1}{A}\int_A Y(\vec{x})\,dx = \frac{1}{A}\int_A f\big[\vec{R}(\vec{x}), \vec{\alpha}(\vec{x})\big]\,dx \tag{6.68}$$

where A is the area of the field. Since the field spatial average Y is an integral, it can be regarded as a sum of random variables with finite mean and variance and therefore Y is approximately normally distributed and characterized entirely by its expectation and variance. Finding these two first central moments by two different types of approximation is the aim of the next subsection.

6.4.1 Computations of Expectation and Variance Using the Taylor Expansion

To derive approximate relationships between the statistical moments of $\overline{Y}$ (Equation [112]) and the moments of $\vec{R}(\vec{x})$ and $\vec{\alpha}(\vec{x})$, second-order Taylor expansion (see Abramowitz and Segun, 1964), about the expectations $E\big[\vec{R}(\vec{x})\big]$ and $E[\vec{\alpha}(\vec{x})]$, is used to give

$$\begin{aligned}
Y\big(R^{(1)}, \cdots R^{(L)}, \alpha^{(1)}, \cdots, \alpha^{(n)}\big) &= Y\big[E\big(R^{(1)}\big), \cdots, E\big(R^{(L)}\big), E\big(\alpha^{(1)}\big), \cdots, E\big(\alpha^{(n)}\big)\big] \\
&+ \sum_{j=1}^{L}\left[\{R^{(j)} - E\big(R^{(j)}\big)\}\frac{\partial Y}{\partial R^{(j)}}\bigg|_{E(R^{(j)})}\right] + \sum_{j=1}^{n}\left[\{\alpha^{(j)} - E\big(\alpha^{(j)}\big)\}\frac{\partial Y}{\partial \alpha^{(j)}}\bigg|_{E(\alpha^{(j)})}\right] \\
&+ \frac{1}{2}\sum_{j=1}^{L}\sum_{k=1}^{L}\big[\{R^{(j)} - E\big(R^{(j)}\big)\}\{R^{(k)} - E\big(R^{(k)}\big)\}\big]\frac{\partial^2 Y}{\partial R^{(j)}\partial R^{(k)}}\bigg|_{E(R^{(j)}),E(R^{(k)})} \\
&+ \frac{1}{2}\sum_{j=1}^{L}\sum_{k=1}^{L}\big[\{\alpha^{(j)} - E\big(\alpha^{(j)}\big)\}\{\alpha^{(k)} - E\big(\alpha^{(k)}\big)\}\big]\frac{\partial^2 Y}{\partial \alpha^{(j)}\partial \alpha^{(k)}}\bigg|_{E(\alpha^{(j)}),E(\alpha^{(k)})}
\end{aligned} \tag{6.69}$$

The expected value of $Y(\vec{x}) = Y\big[\vec{R}(\vec{x}), \vec{\alpha}(\vec{x})\big]$ is obtained by taking the expectation (averaging) of Equation [113] to get

$$\begin{aligned}
E[Y] &= Y\big[E\big(\alpha^{(1)}\big), E\big(\alpha^{(2)}\big)\cdots, E\big(\alpha^{(k)}\big)\big] \\
&+ \frac{1}{2}\sum_{j=1}^{N}\sum_{k=1}^{N} C^{(jk)}(\vec{x}, \vec{x})\frac{\partial^2 Y}{\partial \alpha^{(j)}\partial \alpha^{(k)}}\bigg|_{E(\alpha^{(j)}),E(\alpha^{(k)})}
\end{aligned} \tag{6.70}$$

where $N = L + n$ and α denotes hereafter any soil, man-controlled, and boundary and initial conditions, and $C^{(jk)}$ is the covariance defined by

$$C^{(jk)}(\overrightarrow{x_1},\overrightarrow{x_2}) = E\left[\{\alpha^{(j)}(\overrightarrow{x_1}) - E\left(\alpha^{(j)}(\overrightarrow{x_1})\right)\}\{\alpha^{(k)}(\overrightarrow{x_2}) - E\left(\alpha^{(k)}(\overrightarrow{x_2})\right)\}\right] \quad (6.71)$$

To simplify matters, it is assumed that a are weakly stationary and uncorrelated so that $E\left[\alpha^{(j)}\right] = \text{constant}$, $C^{(jk)} = 0$ for $j \neq k$, and $C^{(jk)} = \sigma^{(j)^2}$

= constant variance for $j = k$. Under these assumptions, the expectation of Y is

$$E[Y] = Y\left[E\left(\alpha^{(1)}\right), E\left(\alpha^{(2)}\right)\cdots, E\left(\alpha^{(N)}\right)\right] + \frac{1}{2}\sum_{j=1}^{N}\sigma^{(j)^2}\left.\frac{\partial^2 Y}{\partial\sigma^{(j)^2}}\right|_{E\left(\alpha^{(j)}\right)} \quad (6.72)$$

This means that the expectation of crop yield in a spatially variable field is approximately equal to the yield that would be achieved in a homogeneous field with the average parameter value plus the sum of products of the variance of each specific parameter and the second derivative of the yield, with respect to the specific parameter, evaluated at the expected value of that parameter. Equation [116] enables one to analyze the variability effect of each parameter on the expected yield.

Note that the second-order Taylor expansion may be a good approximation as long as $\sigma^{(j)^2}$ is relatively small for any soil or man-controlled parameter $i = 1, 2, \ldots, n$. This enables one to neglect even order terms larger than 2 in cases of multivariate normal distribution. In field cases where the variance of a given one or two parameters is relatively large and the other soil or control parameters are relatively uniform, crop yield expectation can be approximated by a numerical quadrature of

$$E\left[Y\left(\alpha^{(1)},\alpha^{(2)}\right)\right] = \iint Y\left(\alpha^{(1)},\alpha^{(2)}\right)f\left(\alpha^{(1)}\right)f\left(\alpha^{(2)}\right)d\alpha^1 d\alpha^2 \quad (6.73)$$

if α^1 and α^1 are independent or by

$$E[Y(\alpha\text{^}\{(1)\}] = \iint Y(\alpha^{(1)}f\left(\alpha^{(1)}\right)d\alpha^1 \quad (6.74)$$

if only one soil parameter is highly variable (the rest are deterministic) or if the influence of the variability of the other parameters on yield is negligibly small. Since $E[Y(x)]$ is independent of x, then

$$E\left[\overline{Y}\right] = E[Y(\vec{x})] \quad (6.75)$$

The variance $\sigma_{\overline{Y}}^2$ of field average yield $\overline{Y}$ (i.e., $\sigma_{\overline{Y}}^2 = \{\overline{Y}(\vec{x}) - E\left[\overline{Y}(\vec{x})\right]\}^2$, is given by

$$\sigma_{\overline{Y}}^2 = \frac{1}{A^2}\int_A\int_A C_Y(x_1, x_2)\ dx_1 dx_2 \qquad (6.76)$$

where

$$C_Y = E[\{Y(\overrightarrow{x_1}) - E[Y(x_1)]\}\{Y(\overrightarrow{x_2}) - E[Y(x_2)]\}] = E[Y'(x_1)Y'(x_2)] \qquad (6.77)$$

is the covariance of Y. Taylor expansion of the residuals $Y'\left(\overrightarrow{\alpha^{(j)}}\right)$ about $E\left[Y\left(\alpha^{(j)}\right)\right]$ yields the first-order expansion

$$Y'\left(\alpha^{(1)}, \alpha^{(2)}, \cdots, \alpha^{(2n)}\right) = \sum_{j=1}^{N}\left(\overrightarrow{\alpha^{(j)}} - E\left[\overrightarrow{\alpha^{(j)}}\right]\right)\frac{\partial Y}{\partial \alpha^{(j)}}\bigg|_{E\left(\alpha^{(j)}\right)} \qquad (6.78)$$

From equations (6.74)-(6.77) one gets

$$\sigma_{\overline{Y}}^2 = \sum_{j=1}^{N}\sum_{k=1}^{N}\left[\frac{1}{A^2}\int_A\int_A C^{(jk)}(\overrightarrow{x_1}, \overrightarrow{x_2})\ d\overrightarrow{x_1}d\overrightarrow{x_2}\right]\left(\frac{\partial Y}{\partial \alpha^{(j)}}\bigg|_{E\left(\alpha^{(j)}\right)}\right)\left(\frac{\partial Y}{\partial \alpha^{(k)}}\bigg|_{E\left(\alpha^{(k)}\right)}\right) \quad (6.79)$$

For stationary $\alpha^{(j)}$

$$C^{(jk)}(\overrightarrow{x_1}, \overrightarrow{x_2}) = C^{(jk)}(\overrightarrow{x_1} - \overrightarrow{x_2}) \qquad (6.80)$$

Using Cauchy algorithm (Feinerman et al., 1985)

$$\iint C^{(jk)}(\overrightarrow{x_1} - \overrightarrow{x_2})\ dx_1 dx_2 = \int C^{(jk)}(\vec{r})H(\vec{r})dr \qquad (6.81)$$

where $\vec{r} = \overrightarrow{x_1} - \overrightarrow{x_2}$ and $H(r)$ is the area of the domain covered jointly by A (the overlapping domain of A) and its translation by r. Thus, if A is a square of sides D, $H(r)$ is given in a cartesian system of coordinates by

$H(x, y) = \left(\frac{D}{2} - |x|\right)\left(\frac{D}{2} - |y|\right)$ for $|\vec{x}| < \frac{D}{2}$ and $|\vec{y}| < \frac{D}{2}$; otherwise, $H = 0$

Similarly, for a circle of diameter D we have

$$H(r) = \frac{D^2}{2}\left[cos^{-1}\left(\frac{r}{D}\right) - \frac{r}{D}\left(1 - \frac{r^2}{D^2}\right)^{1/2}\right] \qquad (6.82)$$

for $r = (x^2 + y^2)^{1/2} < D$; $H = 0$ for $r > D$, while $H(r) = A$ for $r = 0$. Substitute Equation [125] into Equation [123] using Equation [124], and if a are uncorrelated functions then

$$\sigma_{\bar{Y}}^2 = \sum_{j=1}^{N} \frac{\sigma^{(j)^2}}{A^2} \left[\int_A \rho^{(j)}(\vec{r}) H(\vec{r}) d\vec{r} \right] \left(\frac{\partial Y}{\partial \alpha^{(j)}} \Big|_{E(\alpha^{(j)})} \right)^2 \qquad (6.83)$$

where

$$\rho^{(j)}(\vec{r}) = C^{(j)}(\vec{r}) / \sigma^{(j)^2} \qquad (6.84)$$

is the autocorrelation function of the soil parameter or control variable $\alpha^{(j)}$. A simple autocorrelation function commonly used is the exponential

$$\rho^{(j)}(\vec{r}) = exp\left[-r/I^{(j)}\right] \qquad (6.85)$$

where $I^{(j)}$ is the linear integral scale of the variable $\alpha^{(j)}$ defined by

$$\int_0^\infty \rho^{(j)}(\vec{r}) d\vec{r} = I^{(j)} \qquad (6.86)$$

Hence, for an integral scale much smaller than the field "diameter" (D), that is, for $I^{(j)} \ll D, H(r) = A$ and Equation [6.82] becomes

$$\sigma_{\bar{Y}}^2 \cong \sum_{j=1}^{N} \frac{\sigma^{(j)^2}}{A} \left[\int_A \rho^{(j)}(\vec{r}) d\vec{r} \right] \left(\frac{\partial Y}{\partial \alpha^{(j)}} \Big|_{E(\alpha^{(j)})} \right)^2 \qquad (6.87)$$

If, on the other hand, $\alpha^{(j)}$ are fully correlated, that is, $\rho^{(j)}(\vec{r}) = 1$ for any $\vec{r}$ and $\alpha^{(j)}$, then the contribution to $\sigma_{\bar{Y}}^2$ is

$$\sigma_{\bar{Y}}^2 = \sum_{j=1}^{N} \sigma^{(j)^2} \left(\frac{\partial Y}{\partial \alpha^{(j)}} \Big|_{E(\alpha^{(j)})} \right)^2 \qquad (6.88)$$

The modeling problem in order to calculate the two central moments of Equations [6.71] (or Equations [6.72] and [6.73]) and [6.86] or [6.87], boils down to the simulation of $Y\{E[\alpha^{(j)}]\}, j = 1,2, \dots, N$, and the estimation of the respective $\sigma^{(j)^2}$. First and second partial derivatives of Y with respect to each $\alpha^{(j)}$, evaluated at the expectation of the same parameter $E[\alpha^{(j)}]$, can then be obtained from the $Y(E[\alpha^{(j)}])$. This latter function can, in turn, be estimated from any transpiration model including salinity effects by assuming De Wit's relationships (Bresler et al., 1982) between transpiration and dry matter yield (Y)

$$Y = mT_r/E_0 \qquad (6.89)$$

Here T_r, is seasonal transpiration, E_0 is seasonal free water evaporation, and m is a crop coefficient. For a given crop and year with m and E_0 constant, relative yield is obtained from Equation [6.88] as

$$Y/Y_p = T_r/T_p \qquad (6.90)$$

where Y_p , and T_p , are potential yield and potential transpiration, respectively. Deterministic models (Bresler et al., 1982) aimed at calculating transpiration (and therefore dry matter production or in some cases commercial yield) lead to the most general form of crop yield function such as (see Bresler et al., 1982):

$$Y = Y\left(\overrightarrow{\alpha^{(J)}}\right) = Y(\delta, K_s^*, \eta, \beta, h_a, \theta_s, \theta_r, \lambda, b, \psi_{cr}, \phi, m, F, E_o, R, Co, \theta_n, Cn) \quad (6.91)$$

where $\delta, K_s^*, \eta, \beta, h_a, \theta_s, \theta_r,$ and λ are soil parameters characterizing water flow and solute transport; $b, \psi_{cr}, \phi, m,$ and F are plant parameters; $R, Co, \theta_n,$ and Cn, are man-controlled variables characterizing the boundary and initial conditions; and E_0, is a climatic boundary condition replacing *R* during the evapotranspiration stage. Here, *b* represents the area of influence of a root, ψ_{cr} is the critical (lowest possible) plant-root water potential, is the root distribution parameter, F is the crop factor, C_o is solute concentration in water, and $m, \delta, K_s^*, \eta, \beta, h_a, \theta_s, \theta_r, \lambda, E_0, R, \theta_n$ and C_n are as defined before.

The computation procedures for $E\left[Y\left(\overrightarrow{\alpha^{(J)}}\right)\right]$ and $\sigma_{\bar{Y}}^2$ involve the following steps for each $\alpha^{(J)}$ (Equation [136]) for $j = 1, 2, \dots, N$ and $N = 18$:

1. Input $\hat{E}\left[\alpha^{(J)}\right], \widehat{\sigma^{J^2}}, j = 1, 2, \dots, N$ and divide the range between $\hat{E}\left[\alpha^{(J)}\right] + 2\widehat{\sigma^J}$ and $\hat{E}\left[\alpha^{(J)}\right] - 2\widehat{\sigma^J}$ ($\widehat{}$ denotes estimated values) into $M - 1$ equal segments, such that $\alpha_1^{(j)} = \hat{E}\left[\alpha^{(J)}\right] - 2\widehat{\sigma^J}$ and $\alpha_M^{(j)} = \hat{E}\left[\alpha^{(J)}\right] + 2\widehat{\sigma^J}$.

2. Set $i = i + 1$.

3. Calculate $Y_i^{(j)}\{E\left[\overrightarrow{\alpha^{(k)}}\right], \alpha_i^{(j)}\}$ $(k = 1,2, \dots, N; k \neq j)$ from numerical solution of Equation [136]. Note that for $N > j \gg 2, k = 1, 2, \dots, j - 1, j + 1, \dots, N$.

4. If $i < M$, go back to Step 2.

5. Apply spline subroutine and approximate

$$\left.\frac{\partial Y^j}{\partial \alpha^j}\right|_{E[\alpha^{(j)}]}, \left.\frac{\partial^2 Y^j}{\partial {\alpha^j}^2}\right|_{E[\alpha^{(j)}]}$$

6. Calculate σ_Y^2 from Equation [132] or [133] and $E\left[Y^{(j)}\left(\alpha^{(j)}\right)\right]$ from Equation [116] (or [117] or [118], if applied, by a numerical quadrature over the range of $m_\alpha \pm 2\sigma_\alpha$.

7. Change j and repeat from Step 1 above.

6.5 Model Results and Discussion

The simulations represent infiltration and redistribution in Jaipur's sandy loam, followed by solute movement under the same flow conditions. Parameter values were taken from local soil studies, with variability in saturated hydraulic conductivity K_s described by m_Y and σ_Y.

Water Flow Results

Fig. (a): Deterministic S(z) profiles

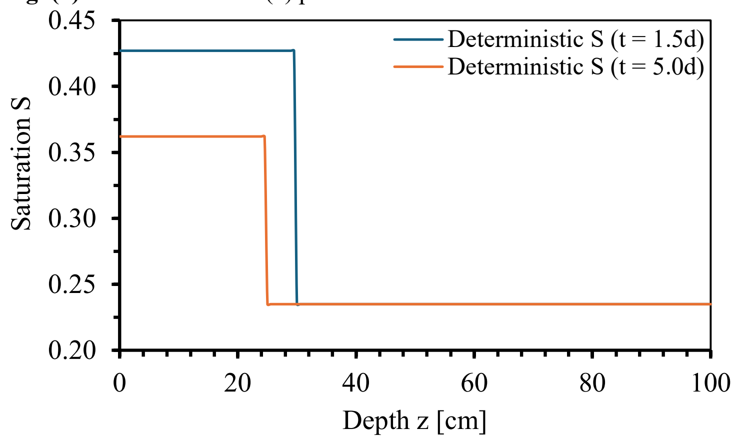

Fig. (b): Stochastic mean E[S(z)]

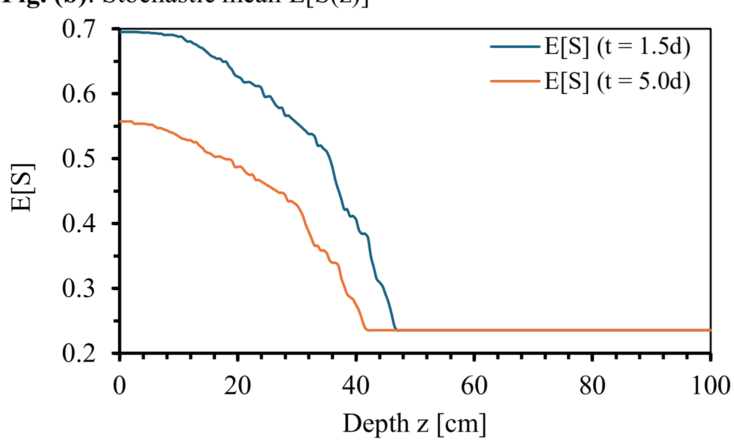

Fig. (c): Coefficient of variation of S(z)

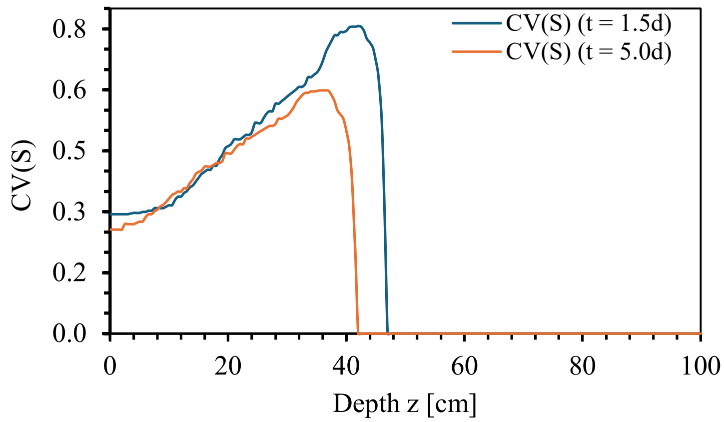

Fig. (d): Deterministic vs stochastic (t = 1.5d)

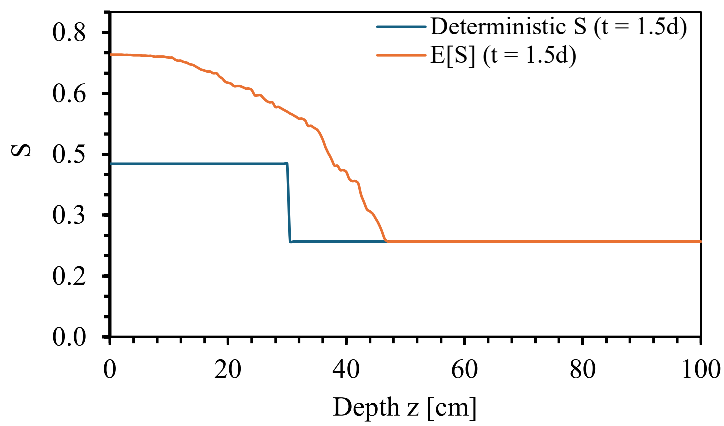

Fig. (e): Deterministic vs stochastic (t = 5d)

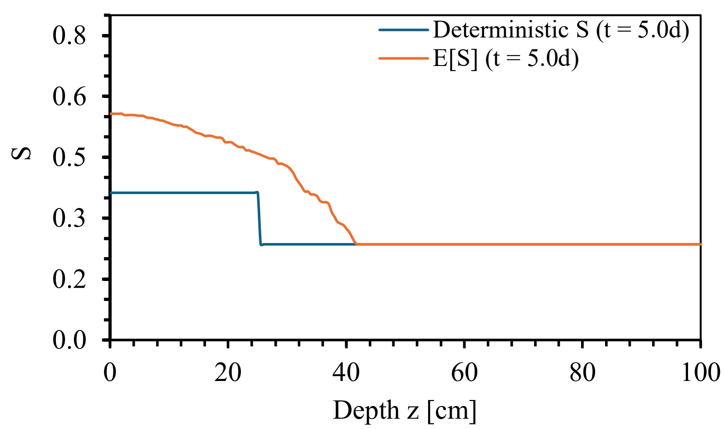

Figure 6.1 Water-flow results for Jaipur sandy loam under stochastic infiltration–redistribution conditions. Fig. (a) to (c) show deterministic S(z), stochastic mean E[S(z)], and coefficient of variation CV(S) at t = 1.5 days and t = 5.0 days and Fig. (d) to (e) compare deterministic and stochastic profiles.

In the deterministic case (uniform K_s), the piston-flow solution shows a sharp wetting front: 40 cm deep at the end of infiltration ($t = 1.5$ days) and 55 cm deep after redistribution ($t = 5.0$ days). This is an idealized pattern that assumes all soil pores are the same size. In the stochastic simulations, which treat K_s as spatially variable, the average wetting front penetrates deeper and is smoother in shape. The coefficient of variation CV(S) peaks near the wetting front and stays high even days after infiltration ends, showing that heterogeneity effects persist well into redistribution. Deterministic models underestimate this depth and miss the effect of preferential flow paths in high-conductivity zones.

Solute Transport Results

Fig. (a) Deterministic C(z) profiles

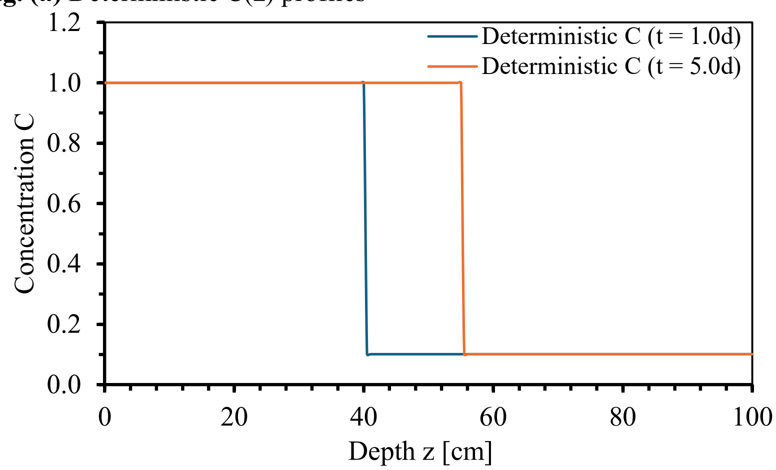

Fig. (b) Stochastic mean E[C(z)]

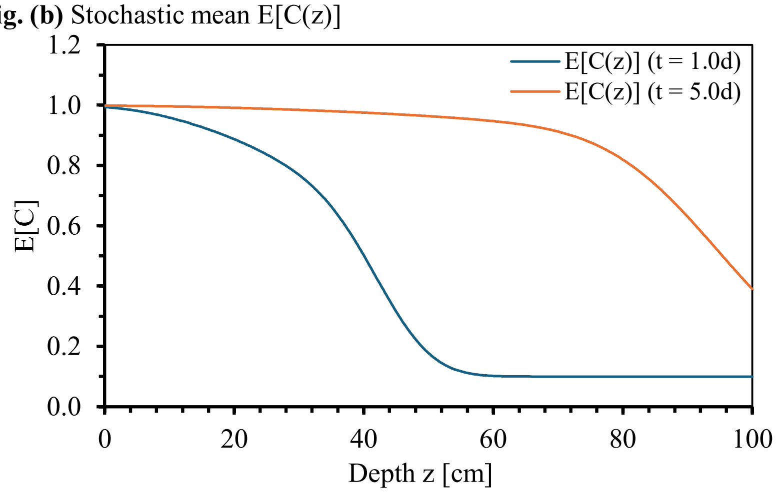

Fig. (c) Coefficient of variation CV(C)

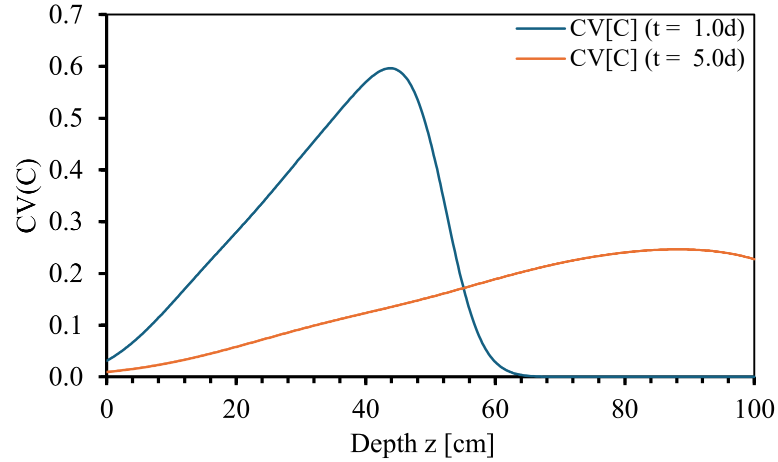

Fig. (d) Deterministic vs Stochastic (t=1.0d)

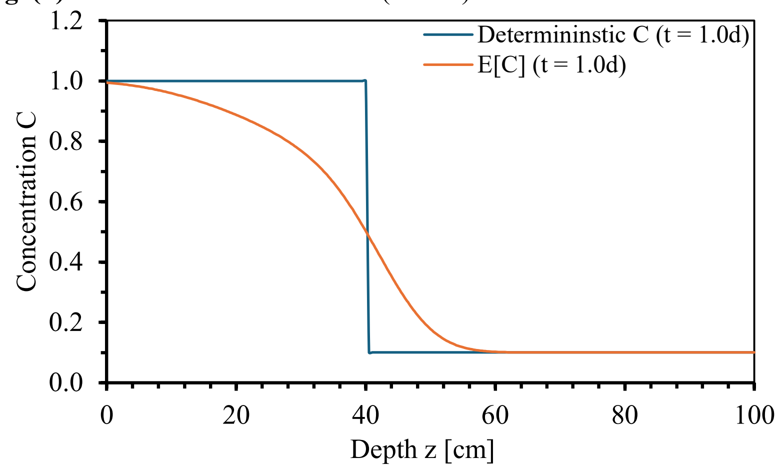

Fig. (e) Deterministic vs Stochastic (t=5.0 d)

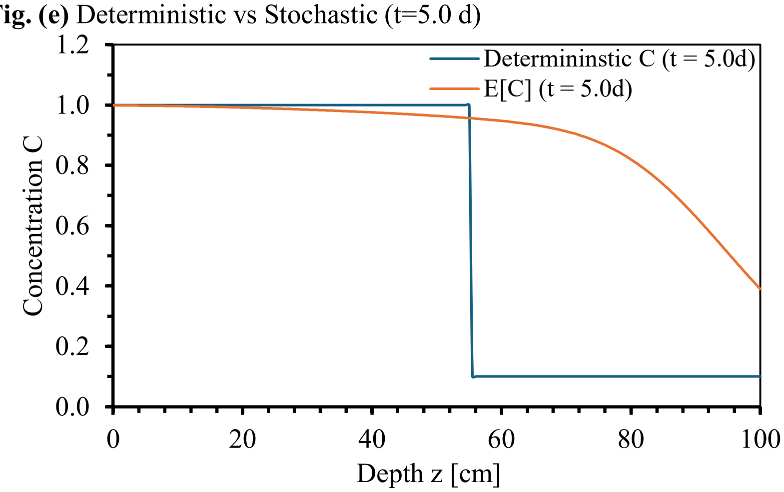

Figure 6.2: Solute-transport results for Jaipur sandy loam under stochastic infiltration–redistribution. Fig. (a) to (c) show deterministic $C(z)$, stochastic mean $E[C(z)]$, and coefficient of variation $CV(C)$ at end infiltration ($t = 1.5$ days) and after redistribution ($t = 5.0$ days) and Fig. (d) to (e) compare deterministic and stochastic profiles.

Using the same flow conditions, solute transport was modeled with an initial concentration C_n in the soil and a higher concentration C_0 applied at the surface for $t \leq t_i$. Deterministic piston-type solutions give sharp solute fronts at 40 cm ($t = 1.0$ day) and 55 cm ($t = 5.0$ days). In stochastic simulations (400 realizations of log-normally distributed K_s), the mean concentration profiles E[C(z)] are smoother and extend deeper than deterministic predictions, again reflecting preferential movement in higher-K_s regions. The variability CV(C) is highest at the moving front and remains significant after redistribution, meaning solute heterogeneity persists long after infiltration stops. Deterministic models underestimate solute depth and cannot capture this variability.

The water-flow results explain the solute-transport patterns: in heterogeneous soils, water moves faster through some pathways, carrying solutes deeper and more unevenly than uniform-soil models predict. Both E[S(z)] and E[C(z)] show deeper penetration in stochastic cases, and both CV(S) and CV(C) remain high after redistribution. This persistence matters for irrigation and pollution control in Jaipur's sandy loam—solutes can travel quickly through preferential flow paths, increasing leaching risk and reducing the effectiveness of surface-applied nutrients.

Implications for Crop Yield Variability

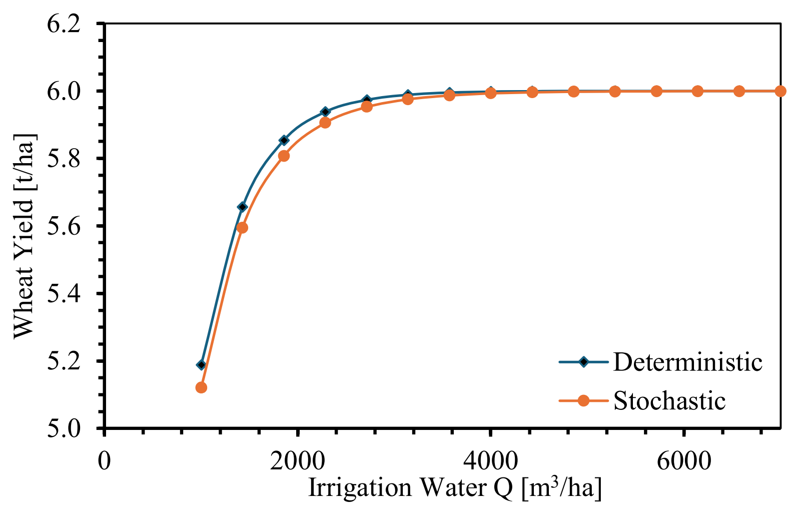

Figure 6.3 Wheat yield response to irrigation water (Q) for Jaipur sandy loam under deterministic and stochastic soil conditions

The deterministic curve assumes a uniform soil with mean α, representing idealized conditions. The stochastic curve accounts for spatial variability in soil properties (σ_α), simulating heterogeneous field conditions using a Mitscherlich-type production function. Results show that yield increases with irrigation water for both cases, but the stochastic yield is consistently lower than the deterministic yield at higher Q due to the impact of soil heterogeneity on water-use efficiency. This highlights the importance of accounting for variability in irrigation planning for Jaipur's wheat crops.

6.6 Conclusion

In Jaipur's sandy loam, stochastic modeling of water flow, solute transport, and wheat yield revealed that soil variability significantly alters infiltration depth, solute migration, and crop productivity compared to uniform-soil (deterministic) predictions. Stochastic simulations captured deeper, smoother wetting fronts, faster solute movement in high-conductivity zones, and persistent variability in both water and solute distributions. These effects translated into more realistic yield–irrigation relationships, highlighting that deterministic models tend to overestimate yields under moderate irrigation and underestimate risks of nutrient loss and yield variability. Overall, incorporating spatial heterogeneity into modeling provides a more accurate basis for irrigation planning and risk assessment in semi-arid agricultural systems.

Chapter 7

Conclusions

and

Future Directions

Chapter 7

Conclusions and Future Directions

The main goal of this research was to develop and test mathematical models that describe how water, nutrients, and pollutants move through soil, how plants take them up, and how these processes influence crop yields in semi-arid conditions. The work combined deterministic and stochastic modeling approaches, using the HYDRUS-1D software to simulate real-world conditions in four agro-climatic zones of Jaipur. The study followed a step-by-step approach:

1. Model water flow and root water uptake (Chapter 3).
2. Extend the model to nutrient transport and uptake with realistic root branching (Chapter 4).
3. Link nutrient and pollutant loads to crop yield through combined response functions (Chapter 5).
4. Incorporate spatial variability into the modeling to reflect real field conditions (Chapter 6).

7.1 Summary of Key Findings

One of the clearest findings of this research is that most water uptake happens close to the surface—within the top 40–60 cm of soil—where the majority of active roots are found. Deeper layers stay wetter for longer, but because roots are scarce there, these layers are also where nutrients are most likely to be lost through leaching.

The movement of nitrate in the soil was shown to be highly dependent on soil type. In sandy soils, nitrate travelled quickly downwards, which meant plants could access it early but also risked losing it beyond the root zone. Loamier soils held nitrate in the active root zone for longer, which improved uptake efficiency. Fine-textured soils tended to keep nitrate near the surface, which sometimes limited deep uptake but still carried the risk of eventual leaching.

Timing proved to be crucial. The models showed that mid-growth stages (T2–T3) were the best period for nutrient uptake, making a strong case for split fertilizer applications or slow-release formulations to match plant demand.

Another key insight is that while nutrients are essential for yield, pollutants can quietly undermine their benefits. When pollutant levels were high, the positive effects of nitrogen were reduced, sometimes significantly.

Finally, the study demonstrated that accounting for soil variability changes the whole picture. Stochastic models, which factor in natural differences across a field, gave more realistic predictions than uniform-soil models. They revealed that yields are often overestimated when variability is ignored, and that the risks of nutrient loss are higher than deterministic models suggest.

7.2 Theoretical and Practical Contributions

Theoretical contributions:

From a theoretical point of view, one of the most significant achievements is the creation of a zone-specific integrated modeling framework. Instead of using a "one-size-fits-all" model, this framework was tailored for four distinct agro-climatic zones in Jaipur. By combining real field data with advanced mathematical modeling, it captures how water moves through the soil, how nutrients and pollutants travel, and how these factors together influence crop yield. This makes the model far more accurate and relevant to local conditions than generic approaches.

Another breakthrough is the inclusion of multiple root branching structures in nutrient uptake simulations. Traditional models often treat roots as simple, uniform structures, but in reality, roots spread out in complex patterns that influence how plants access nutrients. By adding realistic root architecture to the model, this research provides a more accurate picture of how nutrients are actually absorbed, and how this process changes with soil type and moisture levels.

A further innovation is the linking of nutrient response functions and pollutant stress functions with the Advection–Dispersion Equation (ADE). This integration allows the model to reflect both sides of the story: how nutrients boost crop growth and how pollutants can reduce yield. The result is a unified tool that can predict yield under different combinations of nutrient supply and pollution stress, offering a more complete understanding of soil–plant interactions.

Finally, the use of stochastic modeling techniques is a key theoretical contribution. Farming fields are not perfectly uniform—soil properties can vary greatly even within a small area. By including this natural variability in the model, the research provides more realistic predictions of water movement, nutrient behavior, and crop yields. This helps bridge the gap between laboratory-based simulations and real-world farming conditions, where unpredictability is the norm.

Practical contributions:

From a practical perspective, the findings offer clear, actionable recommendations for improving farming practices in semi-arid wheat systems. For example, the model highlights the importance of carefully timed irrigation scheduling. Applying water when plants can use it most effectively not only supports healthy growth but also reduces nutrient losses through deep leaching.

The research also delivers guidelines for fertilizer application, showing that splitting fertilizer into smaller, well-timed doses or using slow-release formulations can significantly improve nutrient use efficiency and prevent wastage. This not only saves money for farmers but also reduces the risk of environmental damage.

Perhaps most importantly, the study offers strategic insights into nitrogen management. Nitrogen is essential for crop growth, but too much of it can harm the environment, especially by contaminating groundwater. The modeling framework developed here can help farmers and policymakers find the right balance—maximizing yields while protecting soil and water resources for the future.

Together, these theoretical advancements and practical recommendations make this research valuable both to the scientific community and to those working directly on the ground in agriculture. They demonstrate how advanced modeling, when combined with local field data, can lead to smarter, more sustainable farming practices.

7.3 Limitations and Sources of Uncertainty

Although the models developed in this research are strong and produce valuable insights, it is important to recognise their boundaries and the uncertainties that remain.

These limitations do not reduce the significance of the findings, but they do highlight where caution is needed in applying the results and where future improvements could be made.

First, the field data used to build and calibrate the models came from only four zones in Jaipur. While these zones were chosen to represent a range of soil textures and agro-climatic conditions, they cannot capture the full diversity of soils and farming practices found in other regions. This means that the models should be tested and adjusted before being applied to new areas.

Second, the modelling work focused mainly on nitrogen as the key nutrient. Nitrogen is indeed critical for wheat growth, but it does not work alone—other nutrients such as phosphorus, potassium, and micronutrients also play vital roles. Interactions between multiple nutrients can sometimes amplify or reduce crop responses, and these effects were not fully explored here.

Third, the models did not explicitly include microbial processes and chemical transformations in the soil, such as nitrification and denitrification. These processes can change the form, availability, and mobility of nitrogen, influencing both crop uptake and environmental losses. Ignoring them simplifies the model but can also overlook important dynamics, especially in wetter or more biologically active soils.

Finally, in the stochastic modeling approach, the variability of soil properties—such as hydraulic conductivity, texture, and organic matter content—was assumed to be constant over time. In reality, soils are dynamic. Management practices, weather patterns, and biological activity can alter these properties seasonally or even within a single growing season. This assumption of stability may therefore underestimate the true variability in water and nutrient movement.

By acknowledging these limitations, the research creates a clear starting point for targeted improvements. Addressing them will make future models more accurate, more adaptable, and even more relevant to real-world agricultural challenges.

7.4 Future Research Directions

While this research answers many important questions, it also opens the door to new ones. There are several promising directions for future work that could make the models even more powerful and the recommendations even more precise.

First, there is a clear need to model multiple nutrients and pollutants together. This study focused mainly on nitrogen, but crops also depend on phosphorus, potassium, and other micronutrients, and these often interact with each other in complex ways. Understanding these combined effects would help in designing more balanced and efficient fertilization strategies.

Second, the models could be expanded to include climate change scenarios. Changes in rainfall patterns, rising temperatures, and more frequent extreme weather events are likely to affect both water movement and nutrient cycling in the soil. Integrating climate projections would help farmers and policymakers prepare for these shifts.

Third, broader field testing is essential. While this work was based on detailed data from four zones in Jaipur, applying the models in other regions and soil types would improve their general applicability and make them more useful for large-scale agricultural planning.

Fourth, future versions of the model should include microbial and chemical transformation processes in greater detail. Processes like nitrification and denitrification, which change the form and availability of nitrogen in the soil, can have a big impact on both yields and environmental outcomes.

Finally, there is great potential in combining these models with remote sensing and machine learning. Satellite and drone data could be used to update model parameters in real time, while machine learning could help spot patterns and improve predictions. This would bring the modeling closer to becoming a dynamic decision-support tool for farmers, giving them guidance that adapts to their fields' conditions day by day.

This thesis brings together soil physics, plant physiology, and environmental science into a single modeling framework that reflects both the complexity of agricultural systems and the need for practical decision-making tools. By linking water flow, nutrient and pollutant dynamics, and yield responses—while accounting for natural variability—it offers both scientific advancements and practical recommendations for sustainable farming in semi-arid regions. The insights gained here can help farmers, researchers, and policymakers work together to improve productivity while safeguarding soil and water resources for the future.

APPENDIX

APPENDIX

Table 1: Daily Rainfall Records for Jaipur District (December 2024 – March 2025)

Date	Rainfall (mm/day)	Date	Rainfall (mm/day)	Date	Rainfall (mm/day)	Date	Rainfall (mm/day)
01-12-24	0	01-01-25	0	01-02-25	0	01-03-25	0
02-12-24	0	02-01-25	0	02-02-25	0	02-03-25	0
03-12-24	0	03-01-25	0	03-02-25	0	03-03-25	0
04-12-24	0	04-01-25	0	04-02-25	0	04-03-25	0
05-12-24	0	05-01-25	0	05-02-25	0	05-03-25	0
06-12-24	0	06-01-25	0	06-02-25	0	06-03-25	0
07-12-24	0	07-01-25	0	07-02-25	0	07-03-25	0
08-12-24	0	08-01-25	0	08-02-25	0	08-03-25	0
09-12-24	0	09-01-25	0	09-02-25	0	09-03-25	0
10-12-24	0	10-01-25	0	10-02-25	0	10-03-25	0
11-12-24	0	11-01-25	4.5	11-02-25	0	11-03-25	0
12-12-24	0	12-01-25	5	12-02-25	0	12-03-25	0
13-12-24	0	13-01-25	0	13-02-25	0	13-03-25	0
14-12-24	0	14-01-25	0	14-02-25	0	14-03-25	0
15-12-24	0	15-01-25	10	15-02-25	0	15-03-25	0
16-12-24	0	16-01-25	10.5	16-02-25	0	16-03-25	0
17-12-24	0	17-01-25	0	17-02-25	0	17-03-25	0
18-12-24	0	18-01-25	0	18-02-25	1	18-03-25	0
19-12-24	0	19-01-25	0	19-02-25	0	19-03-25	0
20-12-24	0	20-01-25	0	20-02-25	0	20-03-25	0
21-12-24	0	21-01-25	0	21-02-25	0	21-03-25	0
22-12-24	0	22-01-25	0	22-02-25	0	22-03-25	0
23-12-24	0	23-01-25	0	23-02-25	0	23-03-25	0
24-12-24	0	24-01-25	0	24-02-25	0	24-03-25	0
25-12-24	0	25-01-25	0	25-02-25	0	25-03-25	0
26-12-24	0	26-01-25	0	26-02-25	0	26-03-25	0
27-12-24	10	27-01-25	0	27-02-25	0	27-03-25	0
28-12-24	10	28-01-25	0	28-02-25	0	28-03-25	0
29-12-24	0	29-01-25	0			29-03-25	0
30-12-24	0	30-01-25	0			30-03-25	0
31-12-24	0	31-01-25	0			31-03-25	0

Source: India-WRIS (https://indiawris.gov.in), *Rainfall time series data retrieved from India-Water Resources Information System, Ministry of Jal Shakti, Government of India for Jaipur District, December 2024 to March 2025.*

Table 2: Daily Evapotranspiration Records for Jaipur District (December 2024 – March 2025)

Date	Evapo-transpiration (in mm)	Transpiration (mm)	Evaporation (mm)	Date	Evapo-transpiration (in mm)	Transpiration (mm)	Evaporation (mm)
01-12-2024	0.1	0.02	0.08	30-01-2025	0.4	0.28	0.12
02-12-2024	0.1	0.02	0.08	31-01-2025	0.37	0.259	0.111
03-12-2024	0.1	0.02	0.08	01-02-2025	0.42	0.294	0.126
04-12-2024	0.1	0.02	0.08	02-02-2025	0.39	0.273	0.117
05-12-2024	0.09	0.018	0.072	03-02-2025	0.41	0.287	0.123
06-12-2024	0.1	0.02	0.08	04-02-2025	0.34	0.238	0.102
07-12-2024	0.1	0.02	0.08	05-02-2025	0.1	0.07	0.03
08-12-2024	0.09	0.018	0.072	06-02-2025	0.39	0.273	0.117
09-12-2024	0.08	0.016	0.064	07-02-2025	0.37	0.259	0.111
10-12-2024	0.08	0.016	0.064	08-02-2025	0.4	0.28	0.12
11-12-2024	0.08	0.016	0.064	09-02-2025	0.33	0.231	0.099
12-12-2024	0.08	0.016	0.064	10-02-2025	0.34	0.238	0.102
13-12-2024	0.09	0.018	0.072	11-02-2025	0.32	0.224	0.096
14-12-2024	0.09	0.018	0.072	12-02-2025	0.31	0.217	0.093
15-12-2024	0.09	0.018	0.072	13-02-2025	0.31	0.217	0.093
16-12-2024	0.09	0.036	0.054	14-02-2025	0.32	0.224	0.096
17-12-2024	0.09	0.036	0.054	15-02-2025	0.31	0.217	0.093
18-12-2024	0.08	0.032	0.048	16-02-2025	0.29	0.174	0.116
19-12-2024	0.08	0.032	0.048	17-02-2025	0.28	0.168	0.112
20-12-2024	0.08	0.032	0.048	18-02-2025	0.24	0.144	0.096
21-12-2024	0.08	0.032	0.048	19-02-2025	0.35	0.21	0.14
22-12-2024	0.08	0.032	0.048	20-02-2025	0.28	0.168	0.112
23-12-2024	0.07	0.028	0.042	21-02-2025	0.33	0.198	0.132
24-12-2024	0.06	0.024	0.036	22-02-2025	0.28	0.168	0.112
25-12-2024	0.07	0.028	0.042	23-02-2025	0.32	0.192	0.128
26-12-2024	0.07	0.028	0.042	24-02-2025	0.31	0.186	0.124
27-12-2024	0.03	0.012	0.018	25-02-2025	0.29	0.174	0.116
28-12-2024	0.83	0.332	0.498	26-02-2025	0.33	0.198	0.132
29-12-2024	0.27	0.108	0.162	27-02-2025	0.3	0.18	0.12
30-12-2024	0.2	0.08	0.12	28-02-2025	0.26	0.156	0.104
31-12-2024	0.15	0.06	0.09	01-03-2025	0.33	0.198	0.132
01-01-2025	0.36	0.252	0.108	02-03-2025	0.31	0.186	0.124
02-01-2025	0.36	0.252	0.108	03-03-2025	0.32	0.192	0.128

03-01-2025	0.39	0.273	0.117	04-03-2025	0.25	0.15	0.1
04-01-2025	0.4	0.28	0.12	05-03-2025	0.28	0.168	0.112
05-01-2025	0.34	0.238	0.102	06-03-2025	0.29	0.174	0.116
06-01-2025	0.28	0.196	0.084	07-03-2025	0.3	0.18	0.12
07-01-2025	0.29	0.203	0.087	08-03-2025	0.29	0.174	0.116
08-01-2025	0.33	0.231	0.099	09-03-2025	0.29	0.174	0.116
09-01-2025	0.34	0.238	0.102	10-03-2025	0.28	0.168	0.112
10-01-2025	0.31	0.217	0.093	11-03-2025	0.28	0.168	0.112
11-01-2025	0.14	0.098	0.042	12-03-2025	0.27	0.162	0.108
12-01-2025	0.92	0.644	0.276	13-03-2025	0.27	0.162	0.108
13-01-2025	0.35	0.245	0.105	14-03-2025	0.25	0.15	0.1
14-01-2025	0.37	0.259	0.111	15-03-2025	0.27	0.162	0.108
15-01-2025	0.33	0.231	0.099	16-03-2025	0.24	0.144	0.096
16-01-2025	0.28	0.196	0.084	17-03-2025	0.24	0.144	0.096
17-01-2025	0.42	0.294	0.126	18-03-2025	0.25	0.15	0.1
18-01-2025	0.4	0.28	0.12	19-03-2025	0.25	0.15	0.1
19-01-2025	0.43	0.301	0.129	20-03-2025	0.25	0.15	0.1
20-01-2025	0.44	0.308	0.132	21-03-2025	0.23	0.138	0.092
21-01-2025	0.44	0.308	0.132	22-03-2025	0.26	0.156	0.104
22-01-2025	0.4	0.28	0.12	23-03-2025	0.25	0.15	0.1
23-01-2025	0.39	0.273	0.117	24-03-2025	0.25	0.15	0.1
24-01-2025	0.39	0.273	0.117	25-03-2025	0.24	0.144	0.096
25-01-2025	0.38	0.266	0.114	26-03-2025	0.24	0.144	0.096
26-01-2025	0.39	0.273	0.117	27-03-2025	0.23	0.138	0.092
27-01-2025	0.39	0.273	0.117	28-03-2025	0.22	0.132	0.088
28-01-2025	0.4	0.28	0.12	29-03-2025	0.22	0.132	0.088
29-01-2025	0.4	0.28	0.12	30-03-2025	0.23	0.138	0.092
				31-03-2025	0.23	0.138	0.092

Source: India-WRIS (https://indiawris.gov.in), *Evapotranspiration data extracted from India-Water Resources Information System, Ministry of Jal Shakti, Government of India for Jaipur District, December 2024 to March 2025.*

Table 3: Soil data obtained from **SoilGrids** for Jaipur District

Site Name	Depth (cm)	Bulk density (cg/cm³)	Clay content (g/kg)	Sand (g/kg)	Silt (g/kg)	Vol. water content at -10 kPa in (10−2 cm³cm⁻³) *10	Vol. water content at -33 kPa in (10−2 cm³cm⁻³) *10	Vol. water content at -1500 kPa in (10−2 cm³cm⁻³) *10
Amer	0-5	146	204	574	222	356	336	99
	5-10	147	192	578	230	355	338	103
	15-30	149	194	577	228	355	329	106
	30-60	157	208	574	218	353	331	103
	60-100	159	197	571	232	351	327	108
	100-200	160	197	580	223	352	333	110
Kotputli	0-5	147	243	460	298	349	301	140
	5-10	148	249	447	304	343	302	144
	15-30	152	276	427	297	346	311	148
	30-60	158	280	415	305	349	322	141
	60-100	159	279	407	314	341	321	151
	100-200	160	264	433	304	344	327	154
Govindgarh	0-5	151	296	460	244	339	295	110
	5-10	150	303	451	247	337	302	111
	15-30	153	301	446	253	335	307	121
	30-60	160	295	451	253	342	323	145
	60-100	161	295	442	263	338	325	147
	100-200	163	279	457	264	342	329	147
Shahpura	0-5	149	241	456	303	342	309	124
	5-10	150	237	456	307	340	311	125
	15-30	153	260	439	300	340	317	134
	30-60	160	277	427	296	343	330	147
	60-100	161	279	417	304	342	324	153
	100-200	163	269	438	292	337	327	152
Virat Nagar	0-5	150	198	535	267	367	343	134
	5-10	151	197	536	267	365	343	139
	15-30	154	208	537	255	365	339	139
	30-60	160	234	511	255	363	343	129
	60-100	160	235	508	256	357	342	135
	100-200	161	225	531	244	354	344	139
Kalwad	0-5	150	260	480	261	332	333	107
	5-10	150	259	479	262	331	336	109
	15-30	153	258	473	269	330	338	117
	30-60	159	276	464	260	333	351	141
	60-100	159	270	457	273	331	346	144
	100-200	161	266	471	263	335	346	144

Dudu	0-5	145	250	356	394	365	335	121
	5-10	146	265	343	391	361	337	123
	15-30	148	262	344	394	361	337	121
	30-60	155	251	356	393	364	338	145
	60-100	156	243	357	399	365	342	149
	100-200	159	250	362	388	366	342	154
Phagi	0-5	147	245	465	291	353	320	123
	5-10	148	246	463	291	348	320	122
	15-30	151	264	448	287	350	324	126
	30-60	157	249	466	285	351	325	145
	60-100	158	245	462	293	355	327	145
	100-200	159	257	465	278	357	330	152
Chaksu	0-5	150	236	492	272	340	335	88
	5-10	151	217	508	274	336	333	92
	15-30	155	242	479	289	338	330	93
	30-60	159	217	497	286	340	335	127
	60-100	160	211	498	291	338	337	132
	100-200	159	203	523	274	343	339	131
Sambhar Lake	0-5	149	267	469	264	349	279	108
	5-10	150	258	473	268	347	283	106
	15-30	153	293	444	263	346	280	106
	30-60	158	285	448	266	348	283	127
	60-100	158	283	441	275	341	293	127
	100-200	159	274	448	279	355	303	133
Bassi	0-5	144	203	558	239	354	326	102
	5-10	147	194	567	239	347	325	106
	15-30	151	188	574	238	350	335	116
	30-60	155	190	565	244	351	342	108
	60-100	157	185	570	246	351	341	114
	100-200	157	177	599	223	349	344	114
Jobner	0-5	149	243	379	378	345	312	115
	5-10	150	239	382	379	345	309	116
	15-30	152	254	375	372	343	307	115
	30-60	157	271	361	368	344	313	143
	60-100	158	269	364	367	342	322	147
	100-200	159	260	374	365	349	332	156

Source: *SoilGrids, ISRIC – World Soil Information (Hengl et al., 2017)*

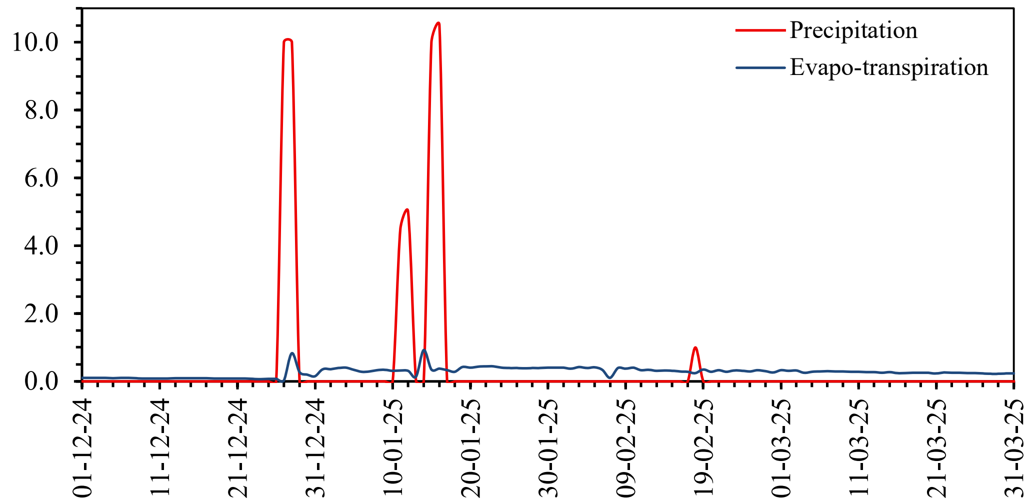

Figure Error! No text of specified style in document.**1:** Daily Precipitation and Evapotranspiration Records for Jaipur District (December 2024 – March 2025) (***Source****: India-WRIS (https://indiawris.gov.in), Rainfall time series data retrieved from India-Water Resources Information System, Ministry of Jal Shakti, Government of India for Jaipur District, December 2024 to March 2025.*)

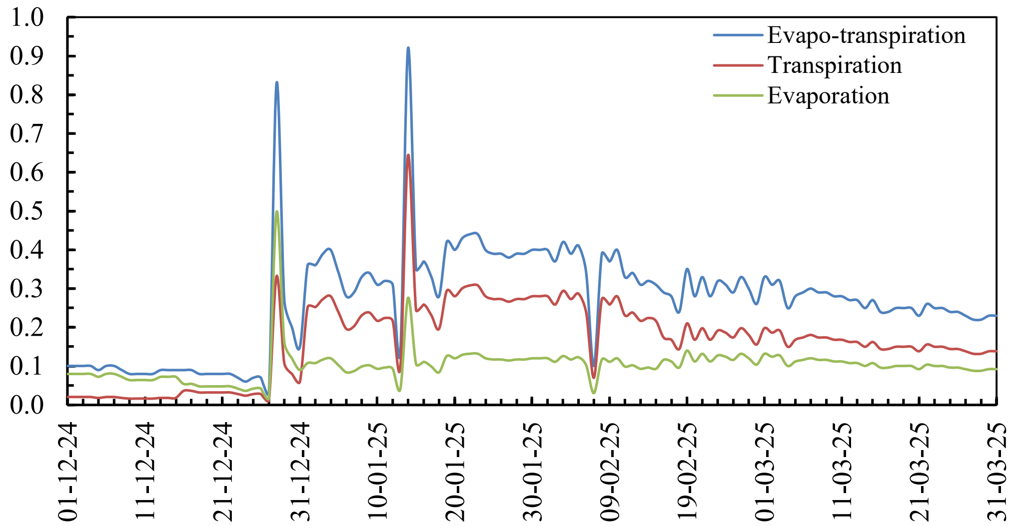

Figure 2: Daily Evapotranspiration, Evaporation and Transpiration Records for Jaipur District (December 2024 – March 2025) (***Source****: India-WRIS (https://indiawris.gov.in), Evapotranspiration data extracted from India-Water Resources Information System, Ministry of Jal Shakti, Government of India for Jaipur District, December 2024 to March 2025.*)

SUMMARY

SUMMARY

This thesis investigates the interconnected processes of water flow, solute transport, nutrient uptake, and pollutant dynamics, and their combined impact on wheat yields in the semi-arid soils of Jaipur, Rajasthan. By developing an integrated modeling framework, it connects physical soil–plant processes with practical agricultural outcomes, using both deterministic and stochastic approaches. The study draws on field data from four agro-climatic zones—Amer, Virat Nagar, Dudu, and Sambhar Lake—ensuring that the models are firmly grounded in local conditions.

The research progresses systematically, beginning with the conceptual and theoretical foundations of soil–water–plant interactions, then advancing to process-based simulations of water flow, nutrient uptake, and yield responses. It culminates in a stochastic framework that accounts for variability and uncertainty in real-world farming. Collectively, the findings highlight the delicate balance between maximizing crop productivity and minimizing environmental risks, offering both scientific contributions and practical strategies for sustainable, climate-resilient agriculture in semi-arid regions.

Chapter 1 – Introduction

This first chapter set the stage for the study by highlighting the importance of water and nutrient management in agriculture, particularly in semi-arid regions like Jaipur, Rajasthan. Agriculture was recognized as central to global food security, but increasing population pressures, limited water availability, and soil degradation were shown to pose serious challenges to sustaining crop yields. The discussion emphasized that imbalances in soil nutrients and inefficient irrigation practices often lead to reduced productivity, making it essential to adopt more scientific and sustainable approaches.

The chapter also introduced the concept of soil–water–plant interactions as the foundation of crop growth. By reviewing how water moves through soil, how nutrients are transported, and how plant roots absorb them, it outlined the complexity of processes that directly influence yield. To address these dynamics, the chapter positioned mathematical modeling as a powerful tool to connect physical processes with practical agricultural outcomes. Models such as Richards' equation for water flow and the advection–dispersion equation for solute transport were identified as key frameworks guiding this study.

Furthermore, the research was placed in a local context, focusing on Jaipur's diverse soils and wheat as the major crop of interest. This ensured both global relevance—addressing sustainability in agriculture—and regional application, making the study meaningful for farmers and policymakers. Finally, the objectives of the thesis were introduced: to develop and apply mathematical and computational models (with the help of HYDRUS and MATLAB) for analyzing solute transport, water flow, and their combined impact on crop yields under varying soil and climatic conditions.

Chapter 2 – Literature Review

This chapter reviewed how research on soil–water–plant interactions has evolved over time. Early studies focused separately on soil physics and plant physiology, but later work recognized their interdependence, leading to the development of mathematical models. Key foundations such as Richards' equation for water flow and the advection–dispersion equation for solute transport were highlighted, along with contributions by van Genuchten and Mualem in defining soil hydraulic functions. More advanced models integrated plant processes, using Michaelis–Menten kinetics for nutrient absorption and the Feddes function for root water uptake under stress. The review also underlined the importance of computational tools such as HYDRUS and MATLAB, which bridge theoretical models with practical applications in agriculture. Despite progress, gaps remain: many models still struggle to represent soil heterogeneity, root architecture, and field variability, while semi-arid regions such as Jaipur are underexplored.

This chapter therefore established the scientific foundation for the research while pointing to the need for context-specific modeling that can improve predictions of nutrient transport and crop yields. It naturally led into Chapter 3, which focused on modeling water flow in soils under transient conditions.

Chapter 3 – Models for Water Flow in Soil and Its Uptake in Plants under Transient Flow Conditions

This chapter examined the fundamental processes governing water movement in soils and its uptake by plant roots. It emphasized that soil water is never static—its availability changes with rainfall, irrigation, evaporation, and plant uptake, creating transient flow conditions. These dynamics directly determine how much water is accessible to crops at different growth stages, making their proper representation essential for agricultural modeling.

The mathematical description of water flow in unsaturated soils is based on Richards' equation, which couples Darcy's law with the continuity equation:

$$\frac{\partial\theta}{\partial t} = \frac{\partial}{\partial z}\left[K(h)\left(\frac{\partial h}{\partial z} + 1\right)\right] - S(z,t)$$

where θ is the volumetric water content [L^3], t is the time [T], z is the vertical coordinate [L] (positive upward), h is the soil water pressure head [L], $K(h)$ is the unsaturated hydraulic conductivity [L/T], $S(z,t)$ is the root water uptake rate (sink term) [1/T].

To make the equation realistic for agricultural soils, van Genuchten–Mualem functions were employed to describe soil hydraulic properties:

$$\theta(h) = \theta_r + \frac{\theta_s - \theta_r}{[1 + (\alpha|h|)^n]^m}, \quad m = 1 - \frac{1}{n}$$

$$K(h) = K_s, S_e^l\left[1 - \left(1 - S_e^{1/m}\right)^m\right]^2$$

where θ_s and θ_r are saturated and residual water contents, K_s is saturated hydraulic conductivity, α, n, m are curve-fitting parameters, S_e is effective saturation, and l is the pore-connectivity parameter. These formulations capture how soil texture controls water retention and movement.

Equally important is the role of plant roots in regulating water uptake. This was represented using the Feddes root water uptake model, which introduces a stress response function $\alpha(h)$:

$$S(h) = \alpha(h) \cdot S_{\text{pot}}$$

where S_{pot} is potential root uptake, and $\alpha(h)$ (0–1) describes the effect of soil moisture stress. Uptake is optimal when h is within a favorable range, but decreases when the soil becomes too dry $h < h_3$ or too wet $h > h_2$. This function realistically accounts for plant–soil interactions.

The practical significance of these models was highlighted through applications to Jaipur's semi-arid soils. Using HYDRUS-1D and zone-specific soil hydraulic parameters, simulations over a 120-day wheat growth cycle revealed distinct patterns:

- Root water uptake was concentrated in the top 40–60 cm across all zones.
- In Amer's sandy loam, surface layers dried rapidly, with pressure heads dropping from −20 cm at Day 0 to below −800 cm by Day 60.
- In finer soils (Sambhar Lake), drying was slower, with pressure heads at 30 cm depth remaining above −400 cm until mid-season.
- Hydraulic conductivity in Amer's top layer declined from ~12 cm/day to below 2 cm/day by Day 90, reducing infiltration capacity.
- Cumulative deep percolation losses ranged from 85 mm in Dudu to 142 mm in Amer, highlighting higher leaching potential in sandy soils.

This chapter demonstrated that transient water flow models not only capture the complexity of soil moisture dynamics but also provide meaningful insights into plant water availability. The results underscored the importance of efficient irrigation planning in semi-arid conditions and set the foundation for Chapter 4, which examined how water flow interacts with solute transport and nutrient uptake.

Chapter 4 – Mathematical Model for Nutrient Uptake in Plants with Multiple Root Branching Structures

This chapter extended the transient water flow framework to investigate how nutrients (specifically nitrate) move through soil and are absorbed by roots with realistic branching structures. The inclusion of root architecture was critical because nutrient uptake depends not only on soil water movement but also on how roots explore and access different zones of the soil profile.

The transport of solutes in the soil was modeled using the Advection–Dispersion Equation (ADE), which accounts for both bulk flow (advection) and spreading (dispersion/diffusion):

$$\frac{\partial (C_T \theta)}{\partial t} = \frac{\partial}{\partial z}\left(D\frac{\partial C}{\partial z} - qC\right) + S(C)$$

where C_T is the total solute concentration in the soil solution $[ML^{-3}]$, θ is the volumetric water content $[L^3L^{-3}]$, D is the dispersion coefficient $[L^2T^{-1}]$, q is the Darcy water flux $[LT^{-1}]$, S is the source or sink term, accounting for processes such as root nutrient uptake, decay, or chemical transformations $[ML^{-3}T^{-1}]$, t is time [T], z is the vertical spatial coordinate [L].

The sink term for root uptake was expressed using Michaelis–Menten kinetics, capturing the saturation behavior of nutrient absorption:

$$S(C) = \frac{V_{max} \cdot C}{K_m + C} \cdot L$$

where V_{max} is the maximum nutrient uptake rate per unit root length $ML^{-1}T^{-1}]$, C is the nutrient concentration in the soil solution $[ML^{-3}]$, K_m is the Michaelis constant, representing the concentration at which uptake is half of V_{max} $[ML^{-3}]$, L is the root length density, representing the total root length per unit volume of soil $[L^{-2}]$ (Barber, 1984).

The inclusion of multiple root branching structures further refined uptake predictions. Instead of treating the root system as a uniform sink, the model accounted for primary roots, lateral branches, and finer rootlets, each contributing differently to nutrient absorption depending on their depth and soil contact.

Simulation results across Jaipur's four agro-climatic zones showed clear contrasts:

- Amer (sandy loam): Nitrate moved beyond 60 cm depth by Day 30, with peak root uptake of 5.55×10^{-4} mmol/cm^3/day at the surface during T3, but leaching losses exceeded 35% of applied nitrogen.
- Virat Nagar and Dudu (loam): Nitrate remained longer in the active root zone, with uptake efficiency above 70% and leaching losses under 20%.
- Sambhar Lake (fine-textured): Nitrate concentrated in the top 20 cm, with uptake below 60 cm contributing less than 10% of total absorption.
- Across all zones, uptake peaked in mid-growth (T2–T3), supporting the value of split or controlled-release nitrogen applications.

This chapter demonstrated that considering root system architecture is essential for realistically modeling nutrient uptake. It showed that soil properties and root branching together shape how efficiently plants access nutrients. These insights highlight the importance of managing both fertilizer application and root-zone conditions to support crop productivity.

Chapter 5 – Model for Nutrient/Pollutant Load and Its Impact on Crop Yield

This chapter built on the earlier water–solute–uptake models to explore how nutrient and pollutant dynamics jointly determine crop yield. While Chapters 3 and 4 described the physical transport and biological uptake processes, Chapter 5 translated these into yield response functions that connect soil conditions directly to crop productivity.

The relationship between soil nutrient concentration (N) and crop yield (Y) is often represented using the Michaelis-Menten equation or its variants:

$$Y = Y_{max} \cdot f(N) = Y_{max} \cdot \frac{N}{N + K_N}$$

where Y is the crop yield, Y_{max} is the maximum achievable yield under optimal nutrient conditions, N is the available nutrient concentration in the soil and K_N is the half-saturation constant, representing the nutrient concentration at which yield is 50% of Y_{max}.

In contrast, pollutants were modeled using a stress function, which accounts for yield reduction due to toxic pollutant concentrations. A typical sigmoidal (logistic) function is used:

$$g(P) = 1 - \frac{1}{1 + e^{-(P - T_P)/S}}$$

where Y_{max} is the maximum yield in the absence of pollutants, P is the pollutant concentration in the soil, T_P is the critical pollutant concentration at which yield is reduced by 50% and k is the slope parameter, that determines the steepness of the yield reduction curve.

Nutrient and pollutant effects are often interdependent. The combined model accounts for these interactions by integrating $f(N)$ and $g(P)$ multiplicatively:

$$Y = Y_{\max} \cdot f(N) \cdot g(P)$$

where $Y_{\max}$ is the maximum potential yield under optimal conditions, $f(N)$ is the nutrient response function and $g(P)$ is the pollutant stress function.

$$Y = Y_{\max} \cdot \frac{N}{K_N + N} \cdot \left(1 - \frac{1}{1 + e^{-(P-T_P)/S}}\right)$$

The simulation results revealed that optimal nitrate availability (0.08–0.12 mmol/cm³ in the upper 30 cm of soil) supported wheat yields of 4.2–4.5 t/ha across zones. Beyond this threshold, yields plateaued at ~4.6 t/ha, while leaching losses increased sharply. In Amer's sandy loam, nitrates moved quickly beyond the 60 cm root zone, with concentrations of 10^{-6}–10^{-7} mmol/cm³ detected at 100 cm depth, indicating groundwater contamination risks. In finer soils such as Dudu, nitrates were retained within the top 40 cm, supporting stable yields of 4.3–4.4 t/ha with lower leaching.

Three key insights emerged:

1. Yield gains diminish beyond optimal fertilizer levels, while environmental risks rise. For example, doubling nitrogen inputs (120 → 240 kg/ha) increased yields by only ~5% but nearly doubled nitrate losses.

2. Excess nitrates accumulate in deeper layers, inaccessible to roots, compounding contamination risks.

3. Sustainable strategies must be site-specific, with sandy soils requiring careful irrigation–fertilizer scheduling and finer soils benefiting from practices that reduce surface accumulation.

This chapter showed that linking solute transport models with yield responses provides a powerful way to understand the trade-offs between crop productivity and environmental sustainability. The findings underline the importance of balancing nutrient inputs with plant demand and soil characteristics: applying the right amount, in the right place, at the right time. These insights lead naturally to the next stage of the thesis, where stochastic models are introduced in Chapter 6 to account for variability and uncertainty in soil and crop systems, offering a more realistic perspective on agricultural outcomes.

Chapter 6 – Stochastic Modeling of Solute Transport and Crop Yield Variability

This study uses stochastic modeling to represent the natural variability of soils, weather, and plant processes in nutrient transport and crop yield prediction. Unlike Deterministic models, which assume these conditions are fixed, making them less able to capture the real variability found in the field, the stochastic approach introduces randomness through a stochastic differential equation,

At a single point, changes in nutrient concentration C(t) can be described using a stochastic differential equation (SDE):

$$dC = f(C,t)\,dt + g(C,t)\,dW_t$$

where $f(C,t)$ is the average change in nutrient concentration, $g(C,t)$ shows the strength of random fluctuations (diffusion), and dW_t represents small random environmental changes, such as irregular rainfall or temperature shifts (Hening et al., 2023). For nutrient movement in the soil profile, the advection–dispersion equation (ADE) can be extended with stochastic terms to include variability:

$$\frac{\partial(\theta C)}{\partial t} = \frac{\partial}{\partial z}\left(\theta D\,\frac{\partial C}{\partial z}\right) - \frac{\partial(qC)}{\partial z} - S(z,t) - k\,\theta C + \xi(z,t),$$

where $\xi(z,t)$ is a random source term representing unpredictable soil or environmental changes. Here, soil and plant parameters are not treated as fixed numbers, but as random variables that can vary from place to place.

Crop yield Y can then be linked to soil water and nutrient availability using a response function:

$$Y = \mathcal{F}(\{C(z,t)\},\{\psi(z,t)\},\boldsymbol{x}) + \varepsilon,$$

where $\mathcal{F}(\cdot)$ is the crop response, x represents management choices (e.g., irrigation and fertilizer timing), and ε accounts for unexplained variation. Instead of one fixed yield estimate, the model produces averages, variances, and probabilities of yield loss or environmental risk (such as nitrate leaching). This framework allows yield outcomes to be assessed not just by single predictions, but by probability distributions and risk measures, supporting more robust water–nutrient management in variable environments such as the semi-arid soils of Jaipur.

Chapter 7 – Conclusion and Future Directions

This final chapter consolidated the central findings. It reflected on the progression from soil–water–plant foundations to advanced models of nutrient uptake, yield responses, and stochastic variability. Together, these contributions deepened understanding of agricultural systems and provided a framework for balancing productivity with sustainability in semi-arid regions.

The chapter revisited the research motivation: sustaining wheat yields in Jaipur while protecting environmental health. It emphasized context-specific strategies, shaped by soil texture, root architecture, and management practices.

Looking ahead, future research should expand beyond nitrogen to include multi-nutrient interactions such as phosphorus and potassium, and incorporate microbial and chemical processes like nitrification, denitrification, and organic matter cycling. Addressing climate variability and change is also critical: linking models with climate projections would help assess the resilience of agricultural practices.

Technological advances provide opportunities for refinement. Remote sensing, GIS mapping, and soil sensors can generate real-time data, while machine learning can uncover hidden patterns in large agricultural datasets. Broader application across regions and crops would test the robustness of the frameworks and support scaling from local to regional strategies.

Finally, this chapter served as both a conclusion and a forward-looking reflection. It consolidated the contributions of the work while pointing toward new directions where models, enriched with data and adapted to changing realities, can guide sustainable and climate-resilient agriculture.

BIBLIOGRAPHY

BIBLIOGRAPHY

Addiscott, T. M., & Wagenet, R. J. (1985). Concepts of solute leaching in soils: A review of modelling approaches. *Journal of Soil Science*, *36*(3), 411-424. https://doi.org/10.1111/j.1365-2389.1985.tb00347.x

Agah, A. E., Meire, P., & Deckere, E. D. (2017). Mathematical Models of Water and Solute Transport in Soil. *Journal of Applied Solution Chemistry and Modeling*, *6*(3), 98–104. https://doi.org/10.6000/1929-5030.2017.06.03.2

Agah, H., Jabarifar, M., & Tabatabaei, S. H. (2017). Modeling solute transport in soil and groundwater: A review. *Environmental Earth Sciences, 76*(22), 1–15. https://doi.org/10.1007/s12665-017-7134-7

Alloway, B. J. (2013). Sources of Heavy Metals and Metalloids in Soils. In B. J. Alloway (Ed.), Heavy Metals in Soils (pp. 11-50). Dordrecht: Springer. https://doi.org/10.1007/978-94-007-4470-7

Barber, S. A. (1984). *Soil nutrient bioavailability: A mechanistic approach*. New York: John Wiley & Sons.

Bear, J. (2005). Modeling solute transport phenomena. In *Encyclopedia of Hydrological Sciences*. https://doi.org/10.1002/0470848944.hsa156

Biggar, J. W., & Nielsen, D. R. (1976). Spatial variability of the leaching characteristics of a field soil. *Water Resources Research, 12*(1), 78–84. https://doi.org/10.1029/WR012i001p00078

Blake, G. R., & Hartge, K. H. (2013a). Bulk density. In *Soil Science Society of America book series* (p. 363). https://doi.org/10.2136/sssabookser5.1.2ed.c13

Blake, G. R., & Hartge, K. H. (2013). Particle density. In *Soil Science Society of America book series* (p. 377). https://doi.org/10.2136/sssabookser5.1.2ed.c14

Blöschl, G., & Sivapalan, M. (1995). Scale issues in hydrological modelling: A review. *Hydrological Processes*, *9*(3-4), 251-290. https://doi.org/10.1002/hyp.3360090305

Bresler, E. (1973). Simultaneous transport of solutes and water under transient unsaturated flow conditions. *Water Resources Research, 9*(4), 975–986. https://doi.org/10.1029/WR009i004p00975

Bresler, E., & Dagan, G. (1983a). Unsaturated flow in spatially variable fields: 1. Derivation of models of infiltration and redistribution. *Water Resources Research, 19*(2), 327–334. https://doi.org/10.1029/WR019i002p00327

Bresler, E., & Dagan, G. (1983b). Unsaturated flow in spatially variable fields: 2. Application of water flow models to various types of variability. *Water Resources Research, 19*(2), 335–340. https://doi.org/10.1029/WR019i002p00335

Bresler, E., & Laufer, A. (1974). Simultaneous transport of solutes and water in soils. *Water Resources Research, 10*(5), 914–920. https://doi.org/10.1029/WR010i005p00914

Brooks, R. H., & Corey, A. T. (1964). *Hydraulic properties of porous media*. Hydrology Papers, No. 3. Fort Collins, CO: Colorado State University.

Buckingham, E. (1907). *Studies on the movement of soil moisture*. Bulletin 38, U.S. Department of Agriculture, Bureau of Soils.

Burdine, N. T. (1953). Relative permeability calculations from pore size distribution data. *Petroleum Transactions, AIME, 198*(1), 71–78.

Campbell, G. S. (1974). A simple method for determining unsaturated conductivity from moisture retention data. *Soil Science, 117*(6), 311–314. https://doi.org/10.1097/00010694-197406000-00001

Carsel, R. F., & Parrish, R. S. (1988). Developing joint probability distributions of soil water retention characteristics. *Water Resources Research, 24*(5), 755–769. https://doi.org/10.1029/WR024i005p00755

Chakraborty, T., & Kadoli, R. (2014). Mathematical and numerical modeling of type N thermocouple. *Universal Journal of Mechanical Engineering, 2*(5), 174. https://doi.org/10.13189/ujme.2014.020505

Chapman, N., Miller, T., Lindsey, K., & Whalley, W. R. (2012). Roots, water, and nutrient acquisition: Let's get physical. *Trends in Plant Science, 17*(12), 701–710. https://doi.org/10.1016/j.tplants.2012.08.001

Chien, S. H., Prochnow, L. I., & Cantarella, H. (2009). Recent developments of fertilizer production and use to improve nutrient efficiency and minimize environmental impacts. In *Advances in agronomy* (Vol. 102, pp. 267–322). Elsevier. https://doi.org/10.1016/S0065-2113(09)01008-6

Choudhary, M., Sharma, K. C., & Sharma, R. K. (2017a). Root distribution pattern and nutrient uptake efficiency of wheat under moisture stress conditions in Rajasthan. *Indian Journal of Agricultural Sciences, 87*(9), 1182.

Choudhary, M., Sharma, K. C., & Sharma, R. K. (2017b). Root distribution pattern and water use efficiency of wheat under different irrigation regimes in semi-arid Rajasthan. *Indian Journal of Agricultural Sciences, 87*(9), 1182.

COMSOL AB. (2020). *COMSOL Multiphysics® v. 5.6*. Stockholm, Sweden: COMSOL AB.

Gardner, W. R. (1958). Some steady-state solutions of the unsaturated moisture flow equation with application to evaporation from a water table. *Soil Science, 85*(4), 228–232. https://doi.org/10.1097/00010694-195804000-00006

Genuchten, M. Th. van. (1980). A closed-form equation for predicting the hydraulic conductivity of unsaturated soils. *Soil Science Society of America Journal, 44*(5), 892–898. https://doi.org/10.2136/sssaj1980.03615995004400050002x

Genuchten, M. Th. van, & Wagenet, R. J. (1989). Two-site/two-region models for pesticide transport and degradation: Theoretical development and analytical solutions. *Soil Science Society of America Journal, 53*(5), 1303–1310. https://doi.org/10.2136/sssaj1989.03615995005300050001x

Goss, M. J., Miller, M. H., Bailey, L. D., & Grant, C. A. (1993). Root growth and distribution in relation to nutrient availability and uptake. *European Journal of Agronomy, 2*(2), 57–67. https://doi.org/10.1016/s1161-0301(14)80135-4

Green, W. H., & Ampt, G. A. (1911). Studies on soil physics: 1. The flow of air and water through soils. *Journal of Agricultural Science, 4*(1), 1–24. https://doi.org/10.1017/S0021859600001441

Gregory, P., & Kirkegaard, J. A. (2016). Growth and function of root systems. In *Encyclopedia of Agriculture and Food Systems* (Vol. 3, pp. 230–245). Elsevier. https://doi.org/10.1016/b978-0-12-394807-6.00127-1

Groenveld, T., Argaman, A., Šimůnek, J., & Lazarovitch, N. (2021). Numerical modeling to optimize nitrogen fertigation with consideration of transient drought and nitrogen stress. *Agricultural Water Management, 254*, 106971. https://doi.org/10.1016/j.agwat.2021.106971

Hamsa, N., & Prakash, N. B. (2020). Heavy metal contamination in soils and crops irrigated with lakes of Bengaluru. *Current Science, 119*(11), 1849–1854. https://doi.org/10.18520/cs/v119/i11/1849-1854

Hanks, R. J., Bowers, S. A., & Roundy, W. T. (1969). Numerical analysis of infiltration, evaporation, and redistribution. *Soil Science Society of America Proceedings, 33*(4), 493–496. https://doi.org/10.2136/sssaj1969.03615995003300040018x

Harbaugh, A. W. (2005). MODFLOW-2005, the U.S. Geological Survey modular ground-water model—the Ground-Water Flow Process. *U.S. Geological Survey Techniques and Methods 6-A16*. Reston, VA.

Haverkamp, R., Parlange, J. Y., Kutilek, M., & Rendon, L. (1977). Determination of the hydraulic conductivity of unsaturated soils from infiltration experiments. *Soil Science Society of America Journal, 41*(2), 285–288. https://doi.org/10.2136/sssaj1977.03615995004100020020x

Healy, R. W. (1990). Simulation of solute transport in variably saturated porous media with supplemental information on modifications to the U.S. Geological

Survey's computer program VS2D. *U.S. Geological Survey Water-Resources Investigations Report 90-4025*. Denver, CO.

Henri, C. V., & Harter, T. (2019). Stochastic assessment of nonpoint source contamination: Joint impact of aquifer heterogeneity and well characteristics on management metrics. *Water Resources Research, 55*(8), 6773–6791. https://doi.org/10.1029/2018wr024230

Hening, A., Hieu, N. T., Nguyen, D. H., & Nguyen, N. N. (2023). Stochastic nutrient-plankton models. *Journal of Differential Equations, 376*, 370–395. https://doi.org/10.1016/j.jde.2023.08.017

Hillel, D. (1980). *Fundamentals of soil physics*. New York: Academic Press.

Hillel, D. (1998). *Environmental soil physics*. San Diego, CA: Academic Press.

Horton, R. E. (1933). The role of infiltration in the hydrologic cycle. *Transactions of the American Geophysical Union, 14*(1), 446–460. https://doi.org/10.1029/TR014i001p00446

Jarvis, N., Jansson, P., Dik, P. E., & Messing, I. (1991). Modelling water and solute transport in macroporous soil. I. Model description and sensitivity analysis. *Journal of Soil Science, 42*(1), 59–70. https://doi.org/10.1111/j.1365-2389.1991.tb00091.x

Jones, J. W., Hoogenboom, G., Porter, C., Boote, K. J., Batchelor, W. D., Hunt, L. A., Wilkens, P. W., Singh, U., Gijsman, A. J., & Ritchie, J. T. (2002). The DSSAT cropping system model. *European Journal of Agronomy, 18*, 235–265. https://doi.org/10.1016/s1161-0301(02)00107-7

Jungk, A., & Claassen, N. (1997). Ion diffusion in the soil–root system. In *Advances in agronomy* (Vol. 61, pp. 53–110). Elsevier. https://doi.org/10.1016/s0065-2113(08)60662-8

Jury, W. A., Gardner, W. R., & Gardner, W. H. (1986). *Soil physics* (5th ed.). Wiley.

Jury, W. A., & Horton, R. (2004). *Soil physics* (6th ed.). Hoboken, NJ: John Wiley & Sons.

Kaushik, P., & Baghel, R. S. (2023). An investigation of the variation in seasonal rainfall patterns over the years. *arXiv*. https://doi.org/10.48550/arXiv.2311.06247

Kostiakov, A. N. (1932). On the dynamics of the coefficient of water percolation in soils and the necessity of studying it from a dynamic point of view for purposes of amelioration. *Transactions of the Sixth Commission, International Society of Soil Science*, Part A, 17–21.

Kroes, J. G., van Dam, J. C., Supit, I., de Wit, A. J. W., Boogaard, H. L., & van Diepen, C. A. (2017). *SWAP version 4: Theory description and user manual*. Wageningen Environmental Research Report 2780, Wageningen University & Research, Wageningen, the Netherlands.

Krishi Vigyan Kendra Jaipur-I. (n.d.). District profile. Retrieved August 21, 2024, from https://jaipur1.kvk2.in/district-profile.php

Leitner, D., Klepsch, S., Bodner, G., & Schnepf, A. (2010). A dynamic root system growth model based on L-Systems. *Plant and Soil, 332*(1), 177–192. https://doi.org/10.1007/s11104-010-0284-7

Li, A., Zhu, L., Xu, W., Liu, L., & Teng, G. (2022). Recent advances in methods for in situ root phenotyping. *PeerJ, 10*, e13638. https://doi.org/10.7717/peerj.13638

Mein, R. G., & Larson, C. L. (1973). Modeling infiltration during a steady rain. *Water Resources Research, 9*(2), 384–394. https://doi.org/10.1029/WR009i002p00384

Mualem, Y. (1976). A new model for predicting the hydraulic conductivity of unsaturated porous media. *Water Resources Research, 12*(3), 513–522. https://doi.org/10.1029/WR012i003p00513

Neuman, S. P., Feddes, R. A., & Bresler, E. (1974). Finite element analysis of two-dimensional flow in soils considering water uptake by roots. *Soil Science Society of America Journal, 39*(2), 224–231. https://doi.org/10.2136/sssaj1975.03615995003900020009x

Nielsen, D. R., van Genuchten, M. Th., & Biggar, J. W. (1986). Water flow and solute transport processes in the unsaturated zone. *Water Resources Research, 22*(9S), 89S–108S. https://doi.org/10.1029/WR022i09Sp0089S

Philip, J. R. (1957). The theory of infiltration: 4. Sorptivity and algebraic infiltration equations. *Soil Science, 84*(3), 257–264. https://doi.org/10.1097/00010694-195709000-00010

Richards, L. A. (1931). Capillary conduction of liquids through porous mediums. *Physics, 1*(5), 318–333. https://doi.org/10.1063/1.1745010

Russo, D., & Bresler, E. (1982a). Soil hydraulic properties as stochastic processes: I. An analysis of field variability. *Soil Science Society of America Journal, 46*(4), 682–687. https://doi.org/10.2136/sssaj1982.03615995004600040006x

Russo, D., & Bresler, E. (1982b). Soil hydraulic properties as stochastic processes: II. Predictions of unsaturated hydraulic conductivity. *Soil Science Society of America Journal, 46*(4), 689–694. https://doi.org/10.2136/sssaj1982.03615995004600040007x

Saffman, P. G. (1959). A theory of dispersion in a porous medium. *Journal of Fluid Mechanics, 6*(3), 321–349. https://doi.org/10.1017/S0022112059000672

Saffman, P. G. (1960). Dispersion due to molecular diffusion and macroscopic mixing in flow through a network of capillaries. *Journal of Fluid Mechanics, 7*(2), 194–208. https://doi.org/10.1017/S0022112060000100

Schnepf, A., Leitner, D., Landl, M., Lobet, G., Mai, T. H., Morandage, S., … & Vereecken, H. (2018). CRootBox: A structural–functional modelling framework for root systems. *Annals of Botany, 121*(5), 1033–1053. https://doi.org/10.1093/aob/mcx221

Segol, G. (1977). A three-dimensional numerical model of transport and dispersion in ground water. *U.S. Environmental Protection Agency Report* EPA-600/3-77-008.

Šimůnek, J., van Genuchten, M. T., & Šejna, M. (2016). Recent developments and applications of the HYDRUS computer software packages. *Vadose Zone Journal, 15*(7). https://doi.org/10.2136/vzj2016.04.0033

Smith, R. E., Parlange, J. Y., & Rose, C. W. (1991). Infiltration models and their solutions. In R. J. Hanks & J. T. Ritchie (Eds.), *Modeling plant and soil systems* (pp. 491–522). Madison, WI: ASA-CSSA-SSSA.

Tilman, D., Balzer, C., Hill, J., & Befort, B. L. (2011). Global food demand and the sustainable intensification of agriculture. *Proceedings of the National Academy of Sciences, 108*(50), 20260–20264. https://doi.org/10.1073/pnas.1116437108

Topp, G. C., & Ferre, P. A. (2002). Water content. In J. H. Dane & G. C. Topp (Eds.), *Methods of soil analysis: Part 4. Physical methods* (pp. 417–545). Madison, WI: Soil Science Society of America.

van Genuchten, M. T. (1980). A closed-form equation for predicting the hydraulic conductivity of unsaturated soils. *Soil Science Society of America Journal, 44*(5), 892–898. https://doi.org/10.2136/sssaj1980.03615995004400050002x

van Genuchten, M. T., & Wagenet, R. J. (1989). Two-site/two-region models for pesticide transport and degradation: Theoretical development and analytical solutions. *Soil Science Society of America Journal, 53*(5), 1303–1310. https://doi.org/10.2136/sssaj1989.03615995005300050001x

Voss, C. I., & Provost, A. M. (2010). SUTRA, A model for saturated–unsaturated variable-density ground-water flow with solute or energy transport. *U.S. Geological Survey Water-Resources Investigations Report* 02-4231. Reston, VA.

Weller, H. G., Tabor, G., Jasak, H., & Fureby, C. (1998). A tensorial approach to computational continuum mechanics using object-oriented techniques. *Computers in Physics, 12*(6), 620–631. https://doi.org/10.1063/1.168744

White, P. J., & Brown, P. H. (2010). Plant nutrition for sustainable development and global health. *Annals of Botany, 105*(7), 1073–1080.

https://doi.org/10.1093/aob/mcq085

World Bank. (2019). Employment in agriculture (% of total employment) (modeled ILO estimate). World Bank. https://data.worldbank.org/indicator/SL.AGR.EMPL.ZS

Zhang, H., Chen, F., & Ouyang, Y. (2021). Nutrient management and environmental sustainability: Challenges and prospects. *Agronomy, 11*(3), 567. https://doi.org/10.3390/agronomy11030567

Zhang, X., Davidson, E. A., Mauzerall, D. L., Searchinger, T. D., Dumas, P., & Shen, Y. (2017). Managing nitrogen for sustainable development. *Nature, 528*(7580), 51–59. https://doi.org/10.1038/nature15743

Zhang, Y., Yang, G., & Li, S. (2014). Significance of conceptual model uncertainty in simulating carbon sequestration in a deep inclined saline aquifer. *Journal of Hazardous, Toxic, and Radioactive Waste, 19*(3). https://doi.org/10.1061/(asce)hz.2153-5515.0000246

PUBLISHED RESEARCH PAPERS IN UGC REFERRED JOURNALS

https://doi.org/ 10.33472/AFJBS.6.Si2.2024.3315-3321

AFJBS

African Journal of Biological Sciences

Journal homepage: http://www.afjbs.com

Research Paper Open Access

Impact of Soil Physicochemical Properties on Crop Productivity in Jaipur's Peri-Urban Ecosystems

Dinesh Kumar Varma[1], Arun Kumar[2*]

[1]Research Scholar, Department of Mathematics, Government College, Kota, University of Kota, Kota, India.

Email: dkmaths89@gmail.com

[2]Professor, Department of Mathematics, Government College, Kota, India.

Email: arunkr71@gmail.com

Article History

Volume 6,Issue Si2, 2024

Received:29 Apr 2024

Accepted : 30 May 2024

doi: 10.33472/AFJBS.6.Si2.2024.3315-3321

Abstract

The nutrients found in the soil are the most crucial components needed for soil fertility and plant growth. Plants need these nutrients in sufficient amounts. This study aimed to assess the chemical characteristics of a few chosen soil ecosystems in Jaipur's outlying regions, including those associated with agriculture, organic farming, forests, and industries. The following factors were examined to determine the soil fertility status: pH, EC, OC, N, P, and K. According to the study, the pH of the soil samples ranged from 7.01 to 7.41 and was somewhat alkaline, but still within the recommended range of 6.5 to 8.5 for crops, except forest soil, which had a lower value. The EC values, which ranged from 0.2 dSm-1 to 0.503 dSm-1, suggested lower salinity in the soil samples. The organic carbon content readings were consistent across all soil samples. Except for organic farming, nitrogen and phosphorus concentrations had a negative influence on all soil samples. Potassium levels are optimal in organic and forest soil samples, but lower in industrial and chemically treated soils.

Keywords: Chemical characteristics, soil nutrients, soil health, forest, organic carbon, EC

Introduction

According to *Velayutham and Bhattacharya* (2000), soil is a naturally occurring substance that is created by pedogenic processes through the weathering of rocks. It has a mineral and organic content as well as specific mineralogical, chemical, physical, and biological qualities that make it an ideal medium for plant growth. In addition to being an essential part of the ecosystem and a major source of food, water, and energy for humans, soil also supports life through a variety of processes such as water purification, biomass production, pollution remediation, ecosystem restoration, and the cycling of carbon, nitrogen, sulfur, and water (*Gaur,* 1997) [9]. Given that agriculture and related industries rely heavily on soil resources, it is the most significant natural resource for humans and other living things. One of the most crucial elements in crop production is soil, which is a thin layer of organic matter on the surface of the earth that also contains nutrients, water, air, and other organic matter that work together to support plant growth. Farmers need to understand that measuring fertility levels is necessary to determine soil fertility, which can lead to increased productivity and profitability.

The world's soil resources are finite and quickly deteriorating due to a variety of anthropogenic activities in natural systems, which causes agricultural land to be used for non-agricultural purposes (Lal, 1998) [13]. Degradation of soil is a serious problem that can be accelerated by salinization, erosion, changes in the soil's organic matter content, loss of plant nutrients, and structural alterations. Soil health is negatively impacted by intensive agricultural practices and excessive use of chemical fertilizers in farming practices for food production. Soil health deteriorated as a result of heavy pesticide use and tainted irrigation water from industrial wastewater (Rayment et al., 2002; Kaur et al., 2014) [17, 11]. As per the report by the Indian Council of Agricultural Research (2010), 37 percent of India's total land area is affected by different types of land degradation, such as acidity, salinity, alkalinity, mining, and industrial waste. These factors have a direct impact on crop productivity throughout the nation. The depleted organic matter needs to be replenished, the degraded soils and ecosystem need to be improved, and food needs need to be met both now and in the future. Food, fuel, water, fiber, herbal, and pharmaceutical items all depend on healthy soils. Physical fertility, chemical fertility, and biological fertility are the three primary components of soil fertility (Christopher Johns et al. 2017) [5].

The ability of plants to absorb nutrients and water is significantly influenced by the physical and chemical characteristics of the soil (B.S. Griffith, 2010) [2]. The size, shape, pore spaces, texture, organic matter, and nutritional composition of the soil are all considered aspects of physical fertility. The soil's pH, electrical conductivity, organic content, and different mineral composition are among its chemical characteristics. Working with various soil ecosystems necessitates an awareness of their various levels of physical and chemical properties. When working with a specific soil, understanding its physical and chemical qualities aids in the soil management methods (N. Brady, 2002) [15]. In addition, the forest provides essential soil ecosystem services that keep terrestrial systems functioning (Abson et al., 2014: Chazdon et al., 2009). [1, 4]. The functions include fuel and fiber (Rojstaczer et al., 2001: Vitousek et al., 1986), as well as products and services required to sustain human populations (Matson, 1997) [14]. [16, 20]. Additionally, they can assist pollination services and regulate pest control (Bale et al., 2008; Kremen et al., 2002). [12]. It's critical to stay current with knowledge regarding the many qualities of soil in order to maximize productivity from any soil ecosystem (B.S. Griffith, 2010). [2]. Soil fertility must be kept at its ideal level in order to improve yields, lower pollution, and implement sustainable agricultural methods (Diaccono & Montemuroo, 2010). [7].

Materials and Methods

The study sites are located in the city-outer part of Jaipur. The composite soil samples were collected from four regions - local forest region, soil with chemically fertilized, soil with organically fertilized soil, and industrial area soil. Three duplicates of the composite soil samples (0–15 cm) were gathered and transported to the lab in tiny, sterile, low-density polythene bags. After being air-dried, the soil samples were run through a 2 mm filter to examine their chemical composition. The soil samples that were treated were utilized to measure pH and In 1:2 soil, electrical conductivity was measured using the conductivity bridge method (Jackson, M.L. 1977) [10] and the potentiometric method (Jackson, M.L. 1977) [10]. Wet digestion was used to measure the organic carbon (Walkley and Black, 1934) [22]. According to Subbaiah and Asija (1956) [18], the alkaline permanganate method is used to evaluate the total nitrogen nutrients level. Available potassium was determined using ammonium acetate extract, and available phosphorus was measured in the Olsen's extract using ascorbic acid (Watanabe and Olsen, 1965) [21].

S. No	Parameters	Methods
1	pH	1:2.0 soil water suspension by Using pH meter.
2	Electrical conductivity	1:2 soil water suspension by using Conductivity bridge.
3	Organic Carbon	Walkley and Black's oxidation method (Walkely, a and Black, I.A. 1934) [22]
4	Total Nitrogen	Alkaline permanganate method (Subbaiah and Asija, 1956) [18]
5	Available Phosphorus	Olsen's extraction method (Olsen, S.R. 1954)
6	Available Potassium	Ammonium acetate extract method (Mervin and Peach, 1951)

The Chemical analysis of the four soil samples was done in triplicates and the data is presented as Mean ± Standard Error. Statistical analysis was done with the help of Microsoft Excel computer software programs.

The term " pH " describes how acidic and alkaline the soil is. Significant changes in the chemical and biological properties of the soils have been demonstrated to occur with slight variations in the pH of the soils. The current study demonstrates that the pH of two agricultural stations was within the ideal range of 6.5 to 8.5, which is needed for crops. The data also revealed that the industrial and forest stations' paddy crops were rather acidic, with the industrial soil having an acidity level of 7.4 and the forest station's 6.15. The soil forest location had the lowest pH value out of the four soils, and organic soil had the highest average value.

According to the results, the pH values of the organic and agricultural soils were similar, and this is roughly in line with past research on the rhizosphere of paddy soil that revealed a pH of 7.23 (*Madhavilatha et al*., 2015) and (Madhavi et al., 2018) [8]. The woodland had a lower pH of 6.12, according to the current data. According to Charman and Murray (2007) [3].

Results

One of the main indicators of salinity or salt content in soil is the electrical conductivity (EC) of the soil. The range of EC values recorded was 0.2 to 0.5 dS m-1, with agriculture exhibiting the greatest average value. Being a measurable part of organic matter, soil organic carbon plays a significant role in soil biological function. The majority of organic matter is made up of decomposing or dead components. The findings revealed moderate in significant quantities in all soil samples. Continuous cultivation, the removal of crop residue without return, and the effects of wind and water erosion, which preferentially remove soil colloids, including the organic components, are all responsible for the low OC.

The three main macronutrients of soil—nitrogen, phosphorus, and potassium—are crucial for plant growth. An essential component of chlorophyll that promotes protein content during vegetative development is nitrogen. A lack of nitrogen causes plants to grow slowly, while too much nitrogen in the soil can also cause problems for plants, as evidenced by their delayed maturity and increased vulnerability to pests and illnesses. The amount of nitrogen in the soil usually indicates fertility and accessible nitrogen ranges from 139.2 kg/acre (organic soil) to 927 kg/acre (industrial). Due to the lack of a nitrogen source, a similar pattern was seen in the forest. Extensive use of chemically fertilized agriculture practices may result in high nitrogen concentration in agricultural soil that exceeds restrictions for this location.

Phosphorus is a crucial component that aids in cell division, promotes the growth and creation of roots, and supplies ATP, the biological energy that increases a plant's resistance to disease, drought, and cold. Phosphorus availability is influenced by both organic carbon and pH. While organic soil is assigned a lower value, forest soil has the highest value. All soil samples do, however, generally contain significant amounts in the area.

Table 1. Physicochemical properties of different Soil (Mean ± SE)

S.No.	Parameters	Agriculture	Organic	Forest	Industrial
1	pH	7.1 ± 0.048	7.1 ± 0.010	6.15 ± 0.012	7.40± 0.126
2	EC (ds m^{-1})	0.504 ± 0.015	0.237 ± 0.015	0.205 ± 0.005	0.307 ± 0.065
3	Organic carbon	0.69 ±0.008	0.72 ±0.014	0.75 ±0.007	0.76 ± 0.024
4	Nitrogen (kg/acre)	872.3 ± 1.45	124.2 ± 0.68	842.6± 1.169	917 ± 3.214
5	Phosphorus (kg/acre)	67.8 ± 0.435	49.45 ± 0.33	74.21 ± 0.76	57.70 ± 0.20
6	Potassium (kg/acre)	30.03 ± 0.688	71 ± 0.577	52.86 ± 0.35	41.5 ± 0.692

Fig 1: P^H values observed in different soil types

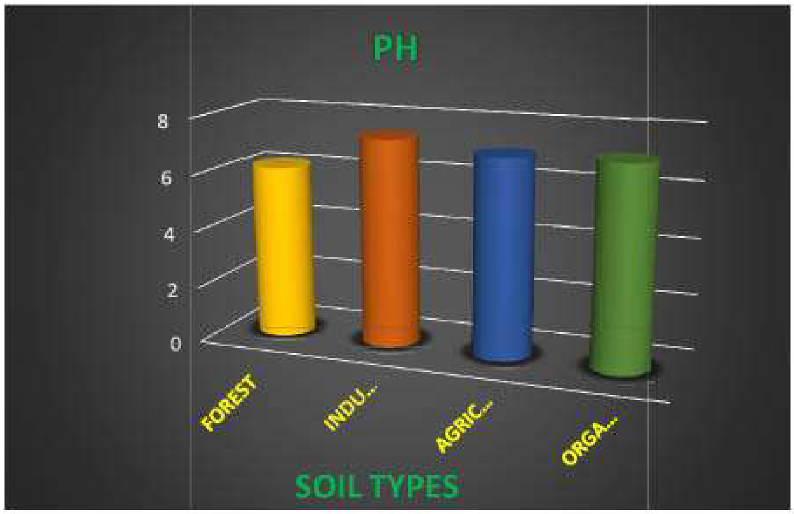

Fig 2. The EC values present in different soil types

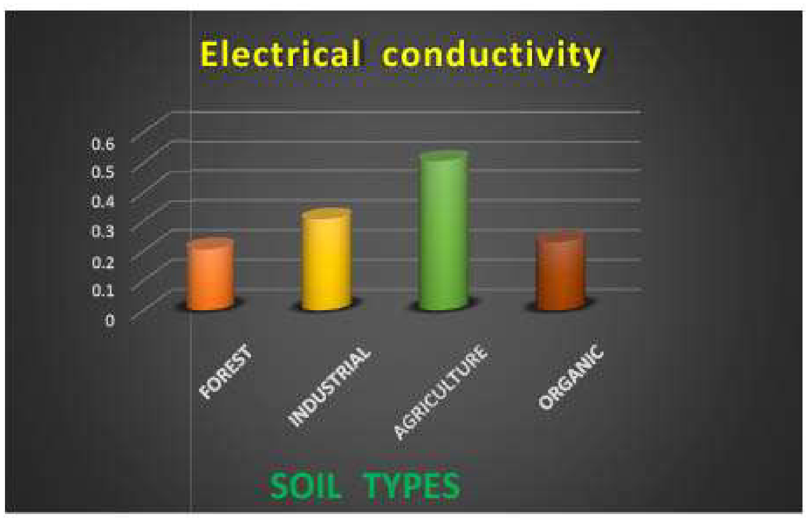

Fig 3. Organic carbon content in different soils

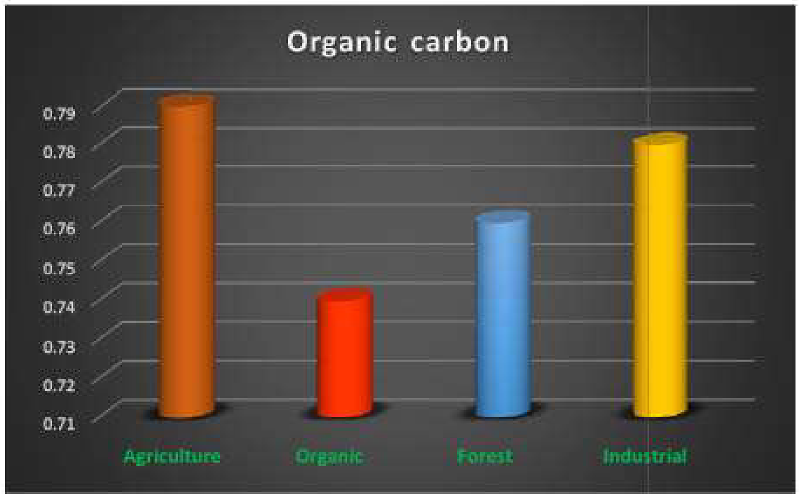

Conclusion

According to the study, soil chemical features such as accessible phosphorus and nitrogen have a detrimental impact on industrial, agricultural, and forest systems, except organic farming soil systems, where phosphorus is the only factor affecting the soil. The soil system's high levels of accessible phosphorus, organic carbon (forest), and nitrogen suggest that it has a significant influence on nutrient build-up and accumulation by lowering losses from soil erosion and leaching brought on by high litter formation. Farmers can benefit from this study, which is the first from Jaipur outside regions. Adopting more environmentally friendly agricultural practices is necessary for sustainable output, and proper soil management techniques can assist in maintaining the health of the soil. To understand the microbial profiles in each of the four soil ecosystems and how they relate to soil management techniques, more research is necessary.

References

1. Abson DJ, Wehrden H, Baumgartner S, Fischer J, Hanspach J, Hardtle W et al. Ecosystem services as a boundary object for sustainability. Ecol. Econ. 2014; 103:29-37.
2. Griffith BS, Ball BC, Daneill TJ, Hallett PD, Nelson R, Wheatley RE et al., Integrating soil quality changes to arable agricultural systems following organic matter addition, or adoption of a ley-arable rotation, Appl. Soil Ecol. 2010; 46:43-53.
3. Charman PEV, Murray BW. Soils and their properties and Management. South Melbourne, Oxford University Press, 2007.
4. Chazdon RL, Harvey CA, Komar O, Griffith DM, Ferguson BG, Martinez-Ramos M et al. Beyond Reserves: a research agenda for conserving biodiversity in human modified tropical landscapes. Biotropica. 2009; 41:142-153.
5. Christopher johns, Living soils: The role of Microorganisms in Soil Health – Future Directions International, 2017.

6. Dhavilewarapu, Madhavi Latha. Studies on soil Microflora in Relation to some physico Chemical Factors from Different Localities of Hyderabad. PhD Thesis, 2015.
7. Diacono M, Montemurro F. Long-term effects of oganic amendments on soil fertility. Agronomy for Sustainable Development, 2010; 30:401.
8. Madhavi E, Shyamkumar B, Raja Sekhar PS. Assessment of Soil Quality under rice (Oryza sativa) Cropping systems. J Pharma Chem Biol Sci. 2018; 6(2):35-41.
9. Gaur G. Soil and Soil waste Pollution and its Management. Sarup and Sons, New Delhi, 1997.
10. Jackson ML. Soil Chemical Analysis. Pentice Hall of India. Private Limited-New Delhi, 1977.
11. Kaur M, Soodan RK, Katnoria JK, Bhardwaj R, Pakade YB, Nagpal AV. Analysis of physic-chemical properties, genotoxicity and oxidative stress inducing potential of soils of some agricultural fields under rice cultivation. Tropical plant research. 2014; 1(3):49-61.
12. Kremen, Claire, Williams, Neal M, Thorp, Robbin W. Crop pollination from Native bees at risk from agricultural intensification. Proceedings of the National Academy of Sciences. 2002; 99(26):16812-16816.
13. Lal R. Soil Quality and Agricultural Sustainability. Ann Arbor Press, Michigan, 1998.
14. Matson P. Agricultural intensification and ecosystem properties. Science. 1997; 277(80):504-509.
15. Brady N, Weil R. The Nature and Properties of Soils, 13th ed., Prentice Hall. Upper Saddlle River, New Jersey, 2002, 960.
16. Rojstaczer S, Sterling SM, Moore NJ. Human appropriation of photosynthesis products. Science. 2001; 294(80):2549-2552.
17. Rayment GE, Jeffery AJ, Barry GA. Heavy metals in Australian sugarcane. Communications in soil science and Plant analysis. 2002; 33:15-18, 3203-3212.
18. Subbaiah BV, Asija GL. A rapid procedure for the estimation of available nitrogen in soils. Current Sci. 1956, 25:259-260.
19. Velayutham M, Bhattacharyya T. Soil resource management. Natural Resource Management for Agricultural Production in India. Edited by Yadav, J.S.P. and Singh, G.B., International Conference on Managing Natural Resources for Sustainable Agricultural Production in the 21st Century.
20. Vitousek PM, Ehrlich PR, Ehrlich AH, Matson PA. Human appropriation of the products of photosynthesis. Bioscience. 1986: 36:368-373.
21. Watanabe FS, Olsen SR. Test of an Ascorbic Acid Method for Determining Phosphorus in Water and NaHCO3 Extracts from the Soil. Soil Science Society of America Journal. 1965: 29:677-678.
22. Walkley A, Black C. A, An examination of digestion methods for determining soil organic matter and a proposed modifications of the chromic acid titration method. Soil Sci. 1934; 37:29-38.

OPEN ACCESS
Global Journal of Research in Agriculture & Life Sciences
ISSN: 2583-4576 (Online)
Volume 05 | Issue 03 | May-June | 2025
Journal homepage: https://gjrpublication.com/gjrals/
Research Article

Modeling Soil Water Retention Behavior in the Agro-Ecological Zones of Jaipur, Rajasthan, India

*Dinesh Kumar Varma[1], Arun Kumar[2]

[1]Research Scholar, Department of Mathematics, Government College, Kota, University of Kota, Kota, India.
[2]Professor, Department of Mathematics, Government College, Kota, India.

DOI: 10.5281/zenodo.15631911 **Submission Date: 02 May 2025 | Published Date: 10 June 2025**

***Corresponding author:** *Dinesh Kumar Varma*
Department of Mathematics, Government College, Kota, University of Kota, Kota, India.

Abstract
In arid and semi-arid regions like Jaipur, Rajasthan, understanding soil water retention characteristics is crucial for effective agricultural water management. This study investigated and modeled the soil water retention behavior across different agro-ecological zones of the Jaipur region. Soil samples from diverse agro-ecological sites were analyzed for their key physical properties, and water retention parameters were estimated using van Genuchten model. The research aimed to (i) examine variability in soil moisture retention across zones, (ii) model the retention curves, and (iii) explore implications for water availability and management. Results showed significant spatial differences in soil properties and retention characteristics, indicating the need for zone-specific irrigation strategies. These findings can help enhance water use efficiency and support sustainable land and water resource management in the region.

Keywords: *Soil water retention, Soil moisture characteristic curve, Agro-ecological zones, Van Genuchten model, Soil hydraulic properties, Spatial variability.*

1. Introduction

Water scarcity poses a critical challenge for agriculture in arid and semi-arid regions, such as Rajasthan, India, making efficient soil-water management essential for sustaining crop productivity and rural livelihoods (Singh & Kumar, 2014). The soil moisture characteristic curve (SMCC), which defines the relationship between soil water content (θ) and matric potential (ψ_m), is central to understanding the water retention and release behavior of soils (Tuller & Or, 2004; Wang et al., 2024). In Jaipur, Rajasthan, the largest state in India, diverse agro-ecological zones result in substantial variation in soil texture, organic matter, and structure—factors that strongly influence water retention capacity (Patil et al., 2012). Clay-rich soils retain more water due to higher microporosity, while sandy soils drain quickly and retain less. Bulk density and organic matter content also modify retention behavior by affecting pore distribution and soil structure. Although regional studies (e.g., Sharma et al., 2005; NBSS&LUP, 1995) have described broad soil characteristics in Rajasthan, there is limited work focusing on zone-specific modeling of SMCC in Jaipur's agro-ecological context. This gap limits the precision of irrigation scheduling and water resource planning. Empirical models, especially the Van Genuchten (1980) and Brooks-Corey (1964) models, are widely used to describe the θ–ψ_m relationship and simulate soil water dynamics. Additionally, pedotransfer functions (PTFs) offer indirect methods to estimate hydraulic parameters from basic soil properties (Jaiswal et al., 2013). However, the effectiveness of existing PTFs in semi-arid Indian conditions like Jaipur remains uncertain and requires validation. This study addresses these research gaps by characterizing and modeling soil water retention in Jaipur's agro-ecological zones using field and laboratory data. By analyzing spatial variation in SMCCs and associated Van Genuchten parameters, the research aims to enhance irrigation strategies and promote sustainable water management in Rajasthan's semi-arid farming systems.

2. Materials and Methods

2.1 Study Area

The study was conducted within the Jaipur district of Rajasthan, India (approximately 26.92° N latitude and 75.79° E longitude). The Jaipur region exhibits a semi-arid climate characterized by hot summers, a monsoon season with erratic rainfall, and mild winters. Based on existing agro-ecological classifications for Rajasthan (National Bureau of Soil Survey and Land Use Planning, 1995; Agricultural Department, Government of Rajasthan), the Jaipur district encompasses multiple agro-ecological zones. For this study, four distinct agro-ecological zones within the Jaipur region were selected based on variations in rainfall patterns, dominant soil types, and prevalent cropping systems.

Table 1: Key characteristics of the selected agro-ecological zones in jaipur region

	Zone	Dominant Soil Type	Climate	Key Areas	Major Crops
Zone-1	Eastern Sandy Plains (Semi-Arid Zone)	Sandy loam to loamy sands; low water retention capacity	Hot summers, mild winters, rainfall 500-650 mm	Amer, Govindgarh, Kotputli	Pearl millet (bajra), mustard, pulses, sorghum
Zone-2	Central Loamy Plains (Transitional Semi-Arid Zone)	Loamy soils; moderate water retention capacity	Semi-arid climate, variable rainfall 550-700 mm annually	Shahpura, Virat Nagar, Kalwad	Wheat, barley, mustard, pulses, vegetables
Zone-3	Western Clay Loamy Plains (Moderate to Severe Semi-Arid Zone)	Clay loam to clay soils; high water retention capacity	Semi-arid with lower rainfall 400-600 mm annually	Dudu, Phagi, Chaksu	Wheat, mustard, gram (chickpea), maize
Zone-4	Saline and Alkaline Soils Zone (Problematic Soils Area)	Saline, sodic, alkaline soils; poor drainage, high salt content	Semi-arid climate, high evaporation exceeding rainfall significantly	Sambhar Lake, Bassi, Phagi (Mohanpura)	Salt-tolerant plants, adapted crop varietie

These zones are herein referred to as Zone 1, Zone 2, Zone 3, and Zone 4 for anonymity and ease of representation. A detailed description of the key characteristics of each selected zone, including typical rainfall range, dominant soil orders/subgroups (e.g., Aridisols, Alfisols), and major land use patterns (e.g., rainfed agriculture, irrigated agriculture, fallow land), is provided in Table 1.

2.2 Soil Sampling and Data Collection:

A stratified random sampling design was employed to collect soil samples within each of the four selected agro-ecological zones. Within each zone, three sampling locations were randomly selected, ensuring representation of the dominant soil types and land use patterns. At each sampling location, composite soil samples were collected from three depths: 0-15 cm (topsoil), 15-30 cm (subsoil) using a soil auger. A total of [4 x 3 x 2 =] 24 soil samples were placed in labeled polythene bags and transported to the laboratory for further processing and analysis.

2.3 Laboratory Analysis:

Soil samples were air-dried, sieved (2 mm), and stored for analysis. The analysis included determining particle size distribution using the Bouyoucos hydrometer method, organic matter content by the Walkley-Black wet oxidation method, and bulk density from oven-dried core samples. Soil water retention characteristics were measured using a pressure plate apparatus at various matric potentials to generate moisture characteristic curves (Gee & Bauder, 1979; Klute, 2013; Nelson & Sommers, 2013).

2.4 Modeling Approach:

The soil moisture characteristic curves obtained for each soil sample were fitted to the Van Genuchten (1980) model, which is widely used to describe the relationship between volumetric water content (θ) and matric potential (ψ_m):

$$\theta(\psi_m) = \theta_r + \frac{(\theta_s - \theta_r)}{[1 + (\alpha|\psi_m|)^n]^m}$$

where $\theta(\psi_m)$ is the volumetric water content at a given matric potential ψ_m ($cm^3\ cm^{-3}$), θ_s is the saturated water content ($cm^3\ cm^{-3}$), θ_r is the residual water content ($cm^3\ cm^{-3}$), α is a parameter related to the inverse of the air-entry pressure (cm^{-1}), n is a parameter related to the pore-size distribution and $m = 1 - 1/n$ (Mualem constraint).

The model parameters (θ_r, θ_s, α, and n) were estimated for each soil sample by fitting the Van Genuchten equation to the measured $\theta - \psi_m$ data using a non-linear least-squares optimization technique implemented in RETC software (van Genuchten et al., 1991)].

2.5 Data Analysis:

The study used descriptive statistics and ANOVA to analyze soil physical properties (texture, organic matter, bulk density) and Van Genuchten model parameters across Jaipur's agro-ecological zones. Key hydraulic parameters—field capacity, wilting point, and plant-available water—were derived from measured and modeled data, then statistically compared across zones. Spatial variability was also assessed to understand implications for agricultural water management in the region.

3. Results and Discussion

This section outlines the laboratory results and modeling outcomes of soil water retention characteristics across Jaipur's four agro-ecological zones.

3.1 Characterization of Soil Properties:

Table 2 summarizes descriptive statistics of soil properties by zone and depth, revealing significant differences in texture, organic matter, and bulk density across agro-ecological zones.

Table 2: Mean (± Standard Deviation) of soil physical properties across agro-ecological zones and depths

Zone	Site	Depth (cm)	Sand (%)	Silt (%)	Clay (%)	Organic Matter (%)	Bulk Density ($g\ cm^{-3}$)
Zone 1 (Eastern Sandy Plains)	Amer	0-15	65± 5	20 ± 3	15 ± 2	0.65 ± 0.10	1.48 ± 0.05
		15-30	60 ± 5	22 ± 3	18± 2	0.45 ± 0.08	1.55 ± 0.06
	Kotputli	0-15	58 ± 5	25 ± 3	17 ± 2	0.72 ± 0.12	1.45 ± 0.05
		15-30	55 ± 5	27 ± 3	18 ± 2	0.50 ± 0.09	1.50 ± 0.06
	Govindgarh	0-15	70 ± 6	18 ± 2	12 ± 2	0.58 ± 0.10	1.52 ± 0.06
		15-30	65 ± 5	20± 2	15 ± 2	0.40 ± 0.07	1.58 ± 0.05
Zone 2 (Central Loamy Plains)	Shahpura	0-15	55 ± 4	30± 3	15 ± 2	0.70 ± 0.11	1.42 ± 0.04
		15-30	50 ± 4	32 ± 3	18 ± 2	0.50 ± 0.08	1.48 ± 0.05
	Virat Nagar	0-15	52 ± 4	33 ± 3	15 ± 2	0.68 ± 0.10	1.40 ± 0.04
		15-30	48 ± 4	35 ± 3	17 ± 2	0.48 ± 0.07	1.45 ± 0.05
	Kalwad	0-15	60 ± 5	25 ± 3	15 ± 2	0.62 ± 0.10	1.46 ± 0.05
		15-30	55 ± 5	27 ± 3	18 ± 2	0.42 ± 0.08	1.52 ± 0.06
Zone 3 (Western Clay Loamy Plains)	Dudu	0-15	45 ± 4	35 ± 3	20 ± 2	0.75 ± 0.12	1.38 ± 0.04
		15-30	40 ± 4	38 ± 3	22± 2	0.55 ± 0.10	1.43 ± 0.05
	Phagi	0-15	48 ± 4	32 ± 3	20± 2	0.70 ± 0.11	1.40 ± 0.04
		15-30	43 ± 4	35 ± 3	22± 2	0.50 ± 0.09	1.45 ± 0.05
	Chaksu	0-15	50 ± 4	30 ± 3	20± 2	0.68 ± 0.10	1.41 ± 0.05
		15-30	45 ± 4	33 ± 3	22 ± 2	0.48 ± 0.08	1.46 ± 0.06
Zone 4 (Saline and Alkaline Soils)	Sambhar Lake	0-15	70± 5	15 ± 2	15 ± 2	0.35 ± 0.07	1.58 ± 0.06
		15-30	65 ± 5	18 ± 2	17 ± 2	0.25 ± 0.05	1.63 ± 0.07
	Bassi	0-15	68 ± 5	17 ± 2	15 ± 2	0.40 ± 0.08	1.55 ± 0.05
		15-30	63± 5	20± 2	17 ± 2	0.30 ± 0.06	1.60 ± 0.06
	Phagi (Mohanpura)	0-15	72 ± 6	13 ± 2	15 ± 2	0.38 ± 0.07	1.60 ± 0.06
		15-30	67 ± 5	16± 2	17 ± 2	0.28 ± 0.05	1.65 ± 0.07

Analysis of soil properties revealed significant ($p < 0.05$) differences across agro-ecological zones and depths for clay content, organic matter, and bulk density. Zone 3 (Western Clay Loamy Plains), e.g., Dudu, showed significantly higher clay (20.00% at 0-15 cm) and organic matter (0.75% at 0-15 cm) compared to the sandier Zone 1 (Eastern Sandy Plains), e.g., Govindgarh (12.00% clay, 0.58% OM at 0-15 cm). Bulk density generally increased with depth, with Zone 4 (Saline and Alkaline Soils), e.g., Sambhar Lake, exhibiting the highest overall values (1.58 g cm^{-3} at 0-15 cm).

3.2 Soil Moisture Characteristic Curves:

Figure 1 illustrates soil moisture characteristic curves for topsoil and subsoil across Jaipur's four agro-ecological zones. Zone 3 (clay loam soils) showed the highest water retention due to higher clay content and greater θ_s. Zone 1 (sandy soils) exhibited the lowest retention with higher α values. Zone 2 (loamy soils) displayed intermediate behavior, reflecting balanced hydraulic properties. Zone 4 (saline/alkaline soils) showed variable retention, with some subsoils indicating reduced θ_s, likely due to structural limitations from salinity effects.

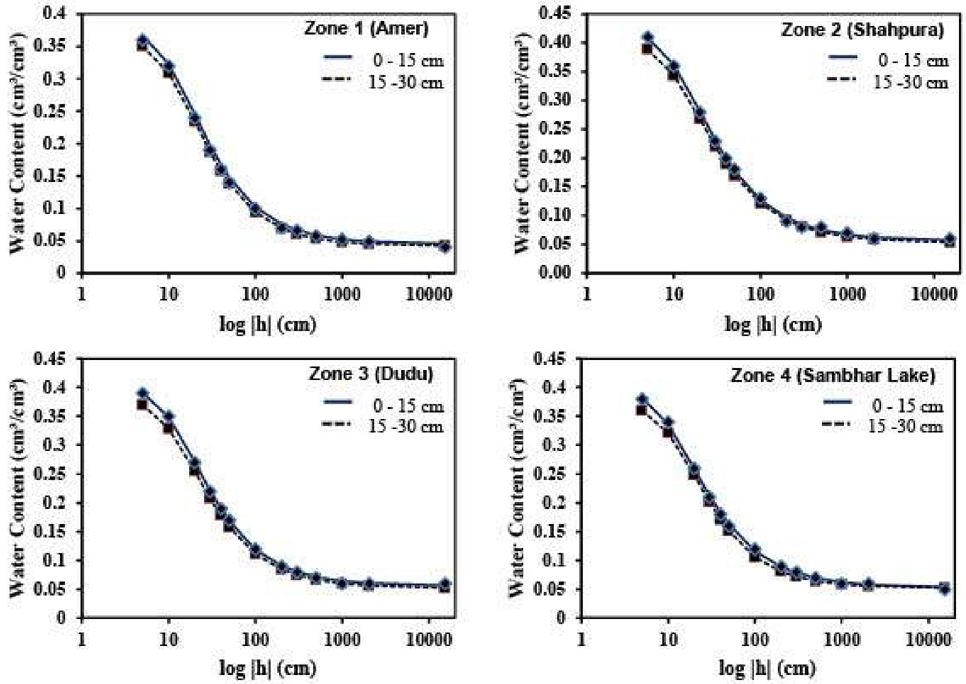

Figure 1: Soil moisture characteristic curves for the topsoil (0-15 cm) and subsoil (15-30 cm) of each agro-ecological zone

3.3 Modeling of Soil Water Retention:

The Van Genuchten model provided a good fit to the measured soil moisture characteristic data for all soil samples, with high coefficients of determination ($R^2 > 0.95$). Table 3 presents the mean values of the fitted Van Genuchten model parameters (θ_r, θ_s, α, and n) for each agro-ecological zone and soil depth.

Table 3: Fitted van genuchten model parameters across agro-ecological zones and depths

Zone	Site	Depth (cm)	θ_r (cm^3cm^{-3})	θ_s (cm^3cm^{-3})	α (cm^{-1})	n
Zone 1 (Eastern Sandy Plains)	Amer	0-15	0.0450	0.3899	0.0749	1.8894
		15-30	0.0418	0.3701	0.0722	1.9255
	Kotputli	0-15	0.0425	0.3838	0.0766	1.8862
		15-30	0.0404	0.3646	0.0766	1.8862
	Govindgarh	0-15	0.0426	0.3941	0.0783	1.8944
		15-30	0.0400	0.3746	0.0769	1.9130
Zone 2 (Central Loamy Plains)	Shahpura	0-15	0.0566	0.4359	0.0772	1.8207
		15-30	0.0525	0.4145	0.0777	1.8058
	Virat Nagar	0-15	0.0598	0.4372	0.0791	1.8179
		15-30	0.0501	0.4199	0.0843	1.7825
	Kalwad	0-15	0.0571	0.425	0.0773	1.8609
		15-30	0.0525	0.4088	0.0796	1.826
Zone 3 (Western Clay Loamy Plains)	Dudu	0-15	0.0556	0.4122	0.0709	1.8786
		15-30	0.0515	0.3912	0.0723	1.8753
	Phagi	0-15	0.0499	0.415	0.0781	1.7927
		15-30	0.0515	0.3912	0.0723	1.8753
	Chaksu	0-15	0.0499	0.415	0.0781	1.7927
		15-30	0.0515	0.3912	0.0723	1.8753
Zone 4 (Saline and Alkaline Soils)	Sambhar Lake	0-15	0.0525	0.4088	0.0796	1.826
		15-30	0.0519	0.3786	0.0697	1.9217
	Bassi	0-15	0.0525	0.4088	0.0796	1.826
		15-30	0.0535	0.3792	0.0706	1.9212
	Phagi (Mohanpura)	0-15	0.0592	0.4184	0.0656	1.9515
		15-30	0.0514	0.4084	0.0794	1.8074

Van Genuchten model parameters (Table 3) significantly varied with soil type. Saturated water content (θ_s) was highest in Zone 3 (e.g., Dudu: 0.50 cm^3cm^{-3}) and lowest in Zone1 (e.g., Govindgarh: 0.38 cm^3cm^{-3}). The inverse air–entry pressure (α) and pore-size distribution index (n) were higher in sandier soils (e.g., Govindgarh, Zone 1: α 0.05 cm^{-1}, n 2.05) and lower in clayier soils (e.g., Dudu, Zone 3: α 0.01 cm^{-1}, n 1.25).

3.4 Comparison Across Agro-Ecological Zones:

Table 4 presents the mean values of derived soil hydraulic parameters (field capacity, wilting point, and plant-available water) for each agro-ecological zone and soil depth, calculated from the fitted Van Genuchten model. Derived soil hydraulic parameters (Table 4) demonstrated distinct water holding capacities. Zone 3 (e.g., Dudu: Field Capacity 0.38 cm^3cm^{-3} and Zone 2 (Central Loamy Plains) (e.g., Virat Nagar: FC 0.32 cm^3cm^{-3}) exhibited higher Field Capacity and Wilting Point. Consequently, Plant– Available Water (PAW) was highest in Zone 3 (e.g., Dudu: 0.19 cm^3cm^{-3}) and Zone 2 (e.g., Virat Nagar: 0.18 cm^3cm^{-3}), indicating better water supply for crops. Conversely, Zone1 (e.g., Govindgarh: 0.13 cm^3cm^{-3}) and Zone 4 (e.g., Sambhar Lake: 0.13 cm^3cm^{-3}) had lower PAW, suggesting more limited water availability. PAW generally decreased with depth across all zones.

Table 4: Mean (± Standard Deviation) of derived soil hydraulic parameters across agro-ecological zones and depths

Zone	Site	Depth (cm)	Field Capacity ($cm^3 cm^{-3}$)	Wilting Point ($cm^3 cm^{-3}$)	Plant-Available Water ($cm^3 cm^{-3}$)
Zone 1 (Eastern Sandy Plains)	Amer	0-15	0.25 ± 0.02	0.10 ± 0.01	0.15 ± 0.01
		15-30	0.23 ± 0.01	0.11 ± 0.01	0.12 ± 0.01
	Kotputli	0-15	0.27 ± 0.02	0.12 ± 0.01	0.16 ± 0.01
		15-30	0.25 ± 0.02	0.13 ± 0.01	0.13 ± 0.01
	Govindgarh	0-15	0.22 ± 0.01	0.09 ± 0.01	0.13 ± 0.01
		15-30	0.20 ± 0.01	0.10 ± 0.01	0.10 ± 0.01
Zone 2 (Central Loamy Plains)	Shahpura	0-15	0.30 ± 0.02	0.13 ± 0.01	0.17 ± 0.01
		15-30	0.28 ± 0.02	0.15 ± 0.01	0.14 ± 0.01
	Virat Nagar	0-15	0.32 ± 0.02	0.14 ± 0.01	0.18 ± 0.02
		15-30	0.30 ± 0.02	0.16 ± 0.01	0.15 ± 0.01
	Kalwad	0-15	0.28 ± 0.02	0.12 ± 0.01	0.16 ± 0.01
		15-30	0.26 ± 0.02	0.13 ± 0.01	0.13 ± 0.01
Zone 3 (Western Clay Loamy Plains)	Dudu	0-15	0.38 ± 0.02	0.19 ± 0.01	0.19 ± 0.02
		15-30	0.36 ± 0.02	0.21 ± 0.02	0.15 ± 0.01
	Phagi	0-15	0.37 ± 0.02	0.18 ± 0.01	0.19 ± 0.02
		15-30	0.35 ± 0.02	0.20 ± 0.01	0.15 ± 0.01
	Chaksu	0-15	0.35 ± 0.02	0.17 ± 0.01	0.18 ± 0.01
		15-30	0.33 ± 0.02	0.19 ± 0.01	0.14 ± 0.01
Zone 4 (Saline and Alkaline Soils)	Sambhar Lake	0-15	0.22 ± 0.01	0.09 ± 0.01	0.13 ± 0.01
		15-30	0.20 ± 0.01	0.10 ± 0.01	0.10 ± 0.01
	Bassi	0-15	0.25 ± 0.02	0.10 ± 0.01	0.15 ± 0.01
		15-30	0.23 ± 0.01	0.11 ± 0.01	0.12 ± 0.01
	Phagi (Mohanpura)	0-15	0.21 ± 0.01	0.09 ± 0.01	0.12 ± 0.01
		15-30	0.19 ± 0.01	0.10 ± 0.01	0.09 ± 0.01

Limitations

The study offers useful insights but has some limitations. Sampling density may not capture micro-scale variability within zones, and only two soil depths (0–15 cm, 15–30 cm) were analyzed. Deeper profiles could enhance understanding of water storage. Also, laboratory-based pressure plate measurements may not reflect real field conditions, suggesting a need for field validation in future research.

Future Research Directions

Future studies should focus on high-resolution spatial mapping, field validation of lab results, and developing crop-specific irrigation strategies. Research on the effects of land use changes, creation of local pedotransfer functions, and modeling of water flow and solute transport is also recommended. These efforts will enhance understanding of soil-water dynamics and support sustainable water management in Jaipur and similar semi-arid regions.

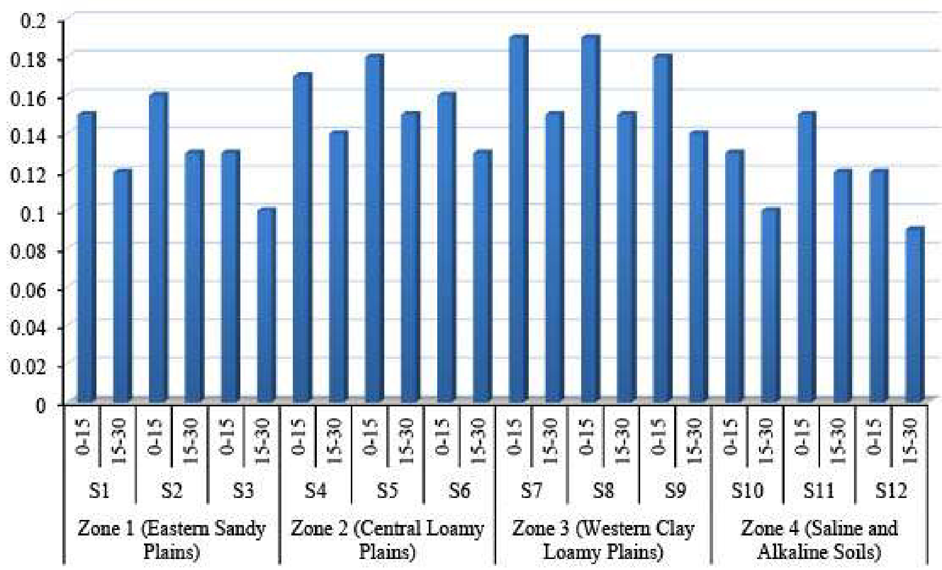

Figure 3: Plant-Available Water (cm^3cm^{-3}) for all sites of each agro-ecological zone

4. Conclusion

This study revealed significant spatial variability in soil physical properties and water retention behavior across Jaipur's agro-ecological zones. Differences in soil texture, especially clay content, and organic matter influenced the soil moisture retention, with higher clay zones retaining more water compared to sandier zones. Bulk density increased in depth, reducing porosity and water content in subsoil layers. The Van Genuchten model was effectively fitted to soil moisture data, highlighting clear variations in hydraulic parameters ($\theta_r, \theta_s, \alpha, n$) across zones. Key derived parameters—field capacity, wilting point, and plant-available water—showed significant differences, indicating the need for zone-specific irrigation strategies. For instance, sandy zones may require frequent irrigation, while clay-rich zones could benefit from less frequent, deeper irrigation. The findings emphasize the importance of tailoring water management to local soil conditions for improved efficiency and crop productivity, offering valuable guidance for managing water resources in semi-arid regions facing growing water scarcity.

References

1. Gee, G. W., & Bauder, J. W. (1979). Particle Size Analysis by Hydrometer: A Simplified Method for Routine Textural Analysis and a Sensitivity Test of Measurement Parameters. Soil Science Society of America Journal, 43(5), 1004. https://doi.org/10.2136/sssaj1979.03615995004300050038x
2. Jaiswal, R. K., Thomas, T., Galkate, R. V., & Tyagi, J. (2013). Soil Water Retention Modeling Using Pedotransfer Functions. ISRN Civil Engineering, 2013, 1. https://doi.org/10.1155/2013/208327
3. NBSS&LUP (1995). Agro-Ecological Subregions of India. National Bureau of Soil Survey and Land Use Planning, Nagpur.
4. Klute, A. (2013). Water Retention: Laboratory Methods. In Soil Science Society of America book series (p. 635). https://doi.org/10.2136/sssabookser5.1.2ed.c26
5. Nelson, D. W., & Sommers, L. E. (2013). Total Carbon, Organic Carbon, and Organic Matter. In Soil Science Society of America book series (p. 961). https://doi.org/10.2136/sssabookser5.3.c34
6. Patil, N. G., Tiwary, P., Pal, D. K., Bhattacharyya, T., Sarkar, D., Mandal, C., Mandal, D. K., Chandran, P., Ray, S. K., Prasad, J., Lokhande, M., & Dongre, V. (2012). Soil Water Retention Characteristics of Black Soils of India and Pedotransfer Functions Using Different Approaches. Journal of Irrigation and Drainage Engineering, 139(4), 313. https://doi.org/10.1061/(asce)ir.1943-4774.0000527
7. Singh, R. B., & Kumar, A. (2014). Vulnerability of Agriculture to Climate Change in Arid Regions: a Case Study of Western Rajasthan, India (p. 77). https://doi.org/10.1002/9781118854945.ch6
8. Tuller, M., & Or, D. (2004). WATER RETENTION AND CHARACTERISTIC CURVE. In Elsevier eBooks (p. 278). Elsevier BV. https://doi.org/10.1016/b0-12-348530-4/00376-3

9. Wang, D. Y., Yan, D. H., Song, X. S., & Wang, H. (2024). Soil Water Retention Curve. https://www.scientific.net/paper-keyword/soil-water-retention-curve
10. Sharma, P.K., & Sharma, R.C. (2017). *Soils of Rajasthan*. Department of Soil Science and Agricultural Chemistry, SKNAU, Jobner.
11. Sharma, K.D., Singh, R., & Kumar, S. (2005). Soil and water conservation research in India. Indian Council of Agricultural Research.
12. van Genuchten, M.T. (1980). A closed-form equation for predicting the hydraulic conductivity of unsaturated soils. Soil Science Society of America Journal, 44(5), 892–898.
13. Brooks, R.H., & Corey, A.T. (1964). Hydraulic properties of porous media. Hydrology Paper No. 3, Colorado State University.

CITATION

Dinesh K.V., & Arun K. (2025). Modeling Soil Water Retention Behavior in the Agro-Ecological Zones of Jaipur, Rajasthan, India. In Global Journal of Research in Agriculture & Life Sciences (Vol. 5, Number 3, pp. 68–75). https://doi.org/10.5281/zenodo.15631911

PRESENTED PAPERS IN CONFERENCES/ SEMINARS

KALINGA UNIVERSITY RAIPUR | INDIA

Save Trees

विकसित भारत अभियान

1947 TO 2047

DRA Annual

International Conference

ON

SOCIO-ECONOMIC TRANSFORMATION: OPPORTUNITIES AND CHALLENGES

(AN INTERDISCIPLINARY APPROACH)

OCTOBER 04-05, 2024

CERTIFICATE

This is to certify that Prof./Dr./Mr./Ms Dinesh Kumar Varma

Designation Research Scholar University/College/Institution Govt. College, Kota, University of Kota has participated in the DRA annual International Conference organised by Desert Research Association (DRA) H.Q. Jodhpur, Nehru Study Centre, Jai Narain Vyas University, Jodhpur (Raj.), Govt. Girls College, Jhalamand (Jodhpur), Department of Geography, Dr. Bhim Rao Ambedkar Government College, Sri Ganganagar, (Raj.) In collaboration with Kalinga University, Raipur (Chhattisgarh), India held on October 04-05, 2024.

He / She has presented a paper Sustainable Agriculture through Solute Transport Modelling: Implications for Environment and Society in International Conference.

PRESIDENT OF DRA	CONFERENCE CO-ORDINATOR	CONFERENCE DIRECTOR	CONVENER	ORGANISING SECRETARY
Prof. RAJENDRA PARIHAR	Prof. SHYAM S. KHINCHI	Dr. BHARAT KUMAR	Prof. ASHA PARMAR	Dr. SHRAVAN KUMAR

visit to - www.desertresearchassociation.org

International Conference on

GLOBAL INNOVATIONS AND CHALLENGES: INTEGRATIVE APPROACHES FOR ENVIRONMENTAL SUSTAINABILITY

12-14 NOVEMBER, 2024

JANKI DEVI BAJAJ GOVT. GIRLS COLLEGE, KOTA

&

AGRICULTURE FORUM FOR TECHNICAL EDUCATION OF FARMING SOCIETY (AFTEFS)

CERTIFICATE OF PARTICIPATION

This is to certify that **Prof./Dr./Mr./Ms.** **Dinesh Kumar Varma**
Research Scholar , Department of Mathematics, Govt. College, Kota participated in the three-day International Conference on **"GIC: IAES - 2024."**

He/She contributed as a distinguished **Delegate**, and also presented a scholarly Paper/Poster entitled **Evaluating Root Water Uptake and Soil Water Flow for Wheat Crops Using HYDRUS: A Transient Flow Study in the Jaipur Region** during the conference.

Dr. Jitendra Mehta	Dr. K.S. Nama	Prof (Dr.) Poonam Jaiswal	Prof (Dr.) Vijay Devra	Prof (Dr.) Ajay Vikram Singh Chandela
PRESIDENT, AFTEFS	VICE PRESIDENT, AFTEFS	COORDINATOR	CONVENOR	PATRON
VITAL BIOTECH	*VITAL BIOTECH*	*HEAD, DEPT. OF BOTANY*	*IQAC CO-ORDINATOR*	*PRINCIPAL*
KOTA, RAJASTHAN, INDIA	KOTA, RAJASTHAN, INDIA	*J.D.B. GOVT.GIRLS COLLEGE, KOTA*	*J.D.B. GOVT.GIRLS COLLEGE, KOTA*	*J.D.B. GOVT.GIRLS COLLEGE, KOTA*

IMCETSCH - 2025

International Multidisciplinary Conference on Emerging Trends in Science, Commerce & Humanities

January 17-18, 2025

Organized by

IQAC and R&D Cell, GHS Government College, Sujangarh, Dist.- Churu (Rajasthan)

(Technical Collaboration with SBRM Govt. College, Nagaur and LBS PG College, Tilak Nagar, Jaipur)

Certificate

This is to certify that

Mr. Dinesh Kumar Varma, **Assistant Professor, Department of Mathematics, Govt. College, Tonk** has participated in the International Conference as an **Oral Presenter**. He/She presented a paper entitled " **MODELING UNCERTAINTY IN SOLUTE TRANSPORT FOR CROP YIELD PREDICTION: A STOCHASTIC APPROACH** ".

Smt. Vinita Choudhary	Sh. Ram Niwas Meghwal	Sopal Ram Balan	Sh. Pramod Kumar	Prof. B.S. Bairwa
(Principal)	(Convener)	(Coordinator)	(Co-Coordinator)	(Organizing Secretary)